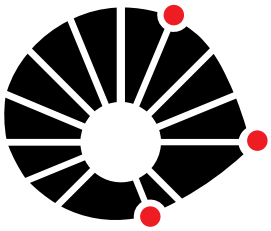

UNICAMP

UNIVERSIDADE ESTADUAL DE CAMPINAS

Instituto de Matemática, Estatística e Computação Científica

THAIS CLARA DA COSTA HAVEROTH

Damage Phase-Field Models with Fractional Derivatives for Viscoelastic Materials

Modelos de Campo de Fase e Derivadas Fracionárias para Dano em Materiais Viscoelásticos

Campinas

2023

Thais Clara da Costa Haveroth

Damage Phase-Field Models with Fractional Derivatives for Viscoelastic Materials

Modelos de Campo de Fase e Derivadas Fracionárias para Dano em Materiais Viscoelásticos

Tese apresentada ao Instituto de Matemática, Estatística e Computação Científica da Universidade Estadual de Campinas como parte dos requisitos exigidos para a obtenção do título de Doutora em Matemática Aplicada.

Thesis presented to the Institute of Mathematics, Statistics and Scientific Computing of the University of Campinas in partial fulfillment of the requirements for the degree of Ph.D. in Applied Mathematics.

Advisor: José Luiz Boldrini

Co-Advisor: Marco Lúcio Bittencourt

Este trabalho corresponde à versão final da Tese defendida pela aluna Thais Clara da Costa Haveroth e orientada pelo Prof. Dr. José Luiz Boldrini.

Campinas

2023

Ficha catalográfica
Universidade Estadual de Campinas
Biblioteca do Instituto de Matemática, Estatística e Computação Científica
Ana Regina Machado - CRB 8/5467

D118d

Da Costa-Haveroth, Thais Clara, 1993-
Damage phase-field models with fractional derivatives for viscoelastic materials / Thais Clara da Costa Haveroth. – Campinas, SP : [s.n.], 2023.

Orientador: José Luiz Boldrini.
Coorientador: Marco Lúcio Bittencourt.
Tese (doutorado) – Universidade Estadual de Campinas, Instituto de Matemática, Estatística e Computação Científica.

1. Modelos de campo de fase. 2. Derivadas fracionárias. 3. Viscoelasticidade. 4. Materiais viscoelásticos - Fratura. I. Boldrini, José Luiz, 1952-. II. Bittencourt, Marco Lúcio, 1964-. III. Universidade Estadual de Campinas. Instituto de Matemática, Estatística e Computação Científica. IV. Título.

Informações Complementares

Título em outro idioma: Modelos de campo de fase e derivadas fracionárias para dano em materiais viscoelásticos
Palavras-chave em inglês:
Phase field models
Fractional derivatives
Viscoelasticity
Viscoelastic materials - Fracture
Área de concentração: Matemática Aplicada
Titulação: Doutora em Matemática Aplicada
Banca examinadora:
José Luiz Boldrini [Orientador]
Giuseppe Romanazzi
Maicon Ribeiro Correa
Sergio Persival Baroncini Proença
Eduardo Alberto Fancello
Data de defesa: 11-05-2023
Programa de Pós-Graduação: Matemática Aplicada

Identificação e informações acadêmicas do(a) aluno(a)
- ORCID do autor: https://orcid.org/0000-0002-0725-8456
- Currículo Lattes do autor: http://lattes.cnpq.br/3285257398864374

Tese de Doutorado defendida em 11 de maio de 2023 e aprovada

pela banca examinadora composta pelos Profs. Drs.

Prof(a). Dr(a). JOSÉ LUIZ BOLDRINI

Prof(a). Dr(a). GIUSEPPE ROMANAZZI

Prof(a). Dr(a). MAICON RIBEIRO CORREA

Prof(a). Dr(a). SERGIO PERSIVAL BARONCINI PROENÇA

Prof(a). Dr(a). EDUARDO ALBERTO FANCELLO

A Ata da Defesa, assinada pelos membros da Comissão Examinadora, consta no SIGA/Sistema de Fluxo de Dissertação/Tese e na Secretaria de Pós-Graduação do Instituto de Matemática, Estatística e Computação Científica.

Acknowledgements

This study was financed in part by the Coordenação de Aperfeiçoamento de Pessoal de Nível Superior - Brasil (CAPES) - Finance Code 001.

I want to extend my heartfelt gratitude to all the people who encouraged me to start this project, persevere with it, and publish it.

I wish to thank my Advisor, Professor José Luiz Boldrini, for all his patience, expert guidance, and immense knowledge that he has given me over the past years.

I am also grateful to my Co-Advisor, Professor Marco Lúcio Bittencourt, for his motivation, encouragement, and help throughout my study.

To all my Professors who have been a constant source of knowledge, inspiration, and renovation.

To the Applied Mathematics Department of the University of Campinas and the Faculty of Mechanical Engineering for the opportunity to carry through this research.

To my amazing husband, Geovane for his support and for encouraging me continuously every step of the way.

To my parents, Leori and Vanir, who always believed in my abilities to achieve my dreams at every stage of my life.

Thank you, everyone!

Resumo

Este trabalho apresenta um modelo inédito e abrangente que utiliza campos de fase e derivadas fracionárias para modelagem de dano em materiais viscoelásticos. Foram utilizados potenciais de energia livre e pseudo potenciais de dissipação apropriados, como uma extensão da estratégia apresentada em Costa-Haveroth et al. (2022), para produzir uma metodologia capaz de descrever fenômenos hereditários com efeitos de memória, grandes deformações e influências térmicas. Os potenciais são acoplados ao modelo de forma termodinamicamente consistente e conduzem a relações tensão/deformação gerais em termos de derivadas fracionárias. Obtemos um sistema não-linear de equações governantes que descrevem a evolução do movimento, dano e temperatura, e mostramos como este conjunto geral de equações pode ser adaptado para recuperar uma grande quantidade de submodelos, incluindo algumas metodologias tradicionais encontrados na literatura. Adaptamos uma estratégia numérica escalonada para resolver o sistema de equações de forma desacoplada; várias simulações foram incluídas no trabalho, tanto para o caso unidimensional quanto bidimensional. Os resultados numéricos são divididos em duas partes: comentários e detalhamentos com respeito aos testes previamente publicamos por nós em Costa-Haveroth et al. (2022), para um submodelo simplificado com representação reológica em paralelo; e novos resultados para um modelo mais abrangente com representação reológica em série. Os testes mostram que a metodologia desenvolvida neste trabalho pode descrever diferentes padrões de danificação, tanto para o regime de pequenas quanto grandes deformações, sendo uma estratégia com grande potencial para tratar de falha em materiais viscoelásticos.

Palavras-chave: Campos de Fase. Dano e Fratura. Viscoelasticidade. Derivadas Fracionárias.

Abstract

This work presents a new and comprehensive damage phase-field model with fractional derivatives for viscoelastic materials. We apply appropriate specific free-energy density and a pseudo-potential of dissipation as an extension of the strategy presented in Costa-Haveroth et al. (2022), producing a framework able to describe hereditary phenomena with memory, large strains, and thermal effects. These potentials are coupled to the model in a thermodynamically consistent way, leading to general fractional stress/strain relations. We obtain a system of nonlinear governing equations to describe the evolution of motion, damage, and temperature. Furthermore, we show how this general set of equations can recover several sub-models, including some traditional approaches widely employed in the literature. We adjust a staggered strategy to solve the governing system numerically and address several one and two-dimensional numerical simulations. We divide the numerical results into two main parts: comments and details on the tests, previously published in Costa-Haveroth et al. (2022), for a simplified parallel sub-model obtained from our general approach; and novelty results for a series model. The tests show that the developed model can describe different damage patterns, both for small and finite strains, being a promising methodology to deal with failure in viscoelastic materials.

Keywords: Phase-field. Damage and Fracture. Viscoelasticity. Fractional Derivatives.

List of Abbreviations and Acronyms

FE	Finite Element
FEM	Finite Element Method
G1	Numerical algorithm used for fractional derivatives
HDPE	High Density Polyethylene
MSD	Mean Square Difference
NR	Newton-Raphson
NM	Newmark Method
PDE	Partial Differential Equation
PM	Parallel Model - Modified fractional Kelvin-Voigt model
PVP	Principle of Virtual Power
SM	Series Model - Modified fractional Zener model

List of Symbols

Sets		
Symbol	Page	Description
$\mathcal{B}$, $\mathcal{B}_{(\cdot)}$	117, 39	Body domains
$C[t_1, t_2]$	27	Continuous function in the interval $[t_1, t_2]$
$\mathbb{N}$	27	Integer non-negative numbers
$\mathbb{R}^n$	20	n-dimensional Euclidean space
Γ, $\Gamma_{(\cdot)}$	31	Boundary of a regular domain
Γ_D, Γ_N	31	Boundaries subject to Dirichlet and Neumann conditions, respectively
Θ	51	Set of variables
$\Upsilon(\cdot)$	46	Set of the independent variables
Ω, $\Omega_{(\cdot)}$	20, 39, 117	Regular domains
Ω_0, $\hat{\Omega}_{(\cdot)}$	20,39,	Initial and intermediate configurations

Operators, superscripts and subscripts		
Symbol	Page	Description
$\mathrm{D}^w(\cdot)$, ${}_{t_1}\mathrm{D}^w_{t_2}(\cdot)$, $\dfrac{\mathrm{d}^w}{\mathrm{d}t^z}(\cdot)$	24, 25, 118	Time derivative of order w
$\boldsymbol{D}$	67	Directional derivative
$\det(\cdot)$	35, 120	Determinant
$\mathrm{div}(\cdot)$, $\mathrm{div}_p(\cdot)$	119	Spatial and material divergence operators
$F(\cdot)$	82	External force
$f(\cdot)$	27	Arbitrary function
$G^{(\cdot)}(\cdot)$	47	Degradation functions
$G_m(\cdot)$, $G_h(\cdot)$	47	Degradation functions associated with memory and hyperelastic effects, respectively
$H(\cdot)$	54	Potential for $(\cdot)$
$\ln(\cdot)$, $\exp(\cdot)$	53, 27	Natural logarithm and exponential functions
$\mathscr{A}(\cdot)$	25	Function that weights the fractional derivative; scalar form of $\boldsymbol{\mathcal{A}}$
$\mathscr{F}(\cdot)$	67	Tensorial valued function
$\mathscr{H}(\cdot)$, $\mathscr{H}_t(\cdot)$	46	Functional associated with memory effects
$\mathscr{N}_A(\cdot,\cdot)$	48	Continuous function of second-order symmetric tensors
$\Gamma(\cdot)$	27	Gamma function

Operators, superscripts and subscripts		
Symbol	Page	Description
$\delta(\cdot)$	34	A virtual quantity of $(\cdot)$
$\tau(\cdot)$	46	Constitutive relation
$\chi(\cdot)$	117	Smooth vector valued mapping for motion
$\nabla_{\boldsymbol{x}}(\cdot)$, $\nabla_p(\cdot)$	119	Spatial and material gradient operators
$\partial_t(\cdot)$	138	Partial time derivative
$\partial_Y(\cdot)$	53	Partial derivative of $(\cdot)$ with respect to Y
$\lceil\cdot\rceil$	27	Ceiling function
$\|\|\cdot\|\|$	71	Norm
$\dot{(\cdot)}$	118	Time derivative of $(\cdot)$
$\ddot{(\cdot)}$	118	Second time derivative of $(\cdot)$
$\tilde{(\cdot)}$	65	Nodal values of the field $(\cdot)$
$\bar{(\cdot)}$	38	Prescribed initial condition for $(\cdot)$
${}^{(d)}(\cdot)$, ${}^{(nd)}(\cdot)$	49	Dissipative and non-dissipative components of $(\cdot)$
$(\cdot)_{\text{symm}}$, $(\cdot)_{\text{skew}}$	42	Symmetric and skew-symmetric parts of $(\cdot)$
$(\cdot)_{n+1}$	65	Variable $(\cdot)$ evaluated at time t_{n+1}
$(\cdot)_i$	71	i-th iteration of the Newton-Raphson method
$(\cdot)^q$	65	q-th element contribution
$(\cdot)^t$	41	Transpose of $(\cdot)$
$(\cdot)^{-t}$	41	Inverse of the transpose of $(\cdot)$
$(\cdot)^{-1}$	40	Inverse of $(\cdot)$

Scalar quantities		
Symbol	Page	Description
A	82	Area
A_m	127	Angular momentum
a, b, c	58	Constants associated with the degradation function
a_1, a_2, a_3	67	Constants for the Newmark method
C, C_1	48	Real constant
$\tilde{b}$	55	Parameter related to the material viscosity
c_v	53	Volumetric heat capacity of the material
$\tilde{c}$	55	Thermal conductivity
E	24	Scalar representation of the Green-Lagrangian Strain
E_Y	24	Young's Modulus
e, e_0	33, 39	Specific internal energy density
f_t	90	Fracture toughness
g_c	54	Critical Griffith fracture energy parameter
j	140	Complex unity

Scalar quantities		
Symbol	Page	Description
k, k_0	34, 40	Volumetric density of energy exchanged by variation of a unity of φ in a unity of time
ℓ	82	Length
m, n, p, q	27, 116	Integer non-negative value
N	27, 116	Number of sub-intervals for the time discretization
N_j	65	Local nodal basis function
R^A, R^B	53, 51	Positive variable associated with damage mechanisms
r, r_0	37	Specific heat source/sink density
S, S_p	24	Scalar representation of the stress
s	47, 117	Some arbitrary non-negative real value
t, $t_{(\cdot)}$	20	Time variables
t_h, $t_{h,0}$	35	Superficial density of energy supplied to the material by the flux
w, $w_{(\cdot)}$, z	20, 116	General scalar field
$\mathcal{I}^A$, $\mathcal{I}^B$	52	Free-energy associated with damage
$\mathcal{K}$	37	Kinect energy
$\mathcal{P}_i$, $\mathcal{P}_e$, $\mathcal{P}_a$, $\mathcal{P}_\varphi$	34, 128	Virtual power of the interior, exterior, inertia and damage forces
$\mathcal{Q}^f$, $\mathcal{Q}^s$	37	Total energy by $\boldsymbol{q}$ and sources/sinks, respectively
$\mathcal{U}$	37	Total internal energy
α	25	Fractional derivative order
β, β_1, $\tilde{\beta}$	137	Real constant associated with α
β_N, γ_N	83	Coefficient of the Newmark method
γ_c	54	Width of the fracture layers
κ	54	Constant associated with α
δ	55	Small positive constant used to avoid singularity
$\hat{\delta}$	140	Small perturbation
δ_{ij}	135	Kronecker delta
$\mathrm{d}\Gamma$, $\mathrm{d}\Gamma_0$	122,	Element of area
$\mathrm{d}\Omega$, $\mathrm{d}\Omega_0$	122	Element of volume
Δt	65	Time increment
ϵ	71	Prescribed tolerance for the Newton-Raphson
η	24	Specific entropy density
η_v	24	Viscous constant
θ, θ_0	37	Absolute temperature
ϑ	65	Quantity of nodes in the element
λ^A, λ^B, μ^A, μ^B	53	Lamé constants

Scalar quantities		
Symbol	Page	Description
$\bar{\lambda}$, $\bar{\mu}$	85	Modified Lamé constants
$\tilde{\lambda}$, c_λ, ζ	55	Material parameters related to the damage change and its derivative
ν	84	Poisson's' ratio
ρ, ρ_0	34, 125	Material densities
τ	27	Integration variable
φ, $\hat{\varphi}^A$, φ^B, φ_0, φ^*	20, 35, 39, 74	Phase field variables
ψ	38, 46, 47	Specific free-energy of Helmholtz
ψ, ψ_c, $\psi_c^{(\cdot)}$	46, 47	Space-time pointwise free-energy densities
ψ_m, $\tilde{\psi}_m$, ψ_m^A, ψ_m^B	47	Free-energies associated with memory effects
ψ_θ, ψ_h	52	Free-energies associated with temperature and hyper-elaticity, respectively
ψ_d,	51	Pseudo-potential of dissipation
ω_m, $\omega_{(\cdot)}$	37	Specific entropy production terms

Vector fields		
Symbol	Page	Description
$\boldsymbol{B}$, $\bar{\boldsymbol{B}}$	66	Matrices of local nodal shape function derivatives
$\boldsymbol{f}$, $\boldsymbol{f}_0$	35, 39, 123	Specific body force vector fields
$\boldsymbol{h}$, $\boldsymbol{h}_0$	34, 40	Energy flux correlated with the spatial variation of a unit of φ in a unit of time
$\boldsymbol{n}$, $\boldsymbol{n}_0$	36,40	Unit normal vectors
$\boldsymbol{N}$, $\bar{\boldsymbol{N}}$	65	Matrices of local nodal shape functions
$\boldsymbol{p}$	117	Lagrangian material point
$\boldsymbol{q}$, $\boldsymbol{q}_0$	37	Heat flux vector field
$\boldsymbol{s}^B$	71	Vector form of $\boldsymbol{S}^B$
$\boldsymbol{u}$	33, 118	Displacement vector field
$\boldsymbol{v}$	33, 118	Velocity vector field
$\boldsymbol{x}$	117	Eulerian (spatial) point
$\boldsymbol{w}$, $\boldsymbol{w}_0$, $\boldsymbol{z}$, $\boldsymbol{z}_0$	114, 116, 119	General vector fields
$\boldsymbol{\Phi}$, $\boldsymbol{\Phi}_{(\cdot)}$	37	Entropy flux
$\boldsymbol{\sigma}$, $\boldsymbol{\sigma}_0$	35, 124	Traction vector fields

Second-order tensors		
Symbol	Page	Description
$\boldsymbol{C}$, $\hat{\boldsymbol{C}}^B$, $\boldsymbol{C}^A$	122, 44	Cauchy-Green deformation tensors
$\boldsymbol{E}$, $\boldsymbol{E}^A$, $\hat{\boldsymbol{E}}^B$, $\boldsymbol{E}_t$	122,42, 42, 47	Green-Lagrange strain tensors

Second-order tensors		
Symbol	Page	Description
$\boldsymbol{F}$, $\boldsymbol{F}^A$, $\boldsymbol{F}^B$	31	Total and partial gradients of deformation
$\bar{\boldsymbol{F}}$	71	Matrix derived from $\boldsymbol{F}$
$\boldsymbol{I}$	31, 119	Second-order identity tensor
$\boldsymbol{J}^{\boldsymbol{u}}$, $\boldsymbol{J}^{\varphi}$, $\boldsymbol{J}^{\boldsymbol{E}^A}$	71, 74, 76	Jacobian matrix for the motion, damage and evolution of $\boldsymbol{E}^A$, respectively
$\boldsymbol{L}$, $\boldsymbol{L}^A$, $\hat{\boldsymbol{L}}^A$ $\boldsymbol{L}^B$	33, 121	Total and partial velocity gradient tensors
$\boldsymbol{M}$	71	Mass matrix
$\boldsymbol{P}$, $\boldsymbol{P}^B$	39	First Piola-Kirschhoff stress tensors
$\boldsymbol{R}$	56	Rotation tensor
$\boldsymbol{R}^{\boldsymbol{u}}$, $\boldsymbol{R}^{\varphi}$, $\boldsymbol{R}^{\boldsymbol{E}^A}$	67, 74, 76	Residue for the motion, damage and evolution of $\boldsymbol{E}^A$
$\boldsymbol{S}$, $\boldsymbol{S}^B$, $\bar{\boldsymbol{S}}$	40, 125, 71	Second Piola-Kirschhoff stress tensor
$\boldsymbol{T}$, $\hat{\boldsymbol{T}}^A$, $\hat{\boldsymbol{T}}^B$, $\boldsymbol{T}^B$, $\hat{\boldsymbol{T}}^A_{\text{skew}}$	34, 124	Cauchy stress tensors
$\boldsymbol{U}$	56	Orthogonal matrix that represents a rotation
$\boldsymbol{Z}$	116	Arbitrary second-order tensor

High-order tensors		
Symbol	Page	Description
$\boldsymbol{\mathcal{A}}$	54	Symmetric fourth-order tensor associated with the fractional derivative
$\boldsymbol{\mathcal{H}}$	70	Fourth-order symmetric positive definite tensor obtained by the derivative of the stress on the strain
$\boldsymbol{\mathcal{I}}$	135	Fourth-order symmetric identity

Contents

INTRODUCTION **15**
A Brief Account of Previous Viscoelastic Damage Models **15**
Shortcomings of Previous Fractional Viscoelastic Damage Models **16**
Proposal of the Present Work **16**
Objectives **16**
Outline of the Thesis **17**
Final Remark **18**

1 HISTORICAL AND MATHEMATICAL OVERVIEW **20**
1.1 Background on Phase-fields Models **20**
1.1.1 Historical Development of Phase-Field Models 21
1.1.2 Damage Phase-Field Models 22
1.2 Background on Viscoelasticity **23**
1.2.1 Traditional Viscoelastic Modeling 23
1.2.2 Fractional Viscoelasticity Modeling 25
1.2.2.1 Historical Overview on Fractional Viscoelasticity 26
1.2.2.2 Caputo Fractional Derivative 27
1.2.3 Parallel versus Series Models 28
1.2.4 Modeling of Failure in Viscoelastic Materials 29

2 GENERAL DAMAGE PHASE-FIELD MODEL **31**
2.1 Incremental Strain and Rheological Connections in Series **31**
2.2 Development of the General Damage Phase-Field Model **33**
2.2.1 The Governing Equations in Eulerian Coordinates 33
2.2.2 The Governing Equations in Lagrangian Coordinates 39
2.2.3 Constitutive Relations in Lagrangian Coordinates 46
2.2.3.1 General Free-Energy 46
2.2.3.2 The Coleman-Noll Method 49
2.2.3.2.1 Terms Derived from the Free-Energy 50
2.2.3.2.2 Dissipative Terms and Pseudo-Potential of Dissipation 51

3 A DAMAGE PHASE-FIELD MODEL WITH FRACTIONAL VISCOELASTICITY **52**
3.1 Viscoelastic Series Model **52**
3.1.1 A Particular Free-Energy Potential 52
3.1.2 Specialization of the Pseudo-Potential of Dissipation 55

3.1.3 Stress Tensors of the Model . . . 55
3.1.4 Degradation Functions . . . 57
3.1.5 System of Equations for the Viscoelastic Series Model . . . 59
3.2 Simplifications and Sub-models . . . 60
3.2.1 Viscoelastic Parallel Model . . . 62

4 NUMERICAL CONSIDERATIONS . . . 65
4.1 Equation of Motion . . . 66
4.1.1 Applying the Newmark Method for Motion . . . 67
4.1.2 Linearization for the Equation of Motion . . . 67
4.1.3 Finite Element Method for Motion Equation . . . 71
4.1.4 Numerical Fractional Derivative - The Algorithm G1 . . . 72
4.2 Equation of Damage . . . 72
4.3 Equations for the Gradients of Deformation . . . 75
4.4 Summary of the Numerical Treatment . . . 78

5 NUMERICAL RESULTS . . . 82
5.1 Results on the Parallel Model . . . 82
5.1.1 Viscoelastic Bar . . . 82
5.1.1.1 Displacement for the Dynamic One-Dimensional Test . . . 83
5.1.1.2 Two-Dimensional Extension . . . 85
5.1.2 I-shaped Viscoelastic Specimen . . . 85
5.1.2.1 Loading-Unloading Simulation without Damage . . . 86
5.1.2.2 Tensile Test with Damage Evolution . . . 87
5.1.3 Comparison with Experimental Results . . . 88
5.1.3.1 Small Strain . . . 89
5.1.3.2 Large Strain and Fracture . . . 91
5.2 Results for the Series Model . . . 94
5.2.1 Comparisons Between SM and PM . . . 95
5.2.2 Damage effect for SM . . . 96

6 CONCLUSIONS . . . 98
6.1 Observations and Contributions . . . 99
6.2 Deficiencies and Limitations . . . 100
6.3 Future Works . . . 101

REFERENCES . . . 102

APPENDIX A – IMPORTANT THEOREMS . . . 114

APPENDIX B – RECURRENT DERIVATIVES . . . 115

APPENDIX C – REVIEW ON CONTINUUM MECHANICS 116
C.1 Tensors . . . 116
C.2 Kinematic of Bodies . . . 117
C.2.1 Displacement, Velocity and Acceleration . . . 117
C.2.2 Lagrangian and Eulerian Configurations . . . 118
C.3 Deformation Gradient . . . 119
C.4 Velocity Gradient Tensor . . . 121
C.5 Strain Tensors . . . 121
C.6 Area and Volume . . . 122
C.7 Forces and Stress . . . 123
C.7.1 Cauchy Stress Tensor . . . 123
C.7.2 Other Stress Measures . . . 124
C.8 Fundamental Equations of Continuum Mechanics . . . 125
C.8.1 Principle of Mass Conservation . . . 125
C.8.2 Balance of Linear Momentum . . . 126
C.8.3 Balance of Angular Momentum . . . 127
C.8.4 First Law of Thermodynamics . . . 127
C.8.4.1 Balance of Power . . . 127
C.8.4.2 Principle of Virtual Power . . . 129
C.8.4.3 Balance of Energies . . . 130
C.8.5 Second Law of Thermodynamics . . . 132
C.9 Voigt notation . . . 133
C.10 Double Scalar Product . . . 133

APPENDIX D – NEO-HOOKEAN MATERIAL 135

APPENDIX E – ALGEBRAIC MANIPULATIONS 136
E.1 Alternative Definition for Caputo Fractional Derivative . . . 136
E.2 Properties for $\mathscr{N}$ . . . 136
E.2.1 On the Obtaining of $\dot{\psi}_m$ . . . 137
E.2.2 Example of $\mathscr{N}$ . . . 138
E.3 On the Obtaining of $\boldsymbol{S}^A$ . . . 139
E.4 On the Obtaining of $\partial_{\boldsymbol{E}^B}\boldsymbol{S}^B$ . . . 140
E.5 On the Obtaining of $\partial_{\boldsymbol{E}^A}\boldsymbol{C}$ and $\partial_{\boldsymbol{E}^A}\boldsymbol{S}^B$ . . . 142
E.6 Simplifications in the Linearization of the Motion Equation . . . 142

Introduction

Modern technology has led to the increased use of viscoelastic materials in several branches of engineering applications as a lighter and cheaper substitute for metals. Nowadays, viscoelastic components are found in a wide range of situations, ranging from the simplest items of daily use to more complex items used in industrial, structural, or biological applications. However, it is widely known that an item made of these materials must meet different mechanical demands according to its conditions of use; thus, a poor design that does not carefully consider those conditions may lead to the item's failure during the operation. Material damage prediction may be the most relevant request in structural applications when designing them.

The damage process for viscoelastic materials generates patterns that are difficult to describe in mathematical terms; this situation explains why most of the classical theories for damage modeling are usually based on the behavior of metals. Furthermore, viscoelastic materials are often used in applications involving large or fast deformations in which the behavior is essentially non-linear - a point that makes the problem still more challenging. This subject attracted the interest of many researchers over the recent years, making modeling damage in viscoelastic materials a trending research topic.

A Brief Account of Previous Viscoelastic Damage Models

The first contributions to damage modeling in viscoelastic material were empiric theories based on the establishment of a critical strain that took place in the 1960s (KNAUSS, 1963; WILLIAMS, 1964; SCHAPERY, 1964). Since then, the proposed models' scientific quality has progressed with works combining theoretical and computational aspects.

Classical damage models assume that sharp interfaces split damaged and undamaged parts of the material. This assumption brings theoretical difficulties: one must have the equations governing the interfaces' evolution and *ad hoc* criteria for the branching and merging the cracking interfaces. Moreover, the sharp interface assumption also brings numerical implementation issues since it demands a complex front-tracking process to follow nontrivial crack propagation. Alternatively to this approach, models based on the phase-field methodology have emerged as an attractive choice to carry out with material damage once they provide a continuum description of state changes. This feature has inspired several proposals on damage phase-field models in the last years (MIEHE et al., 2015; AMENDOLA; FABRIZIO; GOLDEN, 2016; BOLDRINI et al., 2016; HAVEROTH et al., 2020).

Shortcomings of Previous Viscoelastic Damage Models

Despite significant progress in damage modeling for viscoelastic materials, most of the previous viscoelastic damage models describe the damage process based on non-continuous models are restricted to small strain regime. They cannot account simultaneously for the crack nucleation, loading-unloading processes modeling, non-linear viscoelasticity, or thermal influence. Models dealing with non-linear viscoelasticity generally adopt parallel rheological arrangements, which have a simple mathematical development and do not present the flexibility of modeling given by series models.

An essential aspect of being considered is the unclear thermodynamical development of several previous formulations; thermodynamic consistency is a crucial point to be guaranteed since it ensures the physical reliability of the model.

Another issue is how the model includes elastic degradation. In phase-field damage models, this is usually obtained using suitable degradation functions (KUHN; SCHLÜTER; MÜLLER, 2015); this procedure, besides ensuring the elastic degradation, also implies that the driving force related to the elastic effect influences the damage growth. The choice of this degradation function is crucial to obtain a fair model. Costa-Haveroth et al. (2022) propose a novel degradation function to handle damage in viscoelastic materials, which we use in this thesis.

Proposal of the Present Work

Motivated by the abovementioned criticisms, we propose a general damage phase-field framework based on continuum mechanical principles. This model can be used to describe non-linear viscoelasticity and damage by using phase-field variables and fractional derivatives. It is constructed as an extension of our previous work (COSTA-HAVEROTH et al., 2022) and represents rheological arrangement in series which can be particularized to describe several different viscoelastic models. Furthermore, it allows the consideration of finite strain and non-isothermal aspects.

We adopt a scalar variable to describe a diffuse crack transition. It is derived from thermodynamic considerations and is governed by a Partial Differential Equation (PDE). It results in a natural crack nucleation, unlike the discrete fracture models. Additionally, the coupling with fractional viscoelasticity allows using fewer material parameters than models obtained by the classical viscoelastic description for the called power-law materials.

Objectives

The main objectives of this thesis are:

1. Use a damage phase-field methodology to develop a thermodynamically consistent model based on continuum thermo-mechanical principles, able to account for finite strain and non-isothermal effects;
2. Include non-linear viscoelastic behavior in a series model which can be particularized to represent several viscoelastic models;
3. Couple fractional derivatives to the model and establish an appropriate description of the viscoelastic behavior;
4. Propose a suitable and workable numerical approach for the approximation of the model;
5. Develop and implement algorithms based on the previous concepts in MATLAB language and the $(hp)^2$FEM[1] program written in C++ language;
6. Evaluate numerical results and compare them with those obtained by analogous studies and experimental data.

Outline of this thesis

Chapter 1 presents a review concerning mathematical and historical aspects, which underlies the theme of this work. We present the phase-field concept and explain how it has been used to construct damage models. Then, we delineate how traditional and fractional viscoelasticity are commonly used. At the end of this first chapter, we briefly discuss the coupling of phase field theory and fractional derivatives to model failure in viscoelastic materials.

Chapter 2 develops a general damage phase-field model according to a new free-energy potential, based on that proposed by Costa-Haveroth et al. (2022), which includes memory material effects. This model is derived in Eulerian and Lagrangian coordinates using continuum mechanics and thermodynamic principles. Under specific hypotheses, the model derived in this chapter can be associated with a rheological combination of elements in series and is considered a generalization of the model proposed by Costa-Haveroth et al. (2022).

[1] The architecture of the program $(hp)^2$FEM allows flexibility and generalization for implementing high-order finite element methods. It has been implemented using the object-oriented paradigm with the C++ language (see <http://www.fem.unicamp.br/~hp2fem> for details.)

Chapter 3 specializes the general framework for specific viscoelastic materials by choosing a proper free-energy potential and pseudo-potential of dissipation. Particularly, the proposed viscoelastic free-energy potential results in a stress/strain constitutive equation in terms of a fractional order derivative. In the chapter's final, we show that several sub-models, including that presented in Costa-Haveroth et al. (2022), can be obtained from our general fractional viscoelastic damage model using a specific simplification hypothesis.

The method proposed in this work leads to a system of non-linear partial differential equations to describe the evolution of motion, damage, and temperature in viscoelastic materials subject to stress. Chapter 4 describes how the non-linear system is discretized using a staggered scheme for time (semi-implicit/explicit strategy) and the finite element method (FEM) for the spatial domain. We also discuss how the numerical treatment can be simplified to account for sub-models.

Chapter 5 presents a set of one and two-dimensional numerical simulations. These results are divided into two parts: tests with a simplified parallel model, as an extension of those previously published by Costa-Haveroth et al. (2022), and novelty results for a more general series model. Finally, we address the conclusions, remarks, and observations established from the development of this thesis. We also include ideas for future works on this theme.

Final Remark

During the elaboration of this thesis, the author published or presented the following works which have some relation with this thesis:

1. Presentation in the International Symposium on Solid Mechanics - MECSOL - USP(2019)

   Title: Modeling of damage, fracture and fatigue in viscoelastic materials with phase field and fractional derivatives.

   Authors: Costa-Haveroth, T. C.; Bittencourt, M.L.; Boldrini, J.L.

2. Poster presentation in the Workshop of Numerical Analysis and Applications - WANA - IMECC/UNICAMP (2019)

   Title: Phase field and fractional derivatives to model damage, fracture and fatigue in viscoelastic materials.

   Authors: Costa-Haveroth, T. C.; Bittencourt, M.L.; Boldrini, J.L.

3. Presentation in the Workshop of Challenges on numerical simulation for PDE - LabMeC-FEC/UNICAMP(2020)

Title: A phase field model with fractional derivatives for damage in viscoelastic materials.

Authors: Costa-Haveroth, T. C.; Bittencourt, M.L.; Boldrini, J.L.

4. Article published in the Journal Mechanics of Advanced Materials and Structures - Taylor & Francis (2021)

   Title: Aspects on viscoelasticity modeling of HDPE using fractional derivatives: interpolation procedures and efficient numerical scheme.

   Authors: Costa-Haveroth, T. C.; Haveroth, G. A.; Kühl, A.; Boldrini, J.L.; Bittencourt, M.L.; Sasse, F.D.; Polak, M.A.; Muñoz-Rojas, P.A.

5. Article published in the Journal Computational Mechanics - Springer (2022)

   Title: A damage phase-field model for fractional viscoelastic materials in finite strain.

   Authors: Costa-Haveroth, T. C.; Haveroth, G. A.; Bittencourt, M. L.; Boldrini, J. L.

1 Historical and Mathematical Overview

This chapter presents the material background of this work. We start with a brief description of the mathematical and historical aspects which underlie the phase-field models, including a literature review and some of their applications. Next, we explain what is understood by viscoelastic material behavior and the traditional method used to describe this phenomenon. The fractional viscoelastic modeling is also presented by considering the Caputo fractional derivative. Ultimately, these concepts are merged by coupling phase-field theory and fractional derivatives to model failure in viscoelastic materials.

1.1 Background on Phase-fields Models

Phase-field models have been increasingly used as an efficient mathematical tool to describe interface evolution in several state change problems. Differently from non-continuous methods, which adopt instant-sharp interfaces between states, phase-field models introduce a diffuse transition between states (see Fig. 1.1) (STEINBACH, 2009). This feature agrees with practical observations of several state change phenomena, which present transition layers where some physical property changes continuously, although sometimes in a very steep gradient, along each layer width; examples of this situation are melting, solidification, fluid separation, and damage.

Figure 1.1 – Representation of the state changing. Sharp interface (left) and continuum transition by a phase-field variable (right).

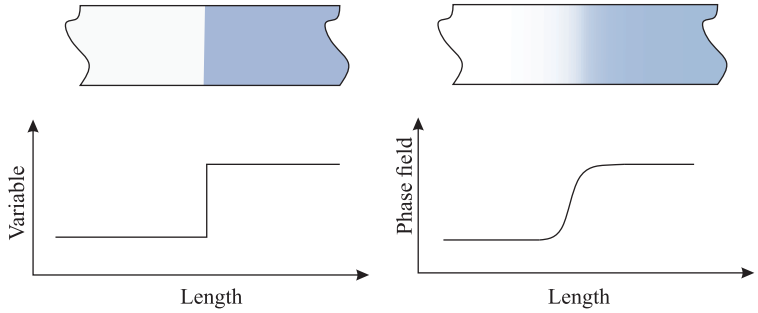

Adapted from Moelans, Blanpain and Wollants (2008).

A rather general mathematical description of phase-field models is illustrated by considering the following situation. Suppose that a physical process involving state changes occurs in evolving regular domains (open, bounded, and connected) $\Omega_t \in \mathbb{R}^3$ over a time interval $[0, t_f]$. Phase-field models associate those states to the values of a certain variable $\varphi(\boldsymbol{x}, t)$ defined for $\boldsymbol{x} \in \Omega_t$ and $t \in [0, t_f]$, which may be related to some material property that varies between different phases. For instance, being $w_1 < w_2$ real

numbers, values of $\varphi \leq w_1$ may correspond to a certain material state **I**, whereas values of $\varphi \geq w_2$ may correspond to another material state **II**. Then, at each time $t \in [0, t_f]$, $\Omega_{w_1}(t) = \{\boldsymbol{x} \in \Omega_t : \varphi(\boldsymbol{x}, t) \leq w_1\}$ is the subset of Ω_t where the material is at state **I**; $\Omega_{w_2}(t) = \{\boldsymbol{x} \in \Omega_t : \varphi(\boldsymbol{x}, t) \geq w_2\}$ is the subset of Ω_t where the material is at state **II**, and $\Omega_{w_1,w_2}(t) = \{\boldsymbol{x} \in \Omega_t : w_1 < \varphi(\boldsymbol{x}, t) < w_2\}$ is the subset associated to the transition layers. Variables of this sort are the phase-field variables (also called order parameters) and are additional unknowns in the corresponding mathematical problem.

This methodology substitutes the required evolution equations for the surfaces used in the sharp interface models, which are rather hard to justify and solve in complex cases, by Partial Differential Equations (PDEs) for the phase fields. These PDEs can be obtained as the usual physical state variable using thermodynamic arguments, as we will show later in this thesis.

1.1.1 Historical Development of Phase-Field Models

The idea of diffusive models started with the work of van der Waals (1979) that presented a model for a liquid-gas phase change problem. This author presented a density function that continuously varies at the interface and considers thermodynamic arguments to conclude that the diffuse state transition overcomes discontinuities in the model, being more reasonable than the assumption of a sharp interface. Landau and Ginzburg (1950) expanded this concept by introducing order parameters (phase fields) evolving according to a non-conservative equation, which followed the condition that the rate of change of these order parameters was directly proportional to the corresponding free-energy functional derivative.

These studies were followed by the contributions of Cahn and Hilliard (CAHN; HILLIARD, 1958; CAHN, 1959), which presented the fourth-order nonlinear Cahn-Hilliard equation for an order parameter to describe fluid separation. In these works, the evolution of the order parameter follows from the mass conservation equation. In contrast, Allen and Cahn (1972) developed the second-order Allen-Cahn equation to describe the phase changing in iron alloys. Both Allen-Cahn and Cahn-Hilliard equations are based on the Ginzburg-Landau free-energy functional (HOHENBERG; KREKHOV, 2015); however, while the Cahn-Hilliard equation is conservative, the original Allen-Cahn equation is non-conservative (CHIARELLI et al., 2017).

Studies about phase-field modeling fall into three main categories. The first uses the diffusion approach, which includes *ad-hoc* additional variables to the problem to generate an appropriate diffuse interface. The second contemplates the works based on the energetic variational concept using the ideas developed by Allen, Cahn, and Hilliard. The third one, called the entropy approach, adopts physical principles as the second law of thermodynamics to generate the proper evolution equation for the phase fields. A detailed

discussion of the differences among these approaches can be found in Haveroth (2020).

The phase-field methodology has found applications in many different scientific areas as, for example, in the solidification (KARMA; RAPPEL, 1996), crystal growth and recrystallization (III; CHEN, 2002), domain microstructure evolutions in ferroelectric materials and dislocation dynamics (WANG et al., 2001; WANG et al., 2004). The prominent acceptance of this theory is due to the advantages from both mathematical and application point-of-view. It is physically motivated, with thermodynamical consistency ensured through rigorous mathematical developments (PENROSE; FIFE, 1990; WANG et al., 1993; BOLDRINI et al., 2016; BOLLADA; JIMACK; MULLIS, 2017). Furthermore, it explicitly allows considering complicated morphological evolution once it is not necessary to know the moving interface (CHOUDHURY, 2017). Moreover, it is relatively easy, at least in theory, to include a variety of physical effects such as plasticity (HAVEROTH et al., 2020), isotropic porous media (ZHOU; ZHUANG, 2020), and anisotropy (MCFADDEN et al., 1993).

In this work, we are particularly interested in the phase-field methodology to model material failure in mechanical components. The following section presents some details in this regard.

1.1.2 Damage Phase-Field Models

Predicting structural failure due to crack nucleation and subsequent propagation is mandatory in several areas and has been the subject of many works during the last century. Classical methodologies approximate the crack by a sharp and discontinuous interface which can lead to challenging numerical problems. In this scenario, phase-field models have gained prominence due to their ability to describe damage processes continuously, creating advantageous features in both theoretical and computational aspects.

The damage phase-field models are diffusive crack methods based on the thermodynamic framework introduced at the beginning of the 20th century by Griffith (1921). Bourdin, Francfort and Marigo (2000) developed the first study on this subject by presenting a scalar phase-field variable to indicate the quasi-static brittle fracture. At the same time, Aranson, Kalatsky and Vinokur (2000) considered damage by coupling dynamic equations and a non-conservative Allen-Cahn-type equation. These works were the basis for most later extensions and improvements.

Miehe and co-workers (MIEHE; HOFACKER; WELSCHINGER, 2010a; MIEHE; WELSCHINGER; HOFACKER, 2010a) presented a damage phase-field model for brittle fracture. In particular, their formulations ensure local irreversibility of the phase-field by preventing the healing of the material. They also contributed to the numerical aspects using a staggered methodology to solve the governing equations. Borden presented a differential

equation for a fourth-order phase-field model (BORDEN, 2012; BORDEN et al., 2014) and Schillinger, Borden and Stolarski (2015) proposed improvements in the crack resolution and the computation time. Duda et al. (2015) proposed a phase-field/gradient-based damage model for brittle fractures in elastic-plastic solids. Ambati, Gerasimov and Lorenzis (2015) presented a formulation that uses the phase-field model for quasi-static fracture and can describe isotropic and anisotropic behaviors. Further developments on damage phase-field models concerning physical aspects were given by Karma, Kessler and Levine (2001), Hakim and Karma (2005), and Hakim and Karma (2009). They used the phase-field variable to model the pattern of the interface evolution to predict the crack for brittle materials. Miehe et al. (2015) defined a generalization of their previous phase-field model by considering finite strains, plasticity, and temperature effects to account for ductile fracture. Amendola, Fabrizio and Golden (2016) also presented similar models, including fatigue description and isothermal cases.

Although several models in the previously cited works are described as thermodynamically consistent, no clear mathematical arguments prove those claims. Boldrini et al. (2016) showed a significant advance in this aspect, presenting a general thermodynamically consistent phase-field model for damage and fatigue, where the behavior of distinct material classes is the consequence of the free-energy and pseudo-potentials of dissipation chosen. Haveroth et al. (2020) coupled plasticity in Boldrini's model and compared simulations with laboratory results. Haveroth (2020) also considered the finite strain in addiction to plasticity.

The studies were done over the last years, and the numerous applications of phase-field methodology to predict mechanical failure, lead to a relatively consolidated framework. Despite that, it is still possible to explore several aspects regarding specific classes of materials. In this context, the following section discusses the modeling of viscoelasticity materials, whose behavior is challenging to account for when subject to damage.

1.2 Background on Viscoelasticity

There are different classes of viscoelastic materials with particular properties and applications. Polymers are a classic example of viscoelastic materials, which allow large-scale applications due to their easy manufacturability and low cost.

Viscoelastic materials present a continuum transition between elastic and viscous states and exhibit a time-dependent stress/strain constitutive relation. If the stress is linearly related to the strain rate, the material is said linear viscoelastic (Newtonian); Otherwise, it is said non-linear viscoelastic (non-Newtonian) (MEYERS; CHAWLA, 2008). Although linear modeling is widely used in academia, most of industrial applications

generally require large or fast deformations in which the behavior is non-linear.

One of the main aspects that must be considered for viscoelastic materials is the non-local time dependence of their strain-stress relations; it is called memory property and must be considered in the modeling process to ensure the accurate description of the material behavior (COLEMAN, 1976).

1.2.1 Traditional Viscoelastic Modeling

In the one-dimensional small strain context, the modeling of viscoelastic materials can be performed using mechanical analogies based on the dualism of viscoelasticity. Generally, Hookean springs represent the elastic part (see Fig. 1.2a). The constitutive equation that relates the stress and strain measurements for this element is the traditional Hooke law, written as

$$S(t) = E_Y \mathrm{D}^0 E(t) \quad \Longleftrightarrow \quad S = E_Y E, \tag{1.1}$$

where S is the stress, E is the strain (in this case, the infinitesimal strain measure), E_Y is the usual spring stiffness constant (sometimes associated with the Young's modulus), and $\mathrm{D}^0(\cdot)$ denotes the derivative of zero-order, i.e., the function itself. On the other hand, the dashpot component represents the viscous part (see Fig. 1.2b). The corresponding stress/strain relation for this component is given by

$$S(t) = \eta_v \mathrm{D}^1 E(t) \quad \Longleftrightarrow \quad S = \eta_v \mathrm{D} E, \tag{1.2}$$

where η_v is the viscous constant and $\mathrm{D}^1(\cdot) = \mathrm{D}(\cdot)$ denotes the usual first derivative.

Figure 1.2 – Rheological Elements.

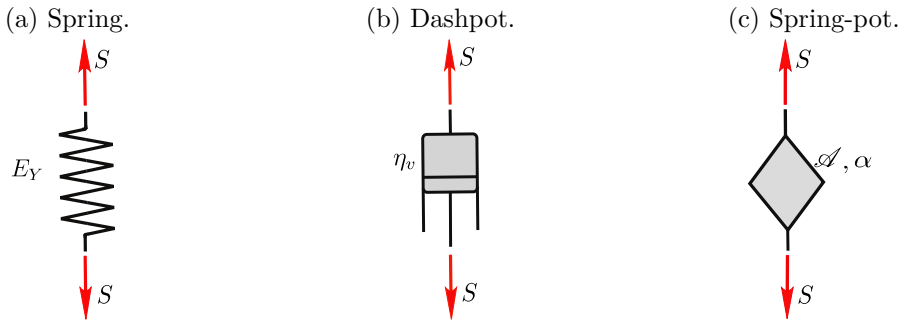

Adapted from Costa-Haveroth (2015).

The development of many traditional viscoelastic mechanical models is based on the arrangement of springs and dashpots, either in series or parallel (see Fig. 1.3). For these models, the corresponding stress/strain relations are defined mathematically by differential equations that can be solved to predict or fit different material.

The stress/strains relations for these models involve exponential functions; then, the materials that can be described by them are called *power-law* behaved (BAGLEY,

1989; BONFANTI et al., 2020). For power-law viscoelastic materials the internal microstructure response is associated with a wide distribution of time-scales. For this reason, they can be described by these traditional models once the exponential terms can associated with different time-scales (FINDLEY; DAVIS, 2013). Under additional conditions, the springs/dashpots models can also be generalized to account for finite strain and multidimensional cases (see Section 1.2.3).

Figure 1.3 – Examples of rheological models in series and parallel.

(a) Generalized Kelvin model.

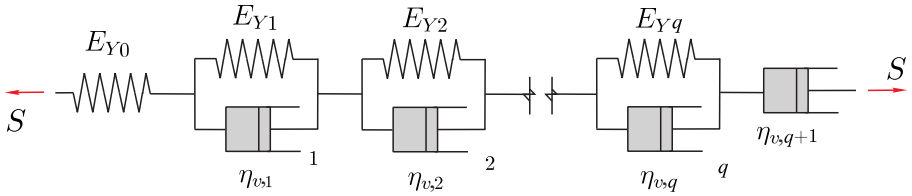

(b) Generalized Maxwell model.

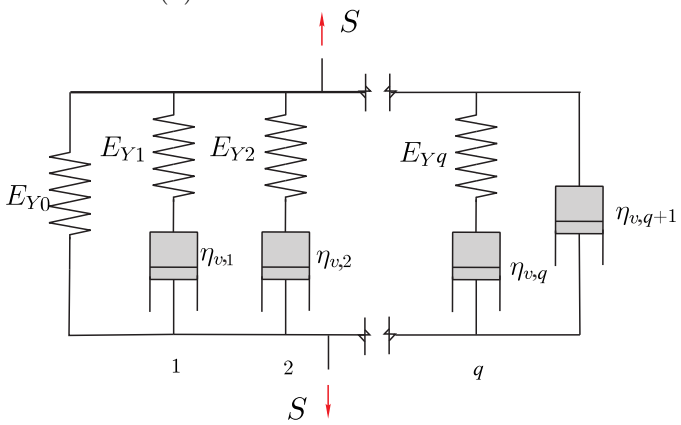

Adapted from Costa-Haveroth (2015).

Despite the simple derivation associated with these models, the number of components necessary to accurately describe a power-law behaved material can be too large. It leads to difficulties for the associated inverse identification problem since each component has a parameter to be adjusted. The following section presents an alternative concept based on the fractional derivative that can overcome this issue.

1.2.2 Fractional Viscoelasticity Modeling

Fractional derivatives have been used as a promising tool to accurately describe the rheological behavior of viscoelastic materials that present power-law behavior, giving rise to the so-called fractional viscoelastic models. They typically demand fewer rheological elements for the stress/strain constitutive relation compared to the traditional models (WELCH; RORRE; DUREN, 1999), reducing the burden of identifying material parameters in inverse problems.

The usual procedure to convert the traditional one-dimensional models into fractional ones is to include another rheological element to draw up a continuum transition between the viscous and elastic states. This particular element is named spring-pot (or Scoot-Blair element) (KOELLER, 1984) (see Fig. 1.2c), and its constitutive stress/strain relation is given by

$$S(t) = \mathscr{A}\, {}_{t_1}\mathrm{D}_t^{\alpha} E(t), \tag{1.3}$$

where $\mathscr{A}$ is a weigh for the fractional derivative (usually as a scalar constant), $\alpha \in [0, 1]$ is the fractional derivative order, and ${}_{t_1}\mathrm{D}_t^{\alpha}(\cdot)$ denotes the fractional derivative operator, over α, in the time interval $[t_1, t]$. Note that if $\alpha = 0$, Eq. (1.3) describes the spring behavior and $\mathscr{A}$ becomes the elastic constant, as shown in Eq. (1.1). On the opposite, if $\alpha = 1$, Eq. (1.3) defines the constitutive equation for the dashpot component, and $\mathscr{A}$ becomes the viscous constant, as we can see in Eq. (1.2). When α comprises values between 0 and 1, the spring-pot represents a rheologic element that behaves partially as a spring and partly as a dashpot. Bonfanti et al. (2020) shows a detailed discussion on the physical and mathematical interpretations for the spring-pot as a representative element to model viscoelastic power-law materials.

These mechanical analogies correspond to the one-dimensional case; however, they can be generalized for the three-dimensional case by using suitable correlated tensors (for details, see Section 3.1.1).

Remark 1.1. *The usual derivative is local because the derivative value at a point depends only on the function values in a small neighborhood around that point. Fractional derivatives are not local; the subscripts that appear quite frequently in the fractional derivative notation,* ${}_{t_1}\mathrm{D}_t(\cdot)$*, are related to this feature; the definition depends on the time domain of the functions under evaluation. If the domain of derivation changes, then the derivative in a specific point also changes. In other words, the derivative computed in a specific time depends on the past values of the function (for more details, see Zhang, Benson and Reeves (2009)). Such non-locality feature makes the fractional derivatives a matching tool for time-dependent problems. In the case of viscoelasticity modeling, the non-local feature is associated with the memory effects.*

1.2.2.1 Historical Overview on Fractional Viscoelasticity

Fractional derivatives were first mentioned in 1695 when Leibniz established the usual notation to represent the derivative, $\frac{\mathrm{d}^w}{\mathrm{d}t^w}(\cdot)$, where t is the independent variable of some function and w is a natural number (LOVERRO, 2004). Some conversations between L'Hopital and Leibniz were concerned with the characterization of this derivative if the index w was not a positive integer number. Such discussion gave rise to the idea of fractional derivatives (NISHIMOTO, 1991).

Throughout the 18th and 19th centuries, famous mathematicians such as Euler, Lagrange, Riemann, Liouville, and Heaviside, among others, dispended some time on this subject (SAMKO; KILBAS; MARICHEV, 1987). However, the relation between fractional derivatives and viscoelasticity outsets only in the 1930s with the works of Gemant and Scott-Blair (GEMANT, 1936; SCOTT-BLAIR, 1944). These pioneers presented fractional differential operators to describe the relaxation process in viscoelastic fluids. After, Caputo and Mainardi presented progress both in the theoretical and practical viewpoints (CAPUTO, 1966; CAPUTO, 1967; CAPUTO; MAINARDI, 1971a; CAPUTO; MAINARDI, 1971b). Their contributions range from proposing new definitions for the fractional derivative to applying fractional models to fit experimental creep curves (CAPUTO; MAINARDI, 1971a).

Bagley and Torvik (1983) proposed a significant advance concerning the basis of fractional derivative modeling. These authors compared the molecular theory of viscoelasticity with the fractional constitutive relations and showed their equivalence. Koeller (1984) showed that the fractional viscoelastic models could be obtained as a generalization of the traditional models. Lion (1997) addressed the fractional Zener model from a thermodynamics point-of-view. Remaining in thermodynamics, Fabrizio (2014) proposed a free-energy that leads to a fractional stress/strain equation. This author also compared his fractional models with the classic theories. Alfano and Musto (2017) change the fractional model developed by Musto and Alfano (2015) and derive a linear viscoelastic model coupled with damage. Zhang et al. (2020) contributed to numerical aspects with a novel method for the finite element approach applied for non-linear fractional viscoelastic materials by using the Caputo's derivative.

Due to their natural ability to model time-dependent phenomena, the most extensive application for fractional derivatives is the viscoelasticity description. (CAPUTO; FABRIZIO, 2016; LAZOPOULOS; KARAOULANIS; LAZOPOULOS, 2016; BALEANU; FERNANDEZ, 2018). Furthermore, comparisons between the traditional and fractional viscoelastic models have been proposed by many authors, showing that the latter can be more advantageous for curve fitting for power law materials (JIA; SHEN; HUA, 2007; FERRANTE; CAPPONI, 2017; COSTA-HAVEROTH, 2015).

1.2.2.2 Caputo Fractional Derivative

For the reader unfamiliar with non-integer derivatives, it is essential to clarify that there are several definitions for fractional derivatives, written in many ways, which are not necessarily equivalent (OLIVEIRA; MACHADO, 2014). These concepts are mostly adaptations of the Riemann-Liouville, Grünwald-Letnikov, or Caputo definitions, the commonly accepted ones. The application at hand usually affects the suitability of the definition to be used.

We adopt the Caputo fractional derivative (CAPUTO, 1966) in this work. It is defined for a function $f(t) \in C[t_1, t_2]$ according to

$$ {}_{t_1}\mathrm{D}_t^{\alpha} f(t) = \frac{1}{\Gamma(1-\alpha)} \int_{t_1}^{t} \frac{\frac{\mathrm{d}^{\lceil \alpha \rceil} f(\tau)}{\mathrm{d}\tau^{\lceil \alpha \rceil}}}{(t-\tau)} \mathrm{d}\tau, $$

where $t_1 < t < t_2$, $\lceil \alpha \rceil$ is the ceiling function of $\alpha \in \mathbb{R}$, and $\Gamma(\cdot)$ is the traditional Gamma function given by

$$ \Gamma(w) = \int_0^{\infty} \exp(-\tau) \tau^{w-1} \mathrm{d}\tau, $$

with $w \in \mathbb{R}$.

When $\alpha \in [0, 1]$, then the following definition is obtained:

$$ {}_{t_1}\mathrm{D}_t^{\alpha} f(t) = \frac{1}{\Gamma(1-\alpha)} \int_{t_1}^{t} \frac{\frac{\mathrm{d}f(\tau)}{\mathrm{d}\tau}}{(t-\tau)} \mathrm{d}\tau. \tag{1.4} $$

According to the manipulations given in Appendix E.1, Eq. (1.4) can be rewritten as

$$ {}_{a}\mathrm{D}_t^{\alpha} f(t) = \frac{1}{\Gamma(1-\alpha)} \frac{f(t) - f(t_1)}{(t-t_1)^{\alpha}} + \alpha \int_{t_1}^{t} \frac{f(t) - f(\tau)}{(t-\tau)^{\alpha+1}} \, \mathrm{d}\tau. \tag{1.5} $$

Equation (1.5) has a central role in the viscoelastic pseudo-potential of dissipation definition, as will be seen later in this work.

From the application viewpoint, there are some advantages of using Caputo's definition. For instance, it provides an interpolation between integer-order derivatives; when α tends to $n \in \mathbb{N}$, we recover the traditional integer-order derivative (PODLUBNY, 1999). It agrees with the physical interpretation of the spring-pot element being suitable to describe viscoelasticity. Additionally, for this operator, the derivative of a constant is zero.

1.2.3 Parallel versus Series Models

Significant differences exist between rheological element arrangements in series and parallel for both traditional and fractional viscoelastic models. To illustrate this difference, consider Fig. 1.4, where A and B represent rheological elements in blocks (or sets). Figure 1.4a shows the arrangement of rheological blocks in parallel, where the total strain in this system equals each rheological block strain. Conversely, if we consider the arrangement of rheological blocks in series, as shown in Fig. 1.4b, the total strain is the sum of the strain in each rheological block. Examples of specific choices for the sets A and B can be seen in Fig. 1.3.

These rheological models can be extended to the finite strain regime by including additional mathematical considerations and replacing linear Hookean springs with non-linear ones. This procedure is simple for parallel models (once the total strain is equal

Figure 1.4 – General parallel and series models.

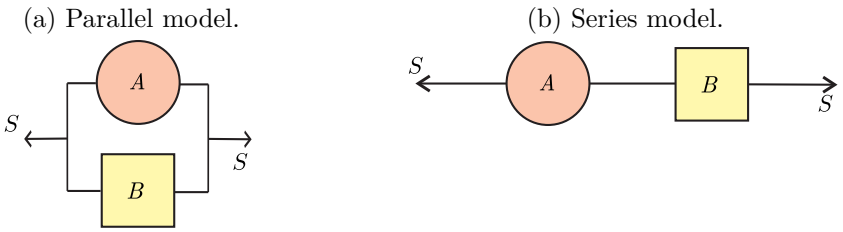

to the strain of each block) and implies a significant simplification in the mathematical development, justifying its wide use in the literature (HAUPT; LION, 2002; SILBERSTEIN; BOYCE, 2010; LIU; FATT, 2011; SHIM; MOHR, 2011). However, it is limited for applications for particular classes of materials.

On the other hand, for series models, the finite strain regime can no longer be described by the additive decomposition of the strains. In this case, the multiplicative decomposition of the deformation gradients generates a challenging task (see Sec. 2.1).

Several authors have previously used the multiplicative decomposition for the deformation gradient for viscoelasticity (see Reese and Govindjee (1998) for a review). However, they do not discuss these decompositions' geometrical or physical meaning. Some clarification about these aspects was given by Ihlemann (2014), who presented a general method for deriving models of multiplicative inelasticity and related them with rheological connections generating the balance of the stresses. Bröcker and Matzenmiller (2014) presented a similar approach; however, differently from Ihlemann's study, they presupposed the balance of the stresses and obtained the decomposition of the stress power as a result.

Despite the advances and improvements achieved by the previously cited studies in the task of modeling viscoelasticity in the finite strain regime, they did not include influences of temperature variance or damage effects.

1.2.4 Modeling of Failure in Viscoelastic Materials

Damage due to load for viscoelastic components generates particular patterns that are difficult to model. If we consider, for instance, the standard case of polymers, the damage process can be broadly summarized by two steps: slippage and chain separation (DANIELS, 1989).

Generally, viscoelastic materials comprise long molecular chains (ANDERSON, 1994). Under tensile stress, the slippage of chains decreases the stiffness, and the localized stress level grows; if the stress on the chain is higher than the bond strength can hold, chain separation arises, resulting in initiation and subsequent coalescence of voids. This process may evolve until fracture (DANIELS, 1989; ANDERSON, 1994; KUKSENKO;

TAMUSZ, 2013). Furthermore, viscoelastic materials are subject to local failure, even at minimal strain levels (CHRISTENSEN, 2012). Then, the slippage is a critical and crucial part of the process and cannot be neglected; it leads to local instabilities which govern the damage evolution. Moreover, the industrial manufacture of viscoelastic materials frequently involves large or fast deformations where the non-linear behavior predominates.

The first contributions on damage modeling for viscoelastic materials date back to the mid-1960s, with the studies of Knauss (KNAUSS, 1963; KNAUSS, 1966; KNAUSS, 1969; WNUK; KNAUSS, 1970), Williams (WILLIAMS, 1964; WILLIAMS, 1965) and Schapery (SCHAPERY, 1964). These works established the crack description empirically by prescribing a critical strain. Nowadays, models progressed, generating works combining advances in mathematical and computational aspects.

Some of the classical models for damage adopt the cohesive zone method (TIJSSENS; GIESSEN; SLUYS, 2000a; TIJSSENS; GIESSEN; SLUYS, 2000b), which, although widely used, presents some shortcomings associated with the description of a sharp interface. Other contributions couple traditional methods for viscoelasticity with statistical approaches to describe failure (SCHAPERY, 1999; SUVOROVA; OHLSON; ALEXEEVA, 2003; VERNEREY et al., 2018). Models based on X-FEM (MOËS; DOLBOW; BELYTSCHKO, 1999) and peridynamics (MADENCI; OTERKUS, 2017) are also used. However, these approaches require extensive reformulation for computational implementation or present issues to account for non-linear viscoelasticity (THAMBURAJA et al., 2019). Then, the continuum approaches arise as an attractive alternative to deal with these problems (NGUYEN et al., 2016; THAMBURAJA et al., 2019).

In particular, the application of phase-fields to model the damage in viscoelastic materials was studied by Schänzel (2015) and Shen, Waisman and Guo (2019). These authors had effective results for material response prediction when subject to load, although the unclear thermodynamic development of the models. Nonetheless, they used classic rheological combinations of dashpots and springs to characterize viscoelasticity, resulting in several material parameters to be identified.

The coupling of fractional viscoelasticity and damage models is very recent in the literature. Krasnobrizha et al. (2016) used a viscoelastoplastic damage model with fractional derivatives that separate the dissipation for each considered effect: material damage, plasticity, and viscoelasticity. Alfano and Musto (2017) re-elaborated the fractional model proposed previously by Musto and Alfano (2015) and addressed thermodynamic considerations resulting in a linear viscoelastic damage model. Tang et al. (2018) presented a fractional viscoplastic continuum damage model to describe creeping in rocks. Good fitting with laboratory data was obtained in this work. Caputo and Fabrizio (2015) used the order of the fractional derivative as a phase-field variable to describe the damage in viscoelastic materials; however, the thermodynamical consistency of this framework is also

unclear. Recently, in Costa-Haveroth et al. (2022), we presented a thermodynamically consistent damage phase-field model for viscoelastic materials. In this previous correlated work, we also proposed a new free-energy potential to consider materials with memory.

The previous discussion shows that many authors have driven further development on modeling failure in viscoelastic materials; however, the research still needs to be explored in some points. Many constitutive models are limited to the parallel combination of rheological blocks. They do not consider simultaneously the crack nucleation, modeling of loading-unloading processes, non-linear viscoelasticity, or even thermal influence. Additionally, excepting the works of Tijssens, Giessen and Sluys (2000a), Tijssens, Giessen and Sluys (2000b), Schänzel (2015), Thamburaja et al. (2019) and Costa-Haveroth et al. (2022) the proposed models are restricted to small strain. The next Chapter intends to deepen these questions by presenting an extension of the model proposed in Costa-Haveroth et al. (2022).

2 General Damage Phase-Field Model

This chapter presents the mathematical development of a general damage phase-field model based on mechanical aspects of the continuum. For the reader who is not familiar with continuum mechanics, we strongly to read Appendix C, which gives a brief review on this theme (for theory details, see the textbooks by Gurtin (1982) and Oden (2012)).

2.1 Incremental Strain and Rheological Connections in Series

Let consider a body $\mathcal{B}_t$ subject to deformations that, at time t, occupies a space defined by a regular domain (open, bounded, connected) $\Omega_t \subset \mathbb{R}^3$ with boundary Γ_t divided into two disjoint parts: Γ_D, $|\Gamma_D| > 0$, and Γ_N, where the body is subject to Dirichlet and Neumann conditions, respectively. The reference configuration $\mathcal{B}_0$ is described by the Lagrangian (material) points $\boldsymbol{p} \in \Omega_0$ whereas the current configuration $\mathcal{B}$ $(= \mathcal{B}_t)$ is given by the Eulerian (spatial) points $\boldsymbol{x} \in \Omega$ $(= \Omega_t)$. The current configuration can be obtained by a smooth vector mapping of $\boldsymbol{p}$, also called body motion, or, as usual, by adopting its linearization represented by the total deformation gradient (see details in Appendix C.3):

$$\boldsymbol{F} = \boldsymbol{I} + \nabla_{\boldsymbol{p}} \boldsymbol{u}\,(\boldsymbol{p}, t)\,,$$

where $\boldsymbol{I}$ is the identity tensor and $\nabla_{\boldsymbol{p}}\boldsymbol{u}$ is the gradient of the displacement field $\boldsymbol{u}$. The tensor $\boldsymbol{F}$ is called a two-point tensor, because it is used to map quantities between material and spatial configurations.

When taking the problem incrementally, that is, including intermediate states between $\mathcal{B}_0$ and $\mathcal{B}$, it is possible to verify that the strain tensors can generally not be obtained by adding incremental strains due to the successive motions in the finite strain setting (CHAVES, 2013). Figure 2.1 illustrates this fact, where we consider the body $\mathcal{B}_0$ subject to deformations in two steps. The application of the partial deformation gradient $\boldsymbol{F}^A$ takes the body in Ω_0 and leads to the intermediate configuration $\hat{\Omega}$, while the application of the partial deformation gradient $\boldsymbol{F}^B$ sends the body in $\hat{\Omega}$ to the current configuration Ω. Then, we straighfoward see that the total deformation gradient can be written as a composition of the partial terms, that is,

$$\boldsymbol{F} = \boldsymbol{F}^B \boldsymbol{F}^A. \tag{2.1}$$

We highlight that the multiplicative decomposition of $\boldsymbol{F}$ in Eq. (2.1) is purely conceptual and can not be determined with experiments (HUBER; TSAKMAKIS, 2000).

Figure 2.1 – Decomposition of the deformation gradient $\boldsymbol{F}$.

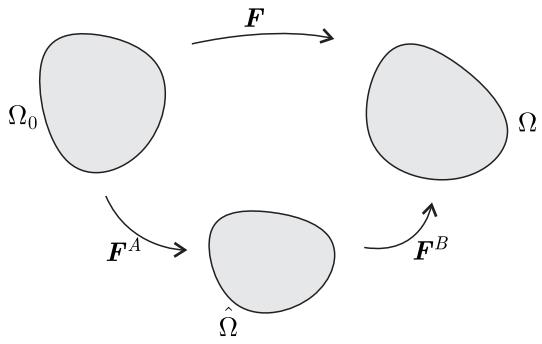

An alternative way to illustrate incremental deformations is to consider an analogy with one-dimensional rheological models. Let consider that the body is composed of a material represented by a rheological connection of two components, A and B, arranged in series as illustrated in Fig. 2.2. When it is subject to stress, the components A and B are affected respectively by the partial deformation gradients $\boldsymbol{F}^A$ and $\boldsymbol{F}^B$ in such a way that the total rheological component is affected according Eq. (2.1). We highlight that the components A and B are general and not necessarily linear (we give a possible specialization in Section 3.1).

Figure 2.2 – Representation of a rheological connection of two components in series. Indeed, A and B can represent different rheological blocks. Possible examples include the Maxwell model, Poynting-Thomson model (BOUKAMEL et al., 2001) or composed chains as the generalized Kelvin model (see Fig. 1.3a).

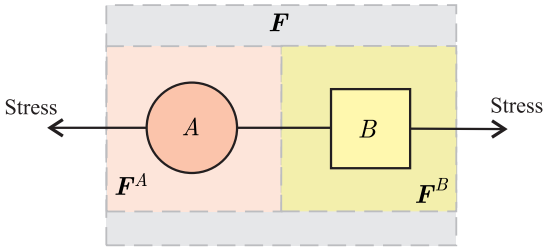

In the previous analogy, we used only two incremental steps for the deformation process, corresponding to parts A and B in the rheological series model. This interpretation can be generalized for q elements, namely $A^1, A^2, ..., A^q$, coupled in series, with the total deformation gradient given by

$$\boldsymbol{F} = \boldsymbol{F}^{A^q} \cdots \boldsymbol{F}^{A^2} \boldsymbol{F}^{A^1}.$$

Formally, the mentioned rheological model is used to represent the one-dimensional case. However, we will use this mechanical analogy throughout the text to help with the physical interpretation of the model in $\mathbb{R}^3$.

Remark 2.1. *Before we move on to the model development, we need to clarify the notation and some measures used in the following. Unless otherwise stated, the subscript* $(\cdot)_0$ *denotes a tensor (or measure) in the reference configuration* Ω_0*, while the corresponding*

in the current setting, Ω, doe not have a subscript. Tensors defined in the intermediate configuration $\hat{\Omega}$ assume the hat symbol $\hat{(\cdot)}$.

The partial velocity gradients associated with the partial deformation gradients $\boldsymbol{F}^A$ and $\boldsymbol{F}^B$ are defined respectively by

$$\hat{\boldsymbol{L}}^A := \dot{\boldsymbol{F}}^A \left(\boldsymbol{F}^A\right)^{-1} \quad \text{and} \quad \boldsymbol{L}^B := \dot{\boldsymbol{F}}^B \left(\boldsymbol{F}^B\right)^{-1}, \tag{2.2-2.3}$$

where $\dot{(\cdot)}$ denotes the derivative on time. Due to the multiplicative decomposition of $\boldsymbol{F}$ given in Eq. (2.1), the total velocity gradient $\boldsymbol{L}$ can be defined as

$$\begin{aligned} \boldsymbol{L} &:= \nabla_{\boldsymbol{x}} \boldsymbol{v} = \dot{\boldsymbol{F}}\boldsymbol{F}^{-1} = \overline{(\boldsymbol{F}^B \dot{\boldsymbol{F}^A})}\left(\boldsymbol{F}^B \boldsymbol{F}^A\right)^{-1} \\ &= \boldsymbol{L}^B + \boldsymbol{L}^A, \end{aligned} \tag{2.4}$$

where

$$\boldsymbol{L}^A := \boldsymbol{F}^B \hat{\boldsymbol{L}}^A \left(\boldsymbol{F}^B\right)^{-1}, \tag{2.5}$$

is the correspondent of $\hat{\boldsymbol{L}}^A$ in the configuration Ω.

2.2 Development of the General Damage Phase-Field Model

This section presents a general damage phase-field model based on the rheological arrangement in series. We derive the governing equations for both Eulerian and Lagrangian configurations, and we obtain the general form of the constitutive relations for the Lagrangian case in terms of the free-energy functional and pseudo-potential of dissipation. The main equations for the model are highlighted by a blue box, and to construct a flowing and concise text, we suppressed some details on basic mechanical principles. The reader will find indications pointing to detailing through the text.

2.2.1 The Governing Equations in Eulerian Coordinates

Let us consider the body $\mathcal{B}$ in the configuration $\Omega \subset \mathbb{R}^3$ (see Fig. 2.1). The fundamental state of $\mathcal{B}$ is given by: (i) the density of mass ρ in Ω, that satisfies the principle of mass conservation; (ii) dynamic variables $\boldsymbol{u}$ and $\boldsymbol{v}$, representing the displacement and velocity vector fields, respectively; and (iii) the specific density of the internal energy e in Ω. The principle of virtual power (PVP) is used to obtain a governing equation for $\boldsymbol{v}$, while the first principle of thermodynamics is employed to determine e. We also assume that the material does not present a preferential direction for the strain evolution.

As in Boldrini et al. (2016), let us presuppose that $\mathcal{B}$ can evolves with damage due to the deformation process. Then we introduce a phase-field variable φ that represents the volumetric fraction of the damaged material and varies in the interval $[0, 1]$; $\varphi = 0$

represents the undamaged material, $\varphi = 1$ the fractured material (voids in the material), and $0 < \varphi < 1$ an intermediate damaged state. Here, the damage is used as a dynamic scalar variable whose corresponding equation will be derived from the PVP. The PVP requires the definition of virtual velocities $\delta\boldsymbol{v}$ and δc, which are, respectively, the admissible macroscopic virtual velocity (the time rate of change of displacement) and the admissible microscopic virtual velocity (the time rate of change of dynamic phase-field φ).

By considering the decomposition of $\boldsymbol{F}$, as shown in Fig. 2.1, and following Frémond and Shitikova (2002) and Boldrini et al. (2016), we derive the basic governing equations in Eulerian coordinates of our model by using the mechanical principles summarized below (see Appendix C.8 for details).

1. For the *principle of mass conservation*, the total quantity of mass in a closed system can not be altered by physical and chemical actions (see Appendix C.8.1). The Eulerian form of this principle is given by

$$\dot{\rho} = -\rho \operatorname{div}_{\boldsymbol{x}}(\boldsymbol{v}), \tag{2.6}$$

   where $\operatorname{div}_{\boldsymbol{x}}(\cdot)$ is the Eulerian divergent operator.

2. The *PVP* states the equilibrium among the virtual powers of inertia $\mathcal{P}_a$, internal $\mathcal{P}_i$ and external $\mathcal{P}_e$ loads for any virtual action $\{\delta\boldsymbol{v}, \delta c\}$ in Ω as

$$\mathcal{P}_a\left(\Omega, \delta\boldsymbol{v}, \delta c\right) = \mathcal{P}_i\left(\Omega, \delta\boldsymbol{v}, \delta c\right) + \mathcal{P}_e\left(\Omega, \delta\boldsymbol{v}, \delta c\right). \tag{2.7}$$

   From the multiplicative decomposition of $\boldsymbol{F}$, given in Eq. (2.1), the total internal virtual power $\mathcal{P}_i$ is composed of a sum of the virtual power generated by $\boldsymbol{F}^A$ and $\boldsymbol{F}^B$, plus a virtual power related to the damage. By considering an adaptation of the total internal virtual power $\mathcal{P}_i$, postulated by Ihlemann (2014), to include the effect of the damage, we define

$$\mathcal{P}_i = \mathcal{P}_A + \mathcal{P}_B + \mathcal{P}_\varphi, \tag{2.8}$$

   where $\mathcal{P}_A$ and $\mathcal{P}_B$ are the virtual internal stress power contributions due to $\boldsymbol{F}^A$ and $\boldsymbol{F}^B$, respectively, and $\mathcal{P}_\varphi$ is the power by the interior loads due to the material damage.

   Based on the usual definitions for the internal power in continuum mechanics, according to Temam and Miranville (2005) and Piero (2009), and defining $\hat{\boldsymbol{T}}^A$ and $\boldsymbol{T}^B$ as the stress tensors related with $\boldsymbol{F}^A$ and $\boldsymbol{F}^B$, respectively, we write

$$\mathcal{P}_A = -\int_{\hat{\Omega}} \hat{\boldsymbol{T}}^A : \delta\hat{\boldsymbol{L}}^A \, \mathrm{d}\hat{\Omega}, \tag{2.9}$$

$$\mathcal{P}_B = -\int_{\Omega} \boldsymbol{T}^B : \delta\boldsymbol{L}^B \, \mathrm{d}\Omega, \tag{2.10}$$

and

$$\mathcal{P}_{\varphi} = -\int_{\Omega} (k\delta c + \boldsymbol{h} \cdot \nabla_{\boldsymbol{x}} \delta c)\, \mathrm{d}\Omega, \tag{2.11}$$

where $\delta(\cdot)$ indicates a virtual quantity[1], k is the volumetric density of energy exchanged by variation of a unity of φ in a unity of time, $\boldsymbol{h}$ is the energy flux correlated with the spatial variation of a unit of φ in a unit of time and $\nabla_{\boldsymbol{x}}(\cdot)$ is the gradient operator in the Eulerian configuration. Equation (2.11) is the same as that proposed by Frémond and Shitikova (2002). We emphasize that, in the present case, $\mathcal{P}_{\varphi}$ represents the virtual power due to the material damage by the application of the total gradient of deformation[2].

The integral in Eq. (2.9) is defined in the intermediate configuration $\hat{\Omega}$; then, from Eq. (2.5), we can rewrite Eq. (2.9) in the current configuration as

$$\begin{aligned} \mathcal{P}_A &= -\int_{\hat{\Omega}} \hat{\boldsymbol{T}}^A : \delta\hat{\boldsymbol{L}}^A \, \mathrm{d}\hat{\Omega} \\ &= -\int_{\Omega} \hat{\boldsymbol{T}}^A : \left(\left(\boldsymbol{F}^B\right)^{-1} \delta\boldsymbol{L}^A \boldsymbol{F}^B\right) \frac{1}{\det(\boldsymbol{F}^B)} \, \mathrm{d}\Omega \\ &= -\int_{\Omega} \boldsymbol{T}^A : \delta\boldsymbol{L}^A \, \mathrm{d}\Omega, \end{aligned} \tag{2.12}$$

where $\boldsymbol{T}^A$ is a stress tensor in Ω given by

$$\boldsymbol{T}^A = \frac{1}{\det(\boldsymbol{F}^B)} \left(\boldsymbol{F}^B\right)^{-t} \hat{\boldsymbol{T}}^A \left(\boldsymbol{F}^B\right)^{t}. \tag{2.13}$$

Then, by replacing Eqs. (2.10), (2.11) and (2.12) in Eq. (2.8), we have

$$\mathcal{P}_i = -\int_{\Omega} \boldsymbol{T}^A : \delta\boldsymbol{L}^A \, \mathrm{d}\Omega - \int_{\Omega} \boldsymbol{T}^B : \delta\boldsymbol{L}^B \, \mathrm{d}\Omega - \int_{\Omega} (k\delta c + \boldsymbol{h} \cdot \nabla_{\boldsymbol{x}} \delta c) \, \mathrm{d}\Omega. \tag{2.14}$$

We also define

$$\mathcal{P}_a = \int_{\Omega} \rho\dot{\boldsymbol{v}} \cdot \delta\boldsymbol{v} \, \mathrm{d}\Omega, \tag{2.15}$$

and

$$\mathcal{P}_e = \int_{\Omega} \rho\boldsymbol{f} \cdot \delta\boldsymbol{v} \, \mathrm{d}\Omega + \int_{\Gamma_N} \boldsymbol{\sigma} \cdot \delta\boldsymbol{v} \, \mathrm{d}\Gamma_N + \int_{\Gamma} t_h \delta c \, \mathrm{d}\Gamma, \tag{2.16}$$

where $\boldsymbol{f}$ is the vector field representing the body force per unit of mass, $\boldsymbol{\sigma}$ is the macroscopic stress vector field, and t_h is the superficial density of energy supplied to the material by the flux $\boldsymbol{h}$. The first term in Eq. (2.16) represents the virtual power by actions at a distance, and the last two are associated with the virtual powers by

[1] From a purely mathematical point of view, we could define, for example, a partial virtual velocity $\delta\boldsymbol{v}^B$ related to the partial gradient of deformation $\boldsymbol{F}^B$. Then, the partial velocity gradient associated with $\delta\boldsymbol{v}^B$ could be written as $\delta\boldsymbol{L}^B = \nabla_{\boldsymbol{x}}(\delta\boldsymbol{v}^B)$.

[2] We could also consider two separated damage variables related to $\boldsymbol{F}^A$ and $\boldsymbol{F}^B$; namely $\hat{\varphi}^A$ and φ^B respectively. In this case, the total internal power related to damage should be considered a sum of the damage power generated by $\hat{\varphi}^A$ in $\hat{\Omega}$ plus φ^B in Ω.

the surface loads. We assume no external microscopic actions influencing the damage (e.g., corrosion or aging).

By replacing Eqs. (2.14), (2.15) and (2.16) into (2.7), we obtain

$$\begin{aligned}\int_\Omega \rho\dot{\boldsymbol{v}}\cdot\delta\boldsymbol{v}\,\mathrm{d}\Omega &= -\int_\Omega \boldsymbol{T}^A:\delta\boldsymbol{L}^A\,\mathrm{d}\Omega-\int_\Omega \boldsymbol{T}^B:\delta\boldsymbol{L}^B\,\mathrm{d}\Omega\\ &\quad-\int_\Omega\left(k\delta c+\boldsymbol{h}\cdot\nabla_{\boldsymbol{x}}\delta c\right)\mathrm{d}\Omega+\int_{\Gamma_N}\boldsymbol{\sigma}\cdot\delta\boldsymbol{v}\,\mathrm{d}\Gamma_N\\ &\quad+\int_\Omega\rho\boldsymbol{f}\cdot\delta\boldsymbol{v}\,\mathrm{d}\Omega+\int_\Gamma t_h\delta c\,\mathrm{d}\Gamma.\end{aligned}\tag{2.17}$$

Since the above equation is valid for any $\{\delta\boldsymbol{v},\delta c,\delta\boldsymbol{L}^A,\delta\boldsymbol{L}_B\}$ in Ω we can assume $\delta c=0$ and $\delta\boldsymbol{L}_A=\boldsymbol{0}$, obtaining $\nabla_{\boldsymbol{x}}\delta\boldsymbol{v}=\delta\boldsymbol{L}_B$ from Eq. (2.4). In this case, Eq. (2.17) leads to

$$\int_\Omega\rho\dot{\boldsymbol{v}}\cdot\delta\boldsymbol{v}\,\mathrm{d}\Omega=\int_{\Gamma_N}\boldsymbol{\sigma}\cdot\delta\boldsymbol{v}\,\mathrm{d}\Gamma_N+\int_\Omega\rho\boldsymbol{f}\cdot\delta\boldsymbol{v}\,\mathrm{d}\Omega-\int_\Omega\boldsymbol{T}^B:\delta\boldsymbol{L}_B\,\mathrm{d}\Omega,\tag{2.18}$$

that is the weak form of the balance of linear momentum associated with macroscopic loads. By considering $\delta\boldsymbol{L}_B=\nabla_{\boldsymbol{x}}(\delta\boldsymbol{v})$ and using integration by parts in the above equation (see Eq. (A.3)), we obtain

$$\begin{aligned}\int_\Omega\rho\dot{\boldsymbol{v}}\cdot\delta\boldsymbol{v}\,\mathrm{d}\Omega &= \int_{\Gamma_N}\boldsymbol{\sigma}\cdot\delta\boldsymbol{v}\,\mathrm{d}\Gamma_N+\int_\Omega\rho\boldsymbol{f}\cdot\delta\boldsymbol{v}\,\mathrm{d}\Omega-\int_\Gamma\left(\boldsymbol{T}^B\boldsymbol{n}\right)\cdot\delta\boldsymbol{v}\,\mathrm{d}\Gamma\\ &\quad+\int_\Omega\mathrm{div}_{\boldsymbol{x}}\left(\boldsymbol{T}^B\right)\cdot\delta\boldsymbol{v}\,\mathrm{d}\Omega,\end{aligned}$$

where $\boldsymbol{n}$ is the unit exterior vector normal to the surface-area element $\mathrm{d}\Gamma$. The above equation is valid for every $\delta\boldsymbol{v}$; then it results in

$$\rho\dot{\boldsymbol{v}}=\rho\boldsymbol{f}+\mathrm{div}_{\boldsymbol{x}}(\boldsymbol{T}^B)\quad\text{in }\Omega,\tag{2.19a}$$

$$\boldsymbol{\sigma}=\boldsymbol{T}^B\boldsymbol{n}\quad\text{on }\Gamma_N,\tag{2.19b}$$

$$\boldsymbol{u}=\bar{\boldsymbol{u}}\quad\text{on }\Gamma_D,\tag{2.19c}$$

that is the local form (or strong form) of the balance of linear momentum in the Eulerian configuration, where $\bar{\boldsymbol{u}}$ is some prescribed value for Dirichlet condition.

Also, by supposing $\delta c=0$ and $\delta\boldsymbol{v}=0$, we obtain $\nabla_{\boldsymbol{x}}\delta\boldsymbol{v}=\boldsymbol{0}$ from Eq. (2.4), which leads to $\delta\boldsymbol{L}^B=-\boldsymbol{F}^B\delta\hat{\boldsymbol{L}}^A\left(\boldsymbol{F}^B\right)^{-1}=-\delta\boldsymbol{L}^A$. In this case, Eq. (2.17) results in

$$\begin{aligned}0 &= -\int_\Omega\boldsymbol{T}^A:\delta\boldsymbol{L}^A\,\mathrm{d}\Omega-\int_\Omega\boldsymbol{T}^B:\delta\boldsymbol{L}^B\,\mathrm{d}\Omega\\ &= -\int_\Omega\boldsymbol{T}^A:\delta\boldsymbol{L}^A\,\mathrm{d}\Omega+\int_\Omega\boldsymbol{T}^B:\delta\boldsymbol{L}^A\,\mathrm{d}\Omega\\ &= -\int_\Omega\left(\boldsymbol{T}^A-\boldsymbol{T}^B\right):\delta\boldsymbol{L}^A\,\mathrm{d}\Omega,\end{aligned}$$

which implies in

$$\boldsymbol{T}^B=\boldsymbol{T}^A\quad\text{in }\Omega.\tag{2.20}$$

We stress the importance of Eq. (2.20). In the one-dimensional case, it shows that the stress $\boldsymbol{T}^A$ acting on A of the rheological arrangement of Fig. 2.2 is the same as that acting at B, recovering the usual stress relation for rheological connection in series. We also found this result for three-dimensional models (GURTIN; FRIED; ANAND, 2010). Additionally, note that we also could have taken $\delta c = 0$ and $\delta\hat{\boldsymbol{L}}^B = \boldsymbol{0}$ in Eq. (2.17); however, due to Eq. (2.20), the result would be the same as that shown in Eq. (2.19a).

Finally, if $\delta\boldsymbol{v} = \delta\boldsymbol{L}^A = \boldsymbol{0}$, then Eq. (2.17) returns

$$\operatorname{div}_{\boldsymbol{x}}(\boldsymbol{h}) - k = 0 \quad \text{in } \Omega, \tag{2.21a}$$

$$t_h = \boldsymbol{h}\cdot\boldsymbol{n} \quad \text{on } \Gamma, \tag{2.21b}$$

that is the balance of linear momentum associated with microscopic loads.

3. The *conservation of angular momentum* requires that

$$\boldsymbol{T}^B = \left(\boldsymbol{T}^B\right)^t \quad \text{in } \Omega, \tag{2.22}$$

where $(\cdot)^t$ is the transpose of $(\cdot)$. In other words, the tensor $\boldsymbol{T}^B$ acts as a Cauchy stress tensor in Ω. By considering Eq. (2.20) we can also conclude that $\boldsymbol{T}^A = \left(\boldsymbol{T}^A\right)^t$.

4. The *first principle of the thermodynamics* (or balance of energy) states that the time rate of change of the total energy is equal to the external power plus the heating of the body (ODEN, 2012):

$$\frac{\mathrm{d}}{\mathrm{d}t}\mathcal{K} + \frac{\mathrm{d}}{\mathrm{d}t}\mathcal{U} = \mathcal{P}_e + \mathcal{Q}^f + \mathcal{Q}^s, \tag{2.23}$$

where

$$\mathcal{K} = \frac{1}{2}\int_\Omega \rho|\boldsymbol{v}|^2 \,\mathrm{d}\Omega, \tag{2.24}$$

is the total kinetic energy,

$$\mathcal{U} = \int_\Omega \rho e \,\mathrm{d}\Omega, \tag{2.25}$$

is the total internal energy, with e being the specific density of internal energy,

$$\mathcal{Q}^f = -\int_\Gamma \boldsymbol{q}\cdot\boldsymbol{n} \,\mathrm{d}\Gamma, \tag{2.26}$$

is the total energy (by unit of time) carried by the energy flux $\boldsymbol{q}$, and

$$\mathcal{Q}^s = \int_\Omega \rho r \,\mathrm{d}\Omega, \tag{2.27}$$

is the total thermal energy (by unit of time) generated in Ω, by the heat sources (or sinks) with specific heat source density r. Replacing Eqs. (2.24-2.27) in (2.23), and after some algebraic manipulations (see Appendix C.8.4.3 for details), we can rewrite the balance of energy in the local form according to

$$\rho\dot{e} = \boldsymbol{T}^A : \boldsymbol{L}^A + \boldsymbol{T}^B : \boldsymbol{L}^B + k\dot{\varphi} + \boldsymbol{h}\cdot\nabla_{\boldsymbol{x}}(\dot{\varphi}) + \rho r - \operatorname{div}_{\boldsymbol{x}}(\boldsymbol{q}) \quad \text{in } \Omega. \tag{2.28}$$

5. We also consider the entropy inequality. As Fabrizio, Giorgi and Morro (2006) and Boldrini et al. (2016), the *second principle of thermodynamics* can be expressed in a generalized form of the Clausius-Duhem inequality (see Truesdell (1952) for details), whose differential form is given by

$$\rho\dot{\eta} \geq -\mathrm{div}_{\boldsymbol{x}}(\boldsymbol{\Phi}) + \rho\omega \quad \text{in } \Omega. \tag{2.29}$$

As in Costa-Haveroth et al. (2022), η denotes the specific entropy density; the total entropy flux is given by $\boldsymbol{\Phi} = \boldsymbol{\Phi}_\theta + \boldsymbol{\Phi}_m$ where $\boldsymbol{\Phi}_\theta = \boldsymbol{q}/\theta$ is the traditional thermal entropy flux, $\theta > 0$ is the temperature, and $\boldsymbol{\Phi}_m$ is some additional entropy flux that can occurs due to other microscopic changes. The total specific entropy production term is split by $\omega = \omega_\theta + \omega_m$, where $\omega_\theta = r/\theta$ is the traditional specific thermal entropy production, and ω_m is some additional specific entropy production term due to other microscopic changes. Here, ω_m is related to damage process. Furthermore, for proper physical modeling, we must have $\int_\Omega \omega_m \, \mathrm{d}\Omega \geq 0$.

The specific free-energy of Helmholtz

$$\psi = e - \theta\eta, \tag{2.30}$$

implies in $e = \psi + \theta\eta$. By replacing it in Eq. (2.28) and comparing with the inequality (2.29), we obtain

$$\begin{aligned} -\rho\left(\dot{\psi} + \dot{\theta}\eta\right) + \boldsymbol{T}^A : \boldsymbol{L}^A + \boldsymbol{T}^B : \boldsymbol{L}^{\boldsymbol{B}} + k\dot{\varphi} + \boldsymbol{h} \cdot \nabla_{\boldsymbol{x}}(\dot{\varphi}) \\ -\frac{1}{\theta}\boldsymbol{q} \cdot \nabla_{\boldsymbol{x}}(\theta) + \theta\mathrm{div}_{\boldsymbol{x}}(\boldsymbol{\Phi}_m) - \theta\rho\omega_m \geq 0 \quad \text{in } \Omega, \end{aligned} \tag{2.31}$$

that must be verified for thermodynamic consistency of all physical admissible processes.

Finally, we summarize the general Eulerian governing equations for our model in the Box 1.

Box 1: General Eulerian governing equations

Consider the general equations:

$$
\begin{aligned}
&\dot{\rho} = -\rho \operatorname{div}_{\boldsymbol{x}}(\boldsymbol{v}) \\
&\dot{\boldsymbol{u}} = \boldsymbol{v} \\
&\rho\dot{\boldsymbol{v}} = \rho\boldsymbol{f} + \operatorname{div}_{\boldsymbol{x}}\left(\boldsymbol{T}^B\right) \\
&\operatorname{div}_{\boldsymbol{x}}(\boldsymbol{h}) - k = 0 \\
&\boldsymbol{T}^A = \boldsymbol{T}^B \\
&\boldsymbol{T}^B = \left(\boldsymbol{T}^B\right)^t \\
&\boldsymbol{F} = \boldsymbol{F}^B\boldsymbol{F}^A \\
&\rho\dot{e} = \boldsymbol{T}^A : \boldsymbol{L}^A + \boldsymbol{T}^B : \boldsymbol{L}^B + k\dot{\varphi} + \boldsymbol{h}\cdot\nabla_{\boldsymbol{x}}\dot{\varphi} + \rho r - \operatorname{div}_{\boldsymbol{x}}(\boldsymbol{q}),
\end{aligned}
$$

in Ω that must satisfying the inequality

$$
\begin{aligned}
-\rho\left(\dot{\psi} + \dot{\theta}\eta\right) + \boldsymbol{T}^A : \boldsymbol{L}^A + \boldsymbol{T}^B : \boldsymbol{L}^{\boldsymbol{B}} + k\dot{\varphi} + \boldsymbol{h}\cdot\nabla_{\boldsymbol{x}}\dot{\varphi} - \frac{1}{\theta}\boldsymbol{q}\cdot\nabla_{\boldsymbol{x}}\theta \\
+\theta\operatorname{div}_{\boldsymbol{p}}(\boldsymbol{\Phi}_m) - \theta\rho\omega_m \geq 0 \quad \text{in } \Omega,
\end{aligned}
$$

for all physical admissible processes.
In this box, we presented eight governing equations. The variables are: $\boldsymbol{u}$, $\boldsymbol{v}$, $\boldsymbol{T}^B$, $\boldsymbol{T}^A$, $\boldsymbol{F}$, $\boldsymbol{F}^B$, $\boldsymbol{F}^A$, $\boldsymbol{L}^A$, $\boldsymbol{L}^B$, $\boldsymbol{q}$, $\boldsymbol{h}$, e and φ.

2.2.2 The Governing Equations in Lagrangian Coordinates

Let consider the body $\mathcal{B}_0$ in the configuration $\Omega_0 \in \mathbb{R}^3$ (see Fig. 2.1). Similarly to the Section 2.2.1, the state of $\mathcal{B}_0$ is described by: (i) the density of mass ρ_0, satisfying the principle of mass conservation; (ii) the dynamic variables $\boldsymbol{u}$ and $\boldsymbol{v}$, describing the displacement and velocity vector fields, respectively; and (iii) the specific density of internal energy e_0. The governing equations for $\boldsymbol{v}$ and e_0 derive from the PVP and by making use of the first principle of thermodynamics, respectively. Moreover, we assume that $\mathcal{B}_0$ can develop damage due to the straining process (without preferential direction), with the corresponding phase-field variable φ_0 lying in the interval $[0, 1]$ ($\varphi_0 = 0$ for undamaged material and $\varphi_0 = 1$ for fractured material). The correspondence $\varphi_0(\boldsymbol{p}, t) = \varphi(\boldsymbol{x}, t)$ is valid.

An immediate way to derive the general Lagrangian governing equations is to follow the same procedure presented in the previous section using Lagrangian variables and tensors. However, such a procedure leads to a cumbersome mathematical manipulation of the internal power due to the pull-back of the tensors in Ω by the total deformation gradient $\boldsymbol{F}$. An alternative to avoid these issues is to derive the Lagrangian equations directly from the Eulerian version, as shown below.

1. According to the discussion on Appendix C.8.1, the Lagrangian version of the *principle of mass conservation* is given by

$$\dot{\rho_0} = 0 \quad \text{in } \Omega_0. \tag{2.32}$$

2. The *balance of linear momentum* can be obtained by changing the domain of integration and the physical quantities in Eq. (2.18) to the reference configuration as

$$\int_{\Omega_0} \rho_0 \dot{\boldsymbol{v}} \cdot \delta \boldsymbol{v} \, \mathrm{d}\Omega_0 = \int_{\Gamma_0} \boldsymbol{\sigma}_0 \cdot \delta \boldsymbol{v} \, \mathrm{d}\Gamma_0 + \int_{\Omega_0} \rho_0 \boldsymbol{f}_0 \cdot \delta \boldsymbol{v} \, \mathrm{d}\Omega_0 - \int_{\Omega_0} \boldsymbol{P}^B : \delta \dot{\boldsymbol{F}} \, \mathrm{d}\Omega_0, \tag{2.33}$$

where $\boldsymbol{\sigma}_0 = \boldsymbol{\sigma}$, $\boldsymbol{f}_0 = \boldsymbol{f}$, $\boldsymbol{P}^B$ is the first Piola-Kirchhoff stress tensor, and $\delta \dot{\boldsymbol{F}} = \nabla_{\boldsymbol{p}} \delta \boldsymbol{v}$, where $\nabla_{\boldsymbol{p}}(\cdot)$ is the Lagrangian gradient operator. Integration by parts can be applied to find

$$\begin{aligned} \int_{\Omega_0} \rho_0 \dot{\boldsymbol{v}} \cdot \delta \boldsymbol{v} \, \mathrm{d}\Omega_0 \;=\; & \int_{\Gamma_0} \boldsymbol{\sigma}_0 \cdot \delta \boldsymbol{v} \, \mathrm{d}\Gamma_0 + \int_{\Omega_0} \rho_0 \boldsymbol{f}_0 \cdot \delta \boldsymbol{v} \, \mathrm{d}\Omega_0 - \int_{\Gamma_0} (\boldsymbol{P}^B \boldsymbol{n}_0) \cdot \delta \boldsymbol{v} \, \mathrm{d}\Gamma_0 \\ & + \int_{\Omega_0} \mathrm{div}_{\boldsymbol{p}}(\boldsymbol{P}^B) \cdot \delta \boldsymbol{v} \, \mathrm{d}\Omega_0, \end{aligned} \tag{2.34}$$

where $\boldsymbol{n}_0$ is the unit vector normal to Γ_0. Once Eq. (2.34) is valid for every $\delta \boldsymbol{v}$, the local form of the balance of linear momentum due to the macroscopic forces in the Lagrangian version is

$$\rho_0 \dot{\boldsymbol{v}} = \rho_0 \boldsymbol{f}_0 + \mathrm{div}_{\boldsymbol{p}} \left(\boldsymbol{P}^B \right) \quad \text{in } \Omega_0, \tag{2.35a}$$

$$\boldsymbol{\sigma}_0 = \boldsymbol{P}^B \boldsymbol{n}_0 \quad \text{on } \Gamma_N, \tag{2.35b}$$

$$\boldsymbol{u} = \bar{\boldsymbol{u}} \quad \text{on } \Gamma_D. \tag{2.35c}$$

Details concerning this derivation can be seen in Appendix C.8.2.

Furthermore, we can define

$$\begin{aligned} \boldsymbol{P}^B &:= \boldsymbol{F} \boldsymbol{S}^B & (2.36) \\ &= \det(\boldsymbol{F}) \, \boldsymbol{T}^B \boldsymbol{F}^{-t}, & (2.37) \end{aligned}$$

where $\boldsymbol{S}^B$ is a symmetric second Piola-Kirchhoff stress tensor ($\boldsymbol{S}^B = \left(\boldsymbol{S}^B \right)^t$). In the one-dimensional case, the tensors $\boldsymbol{T}^B$, $\boldsymbol{P}^B$, and $\boldsymbol{S}^B$, are the stress tensors related to the part B of the rheological model shown in Fig. 2.2. Remember that $\boldsymbol{T}^B$ is an Eulerian quantity while $\boldsymbol{S}^B$ is a Lagrangian measure. Note that, by using Eq. (2.36) and the symmetry of $\boldsymbol{S}^B$, we can manipulate the last term in Eq. (2.33) as

$$\begin{aligned} \boldsymbol{P}^B : \delta \dot{\boldsymbol{F}} = \boldsymbol{F} \boldsymbol{S}^B : \delta \dot{\boldsymbol{F}} = \boldsymbol{S}^B : \boldsymbol{F}^t \delta \dot{\boldsymbol{F}} \;&=\; \boldsymbol{S}^B : \frac{1}{2} \left(\boldsymbol{F}^t \delta \dot{\boldsymbol{F}} + \delta \dot{\boldsymbol{F}}^t \boldsymbol{F} \right) \\ &=\; \boldsymbol{S}^B : \delta \dot{\boldsymbol{E}}, \end{aligned} \tag{2.38}$$

where

$$\delta \dot{\boldsymbol{E}} := \frac{1}{2} \left(\boldsymbol{F}^t \delta \dot{\boldsymbol{F}} + \delta \dot{\boldsymbol{F}}^t \boldsymbol{F} \right),$$

is the time rate of the Green-Lagrange virtual strain tensor. Replacing Eq. (2.38) into Eq. (2.33) we obtain an alternative weak form of the balance of linear momentum associated with macroscopic loads in the Lagrangian configuration:

$$\int_{\Omega_0} \rho_0 \dot{\boldsymbol{v}} \cdot \delta \boldsymbol{v} = \int_{\Gamma_0} \boldsymbol{\sigma}_0 \cdot \delta \boldsymbol{v} \, \mathrm{d}\Gamma_0 + \int_{\Omega_0} \rho_0 \boldsymbol{f}_0 \cdot \delta \boldsymbol{v} \, \mathrm{d}\Omega_0 + \int_{\Omega_0} \boldsymbol{S}^B : \delta \dot{\boldsymbol{E}} \, \mathrm{d}\Omega_0. \tag{2.39}$$

Equation (2.39) is very useful for numerical purposes once the last term on it is the inner product of symmetric tensors.

To develop the balance of linear momentum associated with microscopic loads in the Lagrangian configuration, we consider Eq. (2.17) with $\delta \boldsymbol{v} = \delta \boldsymbol{L}^A = \boldsymbol{0}$:

$$\int_{\Omega} \mathrm{div}_{\boldsymbol{x}}(\boldsymbol{h}) \, \mathrm{d}\Omega - \int_{\Omega} k \, \mathrm{d}\Omega = 0.$$

By applying the divergence theorem (see Appendix. A) and changing the domain of integration to Ω_0, we obtain

$$\begin{aligned} 0 &= \int_{\Gamma} \boldsymbol{h} \cdot \boldsymbol{n} \, \mathrm{d}\Gamma - \int_{\Omega} k \, \mathrm{d}\Omega \\ &= \int_{\Gamma_0} \det(\boldsymbol{F}) \, \boldsymbol{F}^{-1} \boldsymbol{h} \cdot \boldsymbol{n}_0 \, \mathrm{d}\Gamma_0 - \int_{\Omega_0} k_0 \, \mathrm{d}\Omega_0 \\ &= \int_{\Omega_0} \mathrm{div}_{\boldsymbol{p}}(\boldsymbol{h}_0) \, \mathrm{d}\Omega_0 - \int_{\Omega_0} k_0 \, \mathrm{d}\Omega_0, \end{aligned} \tag{2.40}$$

where $\boldsymbol{n} = \det(\boldsymbol{F}) \boldsymbol{F}^{-t} \boldsymbol{n}_0$. Furthermore, $\boldsymbol{h}_0 = \det(\boldsymbol{F}) \boldsymbol{F}^{-1} \boldsymbol{h}$ and $k_0 = \det(\boldsymbol{F}) k$. From Eqs. (2.40) and (2.35b), we finally have the balance of the microscopic loads:

$$\mathrm{div}_{\boldsymbol{p}}(\boldsymbol{h}_0) - k_0 = 0 \quad \text{in } \Omega_0, \tag{2.41a}$$

$$t_{h,0} = \boldsymbol{h}_0 \cdot \boldsymbol{n}_0 \quad \text{on } \Gamma_0, \tag{2.41b}$$

with $t_{h,0}$ representing the superficial density of energy supplied to the material by the flux $\boldsymbol{h}_0$.

3. Let derive the *first principle of the thermodynamics* in the Lagrangian configuration, by considering the integrated version of Eq. (2.28) in Ω:

$$\begin{aligned} \int_{\Omega} \rho \dot{e} \, \mathrm{d}\Omega &= \int_{\Omega} \boldsymbol{T}^A : \boldsymbol{L}^A \, \mathrm{d}\Omega + \int_{\Omega} \boldsymbol{T}^B : \boldsymbol{L}^B \, \mathrm{d}\Omega + \int_{\Omega} k \dot{\varphi} \, \mathrm{d}\Omega + \int_{\Omega} \boldsymbol{h} \cdot \nabla_{\boldsymbol{x}} \dot{\varphi} \, \mathrm{d}\Omega \\ &\quad + \int_{\Omega} \rho r \, \mathrm{d}\Omega - \int_{\Omega} \mathrm{div}_{\boldsymbol{x}}(\boldsymbol{q}) \, \mathrm{d}\Omega. \end{aligned}$$

Some calculation (see details in Appendix C.8.4) implies that the above equation can be rewritten in the reference configuration Ω_0 as

$$\begin{aligned} \int_{\Omega_0} \rho_0 \dot{e}_0 \, \mathrm{d}\Omega_0 &= \int_{\Omega_0} \boldsymbol{T}^A : \boldsymbol{L}^A \det(\boldsymbol{F}) \, \mathrm{d}\Omega_0 + \int_{\Omega_0} \boldsymbol{T}^B : \boldsymbol{L}^B \det(\boldsymbol{F}) \, \mathrm{d}\Omega_0 \\ &\quad + \int_{\Omega_0} k_0 \dot{\varphi}_0 \, \mathrm{d}\Omega_0 + \int_{\Omega_0} \boldsymbol{h}_0 \cdot \nabla_{\boldsymbol{p}} \dot{\varphi}_0 \, \mathrm{d}\Omega_0 + \int_{\Omega_0} \rho_0 r_0 \, \mathrm{d}\Omega_0 \\ &\quad - \int_{\Omega_0} \mathrm{div}_{\boldsymbol{p}}(\boldsymbol{q}_0) \, \mathrm{d}\Omega_0, \end{aligned} \tag{2.42}$$

where $\dot{e} = \dot{e}_0$, $r = r_0$,

$$k\dot{\varphi}\det(\boldsymbol{F}) = \underbrace{k\det(\boldsymbol{F})}_{k_0}\dot{\varphi} = k_0\dot{\varphi}_0,$$

$$\boldsymbol{h}\cdot\nabla_{\boldsymbol{x}}\dot{\varphi}\det(\boldsymbol{F}) = \boldsymbol{h}\cdot\boldsymbol{F}^{-t}\nabla_{\boldsymbol{p}}\dot{\varphi}_0\det(\boldsymbol{F}) = \underbrace{\det(\boldsymbol{F})\boldsymbol{F}^{-1}\boldsymbol{h}}_{\boldsymbol{h}_0}\cdot\nabla_{\boldsymbol{p}}\dot{\varphi}_0 = \boldsymbol{h}_0\cdot\nabla_{\boldsymbol{p}}\dot{\varphi}_0,$$

and

$$\boldsymbol{q}\cdot\boldsymbol{n} = \boldsymbol{q}\cdot\det(\boldsymbol{F})\boldsymbol{F}^{-t}\boldsymbol{n}_0 = \underbrace{\det(\boldsymbol{F})\boldsymbol{F}^{-1}\boldsymbol{q}}_{\boldsymbol{q}_0}\cdot\,\boldsymbol{n}_0 = \boldsymbol{q}_0\cdot\boldsymbol{n}_0.$$

Equation (2.42) implies the following local form of the *balance of energy* in the Lagrangian configuration:

$$\rho_0\dot{e}_0 = \det(\boldsymbol{F})\boldsymbol{T}^A : \boldsymbol{L}^A + \det(\boldsymbol{F})\boldsymbol{T}^B : \boldsymbol{L}^B + k_0\dot{\varphi}_0 + \boldsymbol{h}_0\nabla_{\boldsymbol{p}}\dot{\varphi}_0 + \rho_0 r_0 - \mathrm{div}_{\boldsymbol{p}}(\boldsymbol{q}_0), \tag{2.43}$$

which can be rewritten conveniently by manipulating the first and second terms on the right-hand side. By using Eqs. (2.1), (2.13), and (2.5), the first term in the right hand side of Eq. (2.43) can be transformed according to

$$\begin{aligned}
\det(\boldsymbol{F})\boldsymbol{T}^A : \boldsymbol{L}^A &= \det(\boldsymbol{F})\boldsymbol{T}^A : \boldsymbol{F}^B\hat{\boldsymbol{L}}^A\left(\boldsymbol{F}^B\right)^{-1} \\
&= \det(\boldsymbol{F})\left(\boldsymbol{F}^B\right)^t\boldsymbol{T}^A\left(\boldsymbol{F}^B\right)^{-t} : \hat{\boldsymbol{L}}^A \\
&= \det(\boldsymbol{F}^A)\det(\boldsymbol{F}^B)\left(\boldsymbol{F}^B\right)^t\boldsymbol{T}^A\left(\boldsymbol{F}^B\right)^{-t} : \hat{\boldsymbol{L}}^A \\
&= \det(\boldsymbol{F}^A)\hat{\boldsymbol{T}}^A : \hat{\boldsymbol{L}}^A,
\end{aligned} \tag{2.44}$$

where

$$\hat{\boldsymbol{T}}^A := \det(\boldsymbol{F}^B)\left(\boldsymbol{F}^B\right)^t\boldsymbol{T}^A\left(\boldsymbol{F}^B\right)^{-t}. \tag{2.45}$$

To proceed with the calculation, we split the tensors $\hat{\boldsymbol{T}}^A$ and $\hat{\boldsymbol{L}}^A$ as

$$\hat{\boldsymbol{T}}^A = \hat{\boldsymbol{T}}^A_{\mathrm{symm}} + \hat{\boldsymbol{T}}^A_{\mathrm{skew}} \quad \text{and} \quad \hat{\boldsymbol{L}}^A = \hat{\boldsymbol{D}}^A + \hat{\boldsymbol{W}}^A, \tag{2.46-2.47}$$

where $\hat{\boldsymbol{T}}^A_{\mathrm{symm}}$ and $\hat{\boldsymbol{T}}^A_{\mathrm{skew}}$ are the symmetric and skew-symmetric parts of $\hat{\boldsymbol{T}}^A$, respectively. Similarly, $\hat{\boldsymbol{D}}^A$ (the partial deformation rate tensor) is the symmetric part of $\hat{\boldsymbol{L}}^A$ and $\hat{\boldsymbol{W}}^A$ (the partial spin tensor) is the skew-symmetric counterpart.

The replacement of Eqs. (2.46) and (2.47) into (2.44), implies in

$$\begin{aligned}
\det(\boldsymbol{F})\boldsymbol{T}^A : \boldsymbol{L}^A &= \det(\boldsymbol{F}^A)\hat{\boldsymbol{T}}^A : \hat{\boldsymbol{L}}^A \\
&= \det(\boldsymbol{F}^A)\hat{\boldsymbol{T}}^A_{\mathrm{symm}} : \hat{\boldsymbol{D}}^A + \det(\boldsymbol{F}^A)\hat{\boldsymbol{T}}^A_{\mathrm{skew}} : \hat{\boldsymbol{W}}^A,
\end{aligned} \tag{2.48}$$

and, by Eq. (C.27), we can write

$$\begin{aligned}\det(\boldsymbol{F})\boldsymbol{T}^A : \boldsymbol{L}^A &= \det(\boldsymbol{F}^A)\hat{\boldsymbol{T}}^A_{\text{symm}} : \left(\boldsymbol{F}^A\right)^{-t}\dot{\boldsymbol{E}}^A\left(\boldsymbol{F}^A\right)^{-1} + \det(\boldsymbol{F}^A)\hat{\boldsymbol{T}}^A_{\text{skew}} : \hat{\boldsymbol{W}}^A \\ &= \det(\boldsymbol{F}^A)\left(\boldsymbol{F}^A\right)^{-1}\hat{\boldsymbol{T}}^A_{\text{symm}}\left(\boldsymbol{F}^A\right)^{-t} : \dot{\boldsymbol{E}}^A + \det(\boldsymbol{F}^A)\hat{\boldsymbol{T}}^A_{\text{skew}} : \hat{\boldsymbol{W}}^A \\ &= \boldsymbol{S}^A : \dot{\boldsymbol{E}}^A + \det(\boldsymbol{F}^A)\hat{\boldsymbol{T}}^A_{\text{skew}} : \hat{\boldsymbol{W}}^A, \end{aligned} \tag{2.49}$$

where $\boldsymbol{E}^A$ is the Green-Lagrangian strain tensor, and

$$\boldsymbol{S}^A := \det(\boldsymbol{F}^A)\left(\boldsymbol{F}^A\right)^{-1}\hat{\boldsymbol{T}}^A_{\text{symm}}\left(\boldsymbol{F}^A\right)^{-t}, \tag{2.50}$$

is the Second-Piola Kirchhoff stress tensor. Both tensors, $\boldsymbol{E}^A$ and $\boldsymbol{S}^A$, are associated with the rheological block A.

The symmetry of $\boldsymbol{T}^B$ (see Eq. (2.22)) allows rewriting the second term in the right-hand side of Eq. (2.43) as

$$\begin{aligned}\det(\boldsymbol{F})\boldsymbol{T}^B : \boldsymbol{L}^B &= \det(\boldsymbol{F})\boldsymbol{T}^B : \boldsymbol{D}_B \\ &= \det(\boldsymbol{F})\boldsymbol{T}^B : \left(\boldsymbol{F}^B\right)^{-t}\dot{\hat{\boldsymbol{E}}}^B\left(\boldsymbol{F}^B\right)^{-1} \\ &= \det(\boldsymbol{F}^A)\left(\boldsymbol{F}^B\right)^{-1}\det(\boldsymbol{F}^B)\boldsymbol{T}^B\left(\boldsymbol{F}^B\right)^{-t} : \dot{\hat{\boldsymbol{E}}}^B \\ &= \det(\boldsymbol{F}^A)\hat{\boldsymbol{T}}^B : \dot{\hat{\boldsymbol{E}}}^B, \end{aligned} \tag{2.51}$$

where

$$\hat{\boldsymbol{T}}^B := \left(\boldsymbol{F}^B\right)^{-1}\det(\boldsymbol{F}^B)\boldsymbol{T}^B\left(\boldsymbol{F}^B\right)^{-t}, \tag{2.52}$$

is the stress tensor that is similar to the Cauchy tensor, and $\hat{\boldsymbol{E}}^B$ is a strain tensor similar to Green-Lagrange; these last two tensors are both defined in $\hat{\Omega}$.

Furthermore, by using Eqs. (2.37) and (2.52), we obtain

$$\boldsymbol{S}^B = \det(\boldsymbol{F}^A)\left(\boldsymbol{F}^A\right)^{-1}\hat{\boldsymbol{T}}^B\left(\boldsymbol{F}^A\right)^{-1}, \tag{2.53}$$

where $\boldsymbol{S}^B$ is a symmetric stress tensor that is similar to the second Piola tensor in Ω_0.

Finally, Eqs. (2.43), (2.49) and (2.51) lead to an alternative (to the one given in Eq. (2.42)) local form of the balance of energy:

$$\begin{aligned}\rho_0\dot{e}_0 = \quad & \boldsymbol{S}^A : \dot{\boldsymbol{E}}^A + \det(\boldsymbol{F}^A)\hat{\boldsymbol{T}}^A_{\text{skew}} : \hat{\boldsymbol{W}}^A + \det(\boldsymbol{F}^A)\hat{\boldsymbol{T}}^B : \dot{\hat{\boldsymbol{E}}}^B + k_0\dot{\varphi}_0 \\ & + \boldsymbol{h}_0 \cdot \nabla_{\boldsymbol{p}}\dot{\varphi}_0 + \rho_0 r_0 - \operatorname{div}_{\boldsymbol{p}}\boldsymbol{q}_0, \end{aligned} \tag{2.54}$$

where tensors $\boldsymbol{S}^A$ and $\boldsymbol{E}^A$ are regarded as Lagrangian quantities in the reference configuration Ω_0, while $\hat{\boldsymbol{T}}^B$, $\hat{\boldsymbol{T}}^A_{\text{skew}}$, $\hat{\boldsymbol{W}}^A$ and $\hat{\boldsymbol{E}}^B$ are defined in the intermediate configuration $\hat{\Omega}$.

4. Now, we consider inequality (2.29) integrated in Ω:

$$\int_{\Omega} \rho\dot{\eta}\ \mathrm{d}\Omega \geq -\int_{\Omega} \mathrm{div}_{\boldsymbol{x}}(\boldsymbol{\Phi})\ \mathrm{d}\Omega + \int_{\Omega} \rho\omega\ \mathrm{d}\Omega.$$

This inequality can be rewritten in the Lagrangian configuration as

$$\int_{\Omega_0} \rho_0\dot{\eta}_0\ \mathrm{d}\Omega_0 \geq -\int_{\Omega_0} \mathrm{div}_{\boldsymbol{p}}(\boldsymbol{\Phi}_0)\ \mathrm{d}\Omega_0 + \int_{\Omega_0} \rho_0\omega_0\ \mathrm{d}\Omega_0, \tag{2.55}$$

where $\eta_0(\boldsymbol{p},t) = \eta(\boldsymbol{x},t)$, $\boldsymbol{\Phi}_0 = \det(\boldsymbol{F})\boldsymbol{F}^{-1}\boldsymbol{\Phi}(\boldsymbol{x},t)$ and $\omega_0(\boldsymbol{p},t) = \omega(\boldsymbol{x},t)$ (see details in Appendix C.8.5). Equation (2.55) leads to the local form

$$\rho_0\eta_0 \geq -\mathrm{div}_{\boldsymbol{p}}\boldsymbol{\Phi}_0 + \rho_0\omega_0.$$

Similarly to the Eulerian case, we assume the total entropy flux as $\boldsymbol{\Phi}_0 = \boldsymbol{\Phi}_{0,\theta} + \boldsymbol{\Phi}_{0,m}$ where $\boldsymbol{\Phi}_{0,\theta} = \boldsymbol{q}_0/\theta$ is the classical thermal entropy flux, and $\boldsymbol{\Phi}_{0,m}$ is some additional entropy flux by other microscopic features. The total specific entropy production term is $\omega_0 = \omega_{0,\theta} + \omega_{0,m}$, where $\omega_{0,\theta} = r_0/\theta$ is the traditional specific thermal entropy production, and $\omega_{0,m}$ is some additional specific entropy production term by other microscopic features. In this work, $\omega_{0,m}$ relates to the damage mechanisms. Furthermore, we require that $\int_{\Omega_0} \omega_{0,m}\ \mathrm{d}\Omega_0 \geq 0$.
Replacing the Lagrangian Helmholtz-specific free-energy

$$\psi_0 = e_0 - \theta\eta_0,$$

in Eq. (2.54) and using inequality (2.55), we obtain

$$\begin{aligned} -\rho_0\left(\dot{\psi}_0 + \dot{\theta}\eta_0\right)\boldsymbol{S}^A : \dot{\boldsymbol{E}}^A + \det(\boldsymbol{F}^A)\hat{\boldsymbol{T}}^A_{\mathrm{skew}} : \hat{\boldsymbol{W}}^A + \det(\boldsymbol{F}^A)\hat{\boldsymbol{T}}^B : \dot{\hat{\boldsymbol{E}}}^B + k_0\dot{\varphi}_0 \\ +\boldsymbol{h}_0\cdot\nabla_{\boldsymbol{p}}\dot{\varphi}_0 - \frac{1}{\theta}\boldsymbol{q}_0\cdot\nabla_{\boldsymbol{p}}\theta + \theta\mathrm{div}_{\boldsymbol{p}}(\Phi_{0,m}) - \theta\rho_0\omega_{0,m} \geq 0. \end{aligned} \tag{2.56}$$

5. Herein, we derive important relations among $\boldsymbol{S}^A$, $\hat{\boldsymbol{T}}^A_{\mathrm{skew}}$ and $\hat{\boldsymbol{T}}^B$. From Eqs. (2.20) and (2.45), we get

$$\hat{\boldsymbol{T}}^A = \det(\boldsymbol{F}^B)\left(\boldsymbol{F}^B\right)^t \underbrace{\boldsymbol{T}^A}_{=\boldsymbol{T}^B}\left(\boldsymbol{F}^B\right)^{-t} = \det(\boldsymbol{F}^B)\left(\boldsymbol{F}^B\right)^t\boldsymbol{F}^B\left(\boldsymbol{F}^B\right)^{-1}\boldsymbol{T}^B\left(\boldsymbol{F}^B\right)^{-t}. \tag{2.57}$$

By defining the right Cauchy-Green strain tensor related with $\boldsymbol{F}^B$ as

$$\hat{\boldsymbol{C}}^B := \left(\boldsymbol{F}^B\right)^t\boldsymbol{F}^B = 2\hat{\boldsymbol{E}}^B + \boldsymbol{I},$$

and considering Eqs. (2.52) and (2.57), we obtain

$$\hat{\boldsymbol{T}}^A = \hat{\boldsymbol{C}}^B \hat{\boldsymbol{T}}^B. \tag{2.58}$$

Now, from Eqs. (2.46) and (2.58), by using the definition of $\boldsymbol{S}^A$ presented in Eq. (2.50), we have

$$\frac{1}{\det(\boldsymbol{F}^A)} \boldsymbol{F}^A \boldsymbol{S}^A \left(\boldsymbol{F}^A\right)^t + \hat{\boldsymbol{T}}^A_{\text{skew}} = \hat{\boldsymbol{C}}^B \hat{\boldsymbol{T}}^B. \tag{2.59}$$

Furthermore, Eqs. (2.36) and (2.1) lead to

$$\begin{aligned} \boldsymbol{P}^B = \det(\boldsymbol{F}) \boldsymbol{T}^B \boldsymbol{F}^{-t} &= \det(\boldsymbol{F}^A) \det(\boldsymbol{F}^B) \boldsymbol{F}^B \left(\boldsymbol{F}^B\right)^{-1} \boldsymbol{T}^B \left(\boldsymbol{F}^B\right)^{-t} \left(\boldsymbol{F}^A\right)^{-t} \\ &= \det(\boldsymbol{F}^A) \boldsymbol{F} \left(\boldsymbol{F}^A\right)^{-1} \hat{\boldsymbol{T}}^B \left(\boldsymbol{F}^A\right)^{-t}. \end{aligned} \tag{2.60}$$

This implies that Eq. (2.35a) can be rewritten in terms of $\hat{\boldsymbol{T}}^B$ as

$$\rho_0 \dot{\boldsymbol{v}}_0 = \rho_0 \boldsymbol{f}_0 + \text{div}_{\boldsymbol{p}} \left(\det(\boldsymbol{F}^A) \boldsymbol{F} \left(\boldsymbol{F}^A\right)^{-1} \hat{\boldsymbol{T}}^B \left(\boldsymbol{F}^A\right)^{-t} \right). \tag{2.61}$$

Finally, we summarize the general Lagrangian[3] governing equations in Box 2. We remember that the reader can consult the Eulerian equations of this model in Box 1 and compare them with the Lagrangian version of Box 2.

[3] In a precise mathematical description, the system of equations shown in Box 2 are not Lagrangian, once some of the present tensors are defined in the intermediate configuration $\hat{\Omega}$ (see Appendix C.2.2 for details).

Box 2: General Lagrangian governing equations

Consider the general equations

$$\dot{\rho_0} = 0$$
$$\dot{\boldsymbol{u}} = \boldsymbol{v}$$
$$\rho_0 \dot{\boldsymbol{v}}_0 = \rho_0 \boldsymbol{f}_0 + \mathrm{div}_{\boldsymbol{p}} \left(\det(\boldsymbol{F}^A) \boldsymbol{F} \left(\boldsymbol{F}^A \right)^{-1} \hat{\boldsymbol{T}}^B \left(\boldsymbol{F}^A \right)^{-t} \right)$$
$$\mathrm{div}_{\boldsymbol{p}}(\boldsymbol{h}_0) - k_0 = 0,$$
$$\frac{1}{\det(\boldsymbol{F}^A)} \boldsymbol{F}^A \boldsymbol{S}^A \left(\boldsymbol{F}^A \right)^t + \hat{\boldsymbol{T}}^A_{\mathrm{skew}} = \hat{\boldsymbol{C}}^B \hat{\boldsymbol{T}}^B$$
$$\boldsymbol{S}^B = \left(\boldsymbol{S}^B \right)^t$$
$$\boldsymbol{F} = \boldsymbol{F}^B \boldsymbol{F}^A$$
$$\rho_0 \dot{e}_0 = \boldsymbol{S}^A : \dot{\boldsymbol{E}}^A + \det(\boldsymbol{F}^A) \hat{\boldsymbol{T}}^A_{\mathrm{skew}} : \hat{\boldsymbol{W}}^A + \det(\boldsymbol{F}^A) \hat{\boldsymbol{T}}^B : \dot{\hat{\boldsymbol{E}}}^B + k_0 \dot{\varphi_0} + \boldsymbol{h}_0 \nabla_{\boldsymbol{p}}(\dot{\varphi_0})$$
$$+ \rho_0 r_0 - \mathrm{div}_{\boldsymbol{p}} \boldsymbol{q}_0,$$

in Ω_0 that must satisfying the inequality

$$-\rho_0 \left(\dot{\psi}_0 + \dot{\theta} \eta_0 \right) \boldsymbol{S}^A : \dot{\boldsymbol{E}}^A + \det(\boldsymbol{F}^A) \hat{\boldsymbol{T}}^A_{\mathrm{skew}} : \hat{\boldsymbol{W}}^A + \det(\boldsymbol{F}^A) \hat{\boldsymbol{T}}^B : \dot{\hat{\boldsymbol{E}}}^B + k_0 \dot{\varphi_0}$$
$$+ \boldsymbol{h}_0 \cdot \nabla_{\boldsymbol{p}}(\dot{\varphi}) - \frac{1}{\theta} \boldsymbol{q}_0 . \nabla_{\boldsymbol{p}} \theta \geq 0,$$

for all physical admissible processes.
In this box we presented eight governing equations. The variables are: $\boldsymbol{u}$, $\boldsymbol{v}$, $\hat{\boldsymbol{T}}^B$, $\boldsymbol{S}^A$, $\hat{\boldsymbol{T}}^A_{\mathrm{skew}}$, $\boldsymbol{W}^A$, $\boldsymbol{E}^A$,$\hat{\boldsymbol{E}}^B$, $\boldsymbol{F}$, $\boldsymbol{F}^B$, $\boldsymbol{F}^A$, $\boldsymbol{L}^A$, $\boldsymbol{L}^B$, $\boldsymbol{q}$, $\boldsymbol{h}$, e and φ.

Figure 2.3 presents the main stress tensors used in the previous derivations and summarizes the relations among them.

Figure 2.3 – Stress tensors of the model and their correlations.

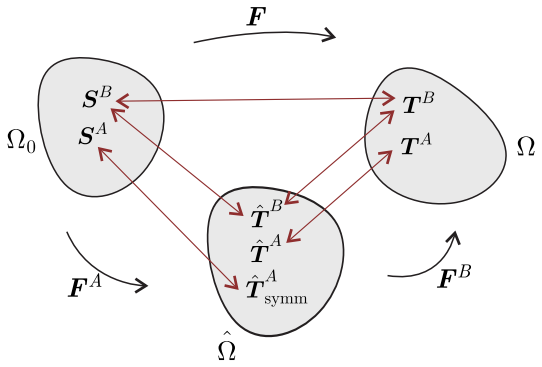

$$\boldsymbol{P}^B = \boldsymbol{F}\boldsymbol{S}^B$$
$$\boldsymbol{P}^B = \det(\boldsymbol{F}) \boldsymbol{T}^B \boldsymbol{F}^{-t}$$
$$\frac{1}{\det(\boldsymbol{F}^A)} \boldsymbol{F}^A \boldsymbol{S}^A \left(\boldsymbol{F}^A \right)^t + \hat{\boldsymbol{T}}^A_{\mathrm{skew}} = \hat{\boldsymbol{C}}^B \hat{\boldsymbol{T}}^B$$
$$\boldsymbol{S}^B = \det(\boldsymbol{F}^A) \left(\boldsymbol{F}^A \right)^{-1} \hat{\boldsymbol{T}}^B \left(\boldsymbol{F}^A \right)^{-1}$$
$$\hat{\boldsymbol{T}}^B = \left(\boldsymbol{F}^B \right)^{-1} \det(\boldsymbol{F}^B) \boldsymbol{T}^B \left(\boldsymbol{F}^B \right)^{-1}$$
$$\hat{\boldsymbol{T}}^B = \det(\boldsymbol{F}^B) \left(\boldsymbol{F}^B \right)^t \boldsymbol{T}^A \left(\boldsymbol{F}^B \right)^{-t}$$
$$\hat{\boldsymbol{T}}^A = \hat{\boldsymbol{T}}^A_{\mathrm{symm}} + \hat{\boldsymbol{T}}^A_{\mathrm{skew}}$$

Remark 2.2. *We adopt the Lagrangian version of the governing equations shown in Box 2 to follow with the derivation of the general model. The Eulerian case can be similarly constructed, but it is not included in this work.*

2.2.3 Constitutive Relations in Lagrangian Coordinates

Let us consider the body $\mathcal{B}_0$ subject to the conditions described at the beginning of Sec. 2.2.2. We want to use the previously established equations of continuum mechanics to determine the behavior of the body (the motion, deformation, temperature, stress, heat flux, entropy, and damage) at each position $\boldsymbol{p}$ and for any time t in some interval $[0, t_f]$. However, until now, we do not have enough information to solve this problem. To "complete" it, we must supplement the basic equations with constitutive equations that characterize the material of which the body is made up. The constitutive equations impose constraints on the possible responses of the material body that describe how a particular material behaves when subjected to different conditions[4].

To proceed, we must define the dependent and independent variables. As Oden (2012) states, variables whose response is experienced by observation are a natural choice for independent ones. By considering that, we define

$$\boldsymbol{S}^A = \tau_1(\Upsilon_1), \quad \hat{\boldsymbol{T}}^A_{skew} = \tau_2(\Upsilon_2), \quad \hat{\boldsymbol{T}}^B = \tau_3(\Upsilon_3), \tag{2.62-2.64}$$

$$\boldsymbol{h}_0 = \tau_4(\Upsilon_4), \quad k_0 = \tau_5(\Upsilon_5), \quad \boldsymbol{q}_0 = \tau_6(\Upsilon_6), \tag{2.65-2.67}$$

where $\tau_{(\cdot)}$ represents a constitutive relation and $\Upsilon_{(\cdot)}$ is a set of independent variables that we might expect to influence the dependent ones that will be those variables will be clear from the following developments.

Now, we want to impose restrictions on the constitutive equations by applying the second law of thermodynamics. Then, the first step is to define the general free-energy density and the pseudo-potential of dissipation used in this model.

2.2.3.1 General Free-Energy

The general free-energy density that we consider in this work is an extension of that presented in Costa-Haveroth et al. (2022) and is given by

$$\begin{aligned} \psi_0 &:= \psi\left(\theta, \nabla_{\boldsymbol{p}}\theta, \boldsymbol{E}^A, \hat{\boldsymbol{E}}^B, \mathscr{H}(\boldsymbol{E}^A), \mathscr{H}(\hat{\boldsymbol{E}}^B), \varphi, \nabla_{\boldsymbol{p}}\varphi\right) \\ &= \psi_c + \psi_m, \end{aligned} \tag{2.68}$$

where

$$\psi_c := \psi_c\left(\theta, \nabla_{\boldsymbol{p}}\theta, \boldsymbol{E}^A, \hat{\boldsymbol{E}}^B, \varphi, \nabla_{\boldsymbol{p}}\varphi\right),$$

is the traditional space-time pointwise potential, and

$$\psi_m := \psi_m\left(\theta, \nabla_{\boldsymbol{p}}\theta, \boldsymbol{E}^A, \hat{\boldsymbol{E}}^B, \mathscr{H}(\boldsymbol{E}^A), \mathscr{H}(\hat{\boldsymbol{E}}^B), \varphi, \nabla_{\boldsymbol{p}}\varphi\right),$$

[4] The constitutive relations must satisfy some fundamental principles (determinism, material frame indifference, physical consistency, amog others). See Oden (2012) for details.

is the potential related to possible memory effects in the strain field [5] (see Sec. 1.2 for comments on the fading memory effects). Furthermore, for simplicity of notation, we use $\psi = \psi_0$ henceforth.

Here, we consider only strain free materials for all time t before the initial analysis time $t_0 = 0$. It means that $\boldsymbol{E}^A(\boldsymbol{p}, t) = \hat{\boldsymbol{E}}^B(\boldsymbol{p}, t) = \boldsymbol{0}$, $\forall t < t_0$, and

$$\mathscr{H}_t(\boldsymbol{E}^A) \;=\; \mathscr{H}(\boldsymbol{E}^A)(\boldsymbol{p}, t) = \{\boldsymbol{E}^A(\boldsymbol{p}, s), 0 < s < t)\}, \tag{2.69}$$

and

$$\mathscr{H}_t(\hat{\boldsymbol{E}}^B) \;=\; \mathscr{H}(\hat{\boldsymbol{E}}^B)(\boldsymbol{p}, t) = \{\hat{\boldsymbol{E}}^B(\boldsymbol{p}, s), 0 < s < t)\}. \tag{2.70}$$

where $\mathscr{H}_t(\hat{\boldsymbol{E}}^A)$ and $\mathscr{H}_t(\hat{\boldsymbol{E}}^B)$ denote the histories of the Green-Lagrange strain tensors $\boldsymbol{E}^A$ and $\hat{\boldsymbol{E}}^B$ up to time t, respectively. Definitions (2.69) and (2.70) are particular cases of that proposed in Fabrizio (2014).

Now let us consider the rheological model presented in Fig. 2.2 to follow the arguments. Conventionally, the rheological arrangements are used to illustrate the one-dimensional case. Herein, we use it to construct an analogy for the three-dimensional case.

If we consider that the body $\mathcal{B}_0$ can be represented by the model of Fig. 2.2, then Eq. (2.68) can be rewritten as

$$\begin{aligned}
\psi \;&=\; \psi_c^A\left(\theta, \nabla_{\boldsymbol{p}}\theta, \varphi, \nabla_{\boldsymbol{p}}\varphi, \boldsymbol{E}^A\right) + \psi_m^A\left(\theta, \nabla_{\boldsymbol{p}}\theta, \varphi, \nabla_{\boldsymbol{p}}\varphi, \mathscr{H}_t(\boldsymbol{E}^A)\right) \\
&\quad + \psi_c^B\left(\theta, \nabla_{\boldsymbol{p}}\theta, \varphi, \nabla_{\boldsymbol{p}}\varphi, \hat{\boldsymbol{E}}^B\right) + \psi_m^B\left(\theta, \nabla_{\boldsymbol{p}}\theta, \varphi, \nabla_{\boldsymbol{p}}\varphi, \mathscr{H}_t(\hat{\boldsymbol{E}}^B)\right) \\
&=\; \psi_c + \psi_m,
\end{aligned} \tag{2.71}$$

where ψ_c^A and ψ_c^B are the classical space-time pointwise potentials associated with the rheological parts A and B, respectively; and ψ_m^A and ψ_m^B are the potentials that account for possible fading memory effects in the strain field for A and B, respectively. Both, $\psi_c := \psi_c^A + \psi_c^B$ and $\psi_m := \psi_m^A + \psi_m^B$, are presented here in a general way. Specialized equations for these functions can be obtained by selecting the material to be modeled (for the case of viscoelastic materials, see Sec. 3.1.1).

We follow Costa-Haveroth et al. (2022) and use the potentials ψ_m^A and ψ_m^B as

$$\psi_m^A\left(\varphi, \mathscr{H}_t(\boldsymbol{E}^A)\right) = \frac{G_m^A(\varphi)}{\rho_0}\tilde{\psi}_m^A\left(\mathscr{H}_t(\boldsymbol{E}^A)\right),$$

and

$$\psi_m^B\left(\varphi, \mathscr{H}_t(\hat{\boldsymbol{E}}^B)\right) = \frac{G_m^B(\varphi)}{\rho_0}\tilde{\psi}_m^B\left(\mathscr{H}_t(\hat{\boldsymbol{E}}^B)\right), \tag{2.72}$$

[5] Christensen (2012, pg.265) also presents the general free-energy density due to the strain and its fading memory parts. It is comparable with the total free-energy ψ of Eq. (2.68), but kept in the general form and not split as proposed here.

where $G_m^A(\varphi), G_m^B(\varphi) \geq 0$ are proper damage degradation functions that will be specified in Sec. 3.1.4, and the potentials $\tilde{\psi}_m^A(\mathscr{H}_t(\boldsymbol{E}^A))$ and $\tilde{\psi}_m^B(\mathscr{H}_t(\hat{\boldsymbol{E}}^B))$ are defined as

$$\tilde{\psi}_m^A\left(\mathscr{H}_t(\boldsymbol{E}^A)\right) = \frac{1}{\Gamma(1-\alpha)}\left[\frac{\mathscr{N}_A\left(\boldsymbol{E}_t^A, \boldsymbol{E}_0^A\right)}{t^\alpha} + \alpha\int_0^t \frac{\mathscr{N}_A\left(\boldsymbol{E}_t^A, \boldsymbol{E}_\tau^A\right)}{(t-\tau)^{1+\alpha}}\,\mathrm{d}\tau\right],$$

and

$$\tilde{\psi}_m^B\left(\mathscr{H}_t(\hat{\boldsymbol{E}}^B)\right) = \frac{1}{\Gamma(1-\alpha)}\left[\frac{\mathscr{N}_B\left(\hat{\boldsymbol{E}}_t^B, \hat{\boldsymbol{E}}_0^B\right)}{t^\alpha} + \alpha\int_0^t \frac{\mathscr{N}_B\left(\hat{\boldsymbol{E}}_t^B, \hat{\boldsymbol{E}}_\tau^B\right)}{(t-\tau)^{1+\alpha}}\,\mathrm{d}\tau\right],$$

where α is a scalar with lies in the interval $(0,1)$, $\Gamma(\cdot)$ is the standard Gamma function (ARTIN, 2015), $\boldsymbol{E}_{(\cdot)}^A := \boldsymbol{E}^A(\boldsymbol{p},\cdot)$ and $\hat{\boldsymbol{E}}_{(\cdot)}^B := \hat{\boldsymbol{E}}^B(\boldsymbol{p},\cdot)$. Furthermore, $\mathscr{N}_{(\cdot)}(\boldsymbol{Z}_1,\boldsymbol{Z}_2)$ is a continuous function of second-order symmetric tensors $\boldsymbol{Z}_{(\cdot)}$ satisfying the conditions defined in Costa-Haveroth et al. (2022):

(a) $\mathscr{N}(\boldsymbol{Z}_1,\boldsymbol{Z}_2) \geq 0,\ \forall\ \boldsymbol{Z}_{(\cdot)}$;

(b) $|\mathscr{N}(\boldsymbol{Z}_1,\boldsymbol{Z}_2)| \leq C(\boldsymbol{Z}_1,\boldsymbol{Z}_2)|\boldsymbol{Z}_1-\boldsymbol{Z}_2|^\beta$, with $\beta \geq 1+\alpha$ and $C(\boldsymbol{Z}_1,\boldsymbol{Z}_2)$ bounded as $|\boldsymbol{Z}_1-\boldsymbol{Z}_2| \to 0_+$;

(c) $|\partial_{\boldsymbol{Z}_1}\mathscr{N}(\boldsymbol{Z}_1,\boldsymbol{Z}_2)| \leq C_1(\boldsymbol{Z}_1,\boldsymbol{Z}_2)|\boldsymbol{Z}_1-\boldsymbol{Z}_2|^{\beta_1}$, with $\beta_1 \geq \alpha$ and $C_1(\boldsymbol{Z}_1,\boldsymbol{Z}_2)$ bounded as $|\boldsymbol{Z}_1-\boldsymbol{Z}_2| \to 0_+$.

We also emphasize that although the gamma function and the domain boundary have the same symbol Γ, the context used in each case is clear, with no ambiguity.

In Costa-Haveroth et al. (2022), we present several examples of possible choices for $\mathscr{N}$ satisfying the conditions (a-c). In particular, Appendix E.2.2 shows a choice for ψ_m, which leads to a constitutive relation stress/strain in terms of fractional derivatives and will be used further on.

We could include the dependence of $\tilde{\psi}_m^A$ and $\tilde{\psi}_m^B$ on θ, $\nabla_{\boldsymbol{p}}\theta$ and $\nabla_{\boldsymbol{p}}\varphi$, as indicated in Eq. (2.71); however, it results in longer computations. To maintain the exposition simple, in this work, we consider $\tilde{\psi}_m^A$ and $\tilde{\psi}_m^B$ depending only on the fading memory effects on the strain field.

By applying the standard chain rule in Eq. (2.71), we obtain the time derivative of ψ:

$$\begin{aligned}
\dot{\psi} &= \dot{\psi}_c + \dot{\psi}_m = \dot{\psi}_c^A + \dot{\psi}_c^B + \dot{\psi}_m^A + \dot{\psi}_m^B \\
&= \partial_\theta\psi_c^A\dot{\theta} + \partial_{\nabla_{\boldsymbol{p}}\theta}\psi_c^A\dot{\overline{\nabla_{\boldsymbol{p}}\theta}} + \partial_{\boldsymbol{E}^A}\psi_c^A : \dot{\boldsymbol{E}}^A + \partial_\varphi\psi_c^A\dot{\varphi} + \partial_{\nabla_{\boldsymbol{p}}\varphi}\psi_c^A\dot{\overline{\nabla_{\boldsymbol{p}}\varphi}} + \partial_\theta\psi_c^B\dot{\theta} \\
&\quad + \partial_{\nabla_{\boldsymbol{p}}\theta}\psi_c^B\dot{\overline{\nabla_{\boldsymbol{p}}\theta}} + \partial_{\hat{\boldsymbol{E}}^B}\psi_c^B : \dot{\hat{\boldsymbol{E}}}^B + \partial_\varphi\psi_c^B\dot{\varphi} + \partial_{\nabla_{\boldsymbol{p}}\varphi}\psi_c^B\dot{\overline{\nabla_{\boldsymbol{p}}\varphi}} \\
&\quad + \boldsymbol{S}_m^A : \dot{\boldsymbol{E}}^A + \frac{G_m^{A\prime}}{\rho_0}\tilde{\psi}_m\dot{\varphi} - R^A + \hat{\boldsymbol{T}}_m^B : \dot{\hat{\boldsymbol{E}}}^B + \frac{G_m^{B\prime}}{\rho_0}\tilde{\psi}_m\dot{\varphi} - R^B,
\end{aligned} \tag{2.73}$$

where $\partial_{(\cdot)}\psi_c^{(\cdot)}$ is the partial derivative of $\psi_c^{(\cdot)}$ on the subscribed variable,

$$\boldsymbol{S}_m^A = \frac{G_m^A(\varphi)}{\rho_0}\frac{1}{\Gamma(1-\alpha)}\left[\frac{\partial_{\boldsymbol{E}_t^A}\mathscr{N}_A(\boldsymbol{E}_t^A,\boldsymbol{E}_0^A)}{t^\alpha} + \alpha\int_0^t \frac{\partial_{\boldsymbol{E}_t^A}\mathscr{N}_A(\boldsymbol{E}_t^A,\boldsymbol{E}_\tau^A)}{(t-\tau)^{1+\alpha}}\,\mathrm{d}\tau\right],$$

$$\hat{\boldsymbol{T}}_m^B = \frac{G_m^B(\varphi)}{\rho_0}\frac{1}{\Gamma(1-\alpha)}\left[\frac{\partial_{\hat{\boldsymbol{E}}_t^B}\mathscr{N}_B(\hat{\boldsymbol{E}}_t^B,\hat{\boldsymbol{E}}_0^B)}{t^\alpha} + \alpha\int_0^t \frac{\partial_{\hat{\boldsymbol{E}}_t^B}\mathscr{N}_B(\hat{\boldsymbol{E}}_t^B,\hat{\boldsymbol{E}}_\tau^B)}{(t-\tau)^{1+\alpha}}\,\mathrm{d}\tau\right],$$

$$R^A = \frac{G_m^A(\varphi)}{\rho_0}\frac{\alpha}{\Gamma(1-\alpha)}\left[\frac{\mathscr{N}_A(\boldsymbol{E}_t^A,\boldsymbol{E}_0^A)}{t^{1+\alpha}} + (1+\alpha)\int_0^t \frac{\mathscr{N}_A(\boldsymbol{E}_t^A,\boldsymbol{E}_\tau^A)}{(t-\tau)^{2+\alpha}}\,\mathrm{d}\tau\right] \geq 0,$$

and

$$R^B = \frac{G_m^B(\varphi)}{\rho_0}\frac{\alpha}{\Gamma(1-\alpha)}\left[\frac{\mathscr{N}_B(\hat{\boldsymbol{E}}_t^B,\hat{\boldsymbol{E}}_0^B)}{t^{1+\alpha}} + (1+\alpha)\int_0^t \frac{\mathscr{N}_B(\hat{\boldsymbol{E}}_t^B,\hat{\boldsymbol{E}}_\tau^B)}{(t-\tau)^{2+\alpha}}\,\mathrm{d}\tau\right] \geq 0. \tag{2.74}$$

where $R^A, R^B \geq 0$, due to the property (b) of the functions $\mathscr{N}_{(\cdot)}$. Appendix E.2.1 show the obtaining of $\dot{\psi}_m^A$ and $\dot{\psi}_m^B$. It also presents a property mandatory for inequality (2.56).

2.2.3.2 The Coleman-Noll Method

In this section, we will apply the Coleman-Noll argument (COLEMAN, 1964a; COLEMAN, 1964b), which restricts the nature of constitutive equations imposed by the second law of thermodynamics. To proceed with, we split additivelly the constitutive relations in Eqs. (2.62), (2.64-2.67) as follows:

$$\boldsymbol{S}^A = {}^{(nd)}\boldsymbol{S}^A + {}^{(d)}\boldsymbol{S}^A, \tag{2.75}$$

$$\hat{\boldsymbol{T}}^B = {}^{(nd)}\hat{\boldsymbol{T}}^B + {}^{(d)}\hat{\boldsymbol{T}}^B, \tag{2.76}$$

$$\boldsymbol{h}_0 = {}^{(nd)}\boldsymbol{h}_0 + {}^{(d)}\boldsymbol{h}_0, \tag{2.77}$$

$$k_0 = {}^{(nd)}k_0 + {}^{(d)}k_0, \tag{2.78}$$

and

$$\boldsymbol{q_0} = {}^{(nd)}\boldsymbol{q}_0 + {}^{(d)}\boldsymbol{q}_0. \tag{2.79}$$

The first part terms, indicated by the left superscript ${}^{(nd)}(\cdot)$, will be derived by using the free-energy density. The remaining ones, indicated by the left superscript ${}^{(d)}(\cdot)$, will be obtained by using pseudo-potential of dissipation[6]. We expect that the ${}^{(nd)}(\cdot)$ terms do not contribute to the entropy increase in the system. On the other hand, the ${}^{(d)}(\cdot)$ part necessarily contributes to the entropy increase; that is, they are essentially dissipative terms (see Sec. 2.2.3.2.2 for further explanation on these aspects). Additionally, we consider

[6] We could also have included the split of the tensor $\hat{\boldsymbol{T}}_{\text{skew}}^A$ in this step; however, we will consider that the effects included by its conjugated tensor, $\boldsymbol{W}_A$, are purely dissipative. Then, the constitutive equation for $\hat{\boldsymbol{T}}_{\text{skew}}^A = {}^{(d)}\hat{\boldsymbol{T}}_{\text{skew}}^A$ will be obtained by using the pseudo-potential of dissipation.

that the heat flux is purely irreversible, or, on other words, ${}^{(nd)}\boldsymbol{q}_0 = \boldsymbol{0}$ and, as in Frémond and Shitikova (2002), we assume that ${}^{(d)}\boldsymbol{h}_0 = \boldsymbol{0}$.

Remember that, for any sufficiently smooth field it is correct to consider $\dot{\overline{\nabla_{\boldsymbol{p}}(\cdot)}} = \nabla_{\boldsymbol{p}}\dot{\overline{(\cdot)}}$. Then, using this relation, replacing Eq. (2.73) in the entropy inequality (2.56) and using the split of the variables into dissipative and nondissipative components given in Eqs. (2.75)-(2.79), we obtain

$$\begin{aligned}
&-\rho_0\left(\eta_0 + \partial_\theta(\psi_c^A + \psi_c^B)\right)\dot{\theta} + \left({}^{(nd)}\boldsymbol{S}^A + {}^{(d)}\boldsymbol{S}^A - \rho_0\partial_{\boldsymbol{E}^A}\psi_c^A - \rho_0\boldsymbol{S}_m^A\right) : \dot{\boldsymbol{E}}^A + \rho_0 R^A \\
&+ \left(\det(\boldsymbol{F}^A)^{(nd)}\hat{\boldsymbol{T}}^B + \det(\boldsymbol{F}^A)^{(d)}\hat{\boldsymbol{T}}^B - \rho_0\partial_{\hat{\boldsymbol{E}}^B}\psi_c^B - \rho_0\hat{\boldsymbol{T}}_m^B\right) : \dot{\hat{\boldsymbol{E}}}^B + \rho_0 R^B \\
&+ \det(\boldsymbol{F}^A)\hat{\boldsymbol{T}}^A_{\text{skew}} : \hat{\boldsymbol{W}}^A - \rho_0\partial_{\nabla_{\boldsymbol{p}}\theta}\left(\psi_c^A + \psi_c^B\right)\nabla_{\boldsymbol{p}}\left(\dot{\theta}\right) - \frac{{}^{(d)}\boldsymbol{q}_0}{\theta}\nabla_{\boldsymbol{p}}(\theta) \\
&+ \left({}^{(nd)}k_0 - G_m^{B'}\tilde{\psi}_m^B - G_m^{A'}\tilde{\psi}_m^A - \rho_0\partial_\varphi\left(\psi_c^A + \psi_c^B\right)\right)\dot{\varphi} \\
&- \left(\rho_0\partial_{\nabla_{\boldsymbol{p}}(\varphi)}\left(\psi_c^A + \psi_c^B\right) - {}^{(nd)}\boldsymbol{h}_0\right)\nabla_{\boldsymbol{p}}\dot{\varphi} + k_0^{(d)}\dot{\varphi} + \theta\text{div}_{\boldsymbol{p}}(\Phi_{0,m}) - \theta\rho_0\omega_{0,m} \geq 0. \quad (2.80)
\end{aligned}$$

This inequality will be crucial in the arguments that follow to obtain the correct constitutive relations.

2.2.3.2.1 Terms Derived from the Free-Energy

The terms derived from the free-energy are generally non-dissipative. To proceed with the arguments, we observe that dissipation is a term associated to the increase of the entropy; that is, terms appearing in the constitutive relations of a given material are considered dissipative when they contribute for the entropy increasing; otherwise, they are considered non-dissipative.

This means that the non-dissipative terms in the inequality (2.80) necessarily must not contribute to the increase of the entropy. In other words, their contribution to (2.80) must be zero. This is done by imposing that

$$\begin{aligned}
&-\rho_0\left(\eta_0 + \partial_\theta\left(\psi_c^A + \psi_c^B\right)\right)\dot{\theta} + \left({}^{(nd)}\boldsymbol{S}^A - \rho_0\partial_{\boldsymbol{E}^A}\psi_c^A - \rho_0\boldsymbol{S}_{mA}\right) : \dot{\boldsymbol{E}}^A \\
&+ \left(\det(\boldsymbol{F}^A)^{(nd)}\hat{\boldsymbol{T}}^B - \rho_0\partial_{\hat{\boldsymbol{E}}^B}\psi_c^B - \rho_0\hat{\boldsymbol{T}}_m^B\right) : \dot{\hat{\boldsymbol{E}}}^B - \rho_0\partial_{\nabla_{\boldsymbol{p}}(\theta)}\left(\psi_c^A + \psi_c^B\right)\nabla_{\boldsymbol{p}}\left(\dot{\theta}\right) \\
&+ \left({}^{(nd)}k_0 - G_m^{B'}\tilde{\psi}_m^B - G_m^{A'}\tilde{\psi}_m^A - \rho_0\partial_\varphi(\psi_c^A + \psi_c^B)\right)\dot{\varphi} \\
&- \left(\rho_0\partial_{\nabla_{\boldsymbol{p}}(\varphi)}\left(\psi_c^A + \psi_c^B\right) - {}^{(nd)}\boldsymbol{h}_0\right)\nabla_{\boldsymbol{p}}\dot{\varphi} = 0. \quad (2.81)
\end{aligned}$$

Since $\dot{\theta}$, $\dot{\boldsymbol{E}}^A$, $\dot{\hat{\boldsymbol{E}}}^B$, $\nabla_{\boldsymbol{p}}\dot{\theta}$, $\dot{\varphi}$ and $\nabla_{\boldsymbol{p}}\dot{\varphi}$ of Eq. (2.81) are independent and arbitrary, the traditional Coleman-Noll method leads to

$$\eta_0 = -\partial_\theta\psi_c, \quad \partial_{\nabla_{\boldsymbol{p}}(\theta)}\psi_c = 0, \quad (2.82\text{-}2.83)$$

$${}^{(nd)}\boldsymbol{S}^A = \rho_0\partial_{\boldsymbol{E}^A}\psi_c^A + \rho_0\boldsymbol{S}_m^A, \quad {}^{(nd)}\hat{\boldsymbol{T}}^B = \frac{1}{\det(\boldsymbol{F}^A)}\left(\rho_0\partial_{\hat{\boldsymbol{E}}^B}\psi_c^B + \rho_0\hat{\boldsymbol{T}}_m^B\right), \quad (2.84\text{-}2.85)$$

$$\boldsymbol{h}_0 = {}^{(nd)}\boldsymbol{h}_0 = \rho_0 \partial_{\nabla_{\boldsymbol{p}}(\varphi)} \psi_c, \quad {}^{(nd)}k_0 = \rho_0 \partial_\varphi \psi_c + \partial_\varphi G_m^B \tilde{\psi}_m^B + \partial_\varphi G_m^A \tilde{\psi}_m^A. \tag{2.86-2.87}$$

Note that we can obtain the constitutive equations for η_0, ${}^{(nd)}\boldsymbol{S}^A$, ${}^{(nd)}\hat{\boldsymbol{T}}^B$, ${}^{(nd)}\boldsymbol{h}_0$ and ${}^{(nd)}k_0$ directly from $\psi_c := \psi_c^A + \psi_c^B$, once it is defined. Furthermore, we note that the free-energy density cannot depend on the gradient of the temperature $\nabla_{\boldsymbol{p}}(\theta)$; a condition captured by Eq. (2.83).

2.2.3.2.2 Dissipative Terms and Pseudo-Potential of Dissipation

Next, to obtain the dissipative terms, we replace in inequality (2.80) the just obtained expressions for the non-dissipative terms; remembering that $\theta > 0$, we are left with

$$\begin{aligned} &\frac{{}^{(d)}\boldsymbol{S}^A}{\theta}\dot{\boldsymbol{E}}^A + \frac{\det(\boldsymbol{F}^A)}{\theta}{}^{(d)}\hat{\boldsymbol{T}}^B : \dot{\hat{\boldsymbol{E}}}^B + \frac{\det(\boldsymbol{F}^A)}{\theta}\hat{\boldsymbol{T}}^A_{\text{skew}} : \hat{\boldsymbol{W}}^A - \frac{{}^{(d)}\boldsymbol{q}_0}{\theta^2}\cdot\nabla_{\boldsymbol{p}}(\theta) + \frac{{}^{(d)}k_0}{\theta}\dot{\varphi} \\ &+\text{div}_{\boldsymbol{p}}(\boldsymbol{\Phi}_{0,m}) - \rho_0\omega_{0,m} + \frac{\rho_0}{\theta}(R^A + R^B) \geq 0. \end{aligned} \tag{2.88}$$

In order to establish a simple theory, we simplify this last expression by taking $\omega_{0,m} = (R^A + R^B)/\theta$ and $\boldsymbol{\Phi}_{0,m} = 0$. The last consideration means that there is no additional flux of entropy and the specific entropy production due to microscopic features other than thermal ones. Then, we obtain that R^A and R^B are related to the damage mechanisms.

Considering these results in (2.88), we obtain the following simplified form of the dissipation inequality:

$$\frac{{}^{(d)}\boldsymbol{S}^A}{\theta}\dot{\boldsymbol{E}}^A + \frac{\det(\boldsymbol{F}^A)}{\theta}{}^{(d)}\hat{\boldsymbol{T}}^B : \dot{\hat{\boldsymbol{E}}}^B + \frac{\det(\boldsymbol{F}^A)}{\theta}\hat{\boldsymbol{T}}^A_{\text{skew}} : \hat{\boldsymbol{W}}^A - \frac{{}^{(d)}\boldsymbol{q}_0}{\theta^2}\cdot\nabla_{\boldsymbol{p}}(\theta) + \frac{{}^{(d)}k_0}{\theta}\dot{\varphi} \geq 0. \tag{2.89}$$

To ensure the inequality (2.89), it is sufficient consider the coefficients ${}^{(ir)}k/\theta$, ${}^{(d)}\boldsymbol{S}^A/\theta$, ${}^{(d)}\hat{\boldsymbol{T}}^B/\theta$, $\hat{\boldsymbol{T}}^A_{\text{skew}}/\theta$, $-{}^{(d)}\boldsymbol{q}/\theta^2$ and ${}^{(d)}k_0/\theta$ as the derivatives of the pseudo-potential of dissipation ψ_d with respect to $\dot{\boldsymbol{E}}^A$, $\dot{\hat{\boldsymbol{E}}}^B$, $\hat{\boldsymbol{W}}^A$, $\nabla_{\boldsymbol{p}}(\theta)$ and $\dot{\varphi}$, respectively.

We follow (BOLDRINI et al., 2016), and adopt ψ_d with the general form

$$\psi_d = \psi_d(\dot{\boldsymbol{E}}^A, \dot{\hat{\boldsymbol{E}}}^B, \hat{\boldsymbol{W}}^A, \nabla_{\boldsymbol{p}}\theta, \dot{\varphi}, \boldsymbol{E}^A, \hat{\boldsymbol{E}}^B, \theta, \varphi, \nabla_{\boldsymbol{p}}\varphi) \geq 0, \tag{2.90}$$

where $\psi_d(\boldsymbol{0}, \boldsymbol{0}, \boldsymbol{0}, \boldsymbol{0}, 0, \Theta) = 0$ with $\Theta = \{\boldsymbol{E}^A, \hat{\boldsymbol{E}}^B, \theta, \varphi, \nabla_{\boldsymbol{p}}\varphi\}$. Furthermore, it must be convex and continuous on the independent variables $\dot{\varphi}$, $\dot{\boldsymbol{E}}^A$, $\dot{\hat{\boldsymbol{E}}}^B$, $\hat{\boldsymbol{W}}^A$, and $\nabla_{\boldsymbol{p}}\theta$ (details on the pseudo-potential of dissipation properties can be found in Frémond and Shitikova (2002, p. 22)). Then, when ψ_d is differentiable. we obtain that

$${}^{(d)}\boldsymbol{S}^A = \theta\partial_{\dot{\boldsymbol{E}}^A}\psi_d, \quad {}^{(d)}\hat{\boldsymbol{T}}^B = \frac{\theta}{\det(\boldsymbol{F}^A)}\partial_{\dot{\hat{\boldsymbol{E}}}^B}\psi_d, \quad \hat{\boldsymbol{T}}^A_{\text{skew}} = \frac{\theta}{\det(\boldsymbol{F}^A)}\partial_{\boldsymbol{W}^A}\psi_d, \tag{2.91-2.93}$$

$${}^{(d)}\boldsymbol{q}_0 = -\theta^2\partial_{\nabla_{\boldsymbol{p}}(\theta)}\psi_d, \quad {}^{(d)}k_0 = \theta\partial_{\dot{\varphi}}\psi_d. \tag{2.94-2.95}$$

For the case where ψ_d is non-differentiable, the previous derivatives must be substituted by subdifferentials.

3 A Damage Phase-Field Model with Fractional Viscoelasticity

The framework derived in Chapter 2 is rather general since suitable free-energy potential, ψ, and pseudo-potential of dissipation, ψ_d, allow us to model different materials. Henceforward, we want to particularize it to the class of viscoelastic materials.

In this chapter, we present a thermodynamically consistent framework that couples the features of phase-field methodology and the fractional derivative to describe the damage in viscoelastic materials. Written in the Lagrangian configuration, the resulting model describes the diffuseness of the crack interface using a scalar phase-field variable. Such model allows for describing finite strain and includes non-isothermal considerations in a thermodynamic consistent way. Furthermore, the model can be particularized to meet different rheological arrangements.

3.1 Viscoelastic Series Model

As discussed in Sec. 2.1, viscoelastic series models can be represented by the rheological arrangement shown in Fig. 2.2. Strictly speaking, rheological arrangements are used to illustrate the one-dimensional case; however, we will use it to give physical meaning to the following arguments and construct an analogy for the three-dimensional case. Remember also that the the multiplicative decomposition of $\boldsymbol{F}$, given in Eq. (2.1), governs the strain process.

3.1.1 A Particular Free-Energy Potential

Consider the rheological arrangement illustrated in Fig. 3.1. If we assume that there is no memory components for part A, then we can take $\psi_m^A = 0$ in Eq. (2.71), which simplifies to

$$\psi = \psi_c^A(\theta, \varphi, \nabla_{\boldsymbol{p}}(\varphi), \boldsymbol{E}^A) + \psi_c^B(\theta, \varphi, \nabla_{\boldsymbol{p}}(\varphi), \hat{\boldsymbol{E}}^B) + \psi_m^B\left(\theta, \varphi, \nabla_{\boldsymbol{p}}(\varphi), \mathscr{H}_t(\hat{\boldsymbol{E}}^B)\right). \quad (3.1)$$

Here, $\psi_c := \psi_c^A + \psi_c^B$ does not depend on $\nabla_{\boldsymbol{p}}(\theta)$ due to Eq. (2.83).

The "local" free-energy density ψ_c^A is split in three terms:

$$\rho_0\psi_c^A\left(\theta, \varphi, \nabla_{\boldsymbol{p}}(\varphi), \boldsymbol{E}^A\right) = G_h^A(\varphi)\,\psi_h^A\left(\boldsymbol{E}^A\right) + \psi_\theta^A(\theta) + \mathcal{I}^A\left(\varphi, \nabla_{\boldsymbol{p}}(\varphi), \boldsymbol{E}^A\right). \quad (3.2)$$

Similarly, for ψ_c^B we have

$$\rho_0\psi_c^B\left(\theta, \varphi, \nabla_{\boldsymbol{p}}(\varphi), \hat{\boldsymbol{E}}^B\right) = G_h^B(\varphi)\,\psi_h^B\left(\hat{\boldsymbol{E}}^B\right) + \psi_\theta^B(\theta) + \mathcal{I}^B\left(\varphi, \nabla_{\boldsymbol{p}}(\varphi), \hat{\boldsymbol{E}}^B\right). \quad (3.3)$$

Figure 3.1 – Rheological connection of two components in series where Part A has no contribution of memory effects. This arrangement is used for the viscoelastic model of this work.

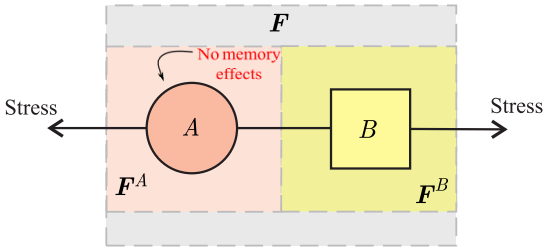

Remark 3.1. *Herein, the energies with the subscript* $\psi_h^{(\cdot)}$ *are related to the hyperelastic deformation and* $G_h^{(\cdot)}(\varphi) \geq 0$ *are proper damage degradation functions of the elastic part of the free-energy which will be characterized and discussed further in Sec. 3.1.4. The energies with the subscript* $\psi_\theta^{(\cdot)}$ *are related to purely thermal effects. Damage contributions are considered in* $\mathcal{I}^{(\cdot)}$.

We consider that both parts, A and B, of the rheological model of Fig. 3.1 will include a hyperelastic compressible Neo-Hookean spring (see Appendix D). In this case, the energy density related to a compressible Neo-Hookean material in part A is given, according to Bonet and Wood (2008), by

$$\begin{aligned} \psi_h^A &:= \psi_h^A\left(\boldsymbol{E}^A\right) \\ &= \frac{\mu^A}{2}\left[\operatorname{tr}\left(\boldsymbol{C}^A\right) - 3\right] - \mu^A \ln\left[\det\left(\boldsymbol{C}^A\right)\right]^{\frac{1}{2}} + \frac{\lambda^A}{2}\left[\ln\left(\det\left(\boldsymbol{C}^A\right)\right)^{\frac{1}{2}}\right]^2, \end{aligned} \tag{3.4}$$

where μ^A and λ^A are the associated Lamé material parameters and $\boldsymbol{C}^A$ is the right Cauchy-Green strain tensor related to part A and defined by

$$\boldsymbol{C}^A := \left(\boldsymbol{F}^A\right)^t \boldsymbol{F}^A = 2\boldsymbol{E}^A + \boldsymbol{I}. \tag{3.5}$$

In the same way, for part B, we have the following energy density:

$$\begin{aligned} \psi_h^B &:= \psi_h^B\left(\hat{\boldsymbol{E}}^B\right) \\ &= \frac{\mu^B}{2}\left[\operatorname{tr}\left(\hat{\boldsymbol{C}}^B\right) - 3\right] - \mu^B \ln\left[\det\left(\hat{\boldsymbol{C}}^B\right)\right]^{\frac{1}{2}} + \frac{\lambda^B}{2}\left[\ln\left(\det\left(\hat{\boldsymbol{C}}^B\right)\right)^{\frac{1}{2}}\right]^2. \end{aligned} \tag{3.6}$$

where μ^B and λ^B are the Lamé material parameters and $\hat{\boldsymbol{C}}^B$ is the right Cauchy-Green strain tensor defined in Eq. (2.58). The non-linear elastic behavior (hyperelasticity) given by Eqs. (3.4) and (3.6) allows to consider finite strain.

The part of the free-energies related to thermal effects are assumed to be as in Frémond and Shitikova (2002):

$$\psi_\theta^{(\cdot)}(\theta) = -c_v \theta \ln \theta,$$

where c_v is the heat capacity.

According to Costa-Haveroth et al. (2022), the energy densities that account for the damage contribution are given by

$$\mathcal{I}^{(\cdot)}\left(\varphi, \nabla_{\boldsymbol{p}}\varphi, \cdot\right) = g_c\left(\frac{\gamma_c}{2}\nabla_{\boldsymbol{p}}\varphi \cdot \boldsymbol{C}^{-1}\nabla_{\boldsymbol{p}}\varphi + \frac{1}{\gamma_c}H(\varphi)\right), \tag{3.7}$$

where $\boldsymbol{C} = \boldsymbol{F}^t\boldsymbol{F}$ (see Eq. (C.25)) represents the total right Cauchy-Green strain tensor for the system. The Griffith fracture constant $g_c > 0$ is fixed (PEREZ, 2016) and

$$H(\varphi) = \frac{\varphi^2}{2}, \tag{3.8}$$

is the potential for $\varphi \in [0, 1]$ (BOLDRINI et al., 2016). The constant $\gamma_c > 0$ characterizes the magnitude of the width for the fractured layers. From Bourdin, Francfort and Marigo (2008), it regulates the crack path diffuseness and can recover the sharp cracks in the limit $\gamma_c \to 0$. Furthermore, according to Haveroth et al. (2020), γ_c is also related to crack propagation speed; as γ_c increases, the crack propagates faster.

Remark 3.2. *The first term in the right-hand side of (3.7), when expressed in Eulerian coordinates is exactly* $\psi^{(\varphi)} = g_c\frac{\gamma_c}{2}|\nabla_{\boldsymbol{x}}(\varphi)|^2$. *This expression corresponds to the standard physical assumption that some quantity of the energy related to damage concentrates in transition layers of the damage phase-field.*

For ψ_m^B, the free-energy density related with memory effects in part B, we consider the definition in Eq. (2.72) with $\tilde{\psi}_m^B$ given by

$$\tilde{\psi}_m^B = \frac{\kappa}{\rho_0}\left[\frac{\left(\hat{\boldsymbol{E}}_t^B - \hat{\boldsymbol{E}}_0\right) : \boldsymbol{\mathcal{A}} : \left(\hat{\boldsymbol{E}}_t^B - \hat{\boldsymbol{E}}_0^B\right)}{t^\alpha} + \alpha\int_0^t \frac{\left(\hat{\boldsymbol{E}}_t^B - \hat{\boldsymbol{E}}_\tau^B\right) : \boldsymbol{\mathcal{A}} : \left(\hat{\boldsymbol{E}}_t^B - \hat{\boldsymbol{E}}_\tau^B\right)}{(t-\tau)^{1+\alpha}}\,\mathrm{d}\tau\right], \tag{3.9}$$

and

$$\kappa = \frac{1}{2\Gamma(1-\alpha)}.$$

Here, $\boldsymbol{\mathcal{A}}$ is a constitutive forth-order symmetric positive definite tensor whose specific form will be described in Sec. 5.1.1. Remember also that, $\hat{\boldsymbol{E}}_{(\cdot)}^B := \hat{\boldsymbol{E}}^B(\boldsymbol{p}, (\cdot))$. See further discussion about the choice of $\tilde{\psi}_m^B$ in Appendix E.2.2.

Deriving Eq. (3.9) with respect to $\hat{\boldsymbol{E}}^B$ leads to the stress associated to the memory effects in part B:

$$\begin{aligned}\hat{\boldsymbol{T}}_m^B \;=\; & \frac{G_m^B(\varphi)}{\rho_0}\Big[\boldsymbol{\mathcal{A}} : {}_0\mathrm{D}_t^{\,\alpha}\hat{\boldsymbol{E}}_t^B + \kappa\frac{\left(\hat{\boldsymbol{E}}_t^B - \hat{\boldsymbol{E}}_0^B\right) : \partial_{\hat{\boldsymbol{E}}^B}\boldsymbol{\mathcal{A}} : \left(\hat{\boldsymbol{E}}_t^B - \hat{\boldsymbol{E}}_0^B\right)}{t^\alpha} \\ & + \kappa\alpha\int_0^t \frac{\left(\hat{\boldsymbol{E}}_t^B - \hat{\boldsymbol{E}}_\tau^B\right) : \partial_{\hat{\boldsymbol{E}}^B}\boldsymbol{\mathcal{A}}(\hat{\boldsymbol{E}}_t^B) : \left(\hat{\boldsymbol{E}}_t^B - \hat{\boldsymbol{E}}_\tau^B\right)}{(t-\tau)^{1+\alpha}}\mathrm{d}\tau\Big],\end{aligned} \tag{3.10}$$

and

$$R_m^B = \frac{G_m^B(\varphi)}{\rho_0}\kappa\left[\frac{\left(\hat{\boldsymbol{E}}_t^B - \hat{\boldsymbol{E}}_0^B\right):\boldsymbol{\mathcal{A}}:\left(\hat{\boldsymbol{E}}_t^B - \hat{\boldsymbol{E}}_0^B\right)}{t^{\alpha+1}} + (\alpha+1)\int_0^t \frac{\left(\hat{\boldsymbol{E}}_t^B - \hat{\boldsymbol{E}}_\tau^B\right):\boldsymbol{\mathcal{A}}:\left(\hat{\boldsymbol{E}}_t^B - \hat{\boldsymbol{E}}_\tau^B\right)}{(t-\tau)^{2+\alpha}}\mathrm{d}\tau\right], \tag{3.11}$$

where R_m^B is defined previously for the general case in (2.74). Equation (3.10) presents the term ${}_0\mathrm{D}_t^{\alpha}\hat{\boldsymbol{E}}^B$, that is the Caputo fractional derivative of $\hat{\boldsymbol{E}}^B$ (see Sec. 1.2.2); the tensor $\boldsymbol{\mathcal{A}}$ weights this fractional derivatives. Appendix E.2.2 details how Eq. (3.10) is obtaining.

3.1.2 Specialization of the Pseudo-Potential of Dissipation

Previously, we established that the specific model presented in this chapter does not have memory components for part A, as can be seen in Fig. 3.1. In other words, part A is non-dissipative and, consequently, the pseudo-potential of dissipation does not depend on $\dot{\boldsymbol{E}}^A$. Therefore, a possible choice for ψ_d, that ensures the conditions in Sec. 2.2.3.2.2, is

$$\psi_d\left(\dot{\hat{\boldsymbol{E}}}^B, \hat{\boldsymbol{W}}^A, \nabla_{\boldsymbol{p}}(\theta), \dot{\varphi}, \Theta\right) = \frac{\tilde{b}(\Theta)}{2}|\dot{\hat{\boldsymbol{E}}}^B|^2 + \frac{\tilde{\epsilon}(\Theta)}{2}|\hat{\boldsymbol{W}}^A|^2 + \frac{\tilde{c}(\Theta)}{2}\nabla_{\boldsymbol{p}}(\theta)\cdot\boldsymbol{C}^{-1}\nabla_{\boldsymbol{p}}\theta + \frac{\tilde{\lambda}(\Theta)}{2}|\dot{\varphi}|^2, \tag{3.12}$$

where $\Theta = \{\boldsymbol{E}^A, \hat{\boldsymbol{E}}^B, \theta, \varphi, \nabla_{\boldsymbol{p}}(\varphi)\}$; $\tilde{b} > 0$ and $\tilde{c} > 0$ are the viscous damping and the heat conductivity associated with the material, respectively (BOLDRINI et al., 2016). The parameter $\tilde{\epsilon} > 0$ can be considered a spin variable associated with the material, and the inverse of $\tilde{\lambda}$ is the rate of change of φ, and we take it as in Boldrini et al. (2016):

$$\frac{1}{\tilde{\lambda}} = \frac{c_\lambda}{(1+\delta-\varphi)^\zeta} > 0, \tag{3.13}$$

where $c_\lambda > 0$ and $\zeta > 0$ are material parameters and δ is a very small perturbation inserted to avoid singularity when $\varphi = 1$. See Costa-Haveroth et al. (2022) for comments on the form of Eq. (3.12).

By considering the pseudo-potential of dissipation of Eq. (3.12), and Eqs. (2.92-2.95), we obtain

$${}^{(d)}\hat{\boldsymbol{T}}^B = \frac{\theta}{\det(\boldsymbol{F}^A)}\tilde{b}(\Theta)\dot{\hat{\boldsymbol{E}}}^B, \qquad \boldsymbol{T}_{skew}^A = \frac{\theta}{\det(\boldsymbol{F}^A)}\tilde{\epsilon}(\Theta)\boldsymbol{W}^A, \tag{3.14-3.15}$$

$${}^{(d)}k_0 = \theta\tilde{\lambda}\dot{\varphi}, \qquad {}^{(d)}\boldsymbol{q}_0 = -\theta^2\tilde{c}(\Theta)\nabla_{\boldsymbol{p}}\theta. \tag{3.16-3.17}$$

3.1.3 Stress Tensors of the Model

We have three stress tensors associated with the proposed model: $\boldsymbol{S}^A$, $\hat{\boldsymbol{T}}^B$ and $\hat{\boldsymbol{T}}^A_{\text{skew}}$. Once $\hat{\boldsymbol{T}}^A_{\text{skew}}$ is given by Eq. (3.15), this section focus on obtaining $\boldsymbol{S}^A$ and $\hat{\boldsymbol{T}}^B$.

The specific viscoelastic model developed in this chapter does not present dissipative terms in part A; then ${}^{(d)}\boldsymbol{S}^A = \boldsymbol{0}$. Furthermore, as part A does not present memory terms, $\boldsymbol{S}^A_m = 0$. From Eqs (2.75), (2.84), and (3.2), it is possible to write the stress tensor $\boldsymbol{S}^A$ according to

$$\boldsymbol{S}^A = \rho_0 \partial_{\boldsymbol{E}^A} \psi^A_c = G^A_h \partial_{\boldsymbol{E}^A} \psi^A_h + \partial_{\boldsymbol{E}^A} \mathcal{I}^A. \tag{3.18}$$

From Eq. (3.4), it is simple to obtain

$$\partial_{\boldsymbol{E}^A} \psi^A_h = \mu^A \left(\boldsymbol{I} - \left(\boldsymbol{C}^A \right)^{-1} \right) + \lambda^A \ln \left(\det \left(\boldsymbol{C}^A \right)^{1/2} \right) \left(\boldsymbol{C}^A \right)^{-1},$$

as show in Appendix D.

On the other hand, the analytic development of $\partial_{\boldsymbol{E}^A} \mathcal{I}^A$ holds extensive algebraic difficulties (see Appendix E.3 for comments); then, it will not explicitly evaluated at this moment.

In summary, Eq. (3.18) can be rewritten, as

$$\boldsymbol{S}^A = G^A_h \left[\mu^A \left(\boldsymbol{I} - \left(\boldsymbol{C}^A \right)^{-1} \right) + \lambda^A \ln \left(\det \left(\boldsymbol{C}^A \right)^{1/2} \right) \left(\boldsymbol{C}^A \right)^{-1} \right] + \partial_{\boldsymbol{E}^A} \mathcal{I}^A. \tag{3.19}$$

The stress tensor $\hat{\boldsymbol{T}}^B$ can be obtained by replacing Eqs. (2.85) and (2.92) in Eq. (2.76):

$$\begin{aligned} \hat{\boldsymbol{T}}^B &= {}^{(nd)}\hat{\boldsymbol{T}}^B + {}^{(d)}\hat{\boldsymbol{T}}^B \\ &= \frac{1}{\det(\boldsymbol{F}^A)} \left(\rho_0 \partial_{\hat{\boldsymbol{E}}^B} \psi^B_c + \rho_0 \hat{\boldsymbol{T}}^B_m + \theta \partial_{\dot{\hat{\boldsymbol{E}}}^B} \psi_d \right). \end{aligned} \tag{3.20}$$

The above equation can be associated with the stress generated by part B of the rheological arrangement given in Fig. 3.1.

By considering Eq. (3.3), we obtain

$$\partial_{\hat{\boldsymbol{E}}^B} \psi^B_c = \frac{1}{\rho_0} \left(G^B_h \partial_{\hat{\boldsymbol{E}}^B} \psi^B_h + \partial_{\hat{\boldsymbol{E}}^B} \mathcal{I}^B \right). \tag{3.21}$$

The derivative in the first right-hand side term is obtained from Eq. (3.6) (see details in Appendix D), which leads to

$$\partial_{\hat{\boldsymbol{E}}^B} \psi^B_h = \mu^B \left(\boldsymbol{I} - \left(\hat{\boldsymbol{C}}^B \right)^{-1} \right) + \lambda^B \ln \left(\det \left(\hat{\boldsymbol{C}}^B \right)^{1/2} \right) \left(\hat{\boldsymbol{C}}^B \right)^{-1},$$

whereas the second one is evaluated by replacing

$$\boldsymbol{C}^{-1} = \boldsymbol{F}^{-1} (\boldsymbol{F})^{-t} = \left(\boldsymbol{F}^A \right)^{-1} \left(\boldsymbol{F}^B \right)^{-1} \left(\boldsymbol{F}^B \right)^{-t} \left(\boldsymbol{F}^A \right)^{-t} = \left(\boldsymbol{F}^A \right)^{-1} \left(\hat{\boldsymbol{C}}^B \right)^{-1} \left(\boldsymbol{F}^A \right)^{-t}. \tag{3.22}$$

in (3.7) and remembering that $\hat{\boldsymbol{C}}^B = 2\hat{\boldsymbol{E}}^B + \boldsymbol{I}$:

$$\partial_{\hat{\boldsymbol{E}}^B}\mathcal{I}^B = 2\partial_{\hat{\boldsymbol{C}}^B}\mathcal{I}^B = \partial_{\hat{\boldsymbol{C}}^B}\left[g_c\gamma_c\nabla_{\boldsymbol{p}}\varphi\cdot\left(\boldsymbol{F}^A\right)^{-1}\left(\hat{\boldsymbol{C}}^B\right)^{-1}\left(\boldsymbol{F}^A\right)^{-1}\nabla_{\boldsymbol{p}}\left(\varphi\right)\right]. \tag{3.23}$$

After algebraic manipulation, Eq. (3.23) becomes

$$\partial_{\hat{\boldsymbol{E}}^B}\mathcal{I}^B = -g_c\gamma_c\left[\left(\hat{\boldsymbol{C}}^B\right)^{-1}\left(\boldsymbol{F}^A\right)^{-t}\nabla_{\boldsymbol{p}}\left(\varphi\right)\right]\otimes\left[\left(\hat{\boldsymbol{C}}^B\right)^{-1}\left(\boldsymbol{F}^A\right)^{-t}\nabla_{\boldsymbol{p}}\left(\varphi\right)\right]. \tag{3.24}$$

For details on obtaining Eq. (3.24), see Appendix E.4.

Taking into account Eqs. (3.20), (3.14) and (3.24), and considering the expression for $\hat{\boldsymbol{T}}_m^B$ given by Eq. (3.10), the second Piola-Kirchhoff stress tensor $\hat{\boldsymbol{T}}^B$ is given by

$$\begin{aligned}\hat{\boldsymbol{T}}^B &= \frac{1}{\det\left(\boldsymbol{F}^A\right)}\left\{G_h^B\left[\mu^B\left(\boldsymbol{I}-\left(\hat{\boldsymbol{C}}^B\right)^{-1}\right)+\lambda^B\ln\left(\det\left(\hat{\boldsymbol{C}}^B\right)^{1/2}\right)\left(\hat{\boldsymbol{C}}^B\right)^{-1}\right]\right.\\
&\quad+\theta\tilde{b}\left(\Theta\right)\dot{\hat{\boldsymbol{E}}}^B - g_c\gamma_c\left[\left(\hat{\boldsymbol{C}}^B\right)^{-1}\left(\boldsymbol{F}^A\right)^{-t}\nabla_{\boldsymbol{p}}\varphi\right]\otimes\left[\left(\hat{\boldsymbol{C}}^B\right)^{-1}\left(\boldsymbol{F}^A\right)^{-t}\nabla_{\boldsymbol{p}}\varphi\right]\\
&\quad+\frac{G_m^B}{\rho_0}\left[\boldsymbol{\mathcal{A}}:{}_0\mathrm{D}_t{}^{\alpha}(\hat{\boldsymbol{E}}_t^B)+\kappa\frac{\left(\hat{\boldsymbol{E}}_t^B-\hat{\boldsymbol{E}}_0^B0\right):\partial_{\hat{\boldsymbol{E}}^B}\boldsymbol{\mathcal{A}}:\left(\hat{\boldsymbol{E}}_t^B-\hat{\boldsymbol{E}}_0^B\right)}{t^{\alpha}}\right.\\
&\quad\left.\left.+\kappa\alpha\int_0^t\frac{\left(\hat{\boldsymbol{E}}_t^B-\hat{\boldsymbol{E}}_\tau^B\right):\partial_{\hat{\boldsymbol{E}}^B}\boldsymbol{\mathcal{A}}:\left(\hat{\boldsymbol{E}}_t^B-\hat{\boldsymbol{E}}_\tau^B\right)}{(t-\tau)^{1+\alpha}}\,\mathrm{d}\tau\right]\right\} \qquad (3.25)\\
&= \hat{\boldsymbol{T}}_{\text{class}}^B+\hat{\boldsymbol{T}}_{\text{frac}}^B, \qquad (3.26)\end{aligned}$$

where

$$\begin{aligned}\hat{\boldsymbol{T}}_{\text{class}}^B &= \frac{1}{\det\left(\boldsymbol{F}^A\right)}\left\{G_h^B\left[\mu^B\left(\boldsymbol{I}-\left(\hat{\boldsymbol{C}}^B\right)^{-1}\right)+\lambda^B\ln\left(\det\left(\hat{\boldsymbol{C}}^B\right)^{1/2}\right)\left(\hat{\boldsymbol{C}}^B\right)^{-1}\right]\right.\\
&\quad\left.+\theta\tilde{b}\left(\Theta\right)\dot{\hat{\boldsymbol{E}}}^B - g_c\gamma_c\left[\left(\hat{\boldsymbol{C}}^B\right)^{-1}\left(\boldsymbol{F}^A\right)^{-t}\nabla_{\boldsymbol{p}}\varphi\right]\otimes\left[\left(\hat{\boldsymbol{C}}^B\right)^{-1}\left(\boldsymbol{F}^A\right)^{-t}\nabla_{\boldsymbol{p}}\left(\varphi\right)\right]\right\},\end{aligned} \tag{3.27}$$

and

$$\begin{aligned}\hat{\boldsymbol{T}}_{\text{frac}}^B &= \frac{1}{\det\left(\boldsymbol{F}^A\right)}\left\{\frac{G_m^B}{\rho_0}\left[\boldsymbol{\mathcal{A}}:{}_0\mathrm{D}_t{}^{\alpha}(\hat{\boldsymbol{E}}_t^B)+\kappa\frac{\left(\hat{\boldsymbol{E}}_t^B-\hat{\boldsymbol{E}}_0^B\right):\partial_{\hat{\boldsymbol{E}}^B}\boldsymbol{\mathcal{A}}:\left(\hat{\boldsymbol{E}}_t^B-\hat{\boldsymbol{E}}_0^B\right)}{t^{\alpha}}\right.\right.\\
&\quad\left.\left.+\kappa\alpha\int_0^t\frac{\left(\hat{\boldsymbol{E}}_t^B-\hat{\boldsymbol{E}}_\tau^B\right):\partial_{\hat{\boldsymbol{E}}^B}\boldsymbol{\mathcal{A}}:\left(\hat{\boldsymbol{E}}_t^B-\hat{\boldsymbol{E}}_\tau^B\right)}{(t-\tau)^{1+\alpha}}\,\mathrm{d}\tau\right]\right\}.\end{aligned} \tag{3.28}$$

As will be discussed in Sec. 3.2, by using the analogy with the rheological arrangement, the first term in (3.27) represents the stress by the Neo-Hookean spring; the second one represents a dashpot; and the last one gives the thermal influences. On the other hand, $\hat{\boldsymbol{T}}_{\text{frac}}^B$, represents the stress by other memory terms. Costa-Haveroth et al. (2022) presented a study on the last two terms of Eq. (3.28) and shown that they give almost no contribution to the total stress, and can be neglected in several cases.

3.1.4 Degradation Functions

In this section, we review the degradation functions $G^{(\cdot)}_{(\cdot)}(\varphi)$, that appear in the stress Equations (3.19) and (3.25). These functions induce the damage effect describing the stiffness variation between undamaged (without voids) and damaged material. According to Miehe, Welschinger and Hofacker (2010b), the degradation function $G^{(\cdot)}_{(\cdot)}(\varphi)$ must satisfy:

$$G^{(\cdot)}_{(\cdot)}(\varphi) > 0, \quad G^{(\cdot)}_{(\cdot)}(\varphi) = \begin{cases} 1 & \text{if } \varphi = 0, \\ 0 & \text{if } \varphi = 1, \end{cases} \quad \text{and} \quad \partial_\varphi G^{(\cdot)}_{(\cdot)}(1) = 0. \tag{3.29}$$

There are many proposals for $G^{(\cdot)}_{(\cdot)}(\varphi)$ depending on the material (KUHN; SCHLÜTER; MÜLLER, 2015; BORDEN et al., 2016; HAVEROTH et al., 2020). For instance, Miehe, Hofacker and Welschinger (2010b) use the function

$$G^{(\cdot)}_{(\cdot)}(\varphi) := G_1(\varphi) = (1-\varphi)^2. \tag{3.30}$$

In fact, Eq. (3.30) is one of the most used in the literature for modeling of crack in metals; however, it is not a suitable option to model viscoelasticity, which presents a distinct fracture pattern.

As commented in Sec. 1.2.4, the damage process in viscoelastic materials combines two failure mechanisms: slippage and chain disjuction. When the slippage along the chains arises, the stiffness decreases. As the slippage evolves, the stress levels increase. In contrast, function G_1 yields a significant loss of stiffness, as shown in Fig. 3.2.

Figure 3.2 – Degradation functions.

(a) G_2 for $b = c = 1$ and a varying. (b) G_2 for $a = c = 1$ and b varying. (c) G_2 for $a = b = 1$ and c varying.

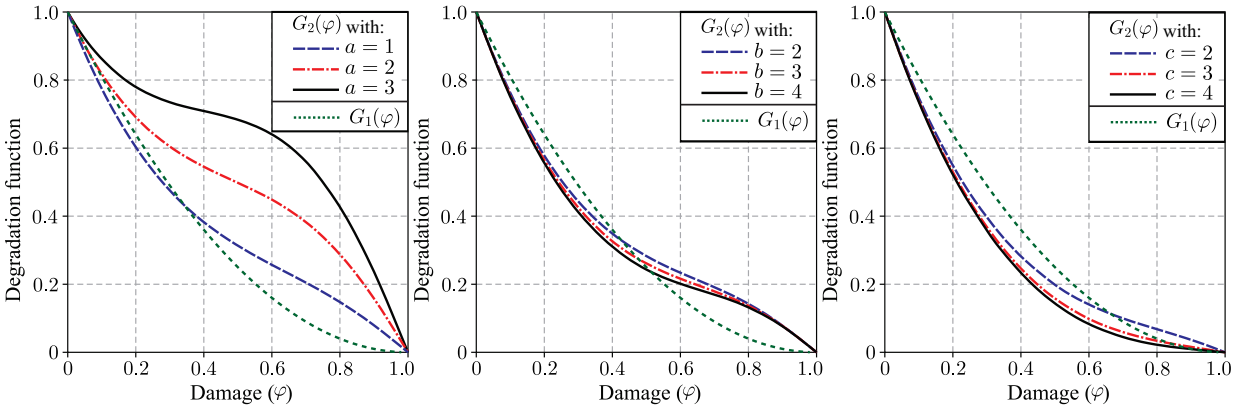

Costa-Haveroth et al. (2022)

Based on the above mentioned criticisms, in Costa-Haveroth et al. (2022), we designed a novel degradation function defined by

$$G^{(\cdot)}_{(\cdot)}(\varphi) := G_2(\varphi) = (1-\varphi)^3 + \frac{a\varphi^d(1-\varphi)^d}{1+b(\varphi-c)^2}, \tag{3.31}$$

where $a, b, c > 0$ and $d = 1.05$. We fix the constant d to obtain the expected behavior in G_2; however it could be included as an extra parameter in the inverse identification. Figure 3.2 presents the response of G_2 by the variation of the parameters a, b and c. Note that, differently from the quadratic function G_1, the new function G_2 is able to introduce transition ranges in the damage process.

For a specific region, function G_2 makes the damage grow slowly. This behavior can be related with the microstructural evolution in strain processes for viscoelastic materials. In fact, the parameters a, b, and c, used in Eq. (3.31) govern G_2 and can be related to the slippage of the chains. In other words, the variation of these parameters changes the concavity of G_2 accordingly, and allows flexibility for modeling materials, once the speed between slippage and the rupture is best controlled.

Section 5.1.3.2 shows the comparisons between G_1 and G_2, as a review on the results previously published in Costa-Haveroth et al. (2022).

3.1.5 System of Equations for the Viscoelastic Series Model

In this section, we outline the final system of equations that accounts for the evolution of motion, damage, and temperature in a body with viscoelastic behavior.

1. Firstly, the *motion* is governed by the balance of linear momentum:

$$\rho_0 \dot{\boldsymbol{v}}_0 = \rho_0 \boldsymbol{f}_0 + \operatorname{div}_{\boldsymbol{p}} \left(\det(\boldsymbol{F}^A) \boldsymbol{F} \left(\boldsymbol{F}^A \right)^{-1} \hat{\boldsymbol{T}}^B \left(\boldsymbol{F}^A \right)^{-t} \right), \tag{3.32}$$

   where $\dot{\boldsymbol{u}} = \boldsymbol{v}$. We recall that $\hat{\boldsymbol{T}}^B$ is the stress given by Eq. (3.25).

2. The equation for the *damage* can be found by replacing k_0 and $\boldsymbol{h}_0$ in Eq. (2.41a) and applying Eqs. (2.77), (2.78) and (2.95). Remembering that $\tilde{\psi}_m^A = 0$ in this model, we obtain

$$\theta \partial_{\dot{\varphi}} \psi_d = \operatorname{div}_{\boldsymbol{p}} (\rho \partial_{\nabla_{\boldsymbol{p}} \varphi} \psi_c) - \rho_0 \partial_{\varphi} \psi_c - \partial_{\varphi} G_m^B \tilde{\psi}_m^B. \tag{3.33}$$

   Note that, Eq. (3.33) is written in terms of the potentials ψ_d, ψ_c and $\tilde{\psi}_m^B$, given by Eqs. (3.12), (3.1) and (3.9), respectively. Then, by solving the derivatives in Eq. (3.33), we obtain

$$\dot{\varphi} = \frac{1}{\tilde{\lambda}\theta} \operatorname{div}_{\boldsymbol{p}} \left(2 g_c \gamma_c (\boldsymbol{C})^{-1} \nabla_{\boldsymbol{p}} (\varphi) \right) - \frac{2 g_c \partial_{\varphi} H(\varphi)}{\gamma_c \tilde{\lambda}\theta} - \frac{\partial_{\varphi} G}{\tilde{\lambda}\theta} \left(\psi_h^A + \psi_h^B + \tilde{\psi}_m^B \right), \tag{3.34}$$

   where $G = G_h^{(\cdot)} = G_m^{(\cdot)}$, meaning that we choose, for simplicity, degrading the hyperelastic part of the model and the part associated with memory effects in the same way.

3. The equation that governs the *temperature* variation is obtained by Eq. (2.54). We use Eqs. (2.94), (2.78), (2.87), and (2.86) to obtain

$$\begin{aligned}\rho_0\dot{e}_0 &= -\mathrm{div}_{\boldsymbol{p}}(\theta^2\partial_{\nabla_{\boldsymbol{p}}(\theta)}\psi_d) + \rho_0 r_0 + \boldsymbol{S}^A : \dot{\boldsymbol{E}}^A + \det(\boldsymbol{F}^A)\hat{\boldsymbol{T}}^A_{\text{skew}} : \hat{\boldsymbol{W}}^A \\ &\quad + \det(\boldsymbol{F}^A)\hat{\boldsymbol{T}}^B : \dot{\hat{\boldsymbol{E}}}^B + \left(\rho\partial_\varphi\psi_c + \theta\partial_{\dot\varphi}\psi_d + \partial_\varphi G\tilde{\psi}_m\right)\dot\varphi + \rho\partial_{\nabla_{\boldsymbol{p}}(\varphi)}\psi_c\cdot\nabla_{\boldsymbol{p}}(\dot\varphi)\,.\end{aligned} \tag{3.35}$$

Replacing the expressions for $\boldsymbol{S}^A$, $\hat{\boldsymbol{T}}^A_{skew}$, and $\hat{\boldsymbol{T}}^B$, given respectively by Eqs. (3.18), (2.93) and (3.20) in Eq. (3.35), and using the specific free-energy of Helmholtz , we can write

$$\begin{aligned}-\rho_0\theta\partial^2_\theta\psi_c\dot\theta &= \mathrm{div}_{\boldsymbol{p}}(\theta^2\partial_{\nabla_{\boldsymbol{p}}\theta}\psi_d) + \rho_0 r_0 + \rho_0\theta\partial_\theta\partial_{\boldsymbol{E}_A}\psi^A_c : \dot{\boldsymbol{E}}^A \\ &\quad +\theta\partial_{\hat{\boldsymbol{W}}_A}\psi_d : \hat{\boldsymbol{W}}^A + \left(\rho_0\theta\partial_\theta\partial_{\boldsymbol{E}^B}\psi^B_c + \theta\partial_{\dot{\boldsymbol{E}}^B}\psi_d\right) : \dot{\boldsymbol{E}}^B \\ &\quad +\rho_0 R^B + (\rho_0\theta\partial_\theta\partial_\varphi\psi_c + \theta\partial_{\dot\varphi}\psi_d)\dot\varphi + \rho_0\theta\partial_\theta\partial_{\nabla_{\boldsymbol{p}}\varphi}\psi_c\nabla_{\boldsymbol{p}}\dot\varphi,\end{aligned} \tag{3.36}$$

where R^B is given by (3.11). The free-energies ψ^A_c and ψ^B_c are given by Eqs. (3.2) and (3.3), respectively, while the pseudo-potential of dissipation ψ_d is given by Eq. (3.12), leading to the equation that governs the temperature:

$$\dot\theta = \frac{1}{2c_v}\left[\mathrm{div}_{\boldsymbol{p}}\left(\theta^2\tilde{c}\boldsymbol{C}^{-1}\nabla_{\boldsymbol{p}}(\theta)\right) + \rho_0 r_0 + \theta\tilde{b}|\dot{\hat{\boldsymbol{E}}}^B|^2 + \theta\tilde{\lambda}|\dot\varphi|^2 + \theta\tilde{\epsilon}|\hat{\boldsymbol{W}}^A|^2 + \rho_0 R^B\right]. \tag{3.37}$$

4. Eqs. (2.1) and (2.59) are also considered for the evolution of the gradient of deformation:

$$\frac{1}{\det(\boldsymbol{F}^A)}\boldsymbol{F}^A\boldsymbol{S}^A\left(\boldsymbol{F}^A\right)^t + \hat{\boldsymbol{T}}^A_{\text{skew}} = \hat{\boldsymbol{C}}^B\hat{\boldsymbol{T}}^B, \tag{3.38}$$

and

$$\boldsymbol{F} = \boldsymbol{F}_B\boldsymbol{F}_A. \tag{3.39}$$

Equations (3.32), (3.34) and (3.37-3.39) constitute a system of nonlinear partial differential equations (PDEs). The numerical approach used to account for the system solution is presented in the next chapter.

Remark 3.3. *We observe that the equations presented in this section do not necessarily ensure the condition $\dot\varphi > 0$. In other words, the proposed model allows the possibility of healing in meso and macro-cracks. Actually, this behavior can be found in real materials (HAYES et al., 2007; LI; NETTLES, 2010; LI, 2014); however, in order to prevent healing and ensure damage irreversibility, we assumed that the damage is irreversible by imposing a numerical constrain that will be described in Sec. 4.2. Further discussion on the damage ireversibility can be found in Costa-Haveroth et al. (2022).*

3.2 Simplifications and Sub-models

The model described in the previous sections allows to consider many simplifications which lead to different material behaviors. In the text that follows, we will discuss some of these possibilities.

Firstly, consider the particularized model obtained if the tensor $\boldsymbol{\mathcal{A}}$ is constant, implying that the last two terms of Eq. (3.25) are null. In this case, the one-dimensional version of the model can be represented by the rheological mechanism of Fig. 3.3a. Here, part A in Fig. 3.1 is composed by the Neo-Hookean spring, and part B is composed by a parallel combination of a Neo-Hookean spring, a dashpot and a spring-pot (fractional element represented by the rhombus; see Sec. 1.2.2). The nature of the mentioned elements, characterizes the stress/strain relation for the model. The dashpot allows to consider viscous dissipative damping in the material and is represented by the term $\theta\tilde{b}\dot{\hat{\boldsymbol{E}}}^B$ in Eq. (3.27). The non-linear springs give suitable description on the contribution of the Neo-Hookean material; the springs of part A and B act on the first two terms of Eq. (3.19) and (3.27), respectivelly. The spring-pot, described by the term $\boldsymbol{\mathcal{A}} : {}_0\mathrm{D}_t^{\alpha}(\hat{\boldsymbol{E}}_t^B)$ in Eq. (3.25), allows to include both, elastic and viscous responses, in the same component. The behavior of the spring-pot is governed by $\boldsymbol{\mathcal{A}}$ and α. It is important to remember that, due to the nature of a fractional derivative element, with interpolates between the behavior of a spring (non-dissipative) and a dashpot (dissipative), it always includes some dissipation. Additionally, the degradation functions $G_h^A(\varphi)$, $G_h^B(\varphi)$ and $G_m(\varphi)$ in Eqs. (3.19) and (3.25) indicate that the Neo-Hookean springs and the spring-pot include damage effects.

Figure 3.3 – Possible interpretations of our model in the one-dimensional case for $\boldsymbol{\mathcal{A}}$ constant. The spring represents the hyperelastic contribution of the Neo-Hookean material and, the dashpot gives the viscous damping. The rhombus represents the fractional rheological element.

(a) General series model.

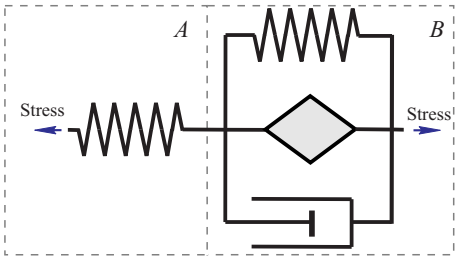

(b) Modified fractional Zener model.

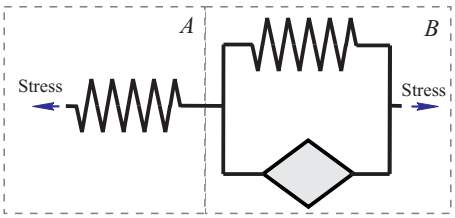

(c) Modified Zener model.

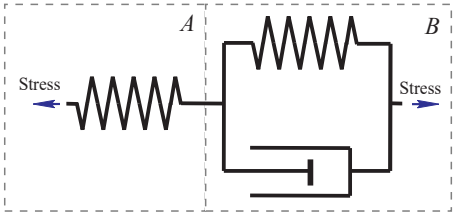

If $\boldsymbol{\mathcal{A}}$ is constant and $\tilde{b} = 0$, then we obtain the modified fractional Zener[1] model of Fig. 3.3b. On the other hand, if $\boldsymbol{\mathcal{A}}$ is constant and viscoelastic effects due to the fractional component are not considered, we recover the modified Zener model of Fig. 3.3c, that is discussed in Costa-Haveroth et al. (2021).

Now, consider that the contribution of the Neo-Hookean spring of part A is not acting for the material considered. Then, we recover a viscoelastic parallel model shown in Fig. 3.4a and widely discussed in Costa-Haveroth et al. (2022). If part A is not acting in the material, tensor $\boldsymbol{\mathcal{A}}$ is constant and $\tilde{b} = 0$, then we obtain the modified fractional Kelvin-Voigt model of Fig. 3.4b. If $\boldsymbol{\mathcal{A}}$ is constant and viscoelastic effects due to the fractional component are not considered, we recover the modified Kelvin-Voigt model of Fig. 3.4c.

Figure 3.4 – Viscoelastic parallel models as a particularization of our model.

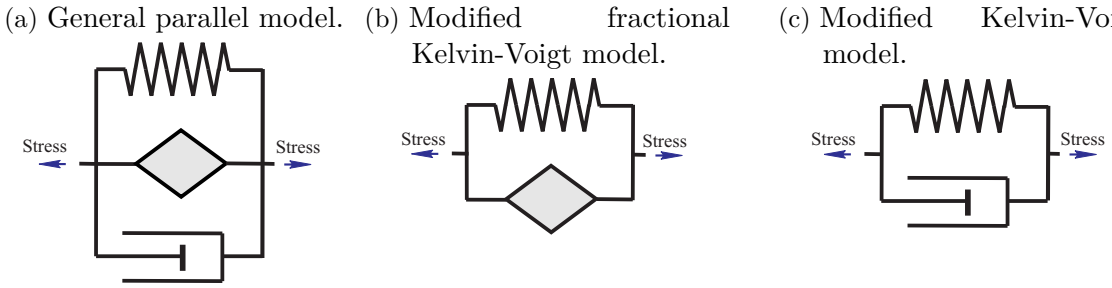

Costa-Haveroth et al. (2022).

Remark 3.4. *Even for the one-dimensional case, we emphasize that for small strain, the Neo-Hookean spring becomes the traditional linear elastic spring. In this case, if part A is not acting in the material,* $\boldsymbol{\mathcal{A}}$ *and* θ *are constants, and no damage is considered, the model described in this work recovers the usual fractional Kelvin-Voigt model, widely discussed in the literature (LEWANDOWSKI; CHORĄŻYCZEWSKI, 2010; XU; XU; HU, 2015; FARNO; BAUDEZ; ESHTIAGHI, 2018). Section 5.1.1.1 presents an example where this simplification is considered. In fact, for that case, Eq. (3.25) is simplified for a widely known equation, for which the thermodynamics were addressed by Lion (LION, 1997); a free-energy potential was even derived with physical justification and the corresponding mechanical dissipation potential was obtained. However, the model presented in this work is more general, including the effects of non-linear dependence of* $\boldsymbol{\mathcal{A}}$ *on* $\hat{\boldsymbol{E}}^B$*, large strain, thermal effects and damage.*

[1] In this work, we refer to modified fractional rheological model when the springs represent Neo-Hookean springs, damage is acting, and termal effects are considered for the material behavior. If the springs represent the traditional linear elastic material and damage or thermal effects are not considered, then we refer to the traditional model.

3.2.1 Viscoelastic Parallel Model

As previously commented, a possible simplification of the general model proposed in this work is obtained when we consider that part A of the rheological arrangement of Fig. 3.3a is not acting. This is equivalent to consider that the spring in A is totally rigid (the elastic constant tends to infinity). Additionally, if viscous damping is not considered ($\tilde{b} = 0$), neither temperature variation, then, the representation is given by a parallel rheological arrangement similar to that show in Fig. 3.4b.

In terms of the gradient decomposition of Eq. (2.1), this particular model is obtained by considering $\boldsymbol{F}^A = \boldsymbol{I}$. In other words, the intermediate configuration $\hat{\Omega}$ is the same as the original configuration Ω_0 and, the total gradient of deformation is given by $\boldsymbol{F} = \boldsymbol{F}^B$. It implies that the total stress acting in the system arises only from part B. Then, the total first Piola-Kirchhoff stress tensor can given by $\boldsymbol{P} = \boldsymbol{P}^B$.

Taking it into account, Eqs. (2.60) and Eq. (2.53) lead to

$$\hat{\boldsymbol{T}}^B = \boldsymbol{S}^B = \boldsymbol{S},$$

and

$$\boldsymbol{P} = \boldsymbol{P}^B = \boldsymbol{F}\hat{\boldsymbol{T}}^B = \boldsymbol{F}\boldsymbol{S}^B = \boldsymbol{F}\boldsymbol{S}, \tag{3.40}$$

where $\boldsymbol{S}$ is taken as the total Second Piola-Kirchhoff stress tensor.

In the same way, the total strain for the system is provided by part B. Then, the total Green-Lagrange strain tensor is taken as $\boldsymbol{E} = \hat{\boldsymbol{E}}^B$. Similarly, the right Cauchy-Green strain tensor is given by $\boldsymbol{C} = \hat{\boldsymbol{C}}^B$.

The governing equations for the evolution of motion, damage and temperature in a body with viscoelastic behavior described by this parallel model can be resumed as follows.

1. Due to Eq. (3.40), the relation (3.32), which express the *motion* in the system, can be rewritten as

$$\rho_0 \dot{\boldsymbol{v}} = \mathrm{div}_{\boldsymbol{p}}(\boldsymbol{P}) + \rho_0 \boldsymbol{b}_0. \tag{3.41}$$

where $\dot{\boldsymbol{u}} = \boldsymbol{v}$ and $\boldsymbol{P} = \boldsymbol{F}\boldsymbol{S}$. The constitutive relation stress/strain for $\boldsymbol{S}$ given by the simplification of Eq. (3.25):

$$\begin{aligned}\boldsymbol{S} \;=\; & G_h\left[\mu(\boldsymbol{I}-\boldsymbol{C}^{-1}) + \lambda \ln\left((\det(\boldsymbol{C}))^{\frac{1}{2}}\right)\boldsymbol{C}^{-1}\right] - g_c\gamma_c\left(\boldsymbol{C}^{-1}\nabla_{\boldsymbol{p}}(\varphi)\right)\otimes\left(\boldsymbol{C}^{-1}\nabla_{\boldsymbol{p}}(\varphi)\right) \\ & + \frac{G_m}{\rho_0}\left[\boldsymbol{\mathcal{A}} : {}_0\mathrm{D}_t^{\alpha}(\boldsymbol{E}_t) + \kappa\frac{(\boldsymbol{E}_t-\boldsymbol{E}_\tau) : \partial_{\boldsymbol{E}}\boldsymbol{\mathcal{A}} : (\boldsymbol{E}_t-\boldsymbol{E}_\tau)}{t^{\alpha}}\right. \\ & \left. + \kappa\alpha\int_0^t \frac{(\boldsymbol{E}_t-\boldsymbol{E}_\tau) : \partial_{\boldsymbol{E}}\boldsymbol{\mathcal{A}} : (\boldsymbol{E}_t-\boldsymbol{E}_\tau)}{(t-\tau)^{1+\alpha}}\mathrm{d}\tau\right],\end{aligned} \tag{3.42}$$

where $G_h = G_m^B$ and $G_m = G_m^B$ are the degradation functions associated with the hyperelastic and the fractional-viscoelastic parts of the material, respectively. If $\boldsymbol{\mathcal{A}}$ is constant, then

$$\begin{aligned}\boldsymbol{S} &= G_h\left[\mu(\boldsymbol{I}-\boldsymbol{C}^{-1})+\lambda\ln\left((\det(\boldsymbol{C}))^{\frac{1}{2}}\right)\boldsymbol{C}^{-1}\right]-g_c\gamma_c\left(\boldsymbol{C}^{-1}\nabla_{\boldsymbol{p}}(\varphi)\right)\otimes\left(\boldsymbol{C}^{-1}\nabla_{\boldsymbol{p}}(\varphi)\right)\\ &\quad+\frac{G_m}{\rho_0}\boldsymbol{\mathcal{A}}:{}_0\mathrm{D}_t{}^{\alpha}(\boldsymbol{E}_t).\end{aligned} \tag{3.43}$$

2. The equation for the *damage* evolution is obtained by simplifying Eq. (3.34) as follow:

$$\dot{\varphi}=\frac{1}{\tilde{\lambda}\theta}\mathrm{div}_{\boldsymbol{p}}\left(g_c\gamma_c\boldsymbol{C}^{-1}\nabla_{\boldsymbol{p}}(\varphi_0)\right)-\frac{g_c\partial_\varphi H(\varphi)}{\gamma_c\tilde{\lambda}\theta}+\frac{1}{\tilde{\lambda}\theta}\partial_\varphi G\psi_h-\frac{\partial_\varphi G}{\tilde{\lambda}\theta}\left(\psi_h+\tilde{\psi}_m\right),$$

where $G = G_h = G_m$, ψ_h is associated with hyperelastic energy of the Neo-Hookean spring and $\tilde{\psi}_m$ is the energy associated with memory parts.

Finally, Equations (3.41) and (3.44) constitute a nonlinear system of PDEs with fractional derivatives and memory terms.

Remark 3.5. *The previously obtained equations, as a particular case of the general model introduced in this thesis, are similar to those presented in Costa-Haveroth et al. (2022).*

4 Numerical Considerations

In this chapter we present the numerical approach used to solve the general system of nonlinear partial differential equations (PDEs) presented in Sec. 3.1.5. This procedure is a generalization of that proposed in Costa-Haveroth et al. (2022).

In order to simplify the numerical treatment, the temperature was remained fixed. Then, it is sufficient describe the evolution of the damage variable, the displacement and the tensors gradients of deformation, $\boldsymbol{F}^A$ and $\boldsymbol{F}^B$, through the time.

The general methodology considers the application of a staggered scheme (also called semi-implicit/explicit time integration scheme) and the Newton-Raphson (NR) method (HAVEROTH et al., 2018). We solve each equation of the system separately by a proper implicit time integration method. It leads to considerable computational gain in comparison with traditional dependent and coupled approaches to solve systems of nonlinear equations.

Details concerning the linearization and numerical considerations for each equation are presented in the following sections. We also present a pseudo-code in Sec. 4.4 which summarizes the numerical treatment.

The time interval $[0, t_f]$ is split into N sub-intervals with time-step $\Delta t = t_n - t_{n-1}$ and $n = 1, \cdots, N+1$. We adopt the subscript $(\cdot)_{n+1}$ to indicate that the variable is updated for the time t_{n+1} .

Remark 4.1. *In the arguments that follow, we assume that we know all the information of the discretized state variables up to time t_n and show how to obtain the corresponding information at t_{n+1}.*

To avoid computational burden, the spatial domain is discretizated for two-dimensional finite element (FE) meshes. We consider the domain Ω_0 divided into m elements Ω_0^q where $q = 1, \cdots, m$, and $\Omega_0 = \cup_{q=1}^{m} \Omega_0^q$ and $\Omega_0^q \cap \Omega_0^p = \emptyset, \forall q \neq p$. The estimation for vector $\boldsymbol{z}$ and scalar z valued-fields are written as a superposition of the local nodal basis function N_i (the know Lagrange polynomials) in each q-th element, $i = 1, \cdots, \vartheta$ and ϑ is the quantity of nodes in the element:

$$z^q \simeq \boldsymbol{N} \tilde{z}^q \quad \text{and} \quad \boldsymbol{z}^q \simeq \bar{\boldsymbol{N}} \tilde{\boldsymbol{z}}^q. \tag{4.1-4.2}$$

The symbol $\tilde{(\cdot)}$ represents the nodal values for variable of interest and the interpolation functions are organized in the matrices

$$\boldsymbol{N} = \begin{bmatrix} N_1 & N_2 & \cdots & N_\vartheta \end{bmatrix}, \tag{4.3}$$

and

$$\bar{\boldsymbol{N}} = \begin{bmatrix} N_1 & 0 & N_2 & 0 & \cdots & N_\vartheta & 0 \\ 0 & N_1 & 0 & N_2 & \cdots & 0 & N_\vartheta \end{bmatrix}. \tag{4.4}$$

The gradient operator is estimated by the global derivatives of the functions N_i with respect to the x and y directions and arranged as

$$\boldsymbol{B} = \begin{bmatrix} N_{1,x} & N_{2,x} & \cdots & N_{\vartheta,x} \\ N_{1,y} & N_{1,y} & \cdots & N_{\vartheta,y} \end{bmatrix}, \tag{4.5}$$

and

$$\bar{\boldsymbol{B}} = \begin{bmatrix} N_{1,x} & 0 & N_{2,x} & 0 & \cdots & N_{\vartheta,x} & 0 \\ N_{1,y} & 0 & N_{2,y} & 0 & \cdots & N_{\vartheta,y} & 0 \\ 0 & N_{1,y} & 0 & N_{2,x} & \cdots & 0 & N_{\vartheta,x} \\ 0 & N_{1,x} & 0 & N_{2,y} & \cdots & 0 & N_{\vartheta,y} \end{bmatrix}. \tag{4.6}$$

4.1 Equation of Motion

The motion is governed by the balance of linear momentum, as shown in Eq. (3.32) or, alternatively, in Eq. (2.35a). To use FE, we must obtain the correlated weak form. Then, we take the inner product of Eq. (2.35a) with some arbitrary virtual velocity $\delta\boldsymbol{v}$ as

$$\int_{\Omega_0} \rho_0 \dot{\boldsymbol{v}} \cdot \delta\boldsymbol{v} \, \mathrm{d}\Omega_0 \;=\; \int_{\Omega_0} \mathrm{div}_{\boldsymbol{p}}(\boldsymbol{P}^B)\delta\boldsymbol{v} \, \mathrm{d}\Omega_0 + \int_{\Omega_0} \rho_0 \boldsymbol{f}_0 \cdot \delta\boldsymbol{v} \, \mathrm{d}\Omega_0. \tag{4.7}$$

Doing integration by parts in the above equation and considering Eqs. (2.35b) and (2.36), we are left with

$$\int_{\Omega_0} \rho_0 \dot{\boldsymbol{v}} \cdot \delta\boldsymbol{v} \, \mathrm{d}\Omega_0 = \int_{\Omega_0} (\boldsymbol{F}\boldsymbol{S}^B) : \nabla_{\boldsymbol{p}}(\delta\boldsymbol{v}) \, \mathrm{d}\Omega_0 + \int_{\Omega_0} \rho_0 \boldsymbol{f}_0 \cdot \delta\boldsymbol{v} \, \mathrm{d}\Omega_0 + \int_{\Gamma_0} \boldsymbol{\sigma}_0 \cdot \delta\boldsymbol{v} \, \mathrm{d}\Gamma_0. \tag{4.8}$$

Considering the symmetry of $\boldsymbol{S}^B$ (see Eq. (2.36)) we have

$$\begin{aligned} \boldsymbol{F}\boldsymbol{S}^B : \nabla_{\boldsymbol{p}}(\delta\boldsymbol{v}) = \boldsymbol{S}^B : \boldsymbol{F}^t \nabla_{\boldsymbol{p}}(\delta\boldsymbol{v}) = \boldsymbol{S}^B : \boldsymbol{F}^t \delta\dot{\boldsymbol{F}} &= \boldsymbol{S}^B : \frac{1}{2}\left(\boldsymbol{F}^t \delta\dot{\boldsymbol{F}} + \delta\dot{\boldsymbol{F}}^t \boldsymbol{F}\right) \\ &= \boldsymbol{S}^B : \delta\dot{\boldsymbol{E}} \end{aligned} \tag{4.9}$$

where $\delta\dot{\boldsymbol{F}} = \nabla_{\boldsymbol{p}}(\delta\boldsymbol{v})$ and

$$\delta\dot{\boldsymbol{E}}(\boldsymbol{u}) := \frac{1}{2}\left(\boldsymbol{F}^t(\boldsymbol{u})\delta\dot{\boldsymbol{F}} + \delta\dot{\boldsymbol{F}}^t \boldsymbol{F}(\boldsymbol{u})\right), \tag{4.10}$$

is the time rate of the Green-Lagrange virtual strain tensor (BONET; WOOD, 2008, p. 148) .

Using Eq. (4.9), we can rewrite Eq. (4.8) as

$$\int_{\Omega_0} \rho_0 \dot{\boldsymbol{v}} \cdot \delta\boldsymbol{v} \, \mathrm{d}\Omega_0 = -\int_{\Omega_0} \boldsymbol{S}^B : \delta\dot{\boldsymbol{E}} \, \mathrm{d}\Omega_0 + \int_{\Omega_0} \rho_0 \boldsymbol{f}_0 \cdot \delta\boldsymbol{v} \, \mathrm{d}\Omega_0 + \int_{\Gamma_0} \boldsymbol{\sigma}_0 \cdot \delta\boldsymbol{v} \, \mathrm{d}\Gamma_0. \tag{4.11}$$

The numerical approximation for Eq. (4.11) involves: discretization of time by the Newmark method (NM), linearization, and spatial discretization by using the FE method. These steps are detailed next.

4.1.1 Applying the Newmark Method for Motion

The NM considers the updated acceleration, at time-step $n+1$, by using:

$$\dot{\boldsymbol{v}}_{n+1} = \ddot{\boldsymbol{u}}_{n+1} = a_1(\boldsymbol{u}_{n+1} - \boldsymbol{u}_n) - a_2\dot{\boldsymbol{u}}_n - a_3\ddot{\boldsymbol{u}}_n, \tag{4.12}$$

where the constants a_i, with $i = 1, \cdots, 3$, are given by

$$a_1 = \frac{1}{\beta_N \Delta t^2}, \quad a_2 = \frac{1}{\beta_N \Delta t}, \quad \text{and,} \quad a_3 = \frac{1 - 2\beta_N}{2\beta_N},$$

and β_N is the Newmark constant (LINDFIELD; PENNY, 2012, p. 266).

By replacing Eq. (4.12) in Eq. (4.11), we obtain the residue for the time discretization of the equation of motion:

$$\begin{aligned} \boldsymbol{R}^{\boldsymbol{u}}_{n+1} \;=\; & \int_{\Omega_0} (a_1(\boldsymbol{u}_{n+1} - \boldsymbol{u}_n) - a_2\dot{\boldsymbol{u}}_n - a_3\ddot{\boldsymbol{u}}_n) \cdot \delta\boldsymbol{v} \; \mathrm{d}\Omega_0 \\ & + \frac{1}{\rho_0} \int_{\Omega_0} \boldsymbol{S}^B(\hat{\boldsymbol{E}}^B(\boldsymbol{u}_{n+1})) : \delta\dot{\boldsymbol{E}}(\boldsymbol{u}_{n+1}) \; \mathrm{d}\Omega_0 \\ & - \int_{\Omega_0} \boldsymbol{f}_{0,n+1}.\delta\boldsymbol{v} \; \mathrm{d}\Omega_0 \; - \frac{1}{\rho_0} \int_{\Gamma_0} \boldsymbol{\sigma}_{0,n+1}.\delta\boldsymbol{v} \; \mathrm{d}\Gamma_0. \end{aligned} \tag{4.13}$$

Here, for simplicity of notation, we explicit the dependency only for mechanical variables.

4.1.2 Linearization for the Equation of Motion

For linearization, it is convenient to recall the general definition of partial directional derivative. We assume that $\boldsymbol{Z}_1$ and $\boldsymbol{Z}_2$ are tensor variables and $\mathscr{F}(\boldsymbol{Z}_1, \boldsymbol{Z}_2)$ is a tensor valued function of $\boldsymbol{Z}_1$ and $\boldsymbol{Z}_2$. Then the partial directional derivative of $\mathscr{F}$ with respect to $\boldsymbol{Z}_1$ at $(\boldsymbol{Z}_1, \boldsymbol{Z}_2)$ in the direction of $\Delta\boldsymbol{Z}_1$ is the limit (when it exists) defined by

$$\boldsymbol{D}_{\boldsymbol{Z}_1}\mathscr{F}(\boldsymbol{Z}_1, \boldsymbol{Z}_2)(\Delta\boldsymbol{Z}_1) = \lim_{s\to 0} \frac{1}{s} \left(\mathscr{F}(\boldsymbol{Z}_1 + s\Delta\boldsymbol{Z}_1, \boldsymbol{Z}_2) - \mathscr{F}(\boldsymbol{Z}_1, \boldsymbol{Z}_2)\right).$$

There are similar definitions for the partial derivative with respect to variable $\boldsymbol{Z}_2$ and for the case of more independent variables.

Here, to shorten the notation, we will use the notation of directional derivative as in Bhatti (2006), which hides some of the details and assumes that the reader can get them from the context:

$$\boldsymbol{D}_{\Delta\boldsymbol{Z}_1}\mathscr{F} = \boldsymbol{D}_{\boldsymbol{Z}_1}\mathscr{F}(\boldsymbol{Z}_1, \boldsymbol{Z}_2)(\Delta\boldsymbol{Z}_1).$$

Now, let us calculate the directional derivative of the residue $\boldsymbol{R}^{\boldsymbol{u}}_{n+1}$, given in Eq. (4.13), on the displacement $\boldsymbol{u}_{n+1}$ in the direction of the displacement increment $\boldsymbol{w}_{n+1}$ defined as

$$\boldsymbol{w}_{n+1} := \Delta\boldsymbol{u}_{n+1}.$$

As we said, we follow the notation of Bhatti (2006), and denote this derivative as

$$\boldsymbol{D}_{\boldsymbol{w}_{n+1}}\boldsymbol{R}^{\boldsymbol{u}}_{n+1} = \boldsymbol{D}_{\Delta\boldsymbol{u}_{n+1}}\boldsymbol{R}^{\boldsymbol{u}}_{n+1}.$$

Consider the first term in the right hand side of Eq. (4.13). Its directional derivative is written as

$$\boldsymbol{D}_{\boldsymbol{w}_{n+1}}\left[\int_{\Omega_0}(a_1(\boldsymbol{u}_{n+1}-\boldsymbol{u}_n)-a_2\dot{\boldsymbol{u}}_n-a_3\ddot{\boldsymbol{u}}_n)\cdot\delta\boldsymbol{v}\;\mathrm{d}\Omega_0\right] = a_1\int_{\Omega_0}\boldsymbol{w}_{n+1}\cdot\delta\boldsymbol{v}\;\mathrm{d}\Omega_0. \quad (4.14)$$

Now, consider the third term in the right hand side of Eq. (4.13). The updated body forces in the initial configuration are represented by $\boldsymbol{f}_{0,n+1}$. Once the displacement does not affect these forces, the directional derivative of this term on the displacement variation $\boldsymbol{w}_{n+1}$ is null. In the same way, we consider the surface loads $\boldsymbol{\sigma}_0$, in the last terms of Eq. (4.13), not dependent on the strain; then its directional derivative is also null.

On the other hand, the second term on the right hand side of Eq. (4.13) is highly nonlinear on the displacement field and demands special care. Note that, $\boldsymbol{S}^B$ depends on the $\boldsymbol{E}^B$, which in turn depends on $\boldsymbol{u}$. Other source on nonlinearity is due to $\delta\dot{\boldsymbol{E}}$, which is also dependent on the displacement.

Observe that the directional derivative of $\boldsymbol{F}_{n+1}$ with respect to the displacement in the direction of an increment of displacement $\boldsymbol{w}_{n+1}$ is

$$\boldsymbol{D}_{\boldsymbol{w}_{n+1}}(\boldsymbol{F}_{n+1}) = \boldsymbol{D}_{\boldsymbol{w}_{n+1}}\left(\boldsymbol{I}+\nabla_{\boldsymbol{p}}(\boldsymbol{u}_{n+1})\right) = \nabla_{\boldsymbol{p}}(\boldsymbol{w}_{n+1}). \quad (4.15)$$

Furthermore, for shortness of notation, we consider

$$\boldsymbol{S}^B(\hat{\boldsymbol{E}}^B(\boldsymbol{u}_{n+1})) := \boldsymbol{S}^B_{n+1}, \qquad \boldsymbol{F}(\boldsymbol{u}_{n+1}) := \boldsymbol{F}_{n+1}, \qquad \text{and} \qquad \delta\dot{\boldsymbol{E}}_{n+1} := \delta\dot{\boldsymbol{E}}(\boldsymbol{u}_{n+1}).$$

We use the product rule of differentiation to obtain the directional derivative of the second term in the right hand side of Eq. (4.13) with respect to displacement along a displacement increment $\boldsymbol{w}_{n+1}$, as follows:

$$\begin{aligned}\boldsymbol{D}_{\boldsymbol{w}_{n+1}}\left[\frac{1}{\rho_0}\int_{\Omega_0}\boldsymbol{S}^B_{n+1}:\delta\dot{\boldsymbol{E}}_{n+1}\;\mathrm{d}\Omega_0\right] &= \frac{1}{\rho_0}\int_{\Omega_0}\boldsymbol{D}_{\boldsymbol{w}_{n+1}}(\boldsymbol{S}^B_{n+1}):\delta\dot{\boldsymbol{E}}_{n+1}\;\mathrm{d}\Omega_0 \\ &\quad +\frac{1}{\rho_0}\int_{\Omega_0}\boldsymbol{S}^B_{n+1}:\boldsymbol{D}_{\boldsymbol{w}_{n+1}}(\delta\dot{\boldsymbol{E}}_{n+1})\;\mathrm{d}\Omega_0. \quad (4.16)\end{aligned}$$

Firstly, consider the directional derivative in the last term of the right hand side of Eq. (4.16). From Eqs. (4.10) and (4.15) we have

$$\boldsymbol{D}_{\boldsymbol{w}_{n+1}}(\delta\dot{\boldsymbol{E}}_{n+1}) = \frac{1}{2}\left[\nabla_{\boldsymbol{p}}(\boldsymbol{w}_{n+1})^t\delta\dot{\boldsymbol{F}}_{n+1}+\delta\dot{\boldsymbol{F}}^t_{n+1}\nabla_{\boldsymbol{p}}(\boldsymbol{w}_{n+1})\right]. \quad (4.17)$$

Now, we work with the derivative in the first term of the right hand side of Eq. (4.16). Note that tensor $\boldsymbol{S}^B$ is given in terms of the partial strain $\hat{\boldsymbol{E}}^B$. In order to derive

$\boldsymbol{S}^B$ in the direction of the increment of displacement $\boldsymbol{w}_{n+1} = \Delta\boldsymbol{u}_{n+1}$, we must rewrite $\boldsymbol{S}^B$ in terms of the total strain $\boldsymbol{E}$. We remember that $\boldsymbol{E} = \frac{1}{2}(\boldsymbol{C} - \boldsymbol{I})$ and use Eqs. (2.1) and (2.58) to obtain

$$\hat{\boldsymbol{E}}^B = \left(\boldsymbol{F}^A\right)^{-t}\left(\boldsymbol{E} + \frac{\boldsymbol{I}}{2}\right)\left(\boldsymbol{F}^A\right)^{-1} - \frac{\boldsymbol{I}}{2} \tag{4.18}$$

$$= \frac{1}{2}\left[\left(\boldsymbol{F}^A\right)^{-t}\boldsymbol{C}\left(\boldsymbol{F}^A\right)^{-1} - \boldsymbol{I}\right]. \tag{4.19}$$

Then, by using Eq. (4.18), the derivative in the first term of the right hand side of Eq. (4.16) can be rewritten with the dependency of the total strain $\boldsymbol{E}$:

$$\boldsymbol{D}_{\boldsymbol{w}_{n+1}}\left(\boldsymbol{S}^B_{n+1}(\hat{\boldsymbol{E}}^B_{n+1})\right) = \boldsymbol{D}_{\boldsymbol{w}_{n+1}}\left[\boldsymbol{S}^B_{n+1}\left(\left(\boldsymbol{F}^A_{n+1}\right)^{-t}\left(\boldsymbol{E}_{n+1} + \frac{\boldsymbol{I}}{2}\right)\left(\boldsymbol{F}^A_{n+1}\right)^{-1} - \frac{\boldsymbol{I}}{2}\right)\right]. \tag{4.20}$$

Note that $\boldsymbol{F}^A_{n+1}$ depends on $\boldsymbol{F}_{n+1}$, that in turn, depends on the displacements. Since this dependency results in difficulties to the chain rule and, to obtain an easier form for (4.20), we take the value of $\boldsymbol{F}^A_{n+1}$ as its known previous time-step value $\boldsymbol{F}^A_n$. Then, Eq. (4.20) is approximated by using

$$\boldsymbol{D}_{\boldsymbol{w}_{n+1}}\left(\boldsymbol{S}^B_{n+1}(\hat{\boldsymbol{E}}^B_{n+1})\right) \simeq \boldsymbol{D}_{\boldsymbol{w}_{n+1}}\left[\boldsymbol{S}^B_{n+1}\left(\left(\boldsymbol{F}^A_{n}\right)^{-t}\left(\boldsymbol{E}_{n+1} + \frac{\boldsymbol{I}}{2}\right)\left(\boldsymbol{F}^A_{n}\right)^{-1} - \frac{\boldsymbol{I}}{2}\right)\right]. \tag{4.21}$$

By using the chain rule for differentiation in Eq. (4.21), and considering Eq. (4.19), we obtain

$$\begin{aligned}\boldsymbol{D}_{\boldsymbol{w}_{n+1}}\left(\boldsymbol{S}^B_{n+1}(\hat{\boldsymbol{E}}^B_{n+1})\right) &\simeq \boldsymbol{D}_{\boldsymbol{w}_{n+1}}\left[\boldsymbol{S}^B_{n+1}\left(\left(\boldsymbol{F}^A_{n}\right)^{-t}\left(\boldsymbol{E}_{n+1} + \frac{\boldsymbol{I}}{2}\right)\left(\boldsymbol{F}^A_{n}\right)^{-1} - \frac{\boldsymbol{I}}{2}\right)\right] \\ &= \left(\partial_{\hat{\boldsymbol{E}}^B}\boldsymbol{S}^B\right)_{n+1} : \left(\partial_{\boldsymbol{E}}\hat{\boldsymbol{E}}^B\right)_{n+1} : \boldsymbol{D}_{\boldsymbol{w}_{n+1}}(\boldsymbol{E}_{n+1}) \\ &= 2\left(\partial_{\hat{\boldsymbol{E}}^B}\boldsymbol{S}^B\right)_{n+1} : \left(\partial_{\boldsymbol{C}}\hat{\boldsymbol{E}}^B\right)_{n+1} : \boldsymbol{D}_{\boldsymbol{w}_{n+1}}(\boldsymbol{E}_{n+1}).\end{aligned} \tag{4.22}$$

Note that $\boldsymbol{S}^B_{n+1}$ is given in terms of $\hat{\boldsymbol{E}}^B_{n+1}$, that in turn is written in terms of $\boldsymbol{F}^B_{n+1}$. We obtain the updated $\boldsymbol{F}^B_{n+1}$ by using Eq. (2.1) to generate the approximation

$$\boldsymbol{F}^B_{n+1} \simeq \boldsymbol{F}_{n+1}\left(\boldsymbol{F}^A_n\right)^{-1}, \tag{4.23}$$

where $\boldsymbol{F}^A_n$ is already known for the time step $n+1$.

The first derivative in the right hand side of Eq. (4.22) demands special care; then, details on its obtaining are discussed in Appendix E.4. The derivative $\partial_{\boldsymbol{C}}\hat{\boldsymbol{E}}_B$, shown in Eq. (4.22), can be obtained by using Eq. (4.19), as show in Appendix E.5:

$$\left(\partial_{\boldsymbol{C}}\hat{\boldsymbol{E}}^B\right)_{n+1} \simeq \left(\frac{1}{2}\left(\boldsymbol{F}^A_n\right)^{-t} \otimes \left(\boldsymbol{F}^A_n\right)^{-1}\right), \tag{4.24}$$

and, the linearization of $\boldsymbol{E}_{n+1}$, also required for the Eq.(4.22), is obtained from

$$\boldsymbol{E} = \frac{1}{2}\left[\nabla(\boldsymbol{u})^t\nabla(\boldsymbol{u}) + \nabla(\boldsymbol{u})^t + \nabla(\boldsymbol{u})\right], \tag{4.25}$$

and simplified as

$$\boldsymbol{D}_{\boldsymbol{w}_{n+1}}(\boldsymbol{E}_{n+1}) = \frac{1}{2}\left[\nabla_{\boldsymbol{p}}(\boldsymbol{w}_{n+1})^t \boldsymbol{F}_{n+1} + \boldsymbol{F}_{n+1}^t \nabla_{\boldsymbol{p}}(\boldsymbol{w}_{n+1})\right]. \tag{4.26}$$

From Eq. (4.22), using (4.24) and (4.26), we get

$$\begin{aligned}
\boldsymbol{D}_{\boldsymbol{w}_{n+1}}\left(\boldsymbol{S}_{n+1}^B(\hat{\boldsymbol{E}}_{n+1}^B)\right) &\simeq \boldsymbol{D}_{\boldsymbol{w}_{n+1}}\left[\boldsymbol{S}_{n+1}^B\left(\left(\boldsymbol{F}_n^A\right)^{-t}\left(\boldsymbol{E}_{n+1}+\frac{\boldsymbol{I}}{2}\right)\left(\boldsymbol{F}_n^A\right)^{-1}-\frac{\boldsymbol{I}}{2}\right)\right] \\
&= 2\left(\partial_{\hat{\boldsymbol{E}}^B}\boldsymbol{S}^B\right)_{n+1} : \left(\partial_{\boldsymbol{C}}\hat{\boldsymbol{E}}^B\right)_{n+1} : \boldsymbol{D}_{\boldsymbol{w}_{n+1}}(\boldsymbol{E}_{n+1}) \\
&= 2\left(\partial_{\hat{\boldsymbol{E}}^B}\boldsymbol{S}^B\right)_{n+1} : \left(\frac{1}{2}\left(\boldsymbol{F}_n^A\right)^{-t}\otimes\left(\boldsymbol{F}_n^A\right)^{-1}\right) : \boldsymbol{D}_{\boldsymbol{w}_{n+1}}(\boldsymbol{E}_{n+1}) \\
&= \boldsymbol{\mathcal{H}}_{n+1} : \left[\frac{1}{2}\left(\nabla_{\boldsymbol{p}}(\boldsymbol{w}_{n+1})^t \boldsymbol{F}_{n+1} + \boldsymbol{F}_{n+1}^t \nabla_{\boldsymbol{p}}(\boldsymbol{w}_{n+1})\right)\right],
\end{aligned} \tag{4.27}$$

where, we denoted

$$\boldsymbol{\mathcal{H}}_{n+1} := \left(\partial_{\hat{\boldsymbol{E}}^B}\boldsymbol{S}^B\right)_{n+1} : \left(\boldsymbol{F}_n^A\right)^{-t}\otimes\left(\boldsymbol{F}_n^A\right)^{-1}. \tag{4.28}$$

Note that, by the definition of $\boldsymbol{\mathcal{H}}$ in Eq. (4.28), it is a fourth-order, symmetric and positive-definite tensor.

By using Eqs. (4.10), (4.17) and (4.27), Eq. (4.16) can be rewritten as

$$\begin{aligned}
&\boldsymbol{D}_{\boldsymbol{w}_{n+1}}\left[\frac{1}{\rho_0}\int_{\Omega_0}\boldsymbol{S}_{n+1}^B : \delta\dot{\boldsymbol{E}}_{n+1}\,\mathrm{d}\Omega_0\right] \\
= &\frac{1}{\rho_0}\int_{\Omega_0}\boldsymbol{\mathcal{H}}_{n+1} : \left[\frac{1}{2}\left(\nabla_{\boldsymbol{p}}(\boldsymbol{w}_{n+1})^t \boldsymbol{F}_{n+1} + \boldsymbol{F}_{n+1}^t \nabla_{\boldsymbol{p}}(\boldsymbol{w}_{n+1})\right)\right] : \delta\dot{\boldsymbol{E}}_{n+1}\,\mathrm{d}\Omega_0 \\
&+\frac{1}{\rho_0}\int_{\Omega_0}\boldsymbol{S}_B : \frac{1}{2}\left[\nabla_{\boldsymbol{p}}(\boldsymbol{w}_{n+1})^t\delta\dot{\boldsymbol{F}}_{n+1} + \delta\dot{\boldsymbol{F}}_{n+1}^t\nabla_{\boldsymbol{p}}(\boldsymbol{w}_{n+1})\right]\mathrm{d}\Omega_0 \\
= &\frac{1}{\rho_0}\int_{\Omega_0}\boldsymbol{\mathcal{H}}_{n+1} : \left[\frac{1}{2}(\nabla_{\boldsymbol{p}}(\boldsymbol{w}_{n+1})^t \boldsymbol{F}_{n+1} + \boldsymbol{F}_{n+1}^t \nabla_{\boldsymbol{p}}(\boldsymbol{w}_{n+1}))\right] : \frac{1}{2}\left[\boldsymbol{F}^t(\boldsymbol{u})\delta\dot{\boldsymbol{F}} + \delta\dot{\boldsymbol{F}}^t\boldsymbol{F}(\boldsymbol{u})\right]\mathrm{d}\Omega_0 \\
&+\frac{1}{\rho_0}\int_{\Omega_0}\boldsymbol{S}_B : \frac{1}{2}\left[\nabla_{\boldsymbol{p}}(\boldsymbol{w}_{n+1})^t\delta\dot{\boldsymbol{F}}_{n+1} + \delta\dot{\boldsymbol{F}}_{n+1}^t\nabla_{\boldsymbol{p}}(\boldsymbol{w}_{n+1})\right]\mathrm{d}\Omega_0.
\end{aligned} \tag{4.29}$$

Appendix E.6 shows that we can use the symmetry of $\boldsymbol{S}^B$ and $\boldsymbol{\mathcal{H}}$ to write

$$\boldsymbol{\mathcal{H}} : \frac{1}{2}\left(\nabla_{\boldsymbol{p}}(\boldsymbol{w})^t\boldsymbol{F} + \boldsymbol{F}^t\nabla_{\boldsymbol{p}}(\boldsymbol{w})\right) : \frac{1}{2}\left(\boldsymbol{F}^t\delta\dot{\boldsymbol{F}} + \delta\dot{\boldsymbol{F}}^t\boldsymbol{F}\right) = \boldsymbol{F}^t\delta\dot{\boldsymbol{F}} : \boldsymbol{\mathcal{H}} : \boldsymbol{F}^t\nabla(\boldsymbol{w}), \tag{4.30}$$

and

$$\boldsymbol{S}^B : \frac{1}{2}\left[\nabla(\boldsymbol{w})^t\delta\dot{\boldsymbol{F}} + \delta\dot{\boldsymbol{F}}^t\nabla(\boldsymbol{w})\right] = \delta\dot{\boldsymbol{F}} : \nabla(\boldsymbol{w})\boldsymbol{S}^B. \tag{4.31}$$

The last two expressions can simplify Eq. (4.29) as

$$\begin{aligned}
\boldsymbol{D}_{\boldsymbol{w}_{n+1}}\left[\frac{1}{\rho_0}\int_{\Omega_0}\boldsymbol{S}_{n+1}^B : \delta\dot{\boldsymbol{E}}_{n+1}\,\mathrm{d}\Omega_0\right] &= \frac{1}{\rho_0}\int_{\Omega_0}\boldsymbol{F}_{n+1}^t\delta\dot{\boldsymbol{F}}_{n+1} : \boldsymbol{\mathcal{H}}_{n+1} : \boldsymbol{F}_{n+1}^t\nabla(\boldsymbol{w}_{n+1})\,\mathrm{d}\Omega_0 \\
&\quad+\frac{1}{\rho_0}\int_{\Omega}\delta\dot{\boldsymbol{F}}_{n+1}^t : \nabla(\boldsymbol{w}_{n+1})\boldsymbol{S}_{n+1}^B\,\mathrm{d}\Omega_0.
\end{aligned} \tag{4.32}$$

Finally, the linearized form of Eq. (4.13) is written from Eqs. (4.14) and (4.32) as

$$\begin{aligned}\boldsymbol{D}_{\boldsymbol{w}_{n+1}}\left(\boldsymbol{R}^{\boldsymbol{u}}_{n+1}\right) &= a_1\int_{\Omega_0}\boldsymbol{w}_{n+1}\cdot\delta\boldsymbol{v}\;\mathrm{d}\Omega_0+\frac{1}{\rho_0}\int_{\Omega_0}\boldsymbol{F}^t_{n+1}\delta\dot{\boldsymbol{F}}_{n+1}:\boldsymbol{\mathcal{H}}_{n+1}:\boldsymbol{F}^t_{n+1}\nabla(\boldsymbol{w}_{n+1})\;\mathrm{d}\Omega_0\\ &\quad+\frac{1}{\rho_0}\int_{\Omega_0}\delta\dot{\boldsymbol{F}}^t_{n+1}:\nabla(\boldsymbol{w}_{n+1})\boldsymbol{S}^B_{n+1}\;\mathrm{d}\Omega_0.\end{aligned}\tag{4.33}$$

4.1.3 Finite Element Method for Motion Equation

We apply the Finite Element Method (FEM) to the motion equation and obtain the final discretized expressions for the associated Jacobian matrix and the residue vector. Therefore, consider the spatial approximations

$$\boldsymbol{u}_{(\cdot)}\simeq\bar{\boldsymbol{N}}\tilde{\boldsymbol{u}}_{(\cdot)},\quad \delta\boldsymbol{v}_{(\cdot)}\simeq\bar{\boldsymbol{N}}\delta\tilde{\boldsymbol{v}}_{(\cdot)},\tag{4.34-4.36}$$

$$\boldsymbol{t}_{(\cdot)}\simeq\bar{\boldsymbol{N}}\tilde{\boldsymbol{t}}_{(\cdot)},\quad \boldsymbol{f}_{(\cdot)}\simeq\bar{\boldsymbol{N}}\tilde{\boldsymbol{f}}_{(\cdot)},\tag{4.37-4.38}$$

where $\bar{\boldsymbol{N}}$ is given in Eq. (4.4). We follow Bhatti (2006, p.496)), and adopt an equivalent product of matrices to write the residue of Eq. (4.13) for each q-th element as

$$\begin{aligned}\boldsymbol{R}^{q,\boldsymbol{u}}_{n+1} &\simeq \boldsymbol{M}^q\left(a_1(\tilde{\boldsymbol{u}}^q_{n+1}+\tilde{\boldsymbol{u}}^q_n-a_2\dot{\tilde{\boldsymbol{u}}}^q_n-a_3\ddot{\tilde{\boldsymbol{u}}}^q_n)+\tilde{\boldsymbol{f}}^q_{n+1}\right)\\ &\quad+\frac{1}{\rho_0}\int_{\Omega^q_0}\bar{\boldsymbol{B}}^t\bar{\boldsymbol{F}}^t_{n+1}\left(\boldsymbol{s}^B{}_{n+1}\right)^q\;\mathrm{d}\Omega^q_0+BT^q,\end{aligned}\tag{4.39}$$

where $\boldsymbol{M}^q$ is the element mass matrix defined as

$$\boldsymbol{M}^q=\int_{\Omega^q_0}\bar{\boldsymbol{N}}^t\bar{\boldsymbol{N}}\;\mathrm{d}\Omega^q_0,\tag{4.40}$$

the matrix $\bar{\boldsymbol{B}}$ is given by Eq. (4.6), BT^q are possible boundary terms from displacements or stresses, $\boldsymbol{s}^B$ is a vector written from the tensor $\boldsymbol{S}^B$, and $\bar{\boldsymbol{F}}$ is derived from $\boldsymbol{F}$:

$$\boldsymbol{s}^B=\begin{bmatrix}S^B_{11} & S^B_{22} & S^B_{12}\end{bmatrix}\quad\text{and}\quad\bar{\boldsymbol{F}}=\begin{bmatrix}F_{11}&0&F_{21}&0\\0&F_{12}&0&F_{22}\\F_{12}&F_{11}&F_{22}&F_{21}\end{bmatrix}.\tag{4.41-4.42}$$

The Jacobian matrix $\boldsymbol{J}^{q,\boldsymbol{u}}_{n+1}$ is obtained by deriving the residue $\boldsymbol{R}^{q,\boldsymbol{u}}_{n+1}$ to $\boldsymbol{w}_{n+1}$. From Eq. (4.33), we have

$$\boldsymbol{J}^{q,\boldsymbol{u}}_{n+1}=\boldsymbol{M}^q a_1+\frac{1}{\rho_0}\int_{\Omega^q_0}\bar{\boldsymbol{B}}^t\bar{\boldsymbol{F}}^t_{n+1}\boldsymbol{H}^q_{n+1}\bar{\boldsymbol{F}}_{n+1}\bar{\boldsymbol{B}}\;\mathrm{d}\Omega^q_0+\frac{1}{\rho_0}\int_{\Omega^q_0}\bar{\boldsymbol{B}}^t\left(\bar{\boldsymbol{S}}^B_{n+1}\right)^q\bar{\boldsymbol{B}}\;\mathrm{d}\Omega^q_0,\tag{4.43}$$

for each q-th element. Matrix $\bar{\boldsymbol{S}}^B$ is a symmetric and block-diagonal matrix constructed from $\boldsymbol{S}$, and given by

$$\bar{\boldsymbol{S}}^B=\begin{bmatrix}S^B_{11}&S^B_{12}&&\\S^B_{12}&S^B_{22}&&\\&&S^B_{11}&S^B_{12}\\&&S^B_{12}&S^B_{22}\end{bmatrix},$$

and $\boldsymbol{H}$ is a symmetric matrix obtained by contracting two indexes in the fourth order tensor $\boldsymbol{\mathcal{H}}$.

Then, we can write the linearized system

$$\boldsymbol{J}^{\boldsymbol{u}}_{n+1,i}\Delta\boldsymbol{u}_{n+1,i} = \boldsymbol{R}^{\boldsymbol{u}}_{n+1,i}, \tag{4.44}$$

where i is the NR iteration. We assemble each q-th local Jacobian matrix $\boldsymbol{J}^{q,\boldsymbol{u}}_{n+1,i}$, to obtain the global Jacobian matrix $\boldsymbol{J}^{\boldsymbol{u}}_{n+1,i}$. Similarly, the global residue $\boldsymbol{R}^{\boldsymbol{u}}_{n+1,i}$ is given by the assembling of each local residue vector $\boldsymbol{R}^{q,\boldsymbol{u}}_{n+1,i}$. We solve the system (4.44) for $\Delta\boldsymbol{u}_{n+1,i}$ and use it to obtain a new approximation for $\boldsymbol{u}_{n+1,i+1}$:

$$\boldsymbol{u}_{n+1,i+1} = \boldsymbol{u}_{n+1,i} + \Delta\boldsymbol{u}_{n+1,i}.$$

This procedure repeats until the difference between the displacements for two consecutive time-steps achieves a prescribed tolerance ϵ_1, i.e., $||\boldsymbol{u}_{n+1,i+1} - \boldsymbol{u}_{n+1,i}|| \leq \epsilon_1$.

4.1.4 Numerical Fractional Derivative - The Algorithm G1

We apply the numerical algorithm known as G1 to approximate the Caputo fractional derivative (OLDHAM; SPANIER, 1974). The fractional derivative of the strain $\hat{\boldsymbol{E}}^B_t$, that appear in Eq. (3.28), will be calculated by

$${}_0\mathrm{D}^{\alpha}_t\,\hat{\boldsymbol{E}}^B_t = (\Delta t)^{-\alpha}\sum_{m=0}^{N} B_{m+1}\hat{\boldsymbol{E}}^B(t - m\Delta t), \tag{4.45}$$

where the coefficients B_{m+1} are defined as

$$B_{m+1} = \frac{\Gamma(m-\alpha)}{\Gamma(-\alpha)\Gamma(m+1)} = \frac{m-1-\alpha}{m}B_m. \tag{4.46}$$

Here, N is the number of sub-intervals for the time. It is important to emphasize that Eq. (4.45) is an approximation for the called Grunwald-Letnikov fractional derivative, that is equal to the Caputo fractional derivative for the circumstances adopted in this work. Further comments on fractional derivatives algorithms can be seen in Costa-Haveroth et al. (2021).

4.2 Equation of Damage

Consider Eq. (3.34), which gives the evolution for damage. By applying the backward Euler method for time discretization, we obtain

$$\begin{aligned}\varphi_{n+1} = \quad & \varphi_n + \frac{\Delta t}{\tilde{\lambda}_{n+1}\theta_{n+1}}\left[\mathrm{div}_{\boldsymbol{p}}\left(2g_c\gamma\boldsymbol{C}^{-1}_{n+1}\nabla_{\boldsymbol{p}}(\varphi_{n+1})\right) - \frac{2g_c}{\gamma}\partial_{\varphi}H_{n+1}\right.\\ & \left.-\partial_{\varphi}G_{n+1}\left(\psi^A_h + \psi^B_h + \tilde{\psi}^B_m\right)_{n+1}\right],\end{aligned} \tag{4.47}$$

where

$$\left(\psi_h^A + \psi_h^B + \tilde{\psi}_m^B\right)_{n+1} := \psi_h^A(\boldsymbol{E}_{n+1}^A) + \psi_h^B(\hat{\boldsymbol{E}}_{n+1}^B) + \tilde{\psi}_m^B(\hat{\boldsymbol{E}}_{n+1}^B),$$

$$\partial_\varphi G_{n+1} := \partial_\varphi G(\varphi_{n+1})$$

and

$$\partial_\varphi H_{n+1} := \partial_\varphi H(\varphi_{n+1}) = \varphi_{n+1}, \tag{4.48}$$

according to the definition of H in Eq. (3.8).

As before, we apply FEs for spatial discretization; but firstly, consider the divergent term in Eq. (4.47) rewritten as

$$\begin{aligned}\varphi_{n+1} \;=\; & \varphi_n + 2\Delta t g_c \gamma \left[\operatorname{div}_{\boldsymbol{p}}\left(\frac{1}{\tilde{\lambda}_{n+1}\theta_{n+1}}\boldsymbol{C}_{n+1}^{-1}\nabla_{\boldsymbol{p}}(\varphi_{n+1})\right)\right. \\ & \left. -\nabla_{\boldsymbol{p}}\left(\frac{1}{\tilde{\lambda}_{n+1}\theta_{n+1}}\right)\cdot\boldsymbol{C}_{n+1}^{-1}\nabla_{\boldsymbol{p}}(\varphi_{n+1})\right] \\ & -\frac{\Delta t}{\tilde{\lambda}_{n+1}\theta_{n+1}}\left[\frac{2g_c}{\gamma}H'_{n+1} + G'_{n+1}\left(\psi_h^A + \psi_h^B + \tilde{\psi}_m^B\right)_{n+1}\right].\end{aligned} \tag{4.49}$$

We multiply Eq. (4.49) by a proper scalar test function w and integrate over the domain Ω_0 to obtain the weak form:

$$\begin{aligned}\int_{\Omega_0}\varphi_{n+1}w\;\mathrm{d}\Omega_0 \;=\; & \int_{\Omega_0}\varphi_n w\mathrm{d}\Omega_0 + 2\Delta t g_c\gamma\int_{\Omega_0}\operatorname{div}_{\boldsymbol{p}}\left(\frac{1}{\tilde{\lambda}_{n+1}\theta_{n+1}}\boldsymbol{C}_{n+1}^{-1}\nabla_{\boldsymbol{p}}(\varphi_{n+1})\right)w\;\mathrm{d}\Omega_0 \\ & -2\Delta t g_c\gamma\int_{\Omega_0}\nabla_{\boldsymbol{p}}\left(\frac{1}{\tilde{\lambda}_{n+1}\theta_{n+1}}\right)\cdot\boldsymbol{C}_{n+1}^{-1}\nabla_{\boldsymbol{p}}(\varphi_{n+1})w\;\mathrm{d}\Omega_0 \\ & -\frac{2\Delta t g_c}{\gamma}\int_{\Omega_0}\frac{1}{\tilde{\lambda}_{n+1}\theta_{n+1}}\partial_\varphi H_{n+1}w\;\mathrm{d}\Omega_0 \\ & -\Delta t\int_{\Omega_0}\frac{\partial_\varphi G_{n+1}}{\tilde{\lambda}_{n+1}\theta_{n+1}}\left(\psi_h^A + \psi_h^B + \tilde{\psi}_m^B\right)_{n+1}w\;\mathrm{d}\Omega_0.\end{aligned} \tag{4.50}$$

Considering Eq. (3.13) we can write

$$\nabla_{\boldsymbol{p}}\left(\frac{1}{\tilde{\lambda}\theta}\right) = \frac{1}{\theta}\nabla_{\boldsymbol{p}}\left(\frac{1}{\tilde{\lambda}}\right) + \frac{1}{\tilde{\lambda}}\nabla_{\boldsymbol{p}}\left(\frac{1}{\theta}\right) = \frac{\zeta c_\lambda}{\theta(1+\tilde{\delta}-\varphi)^{\zeta+1}}\nabla_{\boldsymbol{p}}(\varphi) - \frac{1}{\tilde{\lambda}\theta^2}\nabla_{\boldsymbol{p}}(\theta). \tag{4.51}$$

By replacing Eqs. (4.48) and (4.51) into Eq. (4.50), and assuming θ and λ delayed, we obtain

$$\begin{aligned}\int_{\Omega_0}\varphi_{n+1}w\;\mathrm{d}\Omega_0 \;=\; & \int_{\Omega_0}\varphi_n w\mathrm{d}\Omega_0 - 2\Delta t g_c\gamma\int_{\Omega_0}\frac{1}{\tilde{\lambda}_n\theta_n}\boldsymbol{C}_{n+1}^{-1}\nabla_{\boldsymbol{p}}(\varphi_{n+1})\cdot\nabla_{\boldsymbol{p}}(w)\;\mathrm{d}\Omega_0 \\ & -2\Delta t g_c\gamma\zeta c_\lambda\int_{\Omega_0}\frac{\nabla_{\boldsymbol{p}}(\varphi_n)\cdot\left(\boldsymbol{C}_{n+1}^{-1}\nabla_{\boldsymbol{p}}(\varphi_{n+1})\right)}{\theta_n(1+\tilde{\delta}-\varphi_N)^{\zeta+1}}w\;\mathrm{d}\Omega_0 \\ & +2\Delta t g_c\gamma\int_{\Omega_0}\frac{1}{\tilde{\lambda}_n\theta_n^2}\nabla_{\boldsymbol{p}}(\theta_n)\cdot\left(\boldsymbol{C}_{n+1}^{-1}\nabla_{\boldsymbol{p}}(\varphi_{n+1})\right)w\;\mathrm{d}\Omega_0 \\ & -\frac{2\Delta t g_c}{\gamma}\int_{\Omega_0}\frac{1}{\tilde{\lambda}_n\theta_n}\varphi_{n+1}w\;\mathrm{d}\Omega_0 \\ & -\Delta t\int_{\Omega_0}\frac{1}{\tilde{\lambda}_n\theta_n}\partial_\varphi G_{n+1}\left(\psi_h^A + \psi_h^B + \tilde{\psi}_m^B\right)_{n+1}w\;\mathrm{d}\Omega_0.\end{aligned} \tag{4.52}$$

Now, we adopt the spatial approximations

$$\varphi^q_{(\cdot)} \simeq \boldsymbol{N}\tilde{\varphi}^q_{(\cdot)}, \quad \nabla_{\boldsymbol{p}}(\varphi^q_{(\cdot)}) \simeq \boldsymbol{B}\tilde{\varphi}^q_{(\cdot)}, \tag{4.53-4.54}$$

$$\theta^q_{(\cdot)} \simeq \boldsymbol{N}\tilde{\theta}^q_{(\cdot)}, \quad \nabla_{\boldsymbol{p}}(\theta^q) \simeq \boldsymbol{B}\tilde{\theta}^q_{(\cdot)}, \tag{4.55-4.56}$$

$$w^q \simeq \boldsymbol{N}\tilde{w}^q, \quad \nabla_{\boldsymbol{p}}(w^q) \simeq \boldsymbol{B}\tilde{w}^q, \tag{4.53-4.58}$$

with $\boldsymbol{N}$ and $\boldsymbol{B}$ given by Eqs. (4.3) and (4.5), respectivelly. Henceforth, the gradient $\nabla_{\boldsymbol{p}}(\varphi)$, in the third and fourth terms of the right-hand side of Eq. (4.52), is delayed in time to avoid non-symmetric Jacobian matrix. Then, the residue for each q-th element at time-step $n+1$ for the damage equation can be given by

$$\begin{aligned}
\boldsymbol{R}^{q,\varphi}_{n+1} \;=\; & \int_{\Omega^q_0,} \boldsymbol{N}^t\boldsymbol{N}\left[\left(1+\frac{2\Delta t g_c}{\gamma\tilde{\lambda}^q_n\boldsymbol{N}\tilde{\theta}^q_n}\right)\tilde{\varphi}^q_{n+1}-\tilde{\varphi}^q_n\right]\,\mathrm{d}\Omega^q_0, \\
& +2\Delta t g_c\tilde{\gamma}\int_{\Omega^q_0}\frac{\boldsymbol{B}^t\boldsymbol{C}^{-1\ q}_{n+1}\boldsymbol{B}\tilde{\varphi}^q_n}{\tilde{\lambda}^q_n\boldsymbol{N}\tilde{\theta}^q_n}\,\mathrm{d}\Omega^q_0, \\
& +2\Delta t g_c\gamma\zeta c_\lambda\int_{\Omega^q_0,}\frac{\boldsymbol{N}^t\left(\tilde{\varphi}^q_n\right)^t\boldsymbol{B}^t\boldsymbol{C}^{-t\ q}_{n+1}\boldsymbol{B}\tilde{\varphi}^q_n}{\boldsymbol{N}\tilde{\theta}^q_n(1+\tilde{\delta}-\boldsymbol{N}\tilde{\varphi}^q_n)^{\zeta+1}}\,\mathrm{d}\Omega^q_0, \\
& -2\Delta t g_c\gamma\int_{\Omega^q_0,}\frac{\boldsymbol{N}^t\left(\tilde{\varphi}^q_n\right)^t\boldsymbol{B}^t\boldsymbol{C}^{-t\ q}_{n+1}\boldsymbol{B}\tilde{\theta}^q_n}{\tilde{\lambda}^q_n(\boldsymbol{N}\tilde{\theta}^q_n)^2}\mathrm{d}\Omega^q_0, \\
& +\Delta t\int_{\Omega^q_0,}\frac{\boldsymbol{N}^t\left(\partial_\varphi G^q_{n+1}\right)\left(\psi^A_h+\psi^B_h+\tilde{\psi}^B_m\right)^q_{n+1}}{\tilde{\lambda}^q_n\boldsymbol{N}\tilde{\theta}^q_n}\,\mathrm{d}\Omega^q_0,
\end{aligned} \tag{4.59}$$

where

$$\frac{1}{\tilde{\lambda}^q_n}=\frac{c_\lambda}{(1+\tilde{\delta}-\varphi^q_n)^\zeta}\simeq\frac{c_\lambda}{(1+\tilde{\delta}-\boldsymbol{N}\tilde{\varphi}^q_n)^\zeta}, \tag{4.60}$$

by Eq. (3.13), and we define $G^q_{n+1} := G(\varphi^q_{n+1})$.

The corresponding Jacobian matrix $\boldsymbol{J}^{q,\varphi}_{n+1}$ is obtained by deriving Eq. (4.59) to φ^q_{n+1}:

$$\begin{aligned}
\boldsymbol{J}^{q,\varphi}_{n+1} \;=\; & \int_{\Omega^q_0}\boldsymbol{N}^t\boldsymbol{N}\left(1+\frac{2\Delta t g_c}{\gamma\tilde{\lambda}^q_n\boldsymbol{N}\tilde{\theta}^q_n}\right)\,\mathrm{d}\Omega^q_0+2\Delta t g_c\gamma\int_{\Omega^q_0}\frac{\boldsymbol{B}^t\boldsymbol{C}^{-1\ q}_{n+1}\boldsymbol{B}}{\tilde{\lambda}^q_n\boldsymbol{N}\tilde{\theta}^q_n}\,\mathrm{d}\Omega^q_0 \\
& +\Delta t\int_{\Omega^q_0}\frac{\boldsymbol{N}^t\left(\partial_{\varphi\varphi}G^q_{n+1}\right)\left(\psi^A_h+\psi^B_h+\tilde{\psi}^B_m\right)^q_{n+1}}{\tilde{\lambda}^q_n\boldsymbol{N}\tilde{\theta}^q_n}\,\mathrm{d}\Omega^q_0.
\end{aligned} \tag{4.61}$$

For each time step, we can write the linearized system

$$\boldsymbol{J}^{\varphi}_{n+1,i}\Delta\varphi_{n+1,i}=-\boldsymbol{R}^{\varphi}_{n+1,i}, \tag{4.62}$$

where i is the NR iteration. We assemble each q-th local Jacobian matrix $\boldsymbol{J}^{q,\varphi}_{n+1,i}$ to obtain the global Jacobian matrix $\boldsymbol{J}^{\varphi}_{n+1,i}$. Similarly, the global residue $\boldsymbol{R}^{\varphi}_{n+1,i}$ is obtained by assembling the local residue vector $\boldsymbol{R}^{q,\varphi}_{n+1,i}$.

We solve the system (4.62) for $\Delta\varphi_{n+1,i}$ and use it to obtain a new approximation for $\varphi_{n+1,i+1}$:

$$\varphi_{n+1,i+1} = \varphi_{n+1,i} + \Delta\varphi_{n+1,i}.$$

This procedure repets until the difference between the values for two consecutive time steps achieves a prescribed tolerance ϵ_2, i.e., $||\varphi_{n+1,i+1} - \varphi_{n+1,i}|| \leq \epsilon_2$.

As discussed in Sec. 3.1.5, the damage irreversibility will be established using a predict-corrector procedure: we consider known the state values at time step n and use the governing equation without the additional term in the pseudo-potential to estimate the damage at time step $n+1$, leading to the predicted value φ^*_{n+1} for the damage. Next, we compare φ^*_{n+1} and φ_n, for each node of the mesh; if $\varphi^*_{n+1} \geq \varphi_n$ then we assume $\varphi_{n+1} := \varphi^*_{n+1}$; otherwise $\varphi_{n+1} := \varphi_n$.

Additionally, we adopt $\varphi_0 = 0$ prescribed, i.e., undamaged material to start the analysis; although some level of damage could be assumed to initiate the evolution.

4.3 Equations for the Gradients of Deformation

As commented previously, the model proposed in this work considers only materials which do not present preferential direction for strain evolution. In this sense, we are dealing with isotropic material for which it is usual to postulate zero spin[1]; that is, $\boldsymbol{W}^A = \boldsymbol{0}$. Consequently, $\hat{\boldsymbol{T}}^A_{\text{skew}} = \boldsymbol{0}$ due to Eq. (2.93).

Taking it into account, Eq. (3.38) can be rewritten as

$$\frac{1}{\det(\boldsymbol{F}^A)}\boldsymbol{F}^A\boldsymbol{S}^A\boldsymbol{F}^{A^t} = \hat{\boldsymbol{C}}^B\hat{\boldsymbol{T}}^B. \tag{4.63}$$

Then, Eqs. (2.53) and (4.63) imply in

$$\boldsymbol{F}^A\boldsymbol{S}^A = \left(\boldsymbol{F}^B\right)^t \boldsymbol{F}\boldsymbol{S}^B. \tag{4.64}$$

By imposing time discretization for Eqs. (3.39) and (4.64) we obtain

$$\boldsymbol{F}_{n+1} = \boldsymbol{F}^B_{n+1}\boldsymbol{F}^A_{n+1} \quad \text{and} \quad \boldsymbol{F}^A_{n+1}\boldsymbol{S}^A_{n+1} = \boldsymbol{F}^{B\ t}_{n+1}\boldsymbol{F}_{n+1}\boldsymbol{S}^B_{n+1}, \tag{4.65-4.66}$$

where $\boldsymbol{S}^A_{n+1} := \boldsymbol{S}^A(\boldsymbol{E}^A_{n+1})$ and $\boldsymbol{S}^B_{n+1} := \boldsymbol{S}(\hat{\boldsymbol{E}}^B_{n+1})$.

Remark 4.2. *If $\boldsymbol{F}_{n+1}$, $\boldsymbol{S}^A_{n+1}$, and $\boldsymbol{S}^B_{n+1}$ are known, then Eqs. (4.65) and (4.66) might be simultaneously solved to update the tensors $\boldsymbol{F}^A_{n+1}$ and $\boldsymbol{F}^B_{n+1}$. In this case, since this system is non-linear with respect to $\boldsymbol{F}^A_{n+1}$ and $\boldsymbol{F}^B_{n+1}$, we should apply some iterative method,*

[1] Neto, Peric and Owen (2011, p.584) shown the case of an anisotropic single-crystal, in which a model with non zero spin is considered. Further discussion on the possibility of non zero spin can be found in Dafalias [4, 5].

like the NR, for instance, to numerically solve it. Some preliminary simulated tests using this methodology show convergence lost; then, in the following, we choose an alternative procedure to solve the decoupled system in order to improve the convergence.

As explained in Sec. 4.1.3, we solve the motion equation in the time step $n+1$ by considering $\boldsymbol{F}_n^A$ calculated in the previous time-step. If $\boldsymbol{F}_{n+1}$ and $\boldsymbol{F}_n^A$ are known, Eq. (4.23) can be used to approximate $\boldsymbol{F}_{n+1}^B$. By adopting this, we can calculate $\hat{\boldsymbol{E}}^B$ using Eq. (2.58), the associated stress $\hat{\boldsymbol{T}}_{n+1}^B$ using Eq. (3.25), and $\boldsymbol{S}^B$ through Eq. (2.53).

Next, we need to update the tensor $\boldsymbol{F}_{n+1}^A$ in order to evolve the solution. We use Eq. (4.65) and Eq. (4.66) to write

$$\boldsymbol{F}_{n+1}^A \boldsymbol{S}_{n+1}^A = (\boldsymbol{F}^A)_{n+1}^{-t} \boldsymbol{C}_{n+1} \boldsymbol{S}_{n+1}^B,$$

where $\boldsymbol{C} := \boldsymbol{F}^t \boldsymbol{F}$. Once $\boldsymbol{F}_{n+1}^A$ is not know yet, we can approximate the above equation by using $\boldsymbol{F}_n^A$:

$$\boldsymbol{F}_n^A \boldsymbol{S}_{n+1}^A \simeq (\boldsymbol{F}^A)_n^{-t} \boldsymbol{C}_{n+1} \boldsymbol{S}_{n+1}^B. \tag{4.67}$$

Multiplying both sides of Eq. (4.67) by $(\boldsymbol{F}_n^A)^{-1}$, we obtain

$$\boldsymbol{S}_{n+1}^A = \left(\boldsymbol{C}_n^A\right)^{-1} \boldsymbol{C}_{n+1} \boldsymbol{S}_{n+1}^B, \tag{4.68}$$

where $\left(\boldsymbol{C}_n^A\right)^{-1} = (\boldsymbol{F}_n^A)^{-1}(\boldsymbol{F}_n^A)^{-t}$.

Now, we can use the NR method to solve Eq. (4.68) and find $\boldsymbol{E}_{n+1}^A$. For each iteration i, the residuum[2] is given by

$$\boldsymbol{R}_{n+1,i}^{\boldsymbol{E}^A} = \boldsymbol{S}_{n+1,i}^A - \left(\boldsymbol{C}_n^A\right)^{-1} \boldsymbol{C}_{n+1,i} \boldsymbol{S}_{n+1,i}^B. \tag{4.69}$$

By deriving Eq. (4.69) on the increment of $\boldsymbol{E}_{n+1,i}^A$, which is denoted as $\Delta\boldsymbol{E}_{n+1,i}^A$, we obtain the associated Jacobian:

$$\boldsymbol{J}_{n+1,i}^{\boldsymbol{E}^A} = \partial_{\Delta\boldsymbol{E}_{n+1,i}^A} \boldsymbol{S}_{n+1,i}^A - \left(\boldsymbol{C}_n^A\right)^{-1} \partial_{\Delta\boldsymbol{E}_{n+1,i}^A} \boldsymbol{C}_{n+1,i} \boldsymbol{S}_{n+1,i}^B - \left(\boldsymbol{C}_n^A\right)^{-1} \boldsymbol{C}_{n+1,i} \partial_{\Delta\boldsymbol{E}_{n+1,i}^A} \boldsymbol{S}_{n+1,i}^B. \tag{4.70}$$

Remark 4.3. *It is important to emphasize that we could have calculated the residuum by using Eq. (4.67) instead of (4.68). However, by adopting Eq. (4.68) the subsequent system is composed by three equations. On the other hand, by adopting Eq. (4.67), we need to solve a system with four equations, once (4.67) is non-symmetric.*

[2] We also could have employed the NR method to solve Eq. (4.67) instead of (4.68). However, note that the tensor $\boldsymbol{S}_{n+1}^A$ can be stored in a vector of three components in Voigt notation, if $\boldsymbol{S}^A$ is defined as symmetric. On the other hand, to store $\boldsymbol{F}_n^A \boldsymbol{S}_{n+1}^A$ we need four components for the vector form. In order to reduce the storage, we choose solve Eq.(4.68).

The simplest approximation for the Jacobian of Eq. (4.70) can be given by

$$\begin{aligned}\boldsymbol{J}^{E^A}_{n+1,i} &\simeq \partial_{\Delta \boldsymbol{E}^A_{n+1,i}} \boldsymbol{S}^A_{n+1,i} \\ &= \partial_{\Delta \boldsymbol{E}^A_{n+1}} \left[\mu^A \left(\boldsymbol{I} - \left(\boldsymbol{C}^A_n \right)^{-1} \right) + \lambda^A \ln \left(\det(\boldsymbol{C}^A_n)^{1/2} \right) \left(\boldsymbol{C}^A_{n+1} \right)^{-1} + \partial_{\boldsymbol{E}^A} \mathcal{I}^A_n \right] \\ &\simeq \lambda^A \left(\boldsymbol{C}^A_n \right)^{-1} \otimes \left(\boldsymbol{C}^A_n \right)^{-1} + 2 \left[\mu^A - \lambda^A \ln \left(\det(\boldsymbol{F}^A_n) \right) \right] \boldsymbol{\mathcal{I}} \end{aligned} \tag{4.71}$$

where $\boldsymbol{\mathcal{I}}$ is the fourth order identity. The derivative for the first two terms in the right hand side of Eq. (4.71) is obtained similarly to that shown in Eq. (D.6), while the derivative for the last term is null, once we are using $\boldsymbol{F}^A_n$ delayed.

Some numerical tests shown that the Eq. (4.71) implies in reasonable convergence properties for the NR method without the need of calculate additional costly and difficulty derivatives. Then, Eq. (4.71) is used for the applications presented in this work. The remaining derivatives appearing in Eq. (4.70), he can look them up in Appendix E.5.

As usual, we must solve for $\Delta \boldsymbol{E}^A_{n+1,i}$, the final linearized system

$$\boldsymbol{J}^{\boldsymbol{E}^A}_{n+1,i} \Delta \boldsymbol{E}^A_{n+1,i} = -\boldsymbol{R}^{\boldsymbol{E}^A}_{n+1,i}.$$

in each integration point. A new approximate solution for $\boldsymbol{E}^A_{n+1,i+1}$ is given by

$$\boldsymbol{E}^A_{n+1,i+1} = \boldsymbol{E}^A_{n+1,i} + \Delta \boldsymbol{E}^A_{n+1,i}.$$

The procedure repeats until $||\Delta \boldsymbol{E}^A_{n+1,i}|| \leq \epsilon_3$, where ϵ_3 is a prescribed tolerance. Then $\boldsymbol{E}^A_{n+1} := \boldsymbol{E}^A_{n+1,i+1}$.

After that, the updated value $\boldsymbol{E}^A_{n+1}$ is used to calculate its time derivative by using backward finite differences:

$$\dot{\boldsymbol{E}}^A_{n+1} = \frac{\boldsymbol{E}^A_{n+1} - \boldsymbol{E}^A_n}{\Delta t}.$$

Next, we use Eqs. (2.2) and (2.47) to write the time derivative of $\boldsymbol{F}^A$ as

$$\dot{\boldsymbol{F}}^A_{n+1} = \hat{\boldsymbol{L}}^A_{n+1} \boldsymbol{F}^A_{n+1} = \left(\hat{\boldsymbol{D}}^A_{n+1} + \hat{\boldsymbol{W}}^A_{n+1} \right) \boldsymbol{F}^A_{n+1}.$$

By Eq. (C.27), we have that

$$\dot{\boldsymbol{F}}^A_{n+1} = \left(\boldsymbol{F}^A \right)^{-t}_{n+1} \dot{\boldsymbol{E}}^A_{n+1} + \hat{\boldsymbol{W}}^A_{n+1} \boldsymbol{F}^A_{n+1}. \tag{4.72}$$

Once we adopted $\hat{\boldsymbol{W}}^A = 0$, Eq. (4.72) is simplified to

$$\dot{\boldsymbol{F}}^A_{n+1} = \boldsymbol{F}^{A^{-t}}_n \dot{\boldsymbol{E}}^A_{n+1}. \tag{4.73}$$

Finally, we employ backward finite differences again to update $\boldsymbol{F}^A_{n+1}$:

$$\boldsymbol{F}^A_{n+1} = \boldsymbol{F}^A_n + \Delta t \dot{\boldsymbol{F}}^A_{n+1}. \tag{4.74}$$

It is important to emphasize that, the stress tensor $\boldsymbol{S}^A$ had already been defined as a symmetric one in Eq. (2.50). However, in Eq. (4.68) this property is not evident (due to the simplifications adopted for numerical consideration). In order to ensure the symmetry of $\boldsymbol{S}^A$, we adopt the following configuration in the numerical simulations:

$$\boldsymbol{S}^A = \begin{bmatrix} (\boldsymbol{C}_n^{A^{-1}}\boldsymbol{C}_{n+1}\boldsymbol{S}_{n+1}^B)_{11} & (\boldsymbol{C}_n^{A^{-1}}\boldsymbol{C}_{n+1}\boldsymbol{S}_{n+1}^B)_{12} + (\boldsymbol{C}_n^{A^{-1}}\boldsymbol{C}_{n+1}\boldsymbol{S}_{n+1}^B)_{21} \\ (\boldsymbol{C}_n^{A^{-1}}\boldsymbol{C}_{n+1}\boldsymbol{S}_{n+1}^B)_{12} + (\boldsymbol{C}_n^{A^{-1}}\boldsymbol{C}_{n+1}\boldsymbol{S}_{n+1}^B)_{21} & (\boldsymbol{C}_n^{A^{-1}}\boldsymbol{C}_{n+1}\boldsymbol{S}_{n+1}^B)_{22} \end{bmatrix}. \tag{4.75}$$

4.4 Summary of the Numerical Treatment

This section summarizes the global procedure adopted to solve the system of PDEs presented in Sec. 3.1.5. Algorithm 1 outline the global procedure derived from the numerical treatment indicated in the previous sections to evaluate the damage variable, the displacement and the tensors gradients of deformation, $\boldsymbol{F}^A$ and $\boldsymbol{F}^B$, from a time-step to the next. Remember that temperature was remained constant for the simulations.

In summary, we proceed as follows: we solve the equation for damage evolution and obtain the updated damage value by using the backward Euler method for time and the NR method to deal with nonlinearities (see Sec. 4.2); at this point we use the known displacement of the previous time-step as input. Next, the updated damage values are fixed and used as input to solve the equation of motion. Once we need $\boldsymbol{F}^B$ to solve the motion, we adopt the known total gradient of deformation $\boldsymbol{F}$ and the partial gradient of deformation $\boldsymbol{F}^A$ of the previous time-step to approximate $\boldsymbol{F}^B$, allowing to update the stress $\hat{\boldsymbol{T}}^B$. Remember that, the fractional derivatives appearing in Eq. (3.28) are evaluated by using algorithm G1 (see Sec. 4.1.4). Then, we solve the equation of motion by using the standard NM coupled with the NR procedure. It results in the updated displacement, velocity and acceleration. Finally, we use the NR again to update $\boldsymbol{E}^A$;which is used to update $\dot{\boldsymbol{E}}^A$ and finally, $\boldsymbol{F}^A$. The last one is used as input for the next time-step.

If we consider the simplified parallel model of Sec. 3.2.1 (without temperature evolution), then, the numerical procedure described above simplifies to the same one used in Costa-Haveroth et al. (2022).

Remark 4.4. *As we can see in Findley and Davis (2013, p.130), viscoelastic materials can behave differently under temperature variations; then, thermal influences in viscoelastic materials demand special care. The mechanical properties of most viscoelastic materials are very sensitive to temperature, and thus for many structural applications, a wide understanding of the effect of temperature on the mechanical properties is necessary. Based on those observation, we preferred to proposed a full non-isothermal thermodynamic consistent model in order to give to the reader the possibility to account for the temperature variation. However, once this opens up a very large range of options to be investigated,*

and, since the model needs to be firstly proved in simpler situations, we decided to restrict the examples of the present work to the isothermal case. Comments and suggestions for the inclusion of temperature variation can be found in (HAVEROTH, 2020).

Algorithm 1 – Semi-implicit/explicit time integration scheme coupled with the Newton-Raphson method to solve the system of Sec. 3.1.5.

/* Loop on the time-steps */

1 **for** *time t from $t_0 = 0$ by the increment Δt to the final time t_f*

Input: $\boldsymbol{u}_n$, φ_n, $\boldsymbol{F}_n$, $\boldsymbol{C}_n$, $\boldsymbol{E}^A_n$, $\boldsymbol{F}^A_n$, $\dot{\boldsymbol{C}}_n$, $\dot{\boldsymbol{E}}^A_n$ and $\dot{\boldsymbol{F}}^A_n$.

/* Newton-Rhapson procedure for the damage. */

2 Iteration $i \leftarrow 0$;

3 $\varphi_{n+1,i} \leftarrow \varphi_n$;

4 **while** *(tolerance$<\epsilon_2$ and $i <$maximum number of iterations)* **do**

/* Loop over the Elements (q) */

5 **for** *($q = 1$ to maximum number of elements)*

/* Assemble the Jacobian and the residue */

6 Assemble $\boldsymbol{J}^{\varphi}_{n+1,i}$ by using Eq. (4.61);

7 Assemble $\boldsymbol{R}^{\varphi}_{n+1,i}$ by using Eq. (4.59);

8 **end**

9 Solve $\boldsymbol{J}^{\varphi}_{n+1,i}\Delta\varphi_{n+1,i} = -\boldsymbol{R}^{\varphi}_{n+1,i}$ for $\Delta\varphi_{n+1,i}$;

/* Update φ_{n+1} */

10 $\varphi_{n+1,i+1} \leftarrow \varphi_{n+1,i} + \Delta\varphi_{n+1,i}$;

/* Check the stop criterion */

11 $\epsilon_2 \leftarrow ||\Delta\varphi_{n+1,i}||$;

/* Increment i */

12 $i \leftarrow i + 1$;

13 **end**

Output: $\varphi_{n+1} \leftarrow \varphi_{n+1,i+1}$

/* Newton-Rhapson procedure for the motion. */

19 Iteration $i \leftarrow 0$;

20 $\boldsymbol{u}_{n+1,i} \leftarrow \boldsymbol{u}_n$;

21 **while** *(tolerance$<\epsilon_1$ and $i <$maximum number of iterations)* **do**

/* Loop over the Elements (q) */

22 **for** *($q = 1$ to maximum number of elements)*

/* Loop over the integration points (*int*) */

23 **for** *(int $= 1$ to maximum number of integration points)*

24 Evaluate $\boldsymbol{F}_{n+1,i}$ using $\boldsymbol{u}_{n+1,i}$;

25 Evaluate $\boldsymbol{F}^B_{n+1,i} \leftarrow \boldsymbol{F}_{n+1,i}\left(\boldsymbol{F}^A_n\right)^{-1}$;

26 Evaluate $\hat{\boldsymbol{T}}^B_{n+1,i}$ and $\boldsymbol{S}^B_{n+1,i}$;

27 **end**

/* Assemble the Jacobian and the residue */

28 Assemble $\boldsymbol{J}^{\boldsymbol{u}}_{n+1,i}$ using Eq.(4.43);

29 Assemble $\boldsymbol{R}^{\boldsymbol{u}}_{n+1,i}$ using Eq. (4.39);

30 **end**

31 Solve $\boldsymbol{J}^{\boldsymbol{u}}_{n+1,i}\Delta\boldsymbol{u}_{n+1,i} = -\boldsymbol{R}^{\boldsymbol{u}}_{n+1,i}$ for $\Delta\boldsymbol{u}_{n+1,i}$;

/* Update $\boldsymbol{u}_{n+1}$ */

32 $\boldsymbol{u}_{n+1,i+1} \leftarrow \boldsymbol{u}_{n+1,i} + \Delta\boldsymbol{u}_{n+1,i}$;

/* Check the stop criterion */

33 $\epsilon_1 \leftarrow ||\Delta\boldsymbol{u}_{n+1,i}||$;

/* Increment i */

34 $i \leftarrow i + 1$;

35 **end**

Output: $\boldsymbol{u}_{n+1} \leftarrow \boldsymbol{u}_{n+1,i+1}$

/* Procedure to update $\boldsymbol{E}^A$ */

/* Loop over the integration points */

for *(int* $= 1$ *to maximum number of integration points)*

  Input: $\boldsymbol{F}_n^A$; $\boldsymbol{F}_{n+1}$; $\boldsymbol{C}_{n+1}$ for each integration point

  /* Newton-Rhapson procedure */

  Iteration $i \leftarrow 0$;

  while *(tolerance*$<\epsilon_3$ *and* $i <$*maximum number of iterations)* **do**

    Assemble $\boldsymbol{R}^{\boldsymbol{E}^A}_{n+1,i} = \boldsymbol{S}^A_{n+1,i} - (\boldsymbol{C}^{A^{-1}})_n \boldsymbol{C}_{n+1,i} \boldsymbol{S}^B_{n+1,i}$;

    Assemble $\boldsymbol{J}^{\boldsymbol{E}^A}_{n+1,i} = \partial_{\Delta \boldsymbol{E}^A_{n+1,i}} \boldsymbol{S}^A_{n+1,i}$;

    Solve $\boldsymbol{J}^{\boldsymbol{E}^A}_{n+1,i} \Delta \boldsymbol{E}^A_{n+1,i} = -\boldsymbol{R}^{\boldsymbol{E}^A}_{n+1,i}$ for $\Delta \boldsymbol{E}^A_{n+1,i}$;

    Update $\boldsymbol{E}^A_{n+1,i+1} \leftarrow \boldsymbol{E}^A_{n+1,i} + \Delta \boldsymbol{E}^A_{n+1,i}$.

    /* Check the stop criterion. */

    $\epsilon_3 \leftarrow ||\Delta \boldsymbol{E}^A_{n+1,i}||$;

    /* Increment i */

    $i \leftarrow i + 1$;

  end

end

/* Update $\dot{\boldsymbol{E}}^A$ */

$$\dot{\boldsymbol{E}}^A_{n+1} \leftarrow \frac{\boldsymbol{E}^A_{n+1} - \boldsymbol{E}^A_n}{\Delta t}$$

/* Update $\dot{\boldsymbol{F}}^A_{n+1}$ */

$$\dot{\boldsymbol{F}}^A_{n+1} \leftarrow \boldsymbol{F}_n^{A^{-t}} \dot{\boldsymbol{E}}^A_{n+1}$$

/* Update $\boldsymbol{F}^A_{n+1}$ */

$$\boldsymbol{F}^A_{n+1} \leftarrow \boldsymbol{F}^A_n + \Delta t \dot{\boldsymbol{F}}^A_{n+1}.$$

5 Numerical Results

Numerical results concerning simulations for the models proposed in this work are detailed in this chapter. In order to lead the reader through a progressive and natural understanding of the employed approaches, the examples are ordered from the simplest case to the most complex one, and are divided in two main parts. Firstly, we consider tests with the simplified parallel model of Sec. 3.2.1, as a review of those previously published by Costa-Haveroth et al. (2022). Secondly, we present and discuss novelty results for the series model, for which the governing equations are summarized in Sec. 3.1.5.

5.1 Results on the Parallel Model

This section presents several numerical results related to specializations of the model discussed in Sec. 3.2.1, as a review and an extension of those previously published in Costa-Haveroth et al. (2022). We start by commenting on some aspects of the one-dimensional version of this model and use the conclusions to extend the approach for the two-dimensional case.

5.1.1 Viscoelastic Bar

Consider a viscoelastic bar with density ρ_0, length ℓ, and a squared cross-section area A, fixed at the left end and subject to an external force $F(t)$ on the other end, as shown in Fig. 5.1.

Figure 5.1 – Viscoelastic bar.

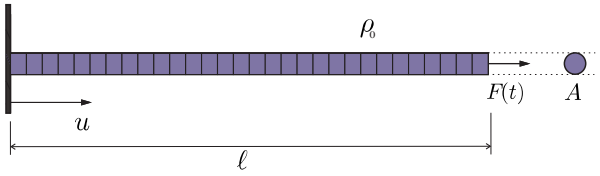

Modified from Costa-Haveroth et al. (2022).

Here we test a simplified version of the model shown in Sec. 3.2.1 to account for this problem. In the first moment, we consider no damage effects ($c_\lambda = 0$); neither dissipation due viscous damping ($\tilde{b} = 0$); furthermore, the bar is strain free for the initial time ($\boldsymbol{E}_0 = \boldsymbol{0}$). We also adopt the results shown in Costa-Haveroth et al. (2022) to disregard the last two terms in Eq. (3.42), that simplifies to:

$$\boldsymbol{S} = \mu(\boldsymbol{I} - \boldsymbol{C}^{-1}) + \lambda \ln\left[(\det(\boldsymbol{C}))^{\frac{1}{2}}\right]\boldsymbol{C}^{-1} + \frac{1}{\rho_0}\boldsymbol{\mathcal{A}} : {}_0\mathrm{D}_t^{\alpha}(\boldsymbol{E}_t). \tag{5.1}$$

Next, one-dimensional dynamic tensile tests for the viscoelastic bar of Fig. 5.1 are performed to measure effect of the fractional viscoelastic parameters.

Remark 5.1. *It is important to emphasize that, concerning this author's best knowledge, previously published works, apart from Costa-Haveroth et al. (2022), do not consider the last two terms shown in Eq. (3.42) when fractional derivatives are used to simulate viscoelasticity. As shown in Appendix E.2.1, these terms appear from the choice of the free-energy density associated with memory terms that was proposed to induce the fractional derivative term in the stress/strain relation. When $\boldsymbol{\mathcal{A}}$ is not dependent on $\boldsymbol{E}$, these terms are null. When $\boldsymbol{\mathcal{A}}$ is allowed to depend on $\boldsymbol{E}$, then, from the purely mathematical point of view, these terms must be included in $\boldsymbol{S}$ for consistent thermodynamics considerations; however, by the tests performed in Costa-Haveroth et al. (2022), we conclude that they can be disregarded for the numerical purposes considered in the present work. Based on these arguments, the following numerical simulations are performed by neglecting the last two terms in Eq. (3.42).*

5.1.1.1 Displacement for the Dynamic One-Dimensional Test

Here, we study the dynamic one-dimensional response of the bar by checking the viscoelastic effect induced by the fractional derivative.

For this problem, we assume Finite Element Method (FEM) with a mesh composed by m Lagrangian linear bar elements. Proper adaptations must be considered for the one-dimensional version of the interpolation shape functions matrices presented in Eqs. (4.3)-(4.6). In the time discretization, we use the Newmark method (NM) (NEWMARK, 1952) with time increment Δt and the usual constants β_N and γ_N as presented in Tab. 5.1. Remember that ϵ_1 represents the tolerance for the motion in the Newton-Raphson (NR) implementation. We implemented the Algorithm 1 for numerical evaluation of the problem we are considering in this subsection by using Matlab language.

Table 5.1 – Parameters for the viscoelastic bar simulations.

Mass Density $\rho_0 = 1420\ kg/m^3$	Length $\ell = 2\ m$	Area $A = 176.71459\ mm^2$	Newmark constant $\beta_N = 0.25$
Newmark constant $\gamma_N = 0.5$	Time-step $\Delta t = 1 \times 10^{-4} s$	Tolerance for NR $\epsilon_1 = 10^{-8}$	Mesh Elements $m = 30$

Costa-Haveroth et al. (2022).

For the tests in this section, damage effects are not considered; furthermore, the applied load is $F = 100\ N$ (for $t > 0$). The intensity of this load, the bar dimensions and the simulation time, implies that the results remain in the small strain regime (in fact,

all the tests results in strain smaller than 0,04%). Following Gaul and Schimidt (2007), we assume that $\mathscr{A}$ weights the fractional derivative without dependence on the strain. It means that in this example we have $\mathscr{A} := p$ is a fixed scalar viscoelastic parameter. The Neo-Hookean spring in Eq. (5.1) is replaced by a linear elastic spring, once we are dealing with small strain. Then, Eq. (5.1) simplifies[1] to

$$S = E_Y E + \frac{p}{\rho_0} \cdot \mathrm{D}_t^{\alpha}(E_t), \tag{5.2}$$

where the unbolded S and E_t are the scalar forms of $\boldsymbol{S}$ and $\boldsymbol{E}_t$, respectively. The Poisson's ratio considered here is $\nu = 0.39$, the Young's modulus is $E_Y = 1430.1 \times 10^6\ Pa$, and the simulation time is $t_f = 0.1\ s$. The values for other parameters are show in Tab. 5.1.

We observe an oscillatory displacement at the free end of the bar induced by the loading. It is shown in Figs. 5.2 and 5.3 for some values of p and α. Once p weights the viscoelasticity influence given by the fractional derivative, the damping effect is augmented when this parameter increases. The same behavior is observed for the variation of α.

Figure 5.2 – Displacement of the viscoelastic bar for $\alpha = 0.5$ fixed and p varying.

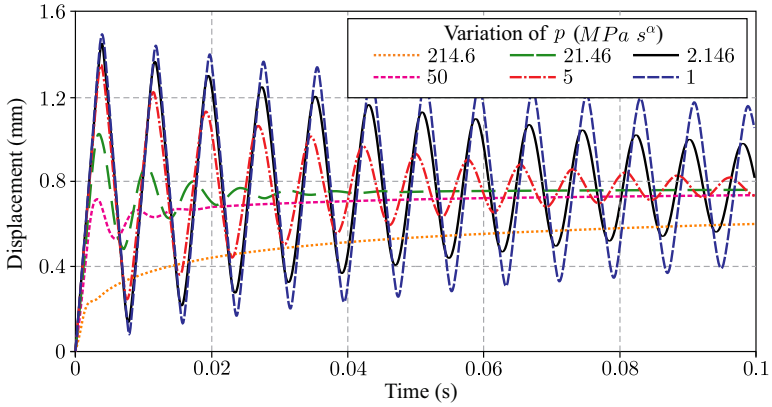

Costa-Haveroth et al. (2022).

The results of this section gives qualitative information that improve our knowledge on the viscoelastic effects associated to the parameters p and α; they guide the two-dimensional tests that will be presented in the next section.

We also stress that the results of Figs. 5.2 and 5.3 agree qualitatively with those presented in the literature for similar viscoelastic problems (EVGENY; HUFENBACH; KROLL, 2003; SCHIMIDT; GAUL, 2006).

5.1.1.2 Two-Dimensional Extension

In this section we perform two-dimensional simulations for the viscoelastic bar of Fig. 5.1 as an extension of the one-dimensional case investigated in the previous

[1] Equation (5.2) is a fractional stress/strain relation widely used in the literature to describe a simple one-dimensional viscoelastic model (FARNO; BAUDEZ; ESHTIAGHI, 2018; MAINARDI, 2010). In the context of this work, it is obtained as a simplification of a more general model (see Sec. 3.2.

Figure 5.3 – Displacement of the viscoelastic bar for $p = 214.6\ \left[(N/m^2)s^{\alpha}\right]$ and α varying.

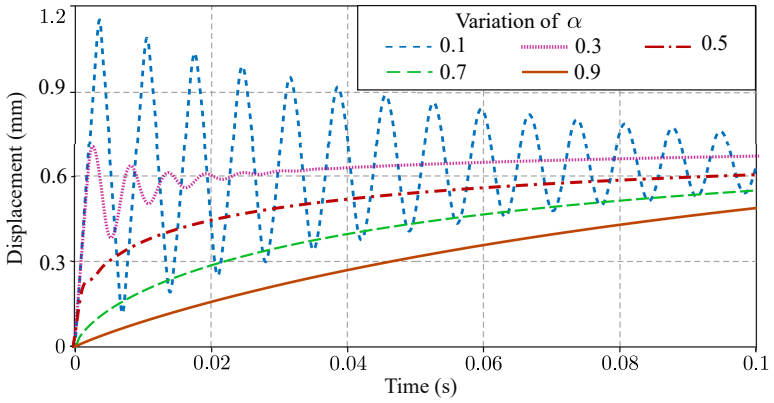

sub-section.

Here, we evaluate the stress by

$$\boldsymbol{S} \;=\; E_Y \boldsymbol{E} + \frac{1}{\rho_0}\boldsymbol{\mathcal{A}} : {}_0\mathrm{D}_t^{\alpha}(\boldsymbol{E}_t), \tag{5.3}$$

that is the multidimensional counterpart of the stress expression of Eq. (5.2).

A key aspect for the two-dimensional extension is a suitable $\boldsymbol{\mathcal{A}}$ choicement, that now must be calculated as a fourth-order tensor. Concerning this aspect, reviewing and extending some of the considerations presented in Costa-Haveroth et al. (2022), we assume that

$$\boldsymbol{\mathcal{A}} := \overline{\lambda}\boldsymbol{C}^{-1} \otimes \boldsymbol{C}^{-1} + 2(\overline{\mu} - \overline{\lambda}\ln\left[(\det(\boldsymbol{C}))^{\frac{1}{2}}\right]\boldsymbol{\mathcal{I}}, \tag{5.4}$$

with

$$\overline{\lambda} = \frac{p\nu}{(1+\nu)(1-2\nu)}, \quad \overline{\mu} = \frac{p}{2(1+\nu)}, \tag{5.5-5.6}$$

which are the expressions of the traditional Lamé parameters but replacing the Young's modulus E_Y by the constant $p = 21.46 \times 10^6\ N/m^2 s^{\alpha}$; here, p is the weighing parameter that has a role similar to that of Young's modulus in the standard elasticity case.

Note that expression (5.4) is an adaptation of the traditional Neo-Hookean elastic tensor and includes the possibility of nonlinearities on $\boldsymbol{\mathcal{A}}$ with respect to the strain. Frequently in the literature, $\boldsymbol{\mathcal{A}}$ is taken fixed and constant, once most of the applications of fractional derivatives are limited to small strains (GAUL; SCHIMIDT, 2007; LEWANDOWSKI; CHORAŚYCZEWSKI, 2010). Although the fractional derivative imposes a nonlinear behavior on the strain for $\alpha \in (0, 1]$, when α tends to 0, the term ${}_0\mathrm{D}_t^{\alpha}(\boldsymbol{E}_t)$ tends to $\boldsymbol{E}_t$. In this case, if we assume a nonlinear dependency of $\boldsymbol{\mathcal{A}}$ on $\boldsymbol{E}$, then the term $\boldsymbol{\mathcal{A}} \cdot {}_0\mathrm{D}_t^{\alpha}(\boldsymbol{E}_t)$ can behave as a nonlinear spring, which is a desirable modeling behavior when dealing with large strains. Then, Eq. (5.4) is used next to simulate the viscoelastic behavior.

5.1.2 I-shaped Viscoelastic Specimen

In this section, we review the plane stress state simulations with an idealized I-shaped viscoelastic specimen (see Fig. 5.4) performed in Costa-Haveroth et al. (2022). The material was considered undamaged (without voids) for the initial time, but, for some cases discussed following, we include the effect of damage as the simulation evolves.

Figure 5.4 – I-shaped viscoelastic specimen.

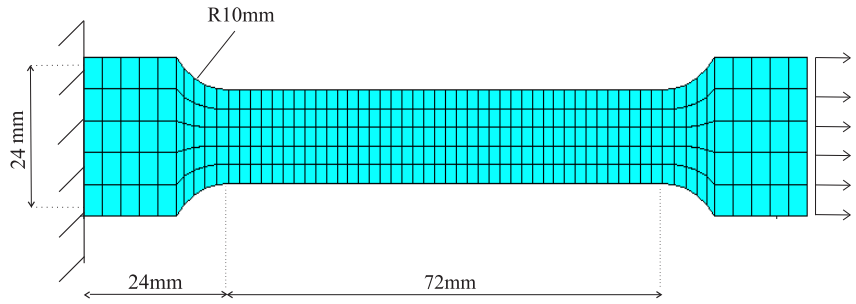

Modified from Costa-Haveroth et al. (2022).

We used m Lagrangian bi-linear quadrilateral elements for the FE discretization, as shown in Fig. 5.4. Table 5.2 presents further simulation data and the adopted material parameters chosen to reproduce the behavior of a generic hard-strong polymeric material (GOWARIKER; VISWANATHAN; SREEDHAR, 1986, p.440). The check point, for which the results are presented, is the center of the specimen (the center of the gauge length).

Table 5.2 – Parameters for the viscoelastic bar simulations.

Mass density $\rho_0 = 2700\ Kg/m^3$	Thickness $t = 0.132934\ mm$	Griffith coefficient $g_c = 4000\ N/m$	Fracture layer $\gamma_c = 0.025\ mm$
Young's modulus $E_Y = 69 \times 10^9\ Pa$	Time-step $\Delta t = 1 \times 10^{-3}\ s$	Poisson's ratio $\nu = 0.33$	Mesh elements $m = 300$

Costa-Haveroth et al. (2022).

5.1.2.1 Loading-Unloading Simulation without Damage

Consider the specimen show in Fig. 5.4 fixed on the left end and subject to an step-by-step distributed load on the other end with constant rate of $5.0 \times 10^6\ N/s$. When the simulation achieves $t_f = 0.8\ s$, the unloading starts to be performed by the opposite rate. We tested the two-dimensional version of our motion equation to describe this loading/unloading problem and scrutnize the influence of the fractional parameter α. The tolerance of the NR procedure for motion is 1×10^{-8}. In this first moment, damage effects are not considered; then, the stress/strain relation can be given by

$$\boldsymbol{S} \;=\; \mu(\boldsymbol{I} - \boldsymbol{C}^{-1}) + \lambda \ln\left((\det(\boldsymbol{C}))^{\frac{1}{2}}\right)\boldsymbol{C}^{-1} + \frac{1}{\rho_0}\boldsymbol{\mathcal{A}} : {}_0\mathrm{D}_t{}^{\alpha}(\boldsymbol{E}_t), \tag{5.7}$$

with $\boldsymbol{\mathcal{A}}$ shown in Eq. (5.4) and $p = 214.6 \times 10^4\ N/m^2 s^\alpha$ fixed.

Figure 5.5a shows the stress/strain plots in the x-direction (horizontal) for α varying. We do not prescribed a residual strain to the specimen after unloading. The behavior shown in Fig. 5.5a is determined naturally by the α choice. As expected, the viscous effect and the residual strain grow as α tends to 1. For α near to 0, the elastic recovering is predominant. These results agree with the background shown in the literature for viscoelastic material under a loading-unloading movement (ZHANG; MOORE, 1997) and give more details on the influence of the parameter α.

Figure 5.5 – Stress/strain diagram in the horizontal direction for some values of α.

(a) Load-unload test without damage effects. Constant strain rate of $5.0{\times}10^6$ N/s.

(b) Tensile test until the specimen breaks with a step-by-step displacement of $1.0 \times 10^{-5}\ mm/t.s$ Damage evolution is included.

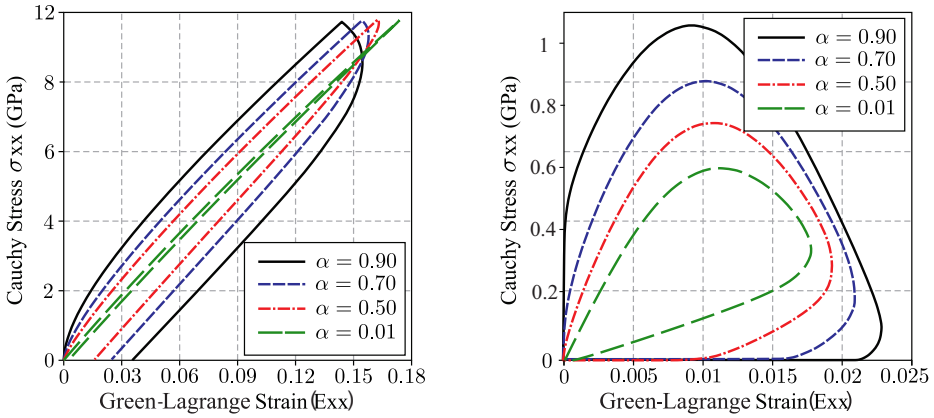

Costa-Haveroth et al. (2022).

5.1.2.2 Tensile Test with Damage Evolution

In order to increment the complexity of the tests, we perform two-dimensional tensile simulations with the specimen of Fig. 5.4, including the damage effects. In this case, the stress tensor considered is given by:

$$\begin{aligned} \boldsymbol{S} \;=\; & G\left[\mu(\boldsymbol{I}-\boldsymbol{C}^{-1}) + \lambda \ln\left((\det(\boldsymbol{C}))^{\frac{1}{2}}\right)\boldsymbol{C}^{-1}\right] - g_c\gamma\left(\boldsymbol{C}^{-1}\nabla_{\boldsymbol{p}}(\varphi)\right)\otimes\left(\boldsymbol{C}^{-1}\nabla_{\boldsymbol{p}}(\varphi)\right) \\ & + \frac{G}{\rho_0}\left(\boldsymbol{\mathcal{A}} : {}_0\mathrm{D}_t^{\alpha}(\boldsymbol{E}_t)\right), \end{aligned} \tag{5.8}$$

with $\boldsymbol{\mathcal{A}}$ and G given respectively by Eqs. (5.4) and (3.30), and $p = 69 \times 10^8\ N/m^2 s^\alpha$. The damage evolution is considered by solving Eq. (3.44). We applied a step-by-step displacement of $1.0 \times 10^{-5}\ mm/t.s$ and monitored the damage increasing until the rupture. The parameter associated with the rate of damage increasing (see Eq. (3.13)) is $c_\lambda = 10^{-7}\ m^2/Ns$ and the remaining parameters are the same as Sec. 5.1.2.1. We adopted the numerical procedure indicated in Sec. 4.4, with the suitable adaptations for this case. The

tolerance of the NR procedure is $\epsilon_2 = 1.0 \times 10^{-8}$ for motion equation and $\epsilon_1 = 1.0 \times 10^{-3}$ for damage equation.

Figure 5.5b presents the stress/strain diagrams for α variation. Note that the nonlinearity due to damage, viscoelasticity and large strains is remarkably in these graphs. When the specimen achieves the rupture, the stress/strain curves recover to the origin, a typical behavior for viscoelastic materials. Figure 5.6 shows the damage evolution for $\alpha = 0.5$ fixed until the specimen breaks. The parameters chosen induces the crack localization. The next section shows a different pattern for damage occurrence.

Figure 5.6 – Damage evolution for $\alpha = 0.5$.

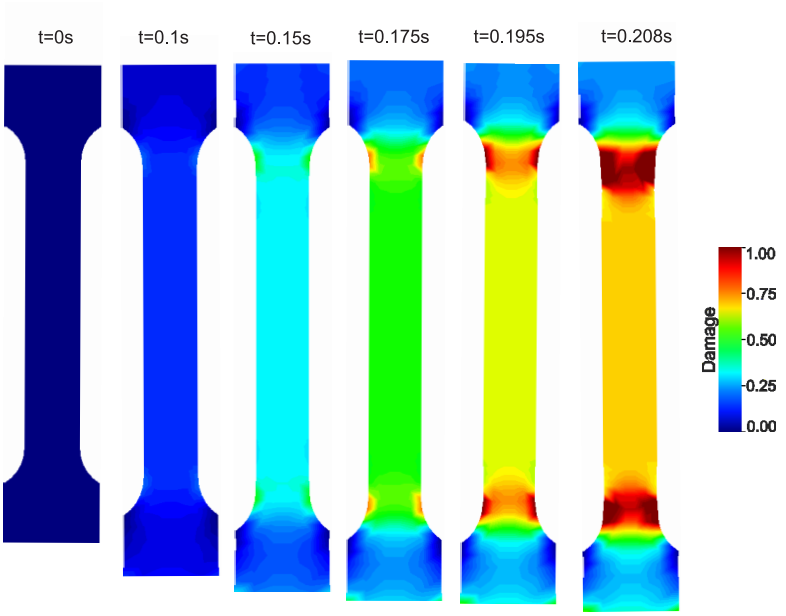

5.1.3 Comparison with Experimental Results

In this section, reviewing results of Costa-Haveroth et al. (2022), we comment on the robustness of the model proposed in Sec. 3.2.1 to fit laboratory data.

The experimental data were obtained from Dusunceli and Colak (2008), who accomplished several tests to characterize material properties of high-density polyethylene (HDPE). They collected samples from extruded PE100 pipes and used the ISO 6259-1 and ISO 6259-3 standards to perform the experiments. For loading-unloading tensile tests, the specimens were fixed at one end, and a load, in the x-direction (horizontal) with a constant strain rate, was applied on the other end. When the test point, at the center of the specimen, achieves a prescribed strain level, the unloading occurs by adopting the opposite strain rate. The geometry of the samples is shown in Fig. 5.7. The laboratory temperature was fixed at 24° C.

In Costa-Haveroth et al. (2022), the setting of these experiments is reproduced for simulations. The formulation proposed in Sec. 3.2.1 is adapted for the plane strain state

Figure 5.7 – HDPE sample used in for curve fitting.

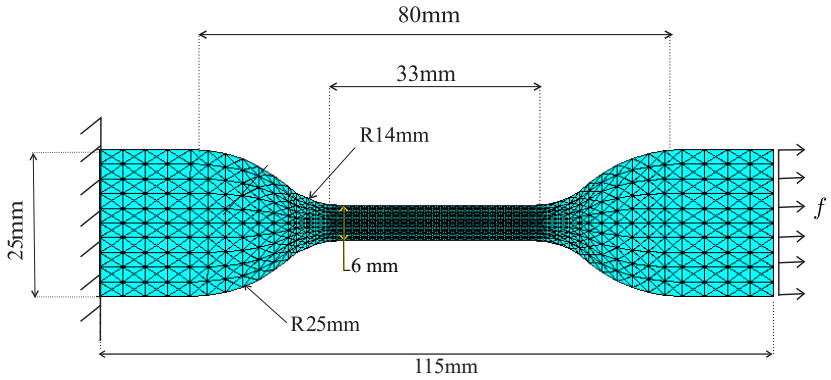

Modified from Costa-Haveroth et al. (2022).

in a quasi-static case; the damage evolves by Eq. (3.44). The irreversibility for damage (see Sec. 4.2) is adopted; thus, damage does not decrease during unloading. The stress used is shown in Eq. (5.8), where the fractional derivative is evaluated by Algorithm G1 (see Sec. 4.1.4).

The Algorithm 1 was adjusted for this problem and implemented in the software hp^2Fem in C++ language. The NR tolerance was $\epsilon_1 = \epsilon_2 = 1 \times 10^{-12}$ for motion and damage equations. A mesh with 2240 finite linear triangular elements of the nodal Lagrange family were used (see Fig. 5.7), and the time step considered was $\Delta t = 0.1\ s$.

It is important to highlight that we had to compare the obtained simulated curves directly with the experimental curve presented in Dusunceli and Colak (2008); a more quantitative comparison was not possible because we did not have access to the laboratory data.

Next, we comment on the effectiveness of our model in fitting the laboratory results in two cases: small and large strains[2].

5.1.3.1 Small Strain

Firstly, the specimen of Fig. 5.7 is loaded slowly by a constant strain rate of 1×10^{-4} until achieves 5% of strain for the test point. Then, the unloading occurs by the opposite strain rate. The damage effects are included for the simulations through Eq. (3.44) and the degradation function $G := G_1$ of Eq. (3.30).

The parameters identification was preceded by several tests to investigate their influence on the model. When the effect of these parameters on the stress/strain curve was identified, we proposed trial values for curve-fitting on the loading part. The values which lead to the best fit were adopted.

[2] There is not consensus in the literature concerning the proper range for small strain; then, in this work, we follow Brinson and Brinson (2015) and Leonov and Prokunin (2012) and assume that small strain for a viscoelastic material occurs if the strain level is less than 5%.

We stress that we do not fit the curve for the unloading part; it is obtained as a natural consequence of the choice of the parameters for the loading. The material parameters identified in Costa-Haveroth et al. (2022) are indicated in Tab. 5.3.

The geometric/material fixed data are thickness $t = 5\ mm$; fracture toughness $f_t = 0.89 \times 10^6\ Pa.m^{\frac{1}{2}}$; length of the fracture layer $\gamma = 0.006\ mm$; Poisson's ratio $\nu = 0.45$; density $\rho = 0.954\ g/m^3$; and $\zeta = 1$. For the plane strain case[3], we follow Perez (2016) by taking the Griffith constant g_c in terms of the fracture toughness:

$$g_c = f_t^2 \frac{(1.0 - \nu^2)}{E}. \tag{5.9}$$

Table 5.3 – Identified parameters for fitting the experimental results.

Young's modulus	Rate of damage increase	Viscoelastic parameter	Fractional derivative order
$E = 0.8 \times\ 10^8 Pa$	$\tilde{c} = 0.18 \times 10^{-2}\ m^2/N.s$	$p = 0.56 \times 10^9\ N/m^2 s^\alpha$	$\alpha = 0.3$

Costa-Haveroth et al. (2022)

The stress/strain diagram obtained for the simulation can be compared with the laboratory result in Fig. 5.8a. Note that the coupling of the straining process and damage evolution, allowed by the model, holds the fitting in the simulations for loading, and naturally promotes the recovering pattern of the experimental results for the unloading. The degradation, as a hereditary phenomenon associated with the damage during the loading process, affects the residual strain for the unloading, resulting in a very approximate behavior when compared with experimental data. Most viscoelastic models found in the literature does not deal properly with unloading.

We consider that the inclusion of damage effects in the process is crucial to obtain suitable results, since viscoelastic materials are susceptible to local failure even at very small strain levels.

Figure 5.8b presents the damage nucleation and subsequent propagation for this simulation. We note the increase of the damage in the center of the specimen, but for this percentage of strain, it is still far from the rupture.

To check the accuracy of the results, we also tested the simulations with $\Delta t = 10^{-3}\ s$. Although we obtained the same qualitative results as those presented for a coarser Δt, some issues related to the fractional derivative evaluation were intensified: simulation effort and memory storage increased greatly. Furthermore, although the algorithm G1, described in Sec. 4.1.4 is attractive due to its simple implementation, its use carries difficulties in coupling an automatic optimization procedure for parameter identification.

[3] The geometry of Fig. 5.7 unfortunately is neither fully in plane strain state nor fully plane stress state; in fact, according to Irwin (1958, p. 656) it is a mixed stress/strain state. Then, to simplify the simulation, we decided to approximate by considering a plane strain situation.

Figure 5.8 – Fitting for the load/unload test in the case of small strain.

(a) Stress/strain diagram for experiment and simulation. Contant strain rate of 1×10^{-4}.

(b) Damage propagation in the sample until 5% strain by using G_1.

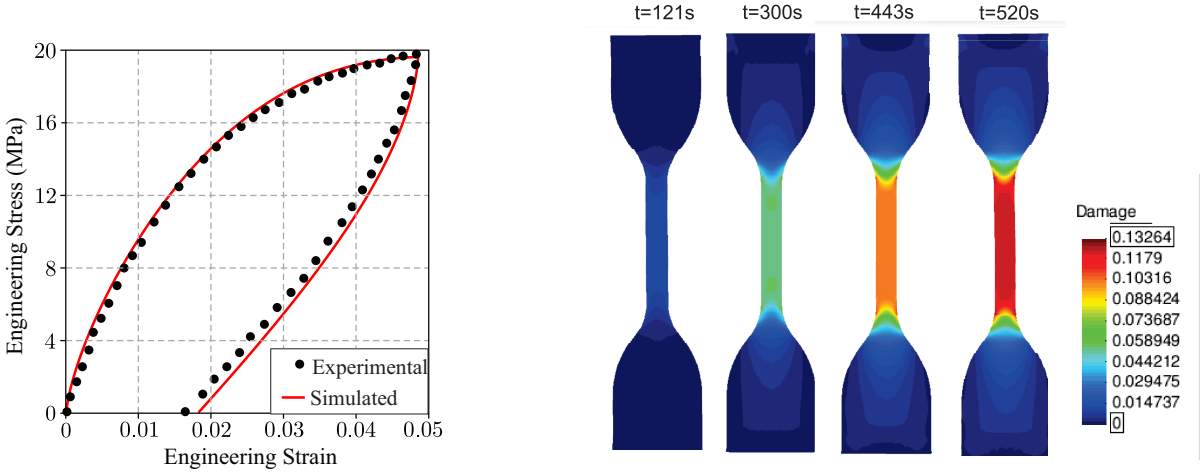

Costa-Haveroth et al. (2022).

Future works on this concern must consider more economic fractional derivative algorithms (see Costa-Haveroth et al. (2021) for some suggestions).

5.1.3.2 Large Strain and Fracture

In this section, we test the robustness of our model to fit laboratory results for the case of large strain; the discussion here is an extension of that we presented in Costa-Haveroth et al. (2022).

The sample shown in Fig. 5.7 is fixed on the left end and subject to an uniaxial load in the x-direction (horizontal) until the sample achieves 15% strain for the test point (the center of the specimem); then an unloading is performed by the opposite strain rate.

We assume this problem as a natural extension of the previous case; then, in a first moment, we try to fit the laboratory results of Dusunceli and Colak (2008) by using the same conditions of Sec. 5.1.3.1 and the previous identified material parameters (see Tab. 5.3). Figure 5.9a shows simulated results and the experimental data.

For the laboratory results, note that the stress level increases until the strain achieves 8%. After that, the loss of stiffness implies in a gradual decreasing of stress. This result diverges remarkably from the simulated one, in which the stress decline quickly after 5% of strain.

The behavior of the stress is strongly determined by the degradation function $G := G_1$, as can be seen in Eq. (5.8). Figure. 5.9b correlates the strain level and the damage values during the simulation by the geometric symbols. Note that as the strain increases, the degradation due damage decreases quickly. In contracts, the damage variable

Figure 5.9 – Trial to fit the experimental results. The geometric symbols associate the strain level with the corresponding degradation for the test.

(a) Stress/strain diagrams for the degradation function $G := G_1$.

(b) Degradation function $G := G_1$.

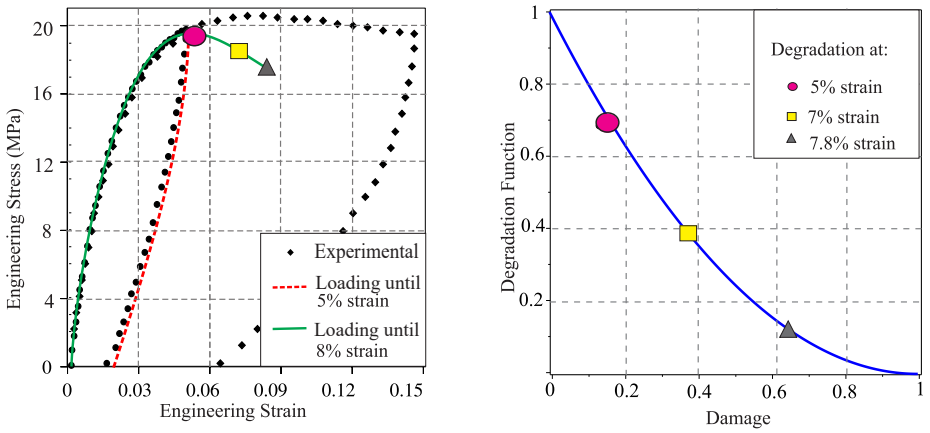

Costa-Haveroth et al. (2022).

increases fast as the process evolves and leads to rupture when the strain exceeds 8,25%. Consequently, as the degradation gets smaller, the stress decreases rapidly (for more comments on the degradation function, see Sec. 3.1.4). Although this behavior is suitable for brittle materials, it is not desirable for the viscoelastic component studied here.

Once the degradation function G_1 does not reproduce the expected behavior for the case of large strains, Costa-Haveroth et al. (2022) tested the alternative function G_2, given by Eq. (3.31), to perform a new fitting. As commented in Sec. 3.1.4, the function G_2 was conceived to characterize the damage in viscoelastic materials based on the microstructure evolution. This function is written in terms of the constants a, b and c, that are additional parameters to be identified. The parameters identified in Costa-Haveroth et al. (2022) are shown in Tab. 5.4.

Table 5.4 – Parameters for fitting the experimental results.

Young's modulus $E_Y = 0.4 \times 10^8\ Pa$	Rate of damage increase $c_\lambda = 0.115 \times 10^{-2}\ m^2/N.s$	Viscoelastic parameter $p = 0.67 \times 10^9\ N/m^2 s^\alpha$	Fractional derivative order $\alpha = 0.35$
Parameters of function G_2	$a = 3.8$	$b = 1.5$	$c = 1.15$

Costa-Haveroth et al. (2022)

Figure 5.10a presents a significantly improvement in the fitting between the new simulation and the laboratory results. Figure 5.10b shows that G_2 has the desirable behavior to properly fit the experimental data, as commented previously. Geometric symbols correlate the degradation and the strain levels. Figure 5.11 shows the damage evolution for the specimen until 15 % strain.

Figure 5.10 – Stress/strain diagrams for the use of the degradation function $G := G_2$. The geometric symbols associate the strains and the degradation levels.

(a) Stress/strain diagram.

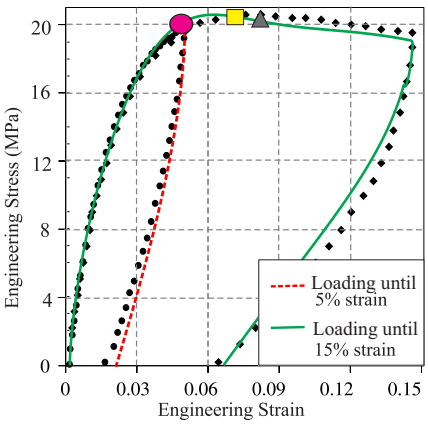

(b) Degradation function G_2 for $a = 3.8$, $b = 1.5$ and $c = 1.15$.

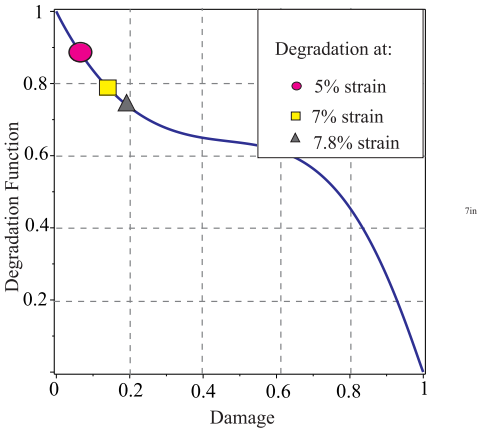

Costa-Haveroth et al. (2022).

Figure 5.11 – Damage evolution in the sample until 15% strain using G_2.

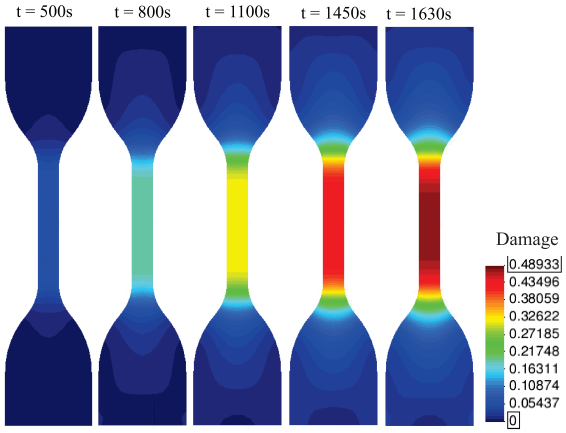

Costa-Haveroth et al. (2022).

Figure 5.10a also shows the simulated results with the parameters of Tab. 5.4 for the case studied in the previous section, where the specimen is loaded just until 5%, then the unloading is performed. Note that in this case, the functions G_1 and G_2 yields very similar stress/strain diagrams. It occurs because the degradations presented by G_1 and G_2 are similar for this levels of strain; nearly to $\varphi = 0.16289$ for both the functions. On this concerning, the fitting provided when the strain level is less then 5% is almost unaffected by the choice of the degradation functions. However, only the function G_2 was able to reproduce the results for the case of large strains.

An additional simulation with the specimen of Fig. 5.7 is performed in our previous work (COSTA-HAVEROTH et al., 2022). To check the crack pattern, we kept the tensile loading until the rupture. We assumed the same parameters shown in Tab. 5.4

for this test. Figure 5.12 shows the damage evolution for this simulation until $t_f = 2654s$. At this point, the strain increased until 23%, and we note the fracture in the center of the specimen.

Figure 5.12 – Damage evolution in the sample until the specimen breaks.

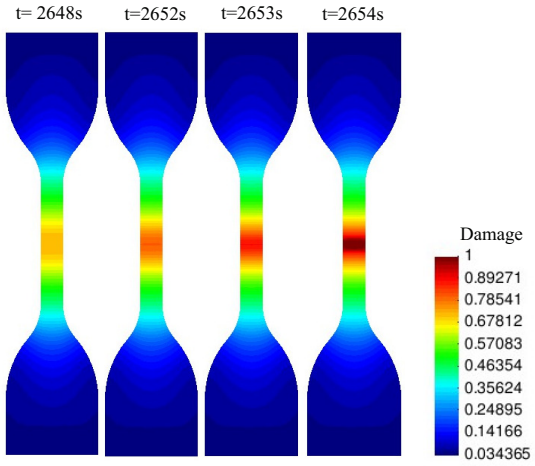

Costa-Haveroth et al. (2022).

5.2 Results for the Series Model

Consider the modified fractional Zener model (SM) and the modified Kelvin-Voigt model (PM) shown in Fig. 5.13. The SM comprises a series arrangement of non-linear springs and a spring-pot, while PM is represented by a non-linear spring and a spring pot arranged in parallel. We observe that, as discussed in Sec. 3.2.1, these models are not purely mechanical since we have also included the damage evolution by coupling the phase-field variable φ in the mathematical modeling.

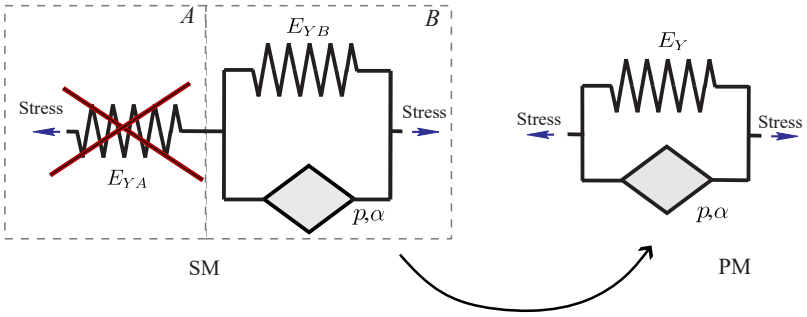

Figure 5.13 – Simplification of the modified fractional Zener model (SM) to the modified Kelvin-Voigt model (PM).

The parameters, E_{YA} and E_{YB}, shown in Fig. 5.13, are related with the stiffness of the non-linear springs in part A and B, respectively, and behave similarly to the Young's modulus. For the SM, if we assume that the non-linear spring, associated with E_{YA}, is much stiffer than the other elements, then the applied forces, and consequently the

displacements, are substantially transferred to the other non-linear spring, described by E_{YB}, and to the spring-pot. In other words, if we neglect part A, then SM simplifies to PM.

In this section, we performed some qualitative comparisons between SM and PM and verified the behavior induced by the material parameters variation in order to enhance the understanding of the behaviors of the models.

In the following, we consider two-dimensional tensile tests for the specimen shown in Fig. 5.7. As before, the specimen is fixed at one end, and a uniaxial load in the x-direction (horizontal) is applied on the other end. The temperature is fixed at 24° C. The stress adopted for PM is shown in Eq. (5.8), where the fractional derivative is evaluated by the Algorithm G1 (see Sec. 4.1.4). For SM, remember that we split the stress on part A and part B (see Sec. 3.1.3). The stress considered for part A is given by Eq. (3.19) and for part B

$$\begin{aligned}\hat{\boldsymbol{T}}^B \;=\; & \frac{1}{\det\left(\boldsymbol{F}^A\right)}\left\{G\left[\mu^B\left(\boldsymbol{I}-\left(\hat{\boldsymbol{C}}^B\right)^{-1}\right)+\lambda^B\ln\left(\det\left(\hat{\boldsymbol{C}}^B\right)\right)^{1/2}\left(\hat{\boldsymbol{C}}^B\right)^{-1}\right]\right. \\ & -g_c\gamma_c\left[\left(\hat{\boldsymbol{C}}^B\right)^{-1}\left(\boldsymbol{F}^A\right)^{-t}\nabla_{\boldsymbol{p}}\varphi\right]\otimes\left[\left(\hat{\boldsymbol{C}}^B\right)^{-1}\left(\boldsymbol{F}^A\right)^{-t}\nabla_{\boldsymbol{p}}\varphi\right] \\ & \left.+\frac{G}{\rho_0}\left[\boldsymbol{\mathcal{A}}:{}_0\mathrm{D}_t^{\alpha}(\hat{\boldsymbol{E}}_t^B)\right]\right\},\end{aligned} \tag{5.10}$$

where G is the degradation function, taken as shown in Eq. (3.31), with the parameters a, b and c given in Tab. 5.4

The numerical implementations of the models are performed by making suitable adaptations on the Algorithm 4.4 for the plane strain case. It is implemented in the software hp^2Fem using C++ language. The tolerance of the NR procedure was $\epsilon = 10^{-12}$ for both motion and damage equations. We considered 2240 linear triangular elements for the FEM, as shown in Fig. 5.7.

The geometric/material data fixed are: thickness $t = 5\ mm$; fracture toughness $f_t = 0.89\times10^6\ Pa.m^{\frac{1}{2}}$; length of the fracture layer $\gamma = 0.006\ mm$; Poisson's ratio $\nu = 0.45$; density $\rho_0 = 0.954\ g/m^3$; and $\zeta = 1$. Again, for the plane strain case, we take the Griffith constant g_c in terms of the fracture toughness as shown in Eq. (5.9).

5.2.1 Comparisons Between SM and PM

Firstly, we compare the behavior of SM and PM (see Fig. 5.13) in the tensile tests by varying the material parameter α associated with the level of viscoelasticity imposed to the models, and fixing the remaining parameters. For this test, we adopt $E_Y = E_{YA} = E_{YB} = 3\times10^9\ Pa$, meaning that the non-linear springs have the same stiffness and $p = 0.67\times10^9 N/m^2 s^{\alpha}$. We apply an incremental distributed load of $10\times10^3\ N/s$ until the time $t_f = 1s$ with $\Delta t = 10^{-2}s$. Figures 5.14a and 5.14b show the stress/strain

diagrams for the case where damage is not considered for the models. For SM, remember that, according to Eq. (2.20), the Cauchy stress tensor has the same value for part A and part B ($\boldsymbol{T}^B = \boldsymbol{T}^A$). Then, in order to promote proper comparisons, we plot the Cauchy stress tensor versus the total strain $\boldsymbol{E}$ for both SM and PM.

Figure 5.14 – Stress/strain diagrams for PM and SM.

(a) PM without damage.

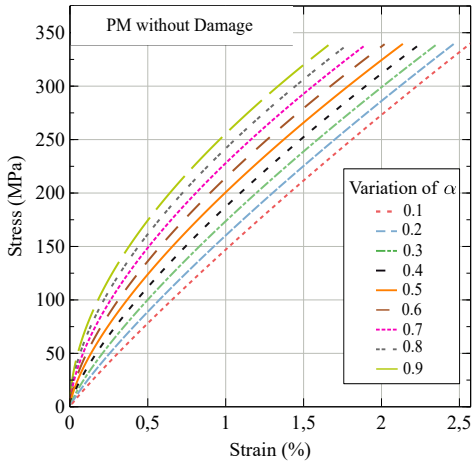

(b) SM without damage.

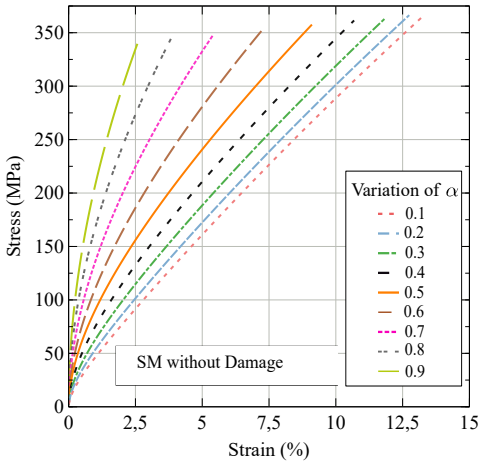

(c) PM with damage.

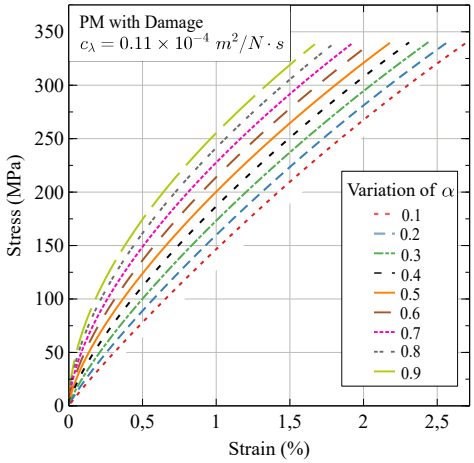

(d) SM with damage.

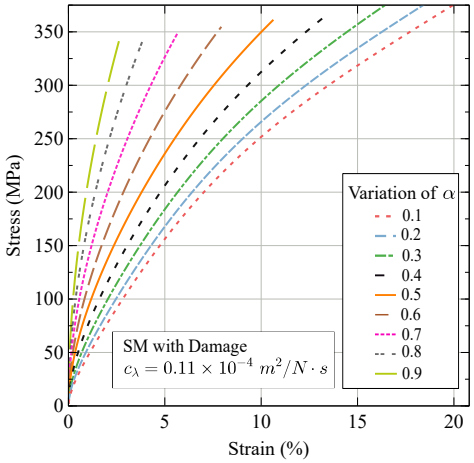

For SM, the level of strain achieved is much higher than for PM, although the level of stress remain similar for both the cases. This behavior was expected, once the extra spring connected in series, for the SM, provides less stiffness to the model.

Figures 5.14c and 5.14d show the stress/strain diagrams for the case where damage was included for the models. We considered $c_\lambda = 0.11 \times 10^{-4} m^2/N \cdot s$. Again, the strain level is higher for the SM then the PM; however, in this case, we can see that the damage effect includes additional nonlinearity to the models. It is noted remarkably in the case of SM, where the strain achieves around to 20% for $\alpha = 0.1$.

5.2.2 Damage effect for SM

In this section, we perform qualitative analysis on the effect caused by the variation of the parameter c_λ, which is associated with the rate of damage increasing, for tensile tests. We apply an incremental distributed load of 10 N/s for the specimen of Fig. 5.7 until the time $t_f = 1s$ with $\Delta t = 10^{-2}s$. Further data is the same as in the previous section. Figure 5.15 show the damage evolution for different values of c_λ and $\alpha = 0.35$, $p = 0.67 \times 10^9$, $E_{YA} = E_{YB} = 0.4 \times 10^8$. fixed. For $c_\lambda = 1 \times 10^{-2}\ m^2/N \cdot s$, the damage nucleation starts near to the radius of the specimen. When c_λ is fixed at $1 \times 10^{-5}\ m^2/N \cdot s$, the damage changes the location and tends to initiate in the center of the sample. By the variation of c_λ, we can obtain different patters for the damaging..

Figure 5.15 – Variation of c_λ for tensile tests and different patters for damage nucleation.

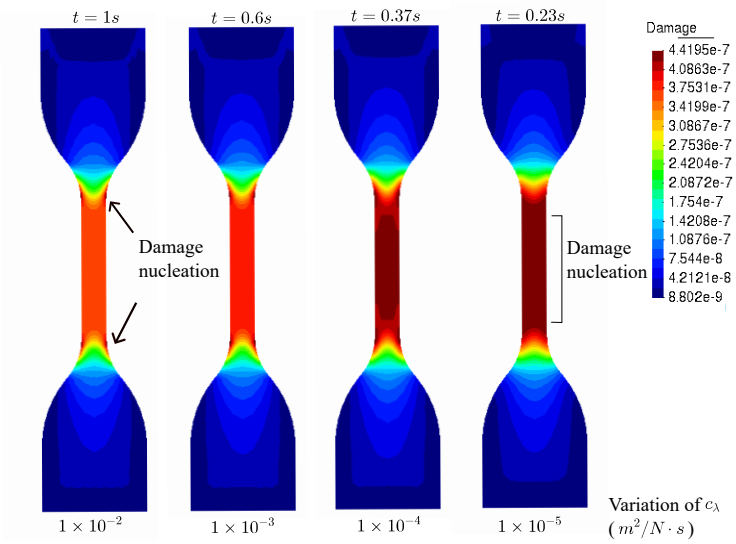

Figure 5.16 shows the damage evolution for the case with $c_\lambda = 1 \times 10^{-3}\ m^2/N \cdot s$. The simulation was performed until the damage location was well defined. Further fixed data is $\alpha = 0.5$, $\Delta t = 10^{-3}$ and an incremental distributed load of 1000 N/s. When we compare the damage pattern presented in this figure with that shown in Fig. 5.12, we can note the flexibility of our model in recover several behaviors that are in fact found for real viscoelastic materials.

Figure 5.16 – Damage evolution for $c_\lambda = 1 \times 10^{-3}\ m^2/N \cdot s$ fixed until the crack.

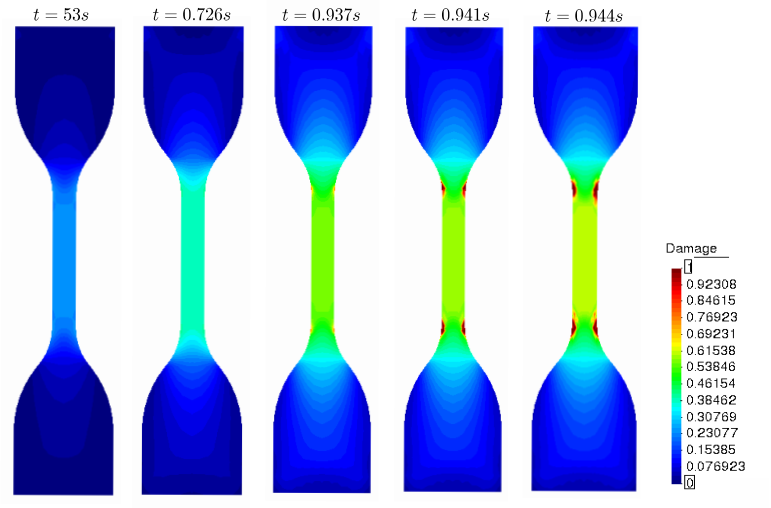

6 Conclusions

In this work, we presented and discussed a new and comprehensive approach in the framework of the damage phase-field model based on the multiplicative decomposition of deformation gradient. It follows the continuum mechanics principles and leads to rather general thermodynamically consistent models.

By adopting a specific free-energy and a particular pseudo-potential of dissipation, we could derive a new family of damage phase-field models with fractional derivatives for materials with fading memory effects. In this thesis, we detailed the arguments for the choice of the free-energy potential, firstly proposed in our previous work (COSTA-HAVEROTH et al., 2022); in particular, we showed in detail how its use ensures the second principle of thermodynamics. This free-energy potential allows damage evolution by including suitable degradation functions, which play an essential role in modeling the stiffness change between the undamaged and the fractured states. As a natural consequence of our choice of free-energy, the stress/strain relation obtained is written in terms of fractional derivatives. Furthermore, the general model can account for finite strain and thermal effects; it is enough to include the thermal dependencies in the chosen potential. A set of partial differential equations mathematically governs the model to describe a body's motion, damage, and temperature.

We applied the degradation function proposed in Costa-Haveroth et al. (2022) to improve the description of viscoelastic fracture to the more general setting of this thesis; this provides more possibilities for realistic characterization of the micro-structural evolution of damage in these materials.

We showed that our general model can be simplified to generate several sub-models to describe damage and viscoelasticity effects in various situations. These sub-models are related to mechanical combinations of rheological components, having thus straightforward physical interpretations.

For the numerical treatment of the system of governing equations, we followed Haveroth et al. (2018) and considered an adapted staggered scheme. This method is also called a semi-implicit/explicit scheme. It consists of solving the equation for each system variable separately by the most appropriate time integration method coupled with the Newton-Rhapson (NR) procedure. We implemented our model in Matlab and C++ and contributed to the software hp^2Fem by including the fractional viscoelasticity.

We verified the performance of our models by several simulations for the isothermal case. The numerical results presented were divided into two parts: a review of the tests provided in Costa-Haveroth et al. (2022) and new simulations for a series

viscoelastic model.

6.1 Observations and Contributions

Here, we summarize the main observations about and conclusions of our work:

1. Firstly, it is essential to emphasize that the general series model proposed in this work is a novelty in the literature. Previous approaches dealing with non-linear viscoelasticity generally relate to parallel rheological arrangements, which have a simple mathematical development and do not present the flexibility of modeling given by series models. Our methodology results in a notably comprehensive model that can be simplified to generate sub-models and deal with different effects, such as large strain, thermal contributions, and distinct damage patterns.

   In Sec. 3.1.1, we used the free-energy potential $\tilde{\psi}_d$, associated with fading memory effects, to ensure the second principle of thermodynamic for the general model proposed in this thesis. This potential, firstly presented in Costa-Haveroth et al. (2022), leads to a stress/strain relation written in terms of fractional derivatives. The form of $\tilde{\psi}_d$ allows the thermodynamically consistent consideration of the non-linear dependency of the tensor $\boldsymbol{\mathcal{A}}$ on the strain (see Sec. E.2.2). It is more general than other potentials associated with fractional viscoelasticity presented in the literature that consider $\boldsymbol{\mathcal{A}}$ as a simple scalar constant.

   As commented in Sec. 3.2, under specific hypotheses, the stress/strain relation obtained in this work can be simplified to generate different relations, including the usual fractional viscoelastic constitutive equations, widely employed in the literature.

2. We extended the discussion provided in Costa-Haveroth et al. (2022) on applying the degradation function G_2 to describe damage for viscoelastic materials. In Sec. 5.1.3.2, we comment on how this function allows the fitting of experimental curves for load/unload tensile tests. These results reinforce that G_2 is a promising alternative to deal with the micro-structure evolution of damage in materials with memory.

3. We presented several one and two-dimensional simulations for the models proposed in this work in different situations. The results indicate that the proposed models successfully describe the response of viscoelastic materials under several conditions: finite strain, damage, fracture, and load/unload process. In Sec. 5.2, we presented new simulated results for our damage viscoelastic series model (SM). We compared SM and its simplified version, a parallel model (PM) previously tested in Costa-Haveroth et al. (2022). We also commented on the behavior induced by the material parameters variation to enhance the understanding of the model. In these tests, we observed the

flexibility of our model in recovering several different behaviors for both, damage evolution and stress/strain relation.

4. We contributed on the expansion of the software $(hp)^2$FEM by implementing a fractional viscoelastic solver in the C++ language. This code was used to generate the simulations presented in Sec. 5.1.3 and 5.2. We presented a pseudo-code summarizing this implementation in Sec. 4.4.

The results presented in this work indicate that the proposed framework successfully describes the response of viscoelastic materials under the conditions tested and is an adequate thermodynamically consistent alternative to deal with large strain and distinct damage patterns.

6.2 Deficiencies and Limitations

The model summarized in Sec. 3.1.5 is comprehensive and can describe several phenomena. However, as a mathematical model becomes more general, it is common to have an increase in algebraic, numerical and interpretative difficulties. Next, we outline the main difficulties identified in this work:

1. As commented in Chapter 4, we adopted several simplifications and strategies to avoid difficulties related to the numerical approach and subsequent computational implementation. Nevertheless, we observed a conspicuous deficiency of the algorithm G1 used to compute the fractional derivatives in our simulations. Although this algorithm is attractive due to its simple implementation, it requires a high computational time. It restricts implementation of automatic optimization procedures for parameter identification to small time intervals. Since the purpose of the present work was to test the effectiveness of the proposed viscoelastic model, we did not investigate the computational aspects of the fractional derivatives here.

2. Due to the limitation associated with the numerical fractional derivative algorithm, it was not possible to implement an automatic inverse parameter identification process. For the fittings presented in this work, the parameters identification was preceded by several tests to investigate their influence on the model. When the effect of these parameters on the stress/strain curve was identified, we proposed trial values for curve-fitting on the loading part. The values with lead to the best fit were adopted. This process is cumbersome, once it demands several non-automatic tests. We hope that the consideration of some economic algorithm for the fractional derivative also allows the implementation of automatic parameter identification processes.

3. Another challenge is the inclusion of thermal effects in viscoelastic materials. This difficulty is not due to limitations of our general model, which is already prepared for the theoretical inclusion of thermal effects, but derives from the necessity of choosing the correct thermal dependencies in particular free-energies and pseudo-potentials of dissipation to recover realistic material behaviors. As commented in Chapter 4, thermal influences in viscoelastic materials demand special care. The mechanical properties of most viscoelastic materials are very sensitive to temperature, and thus for many structural applications, a vast understanding of the effect of temperature on mechanical properties is necessary.

   We did not analyze thermal effects in this work because they open up an extensive range of options to be investigated and mainly because our model needed firstly to be verified in simple situations. For these reasons, we restricted the examples in the present work to the isothermal case.

   However, we also decided to include our full non-isothermal thermodynamic consistent model as a preparation for future investigations taking into account temperature variations.

6.3 Future Works

For future works on the framework of this thesis, we suggest the following:

1. A thorough study on the thermal effects in the viscoelastic materials and the corresponding possibilities, besides the one already presented in this work, of extending the free-energy and pseudo-potential of dissipation to include the dependence on the temperature.

2. The study of the previous item will lead to suitable specific forms for the temperature equation, which can be included in the numerical approach proposed in Chap. 4; subsequent numerical simulations can then be done;

3. Consideration of economic algorithms for fractional derivatives implementation;

4. Comparisons between laboratory results and simulations for the general series model proposed in this work.

5. Further simulations for shear and slow relaxation tests.

REFERENCES

ALFANO, G.; MUSTO, M. Thermodynamic derivation and damage evolution for a fractional cohesive zone model. *Journal of Engineering Mechanics*, American Society of Civil Engineers, v. 143, n. 7, p. D4017001, 2017. Cited 2 times on pages 26 and 29.

ALLEN, S. M.; CAHN, J. W. Ground state structures in ordered binary alloys with second neighbor interactions. *Acta Metallurgica*, Elsevier, v. 20, n. 3, p. 423–433, 1972. Cited on page 21.

AMBATI, M.; GERASIMOV, T.; LORENZIS, L. D. A review on phase-field models of brittle fracture and a new fast hybrid formulation. *Computational Mechanics*, Springer, v. 55, n. 2, p. 383–405, 2015. Cited on page 22.

AMENDOLA, G.; FABRIZIO, M.; GOLDEN, J. M. Thermomechanics of damage and fatigue by a phase field model. *Journal of Thermal Stresses*, Taylor and Francis, v. 39, n. 5, p. 487–499, 2016. Cited 2 times on pages 15 and 23.

ANDERSON, T. *Fracture Mechanics: Fundamentals and Applications, Second Edition*. [S.l.]: Taylor and Francis, 1994. ISBN 9780849342608. Cited on page 29.

ARANSON, I. S.; KALATSKY, V. A.; VINOKUR, V. M. Continuum field description of crack propagation. *Physical review letters*, APS, v. 85, n. 1, p. 118–121, 2000. Cited on page 22.

ARTIN, E. *The gamma function*. [S.l.]: Courier Dover Publications, 2015. Cited on page 48.

BAGLEY, R. L. Power law and fractional calculus model of viscoelasticity. *AIAA journal*, v. 27, n. 10, p. 1412–1417, 1989. Cited on page 24.

BAGLEY, R. L.; TORVIK, P. J. A theoretical basic for the application of fractional calculus to viscoelasticity. *Journal of Rheology*, v. 27, n. 3, p. 201–210, 1983. Cited on page 26.

BALEANU, D.; FERNANDEZ, A. On some new properties of fractional derivatives with mittag-leffler kernel. *Communications in Nonlinear Science and Numerical Simulation*, Elsevier, v. 59, p. 444–462, 2018. Cited on page 27.

BHATTI, M. *Advanced Topics in Finite Element Analysis of Structures: With Mathematica and MATLAB Computations*. Wiley, 2006. ISBN 9780471648079. Available at: <https://books.google.com.br/books?id=fWR5QgAACAAJ>. Cited 3 times on pages 67, 68, and 71.

BOLDRINI, J.; MORAES, E. B. de; CHIARELLI, L.; FUMES, F.; BITTENCOURT, M. A non-isothermal thermodynamically consistent phase field framework for structural damage and fatigue. *Computer Methods in Applied Mechanics and Engineering*, Elsevier, v. 312, p. 395–427, 2016. Cited 9 times on pages 15, 22, 23, 33, 34, 37, 51, 54, and 55.

BOLLADA, P.; JIMACK, P.; MULLIS, A. Bracket formalism applied to phase field models of alloy solidification. *Computational Materials Science*, Elsevier, v. 126, p. 426–437, 2017. Cited on page 22.

BONET, J.; WOOD, R. *Nonlinear Continuum Mechanics for Finite Element Analysis*. Cambridge University Press, 2008. ISBN 9781139467544. Available at: <https://books.google.com.br/books?id=V5Zf1rVeeEsC>. Cited 2 times on pages 53 and 66.

BONFANTI, A.; KAPLAN, J. L.; CHARRAS, G.; KABLA, A. Fractional viscoelastic models for power-law materials. *Soft Matter*, Royal Society of Chemistry, v. 16, n. 26, p. 6002–6020, 2020. Cited 2 times on pages 24 and 26.

BORDEN, M. J. *Isogeometric analysis of phase-field models for dynamic brittle and ductile fracture*. Phd Thesis (PhD Thesis) — University of Texas, 2012. Cited on page 22.

BORDEN, M. J.; HUGHES, T. J.; LANDIS, C. M.; VERHOOSEL, C. V. A higher-order phase-field model for brittle fracture: Formulation and analysis within the isogeometric analysis framework. *Computer Methods in Applied Mechanics and Engineering*, Elsevier, v. 273, p. 100–118, 2014. Cited on page 22.

BORDEN, M. J.; HUGHES, T. J.; LANDIS, C. M.; ANVARI, A.; LEE, I. J. A phase-field formulation for fracture in ductile materials: Finite deformation balance law derivation, plastic degradation, and stress triaxiality effects. *Computer Methods in Applied Mechanics and Engineering*, v. 312, p. 130–166, 2016. Cited on page 58.

BOUKAMEL, A.; MÉO, S.; DÉBORDES, O.; JAEGER, M. A thermo-viscoelastic model for elastomeric behaviour and its numerical application. *Archive of Applied Mechanics*, Springer, v. 71, n. 12, p. 785–801, 2001. Cited on page 32.

BOURDIN, B.; FRANCFORT, G. A.; MARIGO, J.-J. Numerical experiments in revisited brittle fracture. *Journal of the Mechanics and Physics of Solids*, Elsevier, v. 48, n. 4, p. 797–826, 2000. Cited on page 22.

_____. The variational approach to fracture. *Journal of elasticity*, Springer, v. 91, n. 1, p. 5–148, 2008. Cited on page 54.

BRINSON, H.; BRINSON, L. *Polymer Engineering Science and Viscoelasticity: An Introduction*. Springer US, 2015. ISBN 9781489974853. Available at: <https://books.google.com.br/books?id=kmpnBgAAQBAJ>. Cited on page 89.

BRÖCKER, C.; MATZENMILLER, A. On the generalization of uniaxial thermoviscoplasticity with damage to finite deformations based on enhanced rheological models. *Technische Mechanik-European Journal of Engineering Mechanics*, v. 34, n. 3-4, p. 142–165, 2014. Cited on page 28.

CAHN, J. W. Free energy of a nonuniform system. ii. thermodynamic basis. *The Journal of chemical physics*, AIP, v. 30, n. 5, p. 1121–1124, 1959. Cited on page 21.

CAHN, J. W.; HILLIARD, J. E. Free energy of a nonuniform system. i. interfacial free energy. *The Journal of chemical physics*, AIP, v. 28, n. 2, p. 258–267, 1958. Cited on page 21.

CALLEN, H. B. *Thermodynamics and an Introduction to Thermostatistics*. [S.l.]: American Association of Physics Teachers, 1998. Cited on page 132.

CAPUTO, M. Linear models of dissipation whose q is almost frequency independent. *Annali di Geofisica*, 1966. Cited 2 times on pages 26 and 27.

_____. Linear models of dissipation whose q is almost frequency independent. *Geophys. J. R. Astr. Soc.*, 1967. Cited on page 26.

CAPUTO, M.; FABRIZIO, M. Damage and fatigue described by a fractional derivative model. *Journal of Computational Physics*, Elsevier, v. 293, p. 400–408, 2015. Cited on page 30.

_____. Applications of new time and spatial fractional derivatives with exponential kernels. *Progr. Fract. Differ. Appl*, v. 2, n. 2, p. 1–11, 2016. Cited on page 27.

CAPUTO, M.; MAINARDI, F. Linear models of dissipation in inelastic solids. *Riv. Nuovo Cimento*, p. 161–198, 1971. Cited on page 26.

_____. A new dissipation model based on memory mechanism. *Pure Appl. Geophys*, 1971. Cited on page 26.

CHAVES, E. *Notes on Continuum Mechanics*. Springer Netherlands, 2013. (Lecture Notes on Numerical Methods in Engineering and Sciences). ISBN 9789400759862. Available at: <https://books.google.com.br/books?id=2Q1HAAAAQBAJ>. Cited 15 times on pages 31, 115, 116, 117, 118, 119, 120, 121, 122, 127, 132, 133, 134, 135, and 140.

CHIARELLI, L.; FUMES, F.; MORAES, E. B. de; HAVEROTH, G.; BOLDRINI, J.; BITTENCOURT, M. Comparison of high order finite element and discontinuous galerkin methods for phase field equations: Application to structural damage. *Computers & Mathematics with Applications*, Elsevier, 2017. Cited on page 21.

CHOUDHURY, A. Phase-field modeling as a method relevant for modeling phase transformation during interdiffusion. In: *Handbook of Solid State Diffusion, Volume 1*. [S.l.]: Elsevier, 2017. p. 363–389. Cited on page 22.

CHRISTENSEN, R. *Theory of viscoelasticity: an introduction*. [S.l.]: Elsevier, 2012. Cited 2 times on pages 29 and 47.

COLEMAN, B. D. On thermodynamics, strain impulses, and viscoelasticity. *Archive for Rational Mechanics and Analysis*, Springer, v. 17, n. 3, p. 230–254, 1964. Cited on page 49.

_____. Thermodynamics of materials with memory. *Archive for Rational Mechanics and Analysis*, Springer, v. 17, n. 1, p. 1–46, 1964. Cited on page 49.

_____. On the mechanics of materials with fading memory. In: *Applications of Methods of Functional Analysis to Problems in Mechanics*. [S.l.]: Springer, 1976. p. 290–294. Cited on page 23.

COSTA-HAVEROTH, T. C. da. On the use of fractional derivatives for modeling nonlinear viscoelasticity. Universidade do Estado de Santa Catarina, 2015. Cited 3 times on pages 24, 25, and 27.

COSTA-HAVEROTH, T. C. da; HAVEROTH, G. A.; BITTENCOURT, M. L.; BOLDRINI, J. L. A damage phase-field model for fractional viscoelastic materials in finite strain. *Computational Mechanics*, Springer, p. 1–29, 2022. Cited 38 times on pages 6, 7, 16, 17, 18, 30, 37, 46, 47, 48, 54, 55, 57, 58, 59, 60, 62, 64, 65, 78, 82, 83, 84, 85, 86, 87, 88, 89, 90, 91, 92, 93, 94, 98, 99, 136, 140, and 141.

COSTA-HAVEROTH, T. da; HAVEROTH, G.; KÜHL, A.; BOLDRINI, J.; BITTENCOURT, M.; SASSE, F.; POLAK, M.; MUÑOZ-ROJAS, P. Aspects on viscoelasticity modeling of hdpe using fractional derivatives: Interpolation procedures and efficient numerical scheme. *Mechanics of Advanced Materials and Structures*, Taylor & Francis, p. 1–16, 2021. Cited 3 times on pages 61, 72, and 90.

DANIELS, C. A. *Polymers: structure and properties*. [S.l.]: CRC Press, 1989. Cited on page 29.

DUDA, F. P.; CIARBONETTI, A.; SÁNCHEZ, P. J.; HUESPE, A. E. A phase-field/gradient damage model for brittle fracture in elastic–plastic solids. *International Journal of Plasticity*, Elsevier, v. 65, p. 269–296, 2015. Cited on page 22.

DUSUNCELI, N.; COLAK, O. U. The effects of manufacturing techniques on viscoelastic and viscoplastic behavior of high density polyethylene (hdpe). *Materials & Design*, Elsevier, v. 29, n. 6, p. 1117–1124, 2008. Cited 3 times on pages 88, 89, and 91.

EVGENY, B.; HUFENBACH, W.; KROLL, L. Transient response analysis of systems with different damping models. *Computer Methods in Applied Mechanics and Engineering*, v. 192, p. 33–46, 01 2003. Cited on page 85.

FABRIZIO, M. Fractional rheological models for thermomechanical systems. dissipation and free energies. *Fractional Calculus and Applied Analysis*, Springer, v. 17, n. 1, p. 206–223, 2014. Cited 3 times on pages 26, 47, and 139.

FABRIZIO, M.; GIORGI, C.; MORRO, A. A thermodynamic approach to non-isothermal phase-field evolution in continuum physics. *Physica D: Nonlinear Phenomena*, v. 214, n. 2, p. 144 – 156, 2006. ISSN 0167-2789. Available at: <http://www.sciencedirect.com/science/article/pii/S0167278906000066>. Cited on page 37.

FARNO, E.; BAUDEZ, J.-C.; ESHTIAGHI, N. Comparison between classical kelvin-voigt and fractional derivative kelvin-voigt models in prediction of linear viscoelastic behaviour of waste activated sludge. *Science of the Total Environment*, Elsevier, v. 613, p. 1031–1036, 2018. Cited 2 times on pages 62 and 84.

FERRANTE, M.; CAPPONI, C. Viscoelastic models for the simulation of transients in polymeric pipes. *Journal of Hydraulic Research*, Taylor and Francis, v. 55, n. 5, p. 599–612, 2017. Cited on page 27.

FINDLEY, W. N.; DAVIS, F. A. *Creep and Relaxation of Nonlinear Viscoelastic Materials*. Dover Publications, 2013. (Dover Civil and Mechanical Engineering). ISBN 9780486145174. Available at: <http://books.google.com.br/books?id=AZuNioxH_i4C>. Cited 2 times on pages 24 and 78.

FRÉMOND, M.; SHITIKOVA, M. Non-smooth thermomechanics. *Appl. Mech. Rev.*, v. 55, n. 5, p. B99–B100, 2002. Cited 5 times on pages 34, 35, 49, 51, and 53.

GAUL, L.; SCHIMIDT, A. Experimental determination and modeling of material damping. *VDI-Berichte*, p. 17–40, 2007. Cited 2 times on pages 83 and 85.

GEMANT, A. A method of analyzing experimental results obtained from elastiviscous bodies. *Physics 7*, 1936. Cited on page 26.

GOWARIKER, V.; VISWANATHAN, N.; SREEDHAR, J. *Polymer Science*. Wiley, 1986. (Raymond F. Boyer Library Collection). ISBN 9780852263075. Available at: <https://books.google.com.br/books?id=mvCzE_AflUIC>. Cited on page 86.

GRIFFITH, A. A. Vi. the phenomena of rupture and flow in solids. *Philosophical transactions of the royal society of london. Series A, containing papers of a mathematical or physical character*, The royal society London, v. 221, n. 582-593, p. 163–198, 1921. Cited on page 22.

GURTIN, M. *An Introduction to Continuum Mechanics*. Elsevier Science, 1982. (ISSN). ISBN 9780080918495. Available at: <https://books.google.com.br/books?id=W-0b09yIgq4C>. Cited 2 times on pages 31 and 116.

GURTIN, M. E.; FRIED, E.; ANAND, L. *The mechanics and thermodynamics of continua*. [S.l.]: Cambridge University Press, 2010. Cited on page 36.

HAKIM, V.; KARMA, A. Crack path prediction in anisotropic brittle materials. *Physical review letters*, APS, v. 95, n. 23, p. 235501, 2005. Cited on page 22.

_____. Laws of crack motion and phase-field models of fracture. *Journal of the Mechanics and Physics of Solids*, Elsevier, v. 57, n. 2, p. 342–368, 2009. Cited on page 22.

HAUPT, P.; LION, A. On finite linear viscoelasticity of incompressible isotropic materials. *Acta mechanica*, Springer, v. 159, n. 1, p. 87–124, 2002. Cited on page 28.

HAVEROTH, G.; VALE, M.; BITTENCOURT, M.; BOLDRINI, J. A non-isothermal thermodynamically consistent phase field model for damage, fracture and fatigue evolutions in elasto-plastic materials. *Computer Methods in Applied Mechanics and Engineering*, Elsevier, v. 364, p. 112962, 2020. Cited 5 times on pages 15, 22, 23, 54, and 58.

HAVEROTH, G. A. *Phase field models for problems involving fracture, plasticity and finite strains: Modelos de campos de fase para problemas envolvendo fratura, plasticidade e grandes deformações*. Phd Thesis (PhD Thesis) — Universidade Estadual de Campinas, Instituto de Matemática Estatística e Computação Científica, 2020. Cited 3 times on pages 21, 23, and 78.

HAVEROTH, G. A.; MORAES, E. A.; BOLDRINI, J. L.; BITTENCOURT, M. L. Comparison of semi and fully-implicit time integration schemes applied to a damage and fatigue phase field model. *Latin American Journal of Solids and Structures*, SciELO Brasil, v. 15, n. 5, 2018. Cited 2 times on pages 65 and 98.

HAVEROTH, G. A.; STAHLSCHMIDT, J.; MUÑOZ-ROJAS, P. A. Application of the complex variable semi-analytical method for improved displacement sensitivity evaluation in geometrically nonlinear truss problems. *Latin American Journal of Solids and Structures*, SciELO Brasil, v. 12, n. 5, p. 980–1005, 2015. Cited on page 140.

HAYES, S.; ZHANG, W.; BRANTHWAITE, M.; JONES, F. Self-healing of damage in fibre-reinforced polymer-matrix composites. *Journal of the Royal Society Interface*, The Royal Society London, v. 4, n. 13, p. 381–387, 2007. Cited on page 60.

HILDEBRAND, F. *Advanced Calculus for Applications*. Prentice-Hall, 1976. (Bibliyografya ve İndeks). ISBN 9780130111890. Available at: <https://books.google.com.br/books?id=kxZRAAAAMAAJ>. Cited on page 114.

HOHENBERG, P.; KREKHOV, A. An introduction to the ginzburg–landau theory of phase transitions and nonequilibrium patterns. *Physics Reports*, Elsevier, v. 572, p. 1–42, 2015. Cited on page 21.

HUBER, N.; TSAKMAKIS, C. Finite deformation viscoelasticity laws. *Mechanics of materials*, Elsevier, v. 32, n. 1, p. 1–18, 2000. Cited on page 31.

IHLEMANN, J. *Beobachterkonzepte und Darstellungsformen der nichtlinearen Kontinuumsmechanik*. [S.l.]: VDI-Verlag, 2014. Cited 2 times on pages 28 and 34.

III, C. K.; CHEN, L.-Q. Computer simulation of 3-d grain growth using a phase-field model. *Acta materialia*, Elsevier, v. 50, n. 12, p. 3059–3075, 2002. Cited on page 22.

IRWIN, G. Fracture strength relative to onset and arrest of crack propagation. In: *Proc ASTM*. [S.l.: s.n.], 1958. v. 58, p. 640–657. Cited on page 90.

JIA, J. H.; SHEN, X. Y.; HUA, H. X. Viscoelastic behavior analysis and application of the fractional derivative maxwell model. *Jornal of vibration and control*, 2007. Cited on page 27.

KARMA, A.; KESSLER, D. A.; LEVINE, H. Phase-field model of mode iii dynamic fracture. *Physical Review Letters*, APS, v. 87, n. 4, p. 045501, 2001. Cited on page 22.

KARMA, A.; RAPPEL, W.-J. Phase-field method for computationally efficient modeling of solidification with arbitrary interface kinetics. *Physical review E*, APS, v. 53, n. 4, p. R3017, 1996. Cited on page 22.

KNAUSS, W. The time dependent fracture of viscoelastic materials. In: *Proceedings of the First International Conference on Fracture*. [S.l.: s.n.], 1966. Cited on page 29.

_____. Stable and unstable crack growth in viscoelastic media. *Transactions of the Society of Rheology*, The Society of Rheology, v. 13, n. 3, p. 291–313, 1969. Cited on page 29.

KNAUSS, W. G. *Rupture phenomena in viscoelastic materials*. Phd Thesis (PhD Thesis) — California Institute of Technology, 1963. Cited 2 times on pages 15 and 29.

KOELLER, R. C. Application of fractional calculus to the thory of viscoelasticity. *Appl. Mech.*, 1984. Cited 2 times on pages 25 and 26.

KRASNOBRIZHA, A.; ROZYCKI, P.; GORNET, L.; COSSON, P. Hysteresis behaviour modelling of woven composite using a collaborative elastoplastic damage model with fractional derivatives. *Composite Structures*, Elsevier, v. 158, p. 101–111, 2016. Cited on page 29.

KUHN, C.; SCHLÜTER, A.; MÜLLER, R. On degradation functions in phase field fracture models. *Computational Materials Science*, Elsevier, v. 108, p. 374–384, 2015. Cited 2 times on pages 16 and 58.

KUKSENKO, V.; TAMUSZ, V. *Fracture micromechanics of polymer materials*. [S.l.]: Springer Netherlands, 2013. (Fatigue and Fracture). ISBN 9789401715973. Cited on page 29.

LANDAU, L. D.; GINZBURG, V. L. On the theory of superconductivity. *Zh. Eksp. Teor. Fiz.*, v. 20, p. 1064, 1950. Cited on page 21.

LAZOPOULOS, K.; KARAOULANIS, D.; LAZOPOULOS, A. On fractional modelling of viscoelastic mechanical systems. *Mechanics Research Communications*, Elsevier, v. 78, p. 1–5, 2016. Cited on page 27.

LEONOV, A.; PROKUNIN, A. *Nonlinear Phenomena in Flows of Viscoelastic Polymer Fluids*. Springer Netherlands, 2012. ISBN 9789401112581. Available at: <https://books.google.com.br/books?id=sCzpCAAAQBAJ>. Cited on page 89.

LEWANDOWSKI, R.; CHORAŚYCZEWSKI, B. Identification of parameters of the fractional rheological model of viscoelastic dampers. In: *Symposium Vibrations in Physical Systems*. [S.l.: s.n.], 2010. Cited on page 85.

LEWANDOWSKI, R.; CHORĄŻYCZEWSKI, B. Identification of the parameters of the kelvin–voigt and the maxwell fractional models, used to modeling of viscoelastic dampers. *Computers & structures*, Elsevier, v. 88, n. 1-2, p. 1–17, 2010. Cited on page 62.

LI, G. *Self-healing composites: shape memory polymer based structures*. [S.l.]: John Wiley & Sons, 2014. Cited on page 60.

LI, G.; NETTLES, D. Thermomechanical characterization of a shape memory polymer based self-repairing syntactic foam. *Polymer*, Elsevier, v. 51, n. 3, p. 755–762, 2010. Cited on page 60.

LINDFIELD, G.; PENNY, J. *Numerical Methods: Using MATLAB*. [S.l.]: Elsevier Science, 2012. (Matlab examples). ISBN 9780123869425. Cited on page 67.

LION, A. On the thermodynamics of fractional damping elements. *Continuum Mechanics and Thermodynamics*, Springer, v. 9, n. 2, p. 83–96, 1997. Cited 2 times on pages 26 and 62.

LIU, M.; FATT, M. S. H. A constitutive equation for filled rubber under cyclic loading. *International Journal of Non-Linear Mechanics*, Elsevier, v. 46, n. 2, p. 446–456, 2011. Cited on page 28.

LOVERRO, A. Fractional calculus: history, definitions and applications for the engineer. *Rapport technique, Univeristy of Notre Dame: Department of Aerospace and Mechanical Engineering*, 2004. Cited on page 26.

MADENCI, E.; OTERKUS, S. Ordinary state-based peridynamics for thermoviscoelastic deformation. *Engineering Fracture Mechanics*, Elsevier, v. 175, p. 31–45, 2017. Cited on page 29.

MAINARDI, F. *Fractional Calculus and Waves in Linear Viscoelasticity: An Introduction to Mathematical Models*. World Scientific Publishing Company Pte Limited, 2010. ISBN 9781848163300. Available at: <http://books.google.com.br/books?id=3DZ9RuBTHo0C>. Cited on page 84.

MCFADDEN, G.; WHEELER, A.; BRAUN, R.; CORIELL, S.; SEKERKA, R. Phase-field models for anisotropic interfaces. *Physical Review E*, APS, v. 48, n. 3, p. 2016, 1993. Cited on page 22.

MEYERS, M. A.; CHAWLA, K. K. *Mechanical behavior of materials*. [S.l.]: Cambridge university press, 2008. Cited on page 23.

MIEHE, C.; HOFACKER, M.; SCHÄNZEL, L.-M.; ALDAKHEEL, F. Phase field modeling of fracture in multi-physics problems. part ii. coupled brittle-to-ductile failure criteria and crack propagation in thermo-elastic–plastic solids. *Computer Methods in Applied Mechanics and Engineering*, Elsevier, v. 294, p. 486–522, 2015. Cited 2 times on pages 15 and 22.

MIEHE, C.; HOFACKER, M.; WELSCHINGER, F. A phase field model for rate-independent crack propagation: Robust algorithmic implementation based on operator splits. *Computer Methods in Applied Mechanics and Engineering*, Elsevier, v. 199, n. 45-48, p. 2765–2778, 2010. Cited on page 22.

_____. A phase field model for rate-independent crack propagation: robust algorithmic implementation based on operator splits. *Computer Methods in Applied Mechanics and Engineering*, Elsevier, v. 199, n. 45, p. 2765–2778, 2010. Cited on page 58.

MIEHE, C.; WELSCHINGER, F.; HOFACKER, M. Thermodynamically consistent phase-field models of fracture: Variational principles and multi-field fe implementations. *International journal for numerical methods in engineering*, Wiley Online Library, v. 83, n. 10, p. 1273–1311, 2010. Cited on page 22.

_____. Thermodynamically consistent phase-field models of fracture: variational principles and multi-field FE implementations. *International Journal for Numerical Methods in Engineering*, Wiley Online Library, v. 83, n. 10, p. 1273–1311, 2010. Cited on page 57.

MOELANS, N.; BLANPAIN, B.; WOLLANTS, P. An introduction to phase-field modeling of microstructure evolution. *Calphad*, Elsevier, v. 32, n. 2, p. 268–294, 2008. Cited on page 20.

MOËS, N.; DOLBOW, J.; BELYTSCHKO, T. A finite element method for crack growth without remeshing. *International journal for numerical methods in engineering*, Wiley Online Library, v. 46, n. 1, p. 131–150, 1999. Cited on page 29.

MUSTO, M.; ALFANO, G. A fractional rate-dependent cohesive-zone model. *International Journal for Numerical Methods in Engineering*, Wiley Online Library, v. 103, n. 5, p. 313–341, 2015. Cited 2 times on pages 26 and 29.

NETO, E. A. de S.; PERIC, D.; OWEN, D. R. *Computational methods for plasticity: theory and applications*. [S.l.]: John Wiley & Sons, 2011. Cited on page 75.

NEWMARK, N. M. *Computation of dynamic structural response in the range approaching failure*. [S.l.]: Department of Civil Engineering, University of Illinois, 1952. Cited on page 83.

NGUYEN, V.-D.; LANI, F.; PARDOEN, T.; MORELLE, X.; NOELS, L. A large strain hyperelastic viscoelastic-viscoplastic-damage constitutive model based on a multi-mechanism non-local damage continuum for amorphous glassy polymers.

International Journal of Solids and Structures, Elsevier, v. 96, p. 192–216, 2016. Cited on page 29.

NISHIMOTO, K. An essence of nishimoto's fractional calculus (calculus in the 21st century): integrations and differentiations of arbitrary order. *Koriyama*, Japan, 1991. Cited on page 26.

ODEN, J. *An Introduction to Mathematical Modeling: A Course in Mechanics*. Wiley, 2012. (Wiley Series in Computational Mechanics). ISBN 9781118105740. Available at: <https://books.google.com.br/books?id=hIP54aX54xAC>. Cited 10 times on pages 31, 37, 46, 117, 120, 122, 123, 124, 125, and 130.

OGDEN, R. *Non-Linear Elastic Deformations*. Dover Publications, 2013. (Dover Civil and Mechanical Engineering). ISBN 9780486318714. Available at: <https://books.google.com.br/books?id=52XDAgAAQBAJ>. Cited on page 135.

OLDHAM, K. B.; SPANIER, J. *The fractional calculus*. New York-London: Academic Press, 1974. Cited on page 72.

OLIVEIRA, E. C. de; MACHADO, J. A. T. A review of definitions for fractional derivatives and integral. *Mathematical Problems in Engineering*, 2014. Cited on page 27.

PENROSE, O.; FIFE, P. C. Thermodynamically consistent models of phase-field type for the kinetic of phase transitions. *Physica D: Nonlinear Phenomena*, Elsevier, v. 43, n. 1, p. 44–62, 1990. Cited on page 22.

PEREZ, N. *Fracture Mechanics*. Springer International Publishing, 2016. ISBN 9783319249995. Available at: <https://books.google.com.br/books?id=cQTWDAAAQBAJ>. Cited 2 times on pages 54 and 90.

PIERO, G. D. On the method of virtual power in continuum mechanics. *Journal of Mechanics of materials and Structures*, Mathematical Sciences Publishers, v. 4, n. 2, p. 281–292, 2009. Cited on page 34.

PODLUBNY, I. *Fractional Differential Equations*. San Diego-Boston-New York-London-Tokyo-Toronto: Academic Press, 1999. Cited on page 27.

REDDY, J. *An Introduction to Continuum Mechanics*. Cambridge University Press, 2013. (An Introduction to Continuum Mechanics). ISBN 9781107025431. Available at: <https://books.google.com.br/books?id=Rsj-Bwv5FP0C>. Cited on page 116.

REESE, S.; GOVINDJEE, S. A theory of finite viscoelasticity and numerical aspects. *International journal of solids and structures*, Elsevier, v. 35, n. 26-27, p. 3455–3482, 1998. Cited on page 28.

SAMKO, S. G.; KILBAS, A. A.; MARICHEV, O. I. *Fractional integrals and derivatives - theory and applications*. 1a. ed. New York: Gordon and Breach Science Publishers, 1987. Cited on page 26.

SCHÄNZEL, L.-M. *Phase field modeling of fracture in rubbery and glassy polymers at finite thermo-viscoelastic deformations*. [S.l.: s.n.], 2015. Cited 2 times on pages 29 and 30.

SCHAPERY, R. Nonlinear viscoelastic and viscoplastic constitutive equations with growing damage. *International Journal of Fracture*, Springer, v. 97, n. 1-4, p. 33–66, 1999. Cited on page 29.

SCHAPERY, R. A. Application of thermodynamics to thermomechanical, fracture, and birefringent phenomena in viscoelastic media. *Journal of Applied Physics*, American Institute of Physics, v. 35, n. 5, p. 1451–1465, 1964. Cited 2 times on pages 15 and 29.

SCHILLINGER, D.; BORDEN, M. J.; STOLARSKI, H. K. Isogeometric collocation for phase-field fracture models. *Computer Methods in Applied Mechanics and Engineering*, Elsevier, v. 284, p. 583–610, 2015. Cited on page 22.

SCHIMIDT, A.; GAUL, L. On the numerical evaluation of fractional derivatives in multi-dredree-of-freedom systems. *Signal processing*, 2006. Cited on page 85.

SCOTT-BLAIR, G. W. Analytical and integrative aspects of the stress-strain-time problem. *J. Scientific Instruments*, 1944. Cited on page 26.

SHEN, R.; WAISMAN, H.; GUO, L. Fracture of viscoelastic solids modeled with a modified phase field method. *Computer Methods in Applied Mechanics and Engineering*, Elsevier, v. 346, p. 862–890, 2019. Cited on page 29.

SHIM, J.; MOHR, D. Finite strain constitutive model of polyurea for a wide range of strain rates. *International Journal of Plasticity*, p. 868–886, 2011. Cited on page 28.

SILBERSTEIN, M. N.; BOYCE, M. C. Constitutive modeling of the rate, temperature, and hydration dependent deformation response of nafion to monotonic and cyclic loading. *Journal of Power Sources*, Elsevier, v. 195, n. 17, p. 5692–5706, 2010. Cited on page 28.

STEINBACH, I. Phase-field models in materials science. *Modelling and simulation in materials science and engineering*, IOP Publishing, v. 17, n. 7, p. 073001, 2009. Cited on page 20.

SUVOROVA, J.; OHLSON, N.; ALEXEEVA, S. An approach to the description of time-dependent materials. *Materials & design*, Elsevier, v. 24, n. 4, p. 293–297, 2003. Cited on page 29.

TANG, H.; WANG, D.; HUANG, R.; PEI, X.; CHEN, W. A new rock creep model based on variable-order fractional derivatives and continuum damage mechanics. *Bulletin of Engineering Geology and the Environment*, Springer, v. 77, n. 1, p. 375–383, 2018. Cited on page 30.

TEMAM, R.; MIRANVILLE, A. *Mathematical Modeling in Continuum Mechanics*. Cambridge University Press, 2005. ISBN 9781139443210. Available at: <https://books.google.com.br/books?id=7EE9D_4-N5UC>. Cited on page 34.

THAMBURAJA, P.; SARAH, K.; SRINIVASA, A.; REDDY, J. Fracture of viscoelastic materials: Fem implementation of a non-local & rate form-based finite-deformation constitutive theory. *Computer Methods in Applied Mechanics and Engineering*, Elsevier, v. 354, p. 871–903, 2019. Cited 2 times on pages 29 and 30.

TIJSSENS, M.; GIESSEN, E. Van der; SLUYS, L. Modeling of crazing using a cohesive surface methodology. *Mechanics of Materials*, Elsevier, v. 32, n. 1, p. 19–35, 2000. Cited 2 times on pages 29 and 30.

_____. Simulation of mode i crack growth in polymers by crazing. *International Journal of Solids and Structures*, Elsevier, v. 37, n. 48-50, p. 7307–7327, 2000. Cited 2 times on pages 29 and 30.

TRUESDELL, C. The mechanical foundations of elasticity and fluid dynamics. *Journal of Rational Mechanics and Analysis*, JSTOR, v. 1, p. 125–300, 1952. Cited on page 37.

van der Waals, J. The thermodynamic theory of capillarity under the hypothesis of a continuous variation of density; translation of by j. rowlinson. *Journal of Statistical Physics*, Springer, v. 20, n. 2, p. 200–244, 1979. Cited on page 21.

VERNEREY, F. J.; BRIGHENTI, R.; LONG, R.; SHEN, T. Statistical damage mechanics of polymer networks. *Macromolecules*, ACS Publications, v. 51, n. 17, p. 6609–6622, 2018. Cited on page 29.

WANG, J.; SHI, S.-Q.; CHEN, L.-Q.; LI, Y.; ZHANG, T.-Y. Phase-field simulations of ferroelectric/ferroelastic polarization switching. *Acta Materialia*, Elsevier, v. 52, n. 3, p. 749–764, 2004. Cited on page 22.

WANG, S.-L.; SEKERKA, R.; WHEELER, A.; MURRAY, B.; CORIELL, S.; BRAUN, R.; MCFADDEN, G. Thermodynamically-consistent phase-field models for solidification. *Physica D: Nonlinear Phenomena*, Elsevier, v. 69, n. 1-2, p. 189–200, 1993. Cited on page 22.

WANG, Y. U.; JIN, Y.; CUITINO, A.; KHACHATURYAN, A. Nanoscale phase field microelasticity theory of dislocations: model and 3d simulations. *Acta Materialia*, Elsevier, v. 49, n. 10, p. 1847–1857, 2001. Cited on page 22.

WELCH, S. W. J.; RORRE, R. A. L.; DUREN, R. G. J. Application of time-based fractional calculus methods to viscoelastic creep and stress relation of materials. *Mechanic 423s of time- Dependent Materials*, v. 3, p. 279–303, 1999. Cited on page 25.

WILLIAMS, M. Initiation and growth of viscoelastic fracture. *International Journal of Fracture Mechanics*, Springer, v. 1, p. 292–310, 1965. Cited on page 29.

WILLIAMS, M. L. Structural analysis of viscoelastic materials. *AIAA journal*, v. 2, n. 5, p. 785–808, 1964. Cited 2 times on pages 15 and 29.

WNUK, M. P.; KNAUSS, W. G. Delayed fracture in viscoelastic-plastic solids. *International Journal of Solids and Structures*, Elsevier, v. 6, n. 7, p. 995–1009, 1970. Cited on page 29.

XU, Z.-D.; XU, C.; HU, J. Equivalent fractional kelvin model and experimental study on viscoelastic damper. *Journal of Vibration and Control*, SAGE Publications Sage UK: London, England, v. 21, n. 13, p. 2536–2552, 2015. Cited on page 62.

ZHANG, C.; MOORE, I. D. Nonlinear mechanical response of high density polyethylene. part ii: Uniaxial constitutive modeling. *Polymer Engineering & Science*, Wiley Online Library, v. 37, n. 2, p. 414–420, 1997. Cited on page 87.

ZHANG, W.; CAPILNASIU, A.; SOMMER, G.; HOLZAPFEL, G. A.; NORDSLETTEN, D. A. An efficient and accurate method for modeling nonlinear fractional viscoelastic biomaterials. *Computer methods in applied mechanics and engineering*, Elsevier, v. 362, p. 112834, 2020. Cited on page 27.

ZHANG, Y.; BENSON, D. A.; REEVES, D. M. Time and space nonlocalities underlying fractional-derivative models: Distinction and literature review of field applications. *Advances in Water Resources*, Elsevier, v. 32, n. 4, p. 561–581, 2009. Cited on page 26.

ZHOU, S.; ZHUANG, X. Phase field modeling of hydraulic fracture propagation in transversely isotropic poroelastic media. *Acta Geotechnica*, Springer, v. 15, n. 9, p. 2599–2618, 2020. Cited on page 22.

APPENDIX A – Important Theorems

Let Ω be a regular region in $\mathbb{R}^n$ with boundary Γ; let $\boldsymbol{n}$ be its external unitary normal vector field at the boundary. Then, the following results hold:

Teorema 1 (Divergence theorem)**.** *Let $\boldsymbol{w}$ be a regular vector field defined on the closure of Ω. Then, by denoting $\boldsymbol{x} \in \Omega$, we have that*

$$\int_{\Omega} \mathrm{div}_{\boldsymbol{x}}(\boldsymbol{w}) \mathrm{d}\Omega = \int_{\Gamma} \boldsymbol{w} \cdot \boldsymbol{n} \mathrm{d}\Gamma. \tag{A.1}$$

For a regular second order tensor field $\boldsymbol{T}$ defined on the closure of Ω, we have that

$$\int_{\Omega} \mathrm{div}_{\boldsymbol{x}}(\boldsymbol{T}) \mathrm{d}\Omega = \int_{\Gamma} \boldsymbol{T}\boldsymbol{n} \mathrm{d}\Gamma. \tag{A.2}$$

The divergence theorem is applied in Sec. 2.2.2 and Appendices C.8.4.3 and C.8.5.

Teorema 2 (Integration by parts for a second order tensor)**.** *Consider a regular second order tensor field $\boldsymbol{T}$ and a regular vector field $\boldsymbol{w}$, both defined on the closure of Ω; by denoting $\boldsymbol{x} \in \Omega$, we have that*

$$\int_{\Omega} \mathrm{div}_{\boldsymbol{x}}(\boldsymbol{T}) \cdot \boldsymbol{w} \mathrm{d}\Omega = -\int_{\Omega} \boldsymbol{T} : \nabla_{\boldsymbol{x}}(\boldsymbol{w}) \mathrm{d}\Omega + \int_{\Gamma} \boldsymbol{T}\boldsymbol{n} \cdot \boldsymbol{w} \ \mathrm{d}\Gamma, \tag{A.3}$$

where $\boldsymbol{n}$ is the unit vector normal to $\mathrm{d}\Gamma$.

The integration by parts is applied in Sec. 2.2.2 and Appendices E.1 and C.8.5.

Teorema 3 (Reynolds transport theorem)**.** *Let $\boldsymbol{v}$ be a regular velocity field defined on the closure of Ω, and $\boldsymbol{f}$ be a regular tensor, vector or scalar valued field also defined on the closure of Ω. Then,*

$$\frac{\mathrm{d}}{\mathrm{d}t} \int_{\Omega} \boldsymbol{f} \mathrm{d}\Omega = \int_{\Omega} \partial_t \boldsymbol{f} \mathrm{d}\Omega + \int_{\Gamma} (\boldsymbol{v} \cdot \boldsymbol{n}) \, \boldsymbol{f} \ \mathrm{d}\Gamma, \tag{A.4}$$

where $\boldsymbol{v}$ is the velocity vector field. The Reynolds Transport theorem is used in Appendix C.8.4.3.

The proof of the abovementioned theorems is out of this work's scope. Interested readers are referred to the text by Hildebrand (1976).

APPENDIX B – Recurrent Derivatives

1. Derivative of the determinant of a second-order tensor:

$$\partial_{\boldsymbol{C}} \det(\boldsymbol{C}) = \det(\boldsymbol{C})\boldsymbol{C}^{-t}. \tag{B.1}$$

2. Derivative of the trace of a second-order tensor:

$$\partial_{\boldsymbol{C}}(\mathrm{tr}(\boldsymbol{C})) = \boldsymbol{I}. \tag{B.2}$$

3. Derivative of the inverse of a second-order tensor:

$$\partial_{\boldsymbol{C}} \left(\boldsymbol{C}^{-1}\right) = -\boldsymbol{C}^{-1} \otimes \boldsymbol{C}^{-1}. \tag{B.3}$$

These results are used in Appendix D and the correlated proofs can be seen in Chaves (2013).

APPENDIX C – Review on Continuum Mechanics

The following text summarizes some primary information on continuum mechanics. Then, in a simplified way, we review the tensors and the fundamental equations of continuum mechanics used in this work. For details and additional discussions, we recommend the textbooks of Reddy (2013), Chaves (2013) and Gurtin (1982).

C.1 Tensors

Tensors are used to construct mathematical representations of physical phenomena. They are written in a given coordinate system; we can also include the concept of tensor components. Tensors are independent of the coordinate system (they must be the same for different observers); on the other hand, the tensor components change as the system changes.

The tensors can be divided according to their order.

- The zeroth-order tensors have magnitude and no direction. They are scalar quantities and will be denoted by lowercase letters; for instance, z.
- First-order tensors have both magnitude and direction. Usually, they are called vectors and will be denoted by bold lowercase letters $\boldsymbol{z}$ in $\mathbb{R}^n$, and their components by z_i with $i = 1, ..., n$:

$$\boldsymbol{z} = \begin{bmatrix} z_1 \\ z_2 \\ \vdots \\ z_n \end{bmatrix}.$$

- Second-order tensors present magnitude and two directions; they are represented by matrices and will be denoted by bold capital letters $\boldsymbol{Z}$ in $\mathbb{R}^m \times \mathbb{R}^n$, and their components by Z_{ij} with $i = 1, ..., m$ and $j = 1, \cdots, n$:

$$\boldsymbol{Z} = \begin{bmatrix} Z_{11} & Z_{12} & \cdots & Z_{1n} \\ Z_{21} & Z_{22} & \cdots & Z_{2n} \\ \vdots & \vdots & \ddots & \vdots \\ Z_{m1} & Z_{m2} & \cdots & Z_{mn} \end{bmatrix}. \tag{C.1}$$

Higher-order tensors can be defined in the same way as those mentioned above. In particular, this work deals with fourth-order tensors, which are represented by bold calligraphic letters $\boldsymbol{\mathcal{Z}}$ in $\mathbb{R}^m \times \mathbb{R}^n \times \mathbb{R}^p \times \mathbb{R}^q$. Their components are given by Z_{ijkl} with $i = 1, ..., m$, $j = 1, \cdots, n$, $k = 1, ..., p$ and $l = 1, \cdots, q$ (see Appendix C.9 for representing a symmetric fourth-order tensor in Voigt notation).

For generality, this classification is written for tensors defined in spaces which are Cartesian products of Euclidean spaces $\mathbb{R}^n$.

C.2 Kinematic of Bodies

Consider a material body in motion, with an initial state defined at time $t_0 = 0$. This initial configuration, also known as the reference or undeformed configuration (CHAVES, 2013), is a regular domain (open, bounded, and connected) $\Omega_0 \subset \mathbb{R}^3$ with a smooth boundary Γ_0. In this state, the material body is denoted by $\mathcal{B}_0$ and made up of physical points called material points $\boldsymbol{p} = (p_1, p_2, p_3)$, i.e., the coordinates of the place occupied by the body in its reference configuration relative to a fixed Cartesian coordinate system. It is important to emphasize that $\mathcal{B}_0$ is not discrete but a continuous media.

As the body moves, it will have different configurations over time. Then $\mathcal{B}_0$ passes to $\mathcal{B}$ in the current configuration $\Omega \subset \mathbb{R}^3$ (also known as the actual or deformed configuration) with boundary Γ (see Fig. 2.1). Consequently, the material points $\boldsymbol{p}$ in the closure of Ω_0 are mapped into positions $\boldsymbol{x}$ by a smooth vector valued mapping

$$\boldsymbol{x} = \chi(\boldsymbol{p}, t), \tag{C.1}$$

where χ is bijective (implying that the function admits an inverse χ^{-1}), and $\nabla\chi > 0$ (meaning that the material cannot penetrate itself or reverse the orientation of the material coordinates (ODEN, 2012)). The set $\{\chi(\boldsymbol{p}, s), 0 \leq s \leq t\}$ is called trajectory of the body through the time interval $[0, t]$ and χ is the motion.

We have two types of motions. The first is a rigid body motion, which maintains the original shape of the body after motion preserving the distance between particles. This type of motion has two subcategories: translation and rotation. The second one is the motion with deformation, which leads to changes in the distance between particles. Generally, motion is characterized by rigid body motion and deformation, which can arise simultaneously in the body.

C.2.1 Displacement, Velocity and Acceleration

By definition, the displacement vector $\boldsymbol{u}$ of a particle (material point) is given by the difference between the position vector in the current configuration and the position

vector in the reference configuration. If we consider Eq. (C.1), then the displacement can be written as

$$\boldsymbol{u} = \boldsymbol{x} - \boldsymbol{p} = \chi(\boldsymbol{p}, t) - \boldsymbol{p}. \tag{C.2}$$

The rate of change of the position vector defines the velocity $\boldsymbol{v}$. Then, by using Eq. (C.2) it is possible to write

$$\boldsymbol{v} = \frac{\mathrm{d}}{\mathrm{d}t}\boldsymbol{x} = \frac{\mathrm{d}}{\mathrm{d}t}(\boldsymbol{u} + \boldsymbol{p}) = \frac{\mathrm{d}}{\mathrm{d}t}\boldsymbol{u} + \underbrace{\frac{\mathrm{d}}{\mathrm{d}t}\boldsymbol{p}}_{\mathbf{0}} = \frac{\mathrm{d}}{\mathrm{d}t}\boldsymbol{u} = \dot{\boldsymbol{u}},$$

i.e., the velocity is simply the time derivative of the displacement. As shown in the previous equation, we will use the dot notation $\dot{(\cdot)}$ to refer to the time derivative along the text.

Finally, the acceleration vector $\boldsymbol{a}$, is the rate of change of velocity:

$$\boldsymbol{a} = \frac{\mathrm{d}}{\mathrm{d}t}\boldsymbol{v} = \dot{\boldsymbol{v}} = \ddot{\boldsymbol{u}},$$

where $\ddot{(\cdot)}$ denotes the second time derivative.

C.2.2 Lagrangian and Eulerian Configurations

The motion χ of the body, defined in Eq. (C.1), ensures a correlation between the current and reference configurations. Once χ admits an inverse χ^{-1}, the study of motion can be carried out either in the current or reference configuration. In other words, the motion equation can be written in terms of the material points $\boldsymbol{p}$, i.e., the coordinates in the reference configuration, or by spatial coordinates, $\boldsymbol{x}$ in the current configuration (CHAVES, 2013). In general, other physical aspects of the body (temperature, damage) can also be described by equations in these two forms. Suppose the set of equations that describes these attributes is written in terms of the material points. In that case, it is commonly referred to as the *Lagrangian* governing equations of continuum mechanics. If the spatial coordinates are used instead, we refer to it as the *Eulerian* form (or formulation).

In this work, we denote zeroth and first-order Lagrangian tensors by $(\cdot)_0 = (\cdot)(\boldsymbol{p}, t)$, with the subscript denoting that the quantity is given in the reference configuration by material points. On the other hand, zero and first-order Eulerian tensors are denoted by $(\cdot)(\boldsymbol{x}, t)$ (without subscripts). For instance, a given field is written in the Lagrangian form as z_0 and in the Eulerian form as z. These quantities are related by

$$z_0(\boldsymbol{p}, t) = z(\boldsymbol{p}(\boldsymbol{x}, t), t) = z(\boldsymbol{x}, t), \quad \text{and} \quad z(\boldsymbol{x}, t) = z(\xi(\boldsymbol{p}, t), t) = z_0(\boldsymbol{p}, t). \tag{C.3-C.4}$$

There are differences in the way rates of change appear for each formulation. For the Lagrangian case:

$$\frac{\mathrm{d}}{\mathrm{d}t}z_0 = \frac{\mathrm{d}}{\mathrm{d}t}z_0(\boldsymbol{p}, t) = \partial_t z_0(\boldsymbol{p}, t) + \partial_{\boldsymbol{p}} z_0(\boldsymbol{p}, t) \cdot \underbrace{\partial_t \boldsymbol{p}}_{0} = \partial_t z_0(\boldsymbol{p}, t).$$

In the Eulerian case, we have

$$\frac{\mathrm{d}}{\mathrm{d}t}z = \frac{\mathrm{d}}{\mathrm{d}t}z(\boldsymbol{x},t) = \partial_t z(\boldsymbol{x},t) + \partial_{\boldsymbol{x}} z(\boldsymbol{x},t)\cdot\underbrace{\partial_t \boldsymbol{x}}_{v} = \partial_t z(\boldsymbol{x},t) + \partial_{\boldsymbol{x}} z(\boldsymbol{x},t)\cdot\boldsymbol{v}. \tag{C.5}$$

Equation (C.5) is called *material time derivative* in the classical literature.

Additionally, we differentiate the notation for gradient and divergent fields in the Lagrangian and Eulerian formulations. The Lagrangian gradient and divergent are given, respectively, by

$$\nabla_{\boldsymbol{p}}(z_0) = \partial_{\boldsymbol{p}}(z_0), \quad \text{and} \quad \mathrm{div}_{\boldsymbol{p}}(z_0) = \partial_{\boldsymbol{p}}\cdot(z_0). \tag{C.6-C.7}$$

On the other hand, the Eulerian counterparts are given by

$$\nabla_{\boldsymbol{x}}(z) = \partial_{\boldsymbol{x}}(z), \quad \text{and} \quad \mathrm{div}_{\boldsymbol{x}}(z) = \partial_{\boldsymbol{x}}\cdot(z). \tag{C.8-C.9}$$

C.3 Deformation Gradient

This section analyzes how distances between particles change during motion and defines deformation and strain tensors.

In order to proceed, consider two neighboring particles in the reference configuration, denoted by $\boldsymbol{m}_0$ and $\boldsymbol{n}_0$ where $d\boldsymbol{p}$ is a vector that joints these points defining a line element (see Fig. C.1) After motion, particles $\boldsymbol{m}_0$ and $\boldsymbol{n}_0$ occupy new positions $\boldsymbol{m}$ and $\boldsymbol{n}$, respectively. In this new configuration (current configuration), the vector joining the points $\boldsymbol{w}$ and $\boldsymbol{z}$ is represented by $d\boldsymbol{x}$, as shown in Fig. C.1. The relation between $d\boldsymbol{p}$ and $d\boldsymbol{x}$ is given by

$$d\boldsymbol{x} = \boldsymbol{F}d\boldsymbol{p}, \tag{C.10}$$

where

$$\boldsymbol{F} = \partial_{\boldsymbol{p}}\boldsymbol{x}, \tag{C.11}$$

is the material deformation gradient, or simply gradient of deformation (CHAVES, 2013). It is a two-point tensor because it maps quantities between reference and current configuration.

By using Eqs. (C.1) and (C.2), and the gradient definition of Eq. (C.6), it is possible to write $\boldsymbol{F}$ as

$$\boldsymbol{F}(\boldsymbol{p},t) = \nabla_{\boldsymbol{p}}(\chi(\boldsymbol{p},t)) = \boldsymbol{I} + \nabla_{\boldsymbol{p}}(\boldsymbol{u}(\boldsymbol{p},t)), \tag{C.12}$$

where $\boldsymbol{I}$ is the usual second-order identity matrix and $\nabla_{\boldsymbol{p}}(\boldsymbol{u})$ is the displacement gradient tensor.

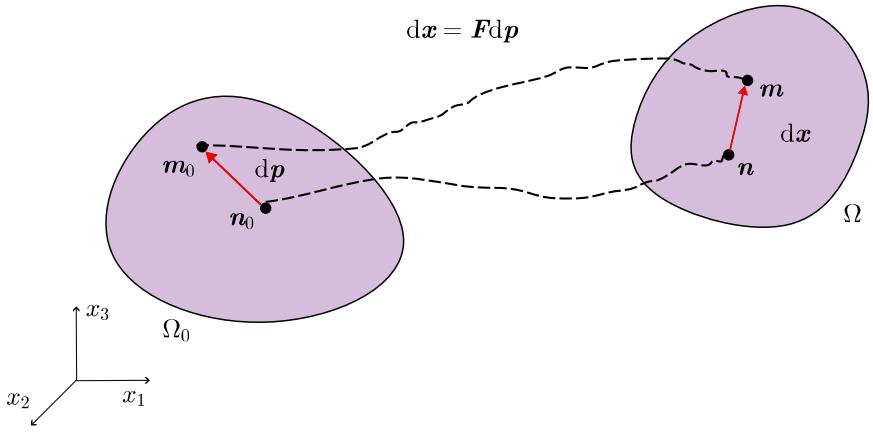

Figure C.1 – Definition for $\boldsymbol{F}$.

We emphasize that $\det \boldsymbol{F} \neq 0$, which means that the physical material cannot penetrate itself or reverse the orientation of material coordinates (ODEN, 2012).

The time derivative of $\boldsymbol{F}$ is given by

$$\dot{\boldsymbol{F}} = \partial_t \nabla_{\boldsymbol{p}}(\boldsymbol{u}(\boldsymbol{p},t)) = \partial_t \frac{\partial}{\partial \boldsymbol{p}}(\boldsymbol{u}(\boldsymbol{p},t)) = \underbrace{\partial_{\boldsymbol{p}}}_{\nabla_{\boldsymbol{p}}} \underbrace{\partial_t(\boldsymbol{u}(\boldsymbol{p},t))}_{v} = \partial_{\boldsymbol{x}}\boldsymbol{v}\partial_{\boldsymbol{p}}\boldsymbol{x} = \nabla_{\boldsymbol{x}}(\boldsymbol{v})\boldsymbol{F}. \quad \text{(C.13)}$$

If $z_0(\boldsymbol{p},t)$ is a scalar field, then we can find the relation between the material gradient $\nabla_{\boldsymbol{p}}(z_0(\boldsymbol{p},t))$ and the spatial gradient $\nabla_x(z(\boldsymbol{x},t))$ by using Eq. (C.3). In terms of components, we have

$$\begin{aligned} [\nabla_{\boldsymbol{p}}(z_0(\boldsymbol{p},t))]_i &= \frac{\partial z_0(\boldsymbol{p},t))}{\partial p_i} = \frac{\partial z(\chi(\boldsymbol{p},t)),t}{\partial \chi_j}\frac{\partial \chi_j}{\partial p_i} = [\nabla_{\boldsymbol{x}}(z(\boldsymbol{x},t))]_j F_{ji} \\ &= F^t_{ij}[\nabla_{\boldsymbol{x}}(z(\boldsymbol{x},t))]_j. \end{aligned} \quad \text{(C.14)}$$

Then,

$$\nabla_{\boldsymbol{p}}(z_0(\boldsymbol{p},t) = \boldsymbol{F}^t \nabla_{\boldsymbol{x}}(z(\boldsymbol{x},t)). \quad \text{(C.15)}$$

Inversely, we can also obtain

$$\nabla_{\boldsymbol{x}}(z(\boldsymbol{x},t)) = \boldsymbol{F}^{-t} \nabla_{\boldsymbol{p}}(z_0(\boldsymbol{p},t)). \quad \text{(C.16)}$$

By using the last result, it is possible to write

$$\nabla_{\boldsymbol{x}}(\boldsymbol{v}) = \nabla_{\boldsymbol{p}}(\boldsymbol{v}_0)\boldsymbol{F}^{-1}. \quad \text{(C.17)}$$

Furthermore, the time derivative of the determinant of $\boldsymbol{F}$ is given by

$$\dot{\det(\boldsymbol{F})} = \mathrm{div}_{\boldsymbol{x}}(\boldsymbol{v}) \det(\boldsymbol{F}). \quad \text{(C.18)}$$

For details on obtaining Eq. (C.18), see Chaves (2013), p. 175.

C.4 Velocity Gradient Tensor

We start this section calculating the material time derivative (defined in Eq. (C.5)) of $\boldsymbol{F}$ by using Eq. (C.11):

$$\dot{\boldsymbol{F}} = \partial_t \partial_{\boldsymbol{p}} \boldsymbol{x} = \partial_{\boldsymbol{p}} \underbrace{\partial_t \boldsymbol{x}}_{\boldsymbol{v}} = \partial_{\boldsymbol{x}} \boldsymbol{v} \partial_{\boldsymbol{p}} \boldsymbol{x} = \nabla_{\boldsymbol{x}}(\boldsymbol{v})\boldsymbol{F} = \boldsymbol{L}\boldsymbol{F},$$

where

$$\boldsymbol{L} = \nabla_{\boldsymbol{x}}(\boldsymbol{v}), \tag{C.19}$$

is an Eulerian quantity called the velocity gradient tensor. In practice, the tensor $\boldsymbol{L}$ is written as an addictive deposition of its symmetric and skew-symmetric parts:

$$\boldsymbol{L} = \boldsymbol{D} + \boldsymbol{W},$$

where $\boldsymbol{D}$ is the deformation rate tensor and $\boldsymbol{W}$ is the spin tensor, which are given respectively by

$$\boldsymbol{D} = \frac{1}{2}(\boldsymbol{L} + \boldsymbol{L}^t) \quad \text{and} \quad \boldsymbol{W} = \frac{1}{2}(\boldsymbol{L} - \boldsymbol{L}^t). \tag{C.20-C.21}$$

When $\boldsymbol{W} = \boldsymbol{0}$, the velocity is said irrotational (CHAVES, 2013).

C.5 Strain Tensors

Broadly, strain is a normalization of deformation. Several strain measures are used in the literature, and some of them are described below.

Firstly, we consider the differential material line segment in the reference configuration and the current configuration, given respectively, by

$$dS_0^2 = \mathrm{d}\boldsymbol{p} \cdot \mathrm{d}\boldsymbol{p}, \quad \text{and} \quad dS^2 = \mathrm{d}\boldsymbol{x} \cdot \mathrm{d}\boldsymbol{x}.$$

The simplest strain definition in the material description is written through the dimensionless rate:

$$\frac{dS^2 - dS_0^2}{dS_0^2}. \tag{C.22}$$

Similarly, the spatial counterpart is written as

$$\frac{dS^2 - dS_0^2}{dS^2}. \tag{C.23}$$

The relationship $dS^2 - dS_0^2$ can be expressed in the material description using (C.10):

$$\begin{aligned} \mathrm{d}S^2 - dS_0^2 &= \mathrm{d}\boldsymbol{x} \cdot \mathrm{d}\boldsymbol{x} - \mathrm{d}\boldsymbol{p} \cdot \mathrm{d}\boldsymbol{p} = \boldsymbol{F}\mathrm{d}\boldsymbol{p} \cdot \boldsymbol{F}\mathrm{d}\boldsymbol{p} - \mathrm{d}\boldsymbol{p} \cdot \mathrm{d}\boldsymbol{p} \\ &= d\boldsymbol{p}^t \boldsymbol{F}^t \boldsymbol{F} \mathrm{d}\boldsymbol{p} - \mathrm{d}\boldsymbol{p}^t d\boldsymbol{p} = \mathrm{d}\boldsymbol{p}^t (\boldsymbol{F}^t \boldsymbol{F} - \boldsymbol{I}) \mathrm{d}\boldsymbol{p} \\ &= \mathrm{d}\boldsymbol{p}^t (\boldsymbol{C} - \boldsymbol{I}) \mathrm{d}\boldsymbol{p} = \mathrm{d}\boldsymbol{p}^t (2\boldsymbol{E}) \mathrm{d}\boldsymbol{p}, \end{aligned} \tag{C.24}$$

where

$$\boldsymbol{C} = \boldsymbol{F}^t\boldsymbol{F}, \tag{C.25}$$

is a symmetric positive definite tensor known as the right Cauchy-Green tensor, and

$$\boldsymbol{E} = \frac{1}{2}(\boldsymbol{C} - \boldsymbol{I}) = \frac{1}{2}(\boldsymbol{F}^t\boldsymbol{F} - \boldsymbol{I}), \tag{C.26}$$

is the symmetric Green-Lagrange strain tensor, also called Lagrangian finite strain tensor or Green-St. Venant strain tensor.

The material time derivative of $\boldsymbol{C}$ is given by

$$\begin{aligned}\dot{\boldsymbol{C}} &= 2\dot{\boldsymbol{E}} = \dot{\overline{\boldsymbol{F}^t\boldsymbol{F}}} = \dot{\boldsymbol{F}}^t\boldsymbol{F} + \boldsymbol{F}^t\dot{\boldsymbol{F}} = \boldsymbol{F}^t\boldsymbol{F}^{-t}\dot{\boldsymbol{F}}^t\boldsymbol{F} + \boldsymbol{F}^t\dot{\boldsymbol{F}}\boldsymbol{F}^{-1}\boldsymbol{F} \\ &= (\boldsymbol{F}^t\dot{\boldsymbol{F}}\boldsymbol{F}^{-1}\boldsymbol{F})^t + \boldsymbol{F}^t\boldsymbol{L}\boldsymbol{F} = (\boldsymbol{F}^t\boldsymbol{L}\boldsymbol{F})^t + \boldsymbol{F}^t\boldsymbol{L}\boldsymbol{F} = 2\boldsymbol{F}^t\boldsymbol{D}\boldsymbol{F},\end{aligned} \tag{C.27}$$

where $\boldsymbol{D}$ is defined in Eq. (C.20).

As commented previously, if the continuum is subjected to rigid body motion, then $\boldsymbol{D} = \boldsymbol{0}$. Due to Eq. (C.27), this condition is equivalent to $\dot{\boldsymbol{E}} = \boldsymbol{0}$ or $\dot{\boldsymbol{C}} = \boldsymbol{0}$.

C.6 Area and Volume

Firstly, consider two line elements $\mathrm{d}\boldsymbol{p}_1$ and $\mathrm{d}\boldsymbol{p}_2$ in the reference configuration to define the area element $\mathrm{d}\Gamma_0$ (see Fig. C.2a). After the motion, these vectors are mapped to $d\boldsymbol{x}_1$ and $d\boldsymbol{x}_2$, respectively, that in turn define the new area element $\mathrm{d}\Gamma$ as shown in Fig. C.2a. According to Oden (2012, p. 18), these area elements can be related by

$$\mathrm{d}\Gamma\boldsymbol{n} = \det(\boldsymbol{F})\boldsymbol{F}^{-t}\boldsymbol{n}_0\mathrm{d}\Gamma_0, \tag{C.28}$$

where $\boldsymbol{n}$ and $\boldsymbol{n}_0$ are unit vectors which are normal to the area elements Γ and Γ_0, respectively. Now, consider a parallelepiped formed by the line elements $d\boldsymbol{p}_1$, $d\boldsymbol{p}_2$ and $d\boldsymbol{p}_3$ in the reference configuration with volume Γ_0. After motion, these vectors are mapped to $d\boldsymbol{x}_1$, $d\boldsymbol{x}_2$ and $d\boldsymbol{x}_3$, respectively, and describe a new parallelepiped $\mathrm{d}\Omega$ as shown in Fig. C.2b. Next, we can establish the relationship between $d\Omega_0$ and $d\Omega$:

$$\mathrm{d}\Omega = \det(\boldsymbol{F})\mathrm{d}\Omega_0. \tag{C.29}$$

Note that if $\det(\boldsymbol{F}) = 1$, the above equation implies that the volume does not change during motion. If $\det(\boldsymbol{F}) > 1$, the volume increases. If $0 < \det(\boldsymbol{F}) < 1$, the volume decrease. On the other hand, if $\det(\boldsymbol{F}) \leq 0$, the material penetrates itself, violating physical interpretation in the continuum mechanics (CHAVES, 2013).

Additionally, for any smooth field $\boldsymbol{w}$, we can use Eq. (C.29) to write

$$\frac{\mathrm{d}}{\mathrm{d}t}\int_\Omega \rho\boldsymbol{w}\ \mathrm{d}\Omega = \frac{\mathrm{d}}{\mathrm{d}t}\int_{\Omega_0} \boldsymbol{w}\rho\det(\boldsymbol{F})\ \mathrm{d}\Omega_0 = \int_{\Omega_0}\frac{\mathrm{d}\boldsymbol{w}}{\mathrm{d}t}\rho_0\ \mathrm{d}\Omega_0 = \int_\Omega \frac{\mathrm{d}\boldsymbol{w}}{\mathrm{d}t}\rho\ \mathrm{d}\Omega. \tag{C.30}$$

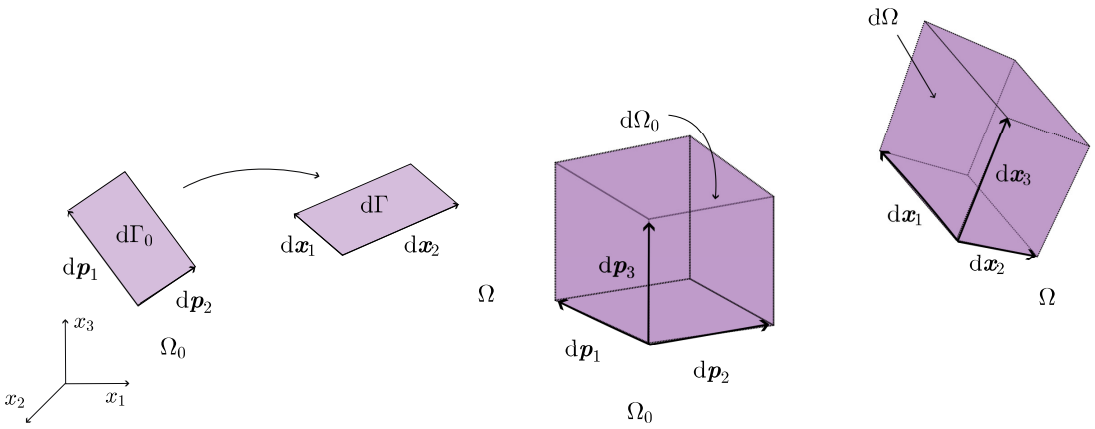

(a) Area element. (b) Volume element.

Figure C.2 – Area and volume elements.

C.7 Forces and Stress

According to Oden (2012), force is a concept used to describe the interaction of the motion of a body with its surrounding. There are two types of forces: body and contact forces. The first one is the forces acting on material points of the body by external agents, and the second characterizes the contact of the boundary surfaces of a body with another body or with the environment.

Body forces are considered a type of external force and will be represented by $\boldsymbol{f}$, which represents force per unit of mass. Then, the total body forces in the domain Ω, represented by F_{body}, are given by

$$F_{body} = \int_{\Omega} \rho \boldsymbol{f} \, \mathrm{d}\Omega,$$

where ρ is the density of mass. Contact forces are associated with the stress tensor $\boldsymbol{\sigma}$, where the total contact forces acting on the body surface can be represented by $F_{surface}$ and obtained through the surface integral

$$F_{surface} = \int_{\Gamma} \boldsymbol{\sigma} \, \mathrm{d}\Gamma. \tag{C.31}$$

Then, it is immediate that the total force acting in a body be given by

$$F_{surface} + F_{body} = \int_{\Gamma} \boldsymbol{\sigma} \mathrm{d}\Gamma + \int_{\Omega} \rho \boldsymbol{f} \, \mathrm{d}\Omega. \tag{C.32}$$

The following section details contact forces and clarify the concept of stress.

C.7.1 Cauchy Stress Tensor

Consider the body shown in Fig. C.3, and the surface Γ, which divides the body into two parts. For each part of the body, a unit normal vector $\boldsymbol{n} = [n_1 n_2 n_3]$ gives orientation to Γ from point $\boldsymbol{x} = (x_1, x_2, x_3)$ at time t. By convention, the direction of $\boldsymbol{n}$ points to the outer side of the surface.

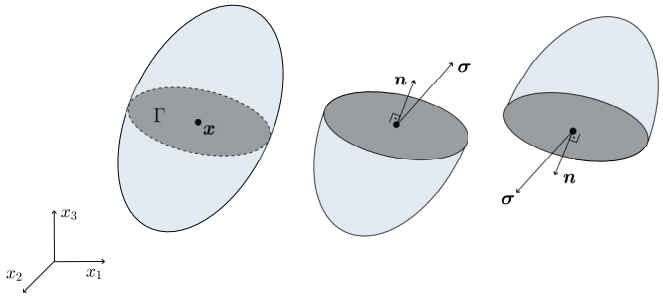

Figure C.3 – Definition for $\boldsymbol{F}$.

The so-called Cauchy hypothesis asserts a vector-valued contact force density, $\boldsymbol{\sigma}$, giving the contact force per unit of area on the surface Γ through $\boldsymbol{x}$, at time t. The orientation of $\boldsymbol{\sigma}$ on one part of the material is opposite to the other part. Furthermore, the total force on surface Γ is given by Eq. (C.31).

The vector $\boldsymbol{\sigma}$ is usually called traction or stress vector and is associated with the normal $\boldsymbol{n}$. The stress state at a point $\boldsymbol{x}$ is completely described when $\boldsymbol{\sigma}$ can be obtained for any arbitrary plane passing through this point. Cauchy's Theorem claims that if we define the traction vector on three mutually perpendicular planes passing through $\boldsymbol{x}$, we can fully describe the stress state at that point. In other words, there exists a symmetric tensor field $\boldsymbol{T}$ such that

$$\boldsymbol{\sigma} = \boldsymbol{T}\boldsymbol{n}, \tag{C.33}$$

where $\boldsymbol{T}$ can be represented in the matrix form:

$$\boldsymbol{T} = \begin{bmatrix} T_{11} & T_{12} & T_{13} \\ T_{21} & T_{22} & T_{23} \\ T_{31} & T_{32} & T_{33} \end{bmatrix}. \tag{C.34}$$

The tensor $\boldsymbol{T}$ is called the Cauchy stress tensor and is used to represent the components of the stress vector. For instance, if $\boldsymbol{n} = [1\ 0\ 0]$, then $\boldsymbol{\sigma} = [T_{11}\ T_{21}\ T_{31}]$ is the vector acting on the plane normal to x_1 direction.In the same way, T_{2i} and T_{3i}, with $i = 1, \cdots, 3$, are components of the stress vector normal to the planes x_2 and x_3, respectively(ODEN, 2012).

C.7.2 Other Stress Measures

The Cauchy stress tensor, presented in the previous section, was derived in the current configuration Ω. However, sometimes it is necessary to adopt the Lagrangian description to describe motion. Then it will be necessary to map the Cauchy stress to a stress tensor in the reference configuration.

Then, we introduce the first Piola-Kirchhoff stress tensor $\boldsymbol{P}$. This tensor represents the force in the current configuration per unit of undeformed area; it is asymmetric

and a two-point tensor like the deformation gradient. The relation between $\boldsymbol{P}$ and $\boldsymbol{T}$ is given by

$$\boldsymbol{P} = \det(\boldsymbol{F})\boldsymbol{T}\boldsymbol{F}^{-t}. \tag{C.35}$$

Furthermore,

$$\mathrm{div}_{\boldsymbol{p}}(\boldsymbol{P}) = \det(\boldsymbol{F})\mathrm{div}_{\boldsymbol{x}}(\boldsymbol{T}). \tag{C.36}$$

See Oden (2012, pp. 41) for comments on obtaining the last equation.

We can also define the symmetric second Piola-Kirchhoff stress tensor $\boldsymbol{S}$, which is defined in the reference configuration, as

$$\boldsymbol{S} = \boldsymbol{F}^{-1}\boldsymbol{P} = \det(\boldsymbol{F})\boldsymbol{F}^{-1}\boldsymbol{T}\boldsymbol{F}^{-t}. \tag{C.37}$$

By Eq. (C.37), we can see that tensor $\boldsymbol{S}$ is the mapping of $\boldsymbol{T}$ to the reference configuration through $\boldsymbol{F}$.

C.8 Fundamental Equations of Continuum Mechanics

This section summarizes the main physical principles and conservative laws used to write the fundamental equations of continuum mechanics.

C.8.1 Principle of Mass Conservation

The principle of mass conservation states that the total mass in a closed system remains constant over time. Then, if ρ_0 and ρ are mass densities for a body in the reference and current configurations, respectively, the total mass m of a system is given by

$$m = \int_{\Omega_0} \rho_0 \, \mathrm{d}\Omega_0 = \int_{\Omega} \rho \, \mathrm{d}\Omega. \tag{C.38}$$

Using Eq. (C.29), we can rewrite the above equation as

$$\int_{\Omega_0} \rho_0 \, \mathrm{d}\Omega_0 = \int_{\Omega} \rho \, \mathrm{d}\Omega = \int_{\Omega_0} \det(\boldsymbol{F})\rho \, \mathrm{d}\Omega_0. \tag{C.39}$$

Since this equation is valid for any volume, we can obtain the local form

$$\rho_0 = \rho \det(\boldsymbol{F}). \tag{C.40}$$

Furthermore, we remember that ρ_0 does not depend on time; then

$$\dot{\rho_0} = 0. \tag{C.41}$$

Equation (C.41) describes the Lagrangian description of the principle of mass conservation. By integrating Eq. (C.41) in Ω_0 and using Eqs. (C.40) and (C.18), we obtain

$$0 = \int_{\Omega_0} \dot{\rho_0}\ \mathrm{d}\Omega_0 = \int_{\Omega_0} \dot{\overline{\rho \det(\boldsymbol{F})}}\ \mathrm{d}\Omega_0 = \int_{\Omega_0} [\dot{\rho} + \rho \mathrm{div}_{\boldsymbol{x}}(\boldsymbol{v})] \det(\boldsymbol{F})\ \mathrm{d}\Omega_0 = \int_{\Omega} (\dot{\rho} + \rho \mathrm{div}_{\boldsymbol{x}}(\boldsymbol{v}))\ \mathrm{d}\Omega.$$

The above equation is the weak form of the principle of mass conservation in the Eulerian configuration. The local form (also called the strong form) is given by

$$\dot{\rho} + \rho \mathrm{div}_{\boldsymbol{x}}(\boldsymbol{v}) = 0. \tag{C.42}$$

Additionally, by using the above relation and the material time derivative of Eq. (C.5), we can write an alternative equation for the mass conservation:

$$0 = \partial_t \rho + \boldsymbol{v} \cdot \nabla_{\boldsymbol{x}}(\rho) + \rho \mathrm{div}_{\boldsymbol{x}}(\boldsymbol{v}) = \partial_t \rho + \mathrm{div}_{\boldsymbol{x}}(\rho \boldsymbol{v}). \tag{C.43}$$

C.8.2 Balance of Linear Momentum

The body's linear momentum is a material property associated with mass and velocity. For the current configuration, it is defined as L_m and given by

$$L_m = \int_{\Omega} \rho \boldsymbol{v}\ \mathrm{d}\Omega, \tag{C.44}$$

where $\boldsymbol{v}$ is the Eulerian velocity field.

The Balance of Linear Momentum states that the time rate of change of L_m, at time t, of an arbitrary part of a continuous medium is the same as the total force acting on the body. In mathematical terms, we can use Eq. (C.32) and Eq. (C.44) to write

$$\int_{\Gamma} \boldsymbol{\sigma}\ \mathrm{d}\Gamma + \int_{\Omega} \rho \boldsymbol{f}\ \mathrm{d}\Omega = \frac{\mathrm{d}}{\mathrm{d}t} \int_{\Omega} \rho \boldsymbol{v}\ \mathrm{d}\Omega, \tag{C.45}$$

that is the Eulerian global form of the principle of conservation of linear momentum. By using (C.33) and (C.30) we can rewrite the above equation as

$$\int_{\Gamma} \boldsymbol{T}\boldsymbol{n}\ \mathrm{d}\Gamma + \int_{\Omega} \rho \boldsymbol{f}\ \mathrm{d}\Omega = \int_{\Omega} \frac{\mathrm{d}\boldsymbol{v}}{\mathrm{d}t} \rho\ \mathrm{d}\Omega,$$

and applying the Eq. (A.2), we obtain

$$\int_{\Omega} \mathrm{div}_{\boldsymbol{x}}(\boldsymbol{T})\ \mathrm{d}\Omega + \int_{\Omega} \rho \boldsymbol{f}\ \mathrm{d}\Omega = \int_{\Omega} \rho \dot{\boldsymbol{v}}\ \mathrm{d}\Omega. \tag{C.46}$$

Once this equation holds for any arbitrary domain, we can write the local form as

$$\mathrm{div}_{\boldsymbol{x}}(\boldsymbol{T}) + \rho \boldsymbol{f} = \rho \dot{\boldsymbol{v}}, \tag{C.47}$$

that is largely known as the equation of motion in the Eulerian description. The Lagrangian counterpart is obtained by replacing Eqs. (C.36) and (C.30) in (C.46):

$$\int_{\Omega_0} \mathrm{div}_{\boldsymbol{p}}(\boldsymbol{P}) \mathrm{d}\Omega_0 + \int_{\Omega_0} \rho_0 \boldsymbol{f}_0 \mathrm{d}\Omega_0 = \int_{\Omega_0} \rho_0 \dot{\boldsymbol{v}} \mathrm{d}\Omega_0,$$

where $\boldsymbol{f}_0 = \boldsymbol{f}$. Then, the local Lagrangian equation of motion is obtained as

$$\mathrm{div}_{\boldsymbol{p}}(\boldsymbol{P}) + \rho_0 \boldsymbol{f}_0 = \rho_0 \dot{\boldsymbol{v}}. \tag{C.48}$$

C.8.3 Balance of Angular Momentum

The angular momentum of a body in the current configuration is given by

$$A_m = \int_\Omega \boldsymbol{x} \times \rho \boldsymbol{v} \, \mathrm{d}\Omega.$$

Its time rate of change can be obtained as

$$\frac{\mathrm{d}}{\mathrm{d}t} \int_\Omega \boldsymbol{x} \times \rho \boldsymbol{v} \, \mathrm{d}\Omega = \int_\Omega \boldsymbol{x} \times \rho \frac{\mathrm{d}\boldsymbol{v}}{\mathrm{d}t} \, \mathrm{d}\Omega.$$

The balance of angular momentum (or rotational equilibrium) states that the time rate of change of angular momentum of a body is equal by the total moment produced by the forces acting on the body. It means that

$$\int_\Omega \boldsymbol{x} \times \rho \frac{\mathrm{d}\boldsymbol{v}}{\mathrm{d}t} \, \mathrm{d}\Omega = \frac{\mathrm{d}}{\mathrm{d}t} \int_\Omega \boldsymbol{x} \times \rho \boldsymbol{f} \, \mathrm{d}\Omega + \frac{\mathrm{d}}{\mathrm{d}t} \int_\Omega \boldsymbol{x} \times \boldsymbol{\sigma} \, \mathrm{d}\Omega. \tag{C.49}$$

The above equation implies that $\boldsymbol{T} = \boldsymbol{T}^t$; consequently, we can also obtain $\boldsymbol{S}^t = \boldsymbol{S}$, by using Eq. (C.37). Details on obtaining these previous properties can be seen in (CHAVES, 2013, p. 303).

C.8.4 First Law of Thermodynamics

In this section, we present equations for the balance of mechanical energy, also referred to as the first law of thermodynamics. We also briefly discuss thermo-mechanical power once the energy balance is written regarding this feature.

C.8.4.1 Balance of Power

Power is a fundamental property of a body in motion when subjected to forces. Mathematically, it is described as the product of force and velocity. Then, by taking the inner product of the equation for the balance of linear momentum, (C.47), with the velocity field $\boldsymbol{v}$ and integrating on Ω, we obtain the called balance of mechanical power in the Eulerian form:

$$\int_\Omega \mathrm{div}_{\boldsymbol{x}}(\boldsymbol{T}) \cdot \boldsymbol{v} \, \mathrm{d}\Omega + \int_\Omega \rho \boldsymbol{f} \cdot \boldsymbol{v} \, \mathrm{d}\Omega = \int_\Omega \rho \dot{\boldsymbol{v}} \cdot \boldsymbol{v} \, \mathrm{d}\Omega. \tag{C.50}$$

Now, integration by parts (see Eq. (A.3)) and using the symmetry of $\boldsymbol{T}$, the first term in Eq. (C.50) can be rewritten as

$$\begin{aligned}
\int_\Omega \mathrm{div}_{\boldsymbol{x}}(\boldsymbol{T}) \cdot \boldsymbol{v} \, \mathrm{d}\Omega &= -\int_\Omega \boldsymbol{T} : \nabla_{\boldsymbol{x}}(\boldsymbol{v}) \, \mathrm{d}\Omega + \int_\Gamma \boldsymbol{T}\boldsymbol{n} \cdot \boldsymbol{v} \, \mathrm{d}\Gamma \\
&= -\int_\Omega \boldsymbol{T} : \underbrace{\nabla_{\boldsymbol{x}}(\boldsymbol{v})}_{\boldsymbol{L}} \, \mathrm{d}\Omega + \int_\Gamma \boldsymbol{T}\boldsymbol{n} \cdot \boldsymbol{v} \, \mathrm{d}\Gamma \\
&= -\int_\Omega \boldsymbol{T} : \boldsymbol{D} \, \mathrm{d}\Omega + \int_\Gamma \boldsymbol{T}\boldsymbol{n} \cdot \boldsymbol{v} \, \mathrm{d}\Gamma,
\end{aligned} \tag{C.51}$$

where $\boldsymbol{D} = \boldsymbol{L}_{\text{symm}}$ is the deformation rate tensor defined in Eq. (C.20). Replacing the above equation into (C.50), we obtain

$$-\int_{\Omega} \boldsymbol{T} : \boldsymbol{D} \, \mathrm{d}\Omega + \int_{\Gamma} \boldsymbol{T}\boldsymbol{n} \cdot \boldsymbol{v} \, \mathrm{d}\Gamma + \int_{\Omega} \rho \boldsymbol{f} \cdot \boldsymbol{v} \, \mathrm{d}\Omega = \int_{\Omega} \rho \dot{\boldsymbol{v}} \cdot \boldsymbol{v} \, \mathrm{d}\Omega. \tag{C.52}$$

Each term in Eq. (C.52) can be associated to particular forces. For instance, the term

$$\mathcal{P}^a = \int_{\Omega} \rho \dot{\boldsymbol{v}} \cdot \boldsymbol{v} \, \mathrm{d}\Omega, \tag{C.53}$$

is the power of acceleration forces acting in the body (the inertia forces). The term

$$\mathcal{P}^i = -\int_{\Omega} \boldsymbol{T} : \boldsymbol{D} \, \mathrm{d}\Omega, \tag{C.54}$$

is the power of internal forces, and

$$\mathcal{P}^e = \int_{\Gamma} \boldsymbol{T}\boldsymbol{n} \cdot \boldsymbol{v} \, \mathrm{d}\Gamma + \int_{\Omega} \rho \boldsymbol{f} \cdot \boldsymbol{v} \, \mathrm{d}\Omega, \tag{C.55}$$

is the power due to external forces.

By using the notation established in Eqs. (C.53)-(C.55), the balance of mechanical power, Eq. (C.52), can be written as

$$\mathcal{P}^a = \mathcal{P}^e + \mathcal{P}^i. \tag{C.56}$$

Alternatively, we can write the powers for the reference configuration. The power of inertia forces, Equation (C.53), can be rewritten as

$$\mathcal{P}^a = \int_{\Omega_0} \rho_0 \dot{\boldsymbol{v}} \cdot \boldsymbol{v} \mathrm{d}\Omega_0.$$

Equations (C.17) and (C.54) result in

$$\begin{aligned} \mathcal{P}^i &= -\int_{\Omega} \boldsymbol{T} : \boldsymbol{D} \, \mathrm{d}\Omega = -\int_{\Omega} \boldsymbol{T} : \nabla_{\boldsymbol{x}}(\boldsymbol{v}) \, \mathrm{d}\Omega = -\int_{\Omega_0} \boldsymbol{T} : \nabla_{\boldsymbol{x}}(\boldsymbol{v}) \det(\boldsymbol{F}) \, \mathrm{d}\Omega_0 \\ &= -\int_{\Omega_0} \boldsymbol{T} : \nabla_{\boldsymbol{p}}(\boldsymbol{v}) \boldsymbol{F}^{-1} \det(\boldsymbol{F}) \, \mathrm{d}\Omega_0. \end{aligned}$$

Manipulating the above relation and using Eqs. (C.35) and (C.13), we obtain

$$\mathcal{P}^i = -\int_{\Omega_0} \det(\boldsymbol{F}) \boldsymbol{T} \boldsymbol{F}^{-t} : \nabla_{\boldsymbol{p}}(\boldsymbol{v}) \, \mathrm{d}\Omega_0 = -\int_{\Omega_0} \boldsymbol{P} : \dot{\boldsymbol{F}} \, \mathrm{d}\Omega_0.$$

Now, remembering that $\boldsymbol{P} = \boldsymbol{F}\boldsymbol{S}$ (see Eq. (C.37)), using the symmetry of $\boldsymbol{S}$ and the time derivative of $\boldsymbol{E}$, given by Eq. (C.27), we are left with

$$\begin{aligned} &= -\int_{\Omega_0} \boldsymbol{F}\boldsymbol{S} : \dot{\boldsymbol{F}} \, \mathrm{d}\Omega_0 = -\int_{\Omega_0} \boldsymbol{S} : \boldsymbol{F}^t \dot{\boldsymbol{F}} \, \mathrm{d}\Omega_0 \\ &= -\int_{\Omega_0} \boldsymbol{S} : \frac{1}{2} \left(\boldsymbol{F}^t \dot{\boldsymbol{F}} + \dot{\boldsymbol{F}}^t \boldsymbol{F} \right) \, \mathrm{d}\Omega_0 = -\int_{\Omega_0} \boldsymbol{S} : \dot{\boldsymbol{E}} \, \mathrm{d}\Omega_0. \end{aligned}$$

In summary, the amount of power generated by the conjugated pair $\boldsymbol{T}$ and $\boldsymbol{D}$ is the same as that generated by $\boldsymbol{P}$ and $\dot{\boldsymbol{F}}$; that in turn is equal to that for $\boldsymbol{S}$ and $\dot{\boldsymbol{E}}$:

$$-\int_{\Omega} \boldsymbol{T} : \boldsymbol{D} \, \mathrm{d}\Omega = -\int_{\Omega_0} \boldsymbol{P} : \dot{\boldsymbol{F}} \, \mathrm{d}\Omega_0 = -\int_{\Omega_0} \boldsymbol{S} : \dot{\boldsymbol{E}} \, \mathrm{d}\Omega_0. \tag{C.57}$$

Now, we can apply Reynold's theorem to write

$$\int_{\Gamma} \underbrace{\boldsymbol{T}\boldsymbol{n}}_{\boldsymbol{\sigma}} \cdot \boldsymbol{b} \, \mathrm{d}\Gamma \;=\; \int_{\Omega} \boldsymbol{T} : \nabla_{\boldsymbol{x}}(\boldsymbol{v}) \, \mathrm{d}\Omega + \int_{\Omega} \mathrm{div}_{\boldsymbol{x}}(\boldsymbol{T})\boldsymbol{v} \, \mathrm{d}\Omega. \tag{C.58}$$

By changing the domain of integration to the reference domain and using Eq. (C.36), we obtain

$$\begin{aligned}
-\int_{\Omega} \boldsymbol{T} : \boldsymbol{D} \, \mathrm{d}\Omega &= \int_{\Omega_0} \boldsymbol{T} : \nabla_{\boldsymbol{x}}(\boldsymbol{v}) \det(\boldsymbol{F}) \, \mathrm{d}\Omega_0 + \int_{\Omega_0} \mathrm{div}_{\boldsymbol{x}}(\boldsymbol{T})\boldsymbol{v} \det(\boldsymbol{F}) \, \mathrm{d}\Omega_0 \\
&= \int_{\Omega_0} \boldsymbol{T} : \nabla_{\boldsymbol{p}}(\boldsymbol{v})\boldsymbol{F}^{-1} \det(\boldsymbol{F}) \, \mathrm{d}\Omega_0 + \int_{\Omega} \frac{1}{\det(\boldsymbol{F})} \mathrm{div}_{\boldsymbol{p}}(\boldsymbol{P})\boldsymbol{v} \det(\boldsymbol{F}) \, \mathrm{d}\Omega_0 \\
&= \int_{\Omega_0} \underbrace{\boldsymbol{T}\boldsymbol{F}^{-t} \det(\boldsymbol{F})}_{\boldsymbol{P}} : \nabla_{\boldsymbol{p}}(\boldsymbol{v}) \, \mathrm{d}\Omega_0 + \int_{\Omega_0} \mathrm{div}_{\boldsymbol{p}}(\boldsymbol{P})\boldsymbol{v} \, \mathrm{d}\Omega_0 \\
&= \int_{\Gamma_0} \underbrace{\boldsymbol{P}\boldsymbol{n}_0}_{\boldsymbol{\sigma}_0} \cdot \boldsymbol{v} \, \mathrm{d}\Gamma_0.
\end{aligned} \tag{C.59}$$

Then, the power due to external forces can be rewritten in the reference configuration as

$$\mathcal{P}^e \;=\; \int_{\Gamma_0} \boldsymbol{P}\boldsymbol{n}_0 \cdot \boldsymbol{v} \, \mathrm{d}\Gamma_0 + \int_{\Omega_0} \rho \boldsymbol{f}_0 \cdot \boldsymbol{v} \, \mathrm{d}\Omega_0. \tag{C.60}$$

C.8.4.2 Principle of Virtual Power

By taking the inner-product of the equation for the balance of linear momentum, (C.47), with any virtual velocity field $\delta\boldsymbol{v}$ and integrating on Ω, we obtain:

$$\int_{\Omega} \mathrm{div}_{\boldsymbol{x}}(\boldsymbol{T}) \cdot \delta\boldsymbol{v} \, \mathrm{d}\Omega + \int_{\Omega} \rho \boldsymbol{f} \cdot \delta\boldsymbol{v} \, \mathrm{d}\Omega = \int_{\Omega} \rho \dot{\boldsymbol{v}} \cdot \delta\boldsymbol{v} \, \mathrm{d}\Omega. \tag{C.61}$$

Similarly to the previous section, the above equation can be rewritten as

$$-\int_{\Omega} \boldsymbol{T} : \nabla_{\boldsymbol{x}}(\delta\boldsymbol{v}) \, \mathrm{d}\Omega + \int_{\Gamma} \boldsymbol{T}\boldsymbol{n} \cdot \delta\boldsymbol{v} \, \mathrm{d}\Gamma + \int_{\Omega} \rho \boldsymbol{f} \cdot \boldsymbol{v} \, \mathrm{d}\Omega = \int_{\Omega} \rho \dot{\boldsymbol{v}} \cdot \boldsymbol{v} \, \mathrm{d}\Omega, \tag{C.62}$$

where

$$\mathcal{P}_a = \int_{\Omega} \rho \dot{\boldsymbol{v}} \cdot \delta\boldsymbol{v} \mathrm{d}\Omega, \tag{C.63}$$

is the virtual power due to the inertia forces,

$$\mathcal{P}_i \;=\; -\int_{\Omega} \boldsymbol{T} : \nabla_{\boldsymbol{x}}(\delta\boldsymbol{v}) \, \mathrm{d}\Omega, \tag{C.64}$$

is the virtual power by the internal forces, and

$$\mathcal{P}_e \;=\; \int_{\Gamma} \boldsymbol{T}\boldsymbol{n} \cdot \delta\boldsymbol{v} \, \mathrm{d}\Gamma + \int_{\Omega} \rho \boldsymbol{f} \cdot \delta\boldsymbol{v} \, \mathrm{d}\Omega, \tag{C.65}$$

is the virtual power due to the external forces. For the previous equations we use the same notation as Eq. (C.56) in order to simplify the exposition.

Equation (C.62) defines the so-called principle of virtual power (or balance of virtual power). Note that the principle of virtual power can be used to obtain the equation of motion. It is equivalent to the momentum balance laws (provided some assumptions are satisfied). When we consider more general situations, which imply additional forces acting on a body, it is easier to define the internal forces associated with these forces by their virtual power than to define them directly (see Sec 2.2.1). Furthermore, the balance of virtual power directly generates the weak forms usually employed in finite element formulations.

C.8.4.3 Balance of Energies

The *first principle of the thermodynamics* (balance of energy) states that the time rate of change of the total energy is balanced by the external power plus the heating of the body (ODEN, 2012):

$$\frac{\mathrm{d}}{\mathrm{d}t}\mathcal{K} + \frac{\mathrm{d}}{\mathrm{d}t}\mathcal{U} = \mathcal{P}_e + \mathcal{Q}^f + \mathcal{Q}^s, \tag{C.66}$$

where

$$\mathcal{K} = \frac{1}{2}\int_\Omega \rho|\boldsymbol{v}|^2 \,\mathrm{d}\Omega, \tag{C.67}$$

is the total kinetic energy,

$$\mathcal{U} = \int_\Omega \rho e \,\mathrm{d}\Omega, \tag{C.68}$$

is the total internal energy with e being the specific density of internal energy,

$$\mathcal{Q}^f = -\int_\Gamma \boldsymbol{q}\cdot\boldsymbol{n} \,\mathrm{d}\Gamma, \tag{C.69}$$

is the total energy (by a unit of time) carried by an energy flux $\boldsymbol{q}$, and

$$\mathcal{Q}^s = \int_\Omega \rho r \,\mathrm{d}\Omega, \tag{C.70}$$

is the total thermal energy (by a unit of time) generated in Ω by the heat sources (or sinks) with specific heat source density r. It is important to emphasize that, although it is possible to include microstructural effects, in the present case, we consider that the involved body is subject simply to macro-mechanic and thermal energies (for a more general case, see Chapter 2).

By using the Reynold's theorem (see Eq. (A.4)) and Eq. (C.67), it is possible to write

$$\begin{aligned}\frac{\mathrm{d}}{\mathrm{d}t}\mathcal{K} &= \frac{1}{2}\frac{\mathrm{d}}{\mathrm{d}t}\int_\Omega \rho|\boldsymbol{v}|^2\,\mathrm{d}\Omega \\ &= \frac{1}{2}\left(\int_\Omega \frac{\partial}{\partial t}\left(\rho|\boldsymbol{v}|^2\right)\,\mathrm{d}\Omega + \int_\Gamma \boldsymbol{v}\cdot\boldsymbol{n}\rho|\boldsymbol{v}|^2\,\mathrm{d}\Gamma\right) \\ &= \frac{1}{2}\left(\int_\Omega \frac{\partial\rho}{\partial t}|\boldsymbol{v}|^2\,\mathrm{d}\Omega + \int_\Omega \rho\frac{\partial|\boldsymbol{v}|^2}{\partial t}\,\mathrm{d}\Omega + \int_\Gamma \boldsymbol{v}\cdot\boldsymbol{n}\rho|\boldsymbol{v}|^2\,\mathrm{d}\Gamma\right). \end{aligned} \tag{C.71}$$

Now, using Eq. (C.43) and the divergence theorem (see Eq. (A.1)), we found

$$\int_\Omega \frac{\partial\rho}{\partial t}|\boldsymbol{v}|^2\,\mathrm{d}\Omega = -\int_\Omega \mathrm{div}_{\boldsymbol{x}}(\rho\boldsymbol{v})|\boldsymbol{v}|^2\,\mathrm{d}\Omega = -\int_\Gamma \rho\boldsymbol{v}\cdot\boldsymbol{n}|\boldsymbol{v}|^2\,\mathrm{d}\Gamma. \tag{C.72}$$

Replacing the above equation in (C.71) we obtain

$$\frac{\mathrm{d}}{\mathrm{d}t}\mathcal{K} = \frac{\mathrm{d}}{\mathrm{d}t}\frac{1}{2}\int_\Omega \rho|\boldsymbol{v}|^2\,\mathrm{d}\Omega = \frac{1}{2}\int_\Omega \rho\frac{\partial|\boldsymbol{v}|^2}{\partial t}\,\mathrm{d}\Omega = \int_\Omega \rho\dot{\boldsymbol{v}}\cdot\boldsymbol{v}\,\mathrm{d}\Omega = \mathcal{P}^a. \tag{C.73}$$

Then, the derivative of the kinematic energy is equal to the power of inertial forces, as we can see in Eq. (C.53).

Using Eq. (C.73) we can rewrite the balance of energy, Eq. (C.66), as

$$\frac{\mathrm{d}}{\mathrm{d}t}\mathcal{U} = -\mathcal{P}_i + \mathcal{Q}^f + \mathcal{Q}^s. \tag{C.74}$$

Now, replacing Eqs. (C.54), (C.68), (C.69) and (C.70) in the above equation, we obtain

$$\frac{\mathrm{d}}{\mathrm{d}t}\int_\Omega \rho e\,\mathrm{d}\Omega = \int_\Omega \boldsymbol{T}:\boldsymbol{D}\mathrm{d}\Omega - \int_\Gamma \boldsymbol{q}\cdot\boldsymbol{n}\,\mathrm{d}\Gamma - \int_\Omega \rho r\,\mathrm{d}\Omega. \tag{C.75}$$

Using Eq. (C.43), (C.30) and the divergence theorem of Eq. (A.1), we obtain

$$\int_\Omega \rho\dot{e}\,\mathrm{d}\Omega = \int_\Omega \boldsymbol{T}:\boldsymbol{D}\mathrm{d}\Omega - \int_\Omega \mathrm{div}_{\boldsymbol{x}}\boldsymbol{q}\,\mathrm{d}\Omega - \int_\Omega \rho r\,\mathrm{d}\Omega, \tag{C.76}$$

that is the integral form of the balance of internal energy. Once it is valid for any arbitrary volume, we can write the local form as

$$\rho\dot{e} = \boldsymbol{T}:\boldsymbol{D} - \rho r - \mathrm{div}_{\boldsymbol{x}}(\boldsymbol{q}). \tag{C.77}$$

Equation (C.77) can be rewritten in the original configuration. For that, consider the last term in the above equation:

$$\begin{aligned}\int_\Omega \mathrm{div}_{\boldsymbol{x}}\boldsymbol{q}\,\mathrm{d}\Omega = \int_\Gamma \boldsymbol{q}\cdot\boldsymbol{n}\,\mathrm{d}\Gamma &= \int_{\Gamma_0} \boldsymbol{q}\cdot\det(\boldsymbol{F})\boldsymbol{F}^{-t}\boldsymbol{n}_0\,\mathrm{d}\Gamma_0 \\ &= \int_{\Gamma_0} \det(\boldsymbol{F})\boldsymbol{F}^{-1}\boldsymbol{q}\cdot\boldsymbol{n}_0\,\mathrm{d}\Gamma_0 \\ &= \int_{\Gamma_0} \boldsymbol{q}_0\cdot\boldsymbol{n}_0\,\mathrm{d}\Gamma_0 \\ &= \int_{\Omega_0} \mathrm{div}_{\boldsymbol{p}}\boldsymbol{q}_0\,\mathrm{d}\Omega_0, \end{aligned} \tag{C.78}$$

that was manipulated by using the Eq. (A.1) and (C.28). Furthermore,

$$\boldsymbol{q}_0 = \det(\boldsymbol{F})\boldsymbol{F}^{-1}\boldsymbol{q}, \tag{C.79}$$

is the energy flux in the original configuration.

Then, by using Eqs. (C.29), (C.57) and (C.78), we can write the Lagrangian version for the balance of energies:

$$\int_{\Omega_0} \rho_0 \dot{e}_0 \, \mathrm{d}\Omega_0 = \int_{\Omega_0} \boldsymbol{S} : \dot{\boldsymbol{E}} \mathrm{d}\Omega_0 - \int_{\Omega_0} \mathrm{div}_{\boldsymbol{p}} \boldsymbol{q}_0 \, \mathrm{d}\Omega_0 - \int_{\Omega_0} \rho_0 r_0 \, \mathrm{d}\Omega_0, \tag{C.80}$$

where the local form is given by

$$\rho_0 \dot{e}_0 = \boldsymbol{S} : \dot{\boldsymbol{E}} - \rho_0 r_0 - \mathrm{div}_{\boldsymbol{p}}(\boldsymbol{q}_0). \tag{C.81}$$

C.8.5 Second Law of Thermodynamics

The second law of thermodynamics is defined in terms of a state function[1] called entropy. This property is commonly used to describe system disorder or uncertainty. In thermodynamics, it is the physical quantity that measures the amount of heating or work that a system can receive (CHAVES, 2013). Then, the concept of entropy can be used to construct a relationship between the internal energy that is available or unavailable for transformations and the resulting heat and work.

The total entropy of a system is given by

$$\int_{\Omega} \rho\eta \, \mathrm{d}\Omega, \tag{C.82}$$

where η is the specific entropy density. The entropy furnished to the system is given by

$$\int_{\Omega} \rho\omega \, \mathrm{d}\Omega, \tag{C.83}$$

where w is the specific density of sources and sinks, called the entropy production term. The entropy that enters the system by the surface is

$$-\int_{\Gamma} \boldsymbol{q} \cdot \boldsymbol{n} \, \mathrm{d}\Gamma. \tag{C.84}$$

The second law of thermodynamics states that the entropy of isolated systems cannot decrease with time. It means that the rate of change of the total entropy is never less than the entropy flow that enters through the body's surface, plus the entropy created inside the body. Mathematically, we can use Eqs. (C.82)-(C.84) to write the integral form of the second principle of thermodynamics, also called entropy inequality, in the Eulerian configuration:

$$\frac{\mathrm{d}}{\mathrm{d}t}\int_{\Omega} \rho\eta \, \mathrm{d}\Omega \geq \int_{\Omega} \rho w \, \mathrm{d}\Omega - \int_{\Gamma} \boldsymbol{q} \cdot \boldsymbol{n} \, \mathrm{d}(\Gamma). \tag{C.85}$$

[1] A *state function* is a property that depends only on the system's current state, independently of how that state came to be achieved (CALLEN, 1998).

We can use Eq. (C.30) to write

$$\frac{\mathrm{d}}{\mathrm{d}t}\int_{\Omega}\rho\eta\ \mathrm{d}\Omega = \int_{\Omega}\rho\dot{\eta}\ \mathrm{d}\Omega. \tag{C.86}$$

Then, by using the above equation and the divergence theorem, Eq. (A.1) in Eq. (C.85), we obtain the alternative form of the entropy inequality, also referred as integral form of Clausius-Duhem inequality:

$$\int_{\Omega}\rho\dot{\eta}\ \mathrm{d}\Omega \geq \int_{\Omega}\rho\omega\ \mathrm{d}\Omega - \int_{\Omega}\mathrm{div}_{\boldsymbol{x}}\boldsymbol{q}\ \mathrm{d}\Omega. \tag{C.87}$$

Note that, by inequality (C.87), if entropy occurs, the process is irreversible; that is, we can not return to the original state without adding work or heat to the system. The process is reversible if the equality is valid for (C.87). The local form of inequality (C.87) is given by

$$\rho\dot{\eta} \geq \rho\omega - \mathrm{div}_{\boldsymbol{x}}\boldsymbol{q}.$$

The Lagrangian version of the entropy inequality can be obtained by using Eq. (C.78) in (C.87):

$$\int_{\Omega_0}\rho_0\dot{\eta}_0\ \mathrm{d}\Omega_0 \geq \int_{\Omega_0}\rho_0\omega_0\ \mathrm{d}\Omega_0 - \int_{\Omega_0}\mathrm{div}_{\boldsymbol{p}}\boldsymbol{q}_0\ \mathrm{d}\Omega_0. \tag{C.88}$$

where $\eta_0(\boldsymbol{p},t) = \eta(\boldsymbol{x},t)$ and $\omega_0(\boldsymbol{p},t) = \omega(\boldsymbol{x},t)$. Since this equation is valid for any volume, we can obtain the local form as

$$\rho_0\dot{\eta}_0 \geq \rho_0\omega_0 - \mathrm{div}_{\boldsymbol{p}}\boldsymbol{q}_0.$$

C.9 Voigt notation

Symmetric fourth-order tensors in the two-dimensional space can be stored in matrices using Voigt notation. The components of $\boldsymbol{\mathcal{Z}} = [Z_{ijkl}]$ are arranged in the matrix $\boldsymbol{Z}$, which represents the contraction of two indexes of $\boldsymbol{\mathcal{Z}}$:

$$\boldsymbol{Z} = \begin{bmatrix} Z_{1111} & Z_{1122} & Z_{1112} \\ Z_{2211} & Z_{2222} & Z_{2212} \\ Z_{1211} & Z_{1222} & Z_{1212} \end{bmatrix} \tag{C.89}$$

Second-order tensors can be written in vector form using the Voigt notation. For instance, the tensor $\boldsymbol{Z}$ can be written as a vector $\boldsymbol{z}$ that represents the contraction of one index. It is given by

$$z = \begin{bmatrix} Z_{11} \\ Z_{12} \\ Z_{21} \\ Z_{22} \end{bmatrix}. \tag{C.90}$$

If $\boldsymbol{Z}$ is symmetrical, then

$$z = \begin{bmatrix} Z_{11} \\ Z_{22} \\ 2Z_{12} \end{bmatrix}. \tag{C.91}$$

We refer to the Voigt notation in Secs. C.1 and 4.3. Further comments on this notation can be seen in Chaves (2013).

C.10 Double Scalar Product

Consider the second order tensors $\boldsymbol{Z}_1$ and $\boldsymbol{Z}_2$. The double scalar product (also called double contraction) between these tensors is given by

$$\boldsymbol{Z}_1 : \boldsymbol{Z}_2 = Z_{1,ij} Z_{2,ij} = \text{tr}\left(\boldsymbol{Z}_1 \boldsymbol{Z}_2^t\right) = \text{tr}\left(\boldsymbol{Z}_1^t \boldsymbol{Z}_2\right). \tag{C.92}$$

Details on the above equation can be see in Chaves (2013).

If we have a fourth-order tensor $\boldsymbol{\mathcal{Z}}$, then

$$\boldsymbol{\mathcal{Z}} : \boldsymbol{Z}_1 = Z_{ijkl} Z_{1,kl} \boldsymbol{e}_i \boldsymbol{e}_j, \tag{C.93}$$

where $\boldsymbol{e}_i$ and $\boldsymbol{e}_j$ are the unitary vectors in the direction of x and y, respectively. It means that Eq. (C.93) results in a second-order tensor.

APPENDIX D – Neo-Hookean Material

We referred to the Neo-Hookean material in Sec. 3.1.1. It is a class of hyperelastic materials, considered an extension of the traditional Hookean material for predicting the nonlinear stress-strain behavior for finite strain. The Neo-Hookean model is based on the behavior of the cross-linked chains and used mainly to describe polymeric materials (OGDEN, 2013).

The energy function for these materials is defined as

$$\psi_h = \frac{\mu}{2}\left(\mathrm{tr}(\boldsymbol{C}-3) - \mu\ln(\det(\boldsymbol{F})) + \frac{\lambda}{2}(\ln(\det(\boldsymbol{F}))^2, \tag{D.1}$$

where $\boldsymbol{C}$ and $\boldsymbol{F}$ are the right Cauchy-Green and the deformation gradient tensors, respectively (see Eqs. (C.25) and (C.11)). These tensors are related by $\boldsymbol{C} = \boldsymbol{F}^t\boldsymbol{F}$.

The second Piola-Kirchhoff stress tensor can be defined in terms of the energy as

$$\boldsymbol{S} = \partial_{\boldsymbol{E}}\psi_h = 2\partial_{\boldsymbol{C}}\psi_h. \tag{D.2}$$

where $\boldsymbol{E}$ is the Green-Lagrange strain tensor defined in Eq. (C.26). The relations (B.1) and (B.2) and the symmetry of $\boldsymbol{C}$ imply in

$$\partial_{\boldsymbol{C}}\left[\ln(\det(\boldsymbol{C})^{1/2})\right] = \frac{1}{2}\boldsymbol{C}^{-t} = \frac{1}{2}\boldsymbol{C}^{-1} \tag{D.3}$$

and

$$\partial_{\boldsymbol{C}}(\ln(\det(\boldsymbol{C})^{1/2})^2 = 2\ln(\det(\boldsymbol{C})^{1/2})\partial_{\boldsymbol{C}}\ln(\det(\boldsymbol{C})^{1/2}) = \ln(\det(\boldsymbol{C})^{1/2})\boldsymbol{C}^{-1}. \tag{D.4}$$

By using the above equations and (D.2) we obtain

$$\boldsymbol{S} = 2\partial_{\boldsymbol{C}}\psi_h = \mu(\boldsymbol{I} - \boldsymbol{C}^{-1}) + \lambda\ln(\det(\boldsymbol{C})^{1/2})\boldsymbol{C}^{-1}. \tag{D.5}$$

The fourth-order tangent tensor corresponding to the Neo-Hookean material can be obtained by differentiation of Eq. (D.5) with respect to $\boldsymbol{C}$. By using Eqs. (B.2) and (B.3) we obtain

$$2\partial_{\boldsymbol{C}}\boldsymbol{S} = 2\left(\mu - \lambda\ln(\det(\boldsymbol{C})^{1/2})\right)\boldsymbol{\mathcal{I}} + \lambda\boldsymbol{C}^{-1}\otimes\boldsymbol{C}^{-1}, \tag{D.6}$$

where $\boldsymbol{\mathcal{I}} = \frac{1}{2}\left(\delta_{ij}\delta_{jl} + \delta_{il}\delta_{jk}\right)$ is the fourth order symmetric identity tensor, with δ_{ij} the usual Kronecker delta:

$$\delta_{ij} = \begin{cases} 1, i = j \\ 0, i \neq j. \end{cases} \tag{D.7}$$

Further comments on the Neo-Hookean material can be seen in Chaves (2013).

APPENDIX E – Algebraic Manipulations

E.1 Alternative Definition for Caputo Fractional Derivative

Consider Eq. (1.4) rewritten as

$$ {}_a\mathrm{D}_t^{\alpha} f(t) = \frac{1}{\Gamma(1-\alpha)} \lim_{C \to t^-} \underbrace{\int_a^C \frac{f'(\tau)}{(t-\tau)}\, \mathrm{d}\tau}_{I}. \tag{E.1} $$

Applying integration by parts with

$$ \begin{aligned} u = \frac{1}{(t-\tau)^{\alpha}} \quad &\Rightarrow \quad \mathrm{d}u = \frac{\alpha}{(t-\tau)^{\alpha+1}}\, \mathrm{d}\tau, \\ \mathrm{d}v = f'(\tau)\mathrm{d}\tau \quad &\Rightarrow \quad v = f(\tau), \end{aligned} $$

we obtain

$$ \begin{aligned} I &= \frac{f(\tau)}{(t-\tau)^{\alpha}}\bigg|_a^C - \alpha \int_a^{\epsilon} \frac{f(\tau)}{(t-\tau)^{\alpha+1}}\, \mathrm{d}\tau. \\ &= \frac{f(C)}{(t-C)^{\alpha}} - \frac{f(a)}{(t-a)^{\alpha}} - \alpha \int_a^C \frac{f(\tau)}{(t-\tau)^{\alpha+1}}\, \mathrm{d}\tau + \alpha \int_a^C \frac{f(C)}{(t-\tau)^{\alpha+1}}\, \mathrm{d}\tau \\ &\quad -\alpha \int_a^C \frac{f(C)}{(t-\tau)^{\alpha+1}}\, \mathrm{d}\tau \\ &= \frac{f(C)}{(t-C)^{\alpha}} - \frac{f(a)}{(t-a)^{\alpha}} + \alpha \int_a^C \frac{f(C)-f(\tau)}{(t-\tau)^{\alpha+1}}\, \mathrm{d}\tau - \alpha f(C) \int_a^C \frac{1}{(t-\tau)^{\alpha+1}}\, \mathrm{d}\tau \\ &= \frac{f(C)}{(t-C)^{\alpha}} - \frac{f(a)}{(t-a)^{\alpha}} + \alpha \int_a^C \frac{f(C)-f(\tau)}{(t-\tau)^{\alpha+1}}\, \mathrm{d}\tau - \frac{f(C)}{(t-C)^{\alpha}} + \frac{f(C)}{(t-a)^{\alpha}} \\ &= -\frac{f(a)}{(t-a)^{\alpha}} + \alpha \int_a^C \frac{f(C)-f(\tau)}{(t-\tau)^{\alpha+1}}\, \mathrm{d}\tau + \frac{f(C)}{(t-a)^{\alpha}}. \end{aligned} $$

By replacing the above expression in Eq. (E.1), then

$$ {}_a\mathrm{D}_t^{\alpha} f(t) = \frac{1}{\Gamma(1-\alpha)} \left(\frac{f(t)-f(a)}{(t-a)^{\alpha}} + \alpha \int_a^t \frac{f(t)-f(\tau)}{(t-\tau)^{\alpha+1}}\, \mathrm{d}\tau \right). $$

E.2 Properties for $\mathscr{N}$

In this Appendix, we discuss some properties for the function $\mathscr{N}(\boldsymbol{Z}_1, \boldsymbol{Z}_2)$, that appears in Sec. 2.2.3.1. This function, proposed originally in Costa-Haveroth et al. (2022), is a suitable continuous function of second-order symmetric tensors with the following properties:

(a) $\mathscr{N}(\boldsymbol{Z}_1, \boldsymbol{Z}_2) \geq 0$, $\forall \boldsymbol{Z}$;

(b) $|\mathscr{N}(\boldsymbol{Z}_1,\boldsymbol{Z}_2)| \leq C(\boldsymbol{Z}_1,\boldsymbol{Z}_2)|\boldsymbol{Z}_1-\boldsymbol{Z}_2|^{\beta}$, with $\beta \geq 1+\alpha$ and $C(\boldsymbol{Z}_1,\boldsymbol{Z}_2)$ bounded as $\boldsymbol{Z}_1-\boldsymbol{Z}_2 \to 0_+$;

(c) $|\partial_{\boldsymbol{Z}_1}\mathscr{N}(\boldsymbol{Z}_1,\boldsymbol{Z}_2)| \leq C_1(\boldsymbol{Z}_1,\boldsymbol{Z}_2)|\boldsymbol{Z}_1-\boldsymbol{Z}_2|^{\beta_1}$, with $\beta_1 \geq \alpha$ and $C_1(\boldsymbol{Z}_1,\boldsymbol{Z}_2)$ bounded as $\boldsymbol{Z}_1-\boldsymbol{Z}_2 \to 0_+$.

Consider now, that $\mathscr{N}$ is applied for $(\boldsymbol{E}_t,\boldsymbol{E}_\tau)$, where $\boldsymbol{E}_{(\cdot)} := \boldsymbol{E}(\boldsymbol{p},(\cdot))$ is the Green-Lagrange strain tensor (as discussed in Sec. 2.2.3.1). By using the previous properties, and the mean value theorem, we obtain

$$\begin{aligned}|\mathscr{N}(\boldsymbol{E}_t,\boldsymbol{E}_\tau)| &\leq C(\boldsymbol{E}_t,\boldsymbol{E}_\tau)|\boldsymbol{E}_t-\boldsymbol{E}_\tau|^{\beta}\\ &\leq C(\boldsymbol{E}_t,\boldsymbol{E}_\tau)\max\{|\dot{\boldsymbol{E}}_s|, s\in[0,t)\}^{\beta}|t-\tau|^{\beta},\end{aligned} \tag{E.2}$$

and

$$\begin{aligned}|\partial_{\boldsymbol{E}_t}\mathscr{N}(\boldsymbol{E}_t,\boldsymbol{E}_\tau)| &\leq C_1(\boldsymbol{E}_t,\boldsymbol{E}_\tau)|\boldsymbol{E}_t-\boldsymbol{E}_\tau|^{\beta_1}\\ &\leq C_1(\boldsymbol{E}_t,\dot{\boldsymbol{E}}_\tau)\max\{|\boldsymbol{E}_s|, s\in[0,t)\}^{\beta_1}|t-\tau|^{\beta_1}.\end{aligned} \tag{E.3}$$

Inequality (E.2) leads to

$$\lim_{\tau\to t-}\frac{\mathscr{N}(\boldsymbol{E}_t,\boldsymbol{E}_t au)}{(t-\tau)^{1+\alpha}} = 0, \quad 0<\alpha<1. \tag{E.4}$$

Moreover, we also consider that $\dfrac{\mathscr{N}(\boldsymbol{E}_t,\boldsymbol{E}_\tau)}{(t-\tau)^{2+\alpha}}$ and $\dfrac{\partial_{\boldsymbol{E}_t}\mathscr{N}(\boldsymbol{E}_t,\boldsymbol{E}_\tau)}{(t-\tau)^{1+\alpha}}$ are integrable in $[0,t)$ with respect to τ.

E.2.1 On the Obtaining of $\dot{\psi}_m$

Consider ψ_m and $\tilde{\psi}_m$, as presented in Sec. 2.2.3.1, given respectively by

$$\psi_m\left(\varphi,\mathscr{H}_t(\boldsymbol{E})\right) = \frac{G_m(\varphi)}{\rho_0}\tilde{\psi}_m\left(\mathscr{H}_t(\boldsymbol{E})\right), \tag{E.5}$$

and

$$\tilde{\psi}_m\left(\mathscr{H}_t(\boldsymbol{E})\right) = \frac{1}{\Gamma(1-\alpha)}\left[\frac{\mathscr{N}\left(\boldsymbol{E}_t,\boldsymbol{E}_0\right)}{t^{\alpha}} + \alpha\int_0^t \frac{\mathscr{N}\left(\boldsymbol{E}_t,\boldsymbol{E}_\tau\right)}{(t-\tau)^{1+\alpha}}\mathrm{d}\tau\right], \tag{E.6}$$

where

$$\begin{aligned}\mathscr{H}_t(\boldsymbol{E}) &= \mathscr{H}(\boldsymbol{E})(\boldsymbol{p},t)\\ &= \{\boldsymbol{E}(\boldsymbol{p},t-s), 0<s<\infty)\}\\ &= \{\boldsymbol{E}(\boldsymbol{p},s), 0<s<t)\},\end{aligned} \tag{E.7}$$

as show in Eq. (2.69). Under the conditions for $\mathscr{N}$, established in the previous section, the time derivative $\dot{\psi}_m$ for strains are continuous at time $t=0+$ and has bounded rates

(i.e, $|\dot{\boldsymbol{E}}(\boldsymbol{p},t)|$ bounded as $t \to 0_+$), can be obtained as

$$\begin{aligned}\dot{\psi}_m(\varphi, \mathscr{H}_t(\boldsymbol{E})) &= \frac{\dot{G}_m(\varphi)}{\rho_0}\tilde{\psi}_m + \frac{G_m(\varphi)}{\rho_0}\dot{\tilde{\psi}}_m(\mathscr{H}_t(\boldsymbol{E})) \\ &= \frac{\dot{G}_m(\varphi)}{\rho_0}\tilde{\psi}_m + \frac{G_m}{\rho_0}\left(\partial_{\mathscr{H}_t(\boldsymbol{E})}\tilde{\psi}_m : \dot{\overline{\mathscr{H}_t(\boldsymbol{E})}} + \partial_t\tilde{\psi}_m\right). \end{aligned} \tag{E.8}$$

Firstly, we consider

$$\begin{aligned}&\partial_{\mathscr{H}_t(\boldsymbol{E})}\tilde{\psi}_m : \dot{\overline{\mathscr{H}_t(\boldsymbol{E})}} \\ =\ & \frac{1}{\Gamma(1-\alpha)}\left[\frac{\partial_{\mathscr{H}_t(\boldsymbol{E})}\mathscr{N}(\boldsymbol{E}_t,\boldsymbol{E}_0)}{t^\alpha} + \alpha\int_0^t \frac{\partial_{\mathscr{H}_t(\boldsymbol{E})}\mathscr{N}(\boldsymbol{E}_t,\boldsymbol{E}_\tau)}{(t-\tau)}\mathrm{d}\tau\right] : \dot{\overline{\mathscr{H}_t(\boldsymbol{E})}}, \end{aligned} \tag{E.9}$$

Now, we calculate

$$\begin{aligned}\partial_t\tilde{\psi}_m &= \frac{1}{\Gamma(1-\alpha)}\left[\frac{-\alpha\mathscr{N}(\boldsymbol{E}_t,\boldsymbol{E}_0)}{t^{\alpha+1}} + \alpha\frac{\mathrm{d}}{\mathrm{d}t}\int_0^t \frac{\mathscr{N}(\boldsymbol{E}_t,\boldsymbol{E}_\tau)}{(t-\tau)^{1+\alpha}}\mathrm{d}\tau\right] \\ &= \frac{1}{\Gamma(1-\alpha)}\left[\frac{-\alpha\mathscr{N}(\boldsymbol{E}_t,\boldsymbol{E}_0)}{t^{\alpha+1}} + \alpha\left(\frac{\mathscr{N}(\boldsymbol{E}_t,\boldsymbol{E}_\tau)}{(t-\tau)^{1+\alpha}}\bigg|_{\tau=t} + \int_0^t \partial_t\left(\frac{\mathscr{N}(\boldsymbol{E}_t,\boldsymbol{E}_\tau)}{(t-\tau)^{1+\alpha}}\right)\mathrm{d}\tau\right)\right]. \end{aligned} \tag{E.10}$$

The result of Eq. (E.4) implies that

$$\partial_t\tilde{\psi}_m = -\alpha(1+\alpha)\int_0^t \frac{\mathscr{N}(\boldsymbol{E}_t,\boldsymbol{E}_\tau)}{(t-\tau)^{2+\alpha}}\mathrm{d}\tau. \tag{E.11}$$

Then, Eq. (E.8) becomes

$$\dot{\psi}_m = \boldsymbol{S}_m : \dot{\boldsymbol{E}}_t + \frac{\dot{G}_m}{\rho}\tilde{\psi}_m - R, \tag{E.12}$$

where

$$\boldsymbol{S}_m = \frac{G_m}{\rho_0\Gamma(1-\alpha)}\left[\frac{\partial_{\boldsymbol{E}_t}\mathscr{N}(\boldsymbol{E}_t,\boldsymbol{E}_0)}{t^\alpha} + \alpha\int_0^t \frac{\partial_{\boldsymbol{E}_t}\mathscr{N}(\boldsymbol{E}_t,\boldsymbol{E}_\tau)}{(t-\tau)^{1+\alpha}}\mathrm{d}\tau\right], \tag{E.13}$$

and

$$R = \frac{G_m\alpha}{\rho_0\Gamma(1-\alpha)}\left[\frac{\mathscr{N}(\boldsymbol{E}_t,\boldsymbol{E}_0)}{t^{1+\alpha}} + (1+\alpha)\int_0^t \frac{\mathscr{N}(\boldsymbol{E}_t,\boldsymbol{E}_\tau)}{(t-\tau)^{2+\alpha}}\mathrm{d}\tau\right]. \tag{E.14}$$

Note that $R \geq 0$, due to the property (b) defined previously for $\mathscr{N}$.

E.2.2 Example of $\mathscr{N}$

Consider $\mathscr{N}(\boldsymbol{E}_t,\boldsymbol{E}_\tau) = \frac{1}{2}(\boldsymbol{E}_t - \boldsymbol{E}_\tau) : \boldsymbol{\mathcal{A}}(\boldsymbol{E}_t) : (\boldsymbol{E}_t,\boldsymbol{E}_\tau)$ with $\boldsymbol{\mathcal{A}}(\boldsymbol{E}_t)$ a fourth order symmetric-positive definite tensor continuously depending on $\boldsymbol{E}_t$. Then (E.6) becomes

$$\tilde{\psi}_m = \frac{\kappa}{\rho}\left[\frac{[\boldsymbol{E}_t - \boldsymbol{E}_0] : \boldsymbol{\mathcal{A}} : [\boldsymbol{E}_t - \boldsymbol{E}_0]}{t^\alpha} + \alpha\int_0^t \frac{[\boldsymbol{E}_t - \boldsymbol{E}_\tau] : \boldsymbol{\mathcal{A}} : [\boldsymbol{E}_t - \boldsymbol{E}_\tau]}{(t-\tau)^{1+\alpha}}\,\mathrm{d}\tau\right]. \tag{E.15}$$

In this case, some algebraic manipulation and Eq. (E.13) lead to

$$\begin{aligned} \boldsymbol{S}_m &= \frac{G_m}{\rho}\left[\boldsymbol{\mathcal{A}} : {}_0\mathrm{D}_t^{\alpha}\boldsymbol{E}_t + \kappa\frac{(\boldsymbol{E}_t-\boldsymbol{E}_0):\partial_{\boldsymbol{E}}\boldsymbol{\mathcal{A}}:(\boldsymbol{E}_t-\boldsymbol{E}_0)}{t^{\alpha}}\right. \\ &\left. +\kappa\alpha\int_0^t \frac{(\boldsymbol{E}_t-\boldsymbol{E}_\tau):\partial_{\boldsymbol{E}}\boldsymbol{\mathcal{A}}:(\boldsymbol{E}_t-\boldsymbol{E}_\tau)}{(t-\tau)^{1+\alpha}}\mathrm{d}\tau\right], \end{aligned} \tag{E.16}$$

were ${}_0\mathrm{D}_t^{\alpha}\boldsymbol{E}$ is the Caputo fractional derivative of $\boldsymbol{E}$, as shown in Eq. (1.5). Furthermore, Eq. (E.14) can be rewritten as

$$\begin{aligned} R_m &= \frac{G_m}{\rho_0}\kappa\left[\frac{\left(\boldsymbol{E}_t-\hat{E}_0\right):\boldsymbol{\mathcal{A}}:(\boldsymbol{E}_t-\boldsymbol{E}_0)}{t^{\alpha+1}}\right. \\ &\left. +(\alpha+1)\int_0^t \frac{(\boldsymbol{E}_t-\boldsymbol{E}_\tau):\boldsymbol{\mathcal{A}}:\left(\boldsymbol{E}_t-\hat{E}_\tau\right)}{(t-\tau)^{2+\alpha}}\mathrm{d}\tau\right], \end{aligned} \tag{E.17}$$

An interesting possibility is to take $\boldsymbol{\mathcal{A}}(\boldsymbol{E}) = \partial^2_{\boldsymbol{E}}\psi_e(\boldsymbol{E})$, where $\psi_e(\boldsymbol{E})$ is any standard elastic specific free-energy with continuous derivatives with respect to $\boldsymbol{E}$ up to order 3.

It is important to emphasize that Equation (E.15) is a modification of the free-energy potential proposed in Fabrizio (2014). The author shows that his proposal for the free-energy implies in a stress equation in terms of fractional derivatives. However, the arguments presented in Fabrizio (2014) do not make clear why the definition of fractional derivatives must appear. In the present paper we modified Fabrizio's suggestion including the first term of Eq. (E.15) to properly lead to the fractional derivative definition that appears in the associated stress $\boldsymbol{S}_m$ (see Eq. (E.16)). We also extend his suggestion for the three-dimensional case, and added the possibility to consider $\boldsymbol{\mathcal{A}}(\boldsymbol{E})$ nonlinear in relation to $\boldsymbol{E}$.

E.3 On the Obtaining of $\boldsymbol{S}^A$

How to compute the derivative of $\mathcal{I}^A$ with respect to the strain tensor $\boldsymbol{E}^A$, as demanded by Eq. (3.18)? The text that follows explicit the difficult to obtain this derivative analytically.

Note that

$$\mathcal{I}^A\left(\varphi, \nabla_{\boldsymbol{p}}\varphi, \boldsymbol{E}^A\right) = g_c\left(\frac{\gamma_c}{2}\nabla_{\boldsymbol{p}}\varphi\cdot\boldsymbol{C}^{-1}\nabla_{\boldsymbol{p}}\varphi + \frac{1}{\gamma_c}H(\varphi)\right), \tag{E.18}$$

is given in terms of the inverse of total right Cauchy-Green strain tensor $\boldsymbol{C} = \boldsymbol{F}^t\boldsymbol{F}$. We can use the multiplicative decomposition of $\boldsymbol{F}$ in Eq. (2.1), and the definiton of $\hat{\boldsymbol{C}}^B$ in Eq.

(2.58) to obtain

$$\begin{aligned}\boldsymbol{C}^{-1} &= \boldsymbol{F}^{-1}(\boldsymbol{F})^{-t} \\ &= \left(\boldsymbol{F}^{A}\right)^{-1}\left(\boldsymbol{F}^{B}\right)^{-1}\left(\boldsymbol{F}^{B}\right)^{-t}\left(\boldsymbol{F}^{A}\right)^{-t} \\ &= \left(\boldsymbol{F}^{A}\right)^{-1}\left(\hat{\boldsymbol{C}}^{B}\right)^{-1}\left(\boldsymbol{F}^{A}\right)^{-t}. \end{aligned} \tag{E.19}$$

Moreover, we can consider the polar decomposition $\boldsymbol{F}^A = \boldsymbol{R}^A\boldsymbol{U}^A$, where $\boldsymbol{R}^A$ is an orthogonal matrix that represents a rotation and $\boldsymbol{U}^A$ is a symmetric positive definite matrix that represents a distortion and can be related with $\boldsymbol{C}^A$ by $\boldsymbol{U}^A = \left(\boldsymbol{C}^A\right)^{1/2}$ (CHAVES, 2013). It enables to write the following identity:

$$\left(\boldsymbol{F}^{A}\right)^{-1}\left(\hat{\boldsymbol{C}}^{B}\right)^{-1}\left(\boldsymbol{F}^{A}\right)^{-t} = \left(\boldsymbol{C}^{A}\right)^{-1/2}\left(\boldsymbol{R}^{A}\right)^{-1}\left(\hat{\boldsymbol{C}}^{B}\right)^{-1}\left(\boldsymbol{R}^{A}\right)^{-t}\left(\boldsymbol{C}^{A}\right)^{-t/2}.$$

Then, remembering that $\boldsymbol{C}^A = 2\boldsymbol{E}^A + \boldsymbol{I}$ and using the above equation, we have

$$\begin{aligned}\partial_{\boldsymbol{E}^A}\mathcal{I}^A &= 2\partial_{\boldsymbol{C}^A}\mathcal{I}^A \\ &= g_c\gamma\partial_{\boldsymbol{C}^A}\left[\nabla_{\boldsymbol{p}}\varphi\cdot\left(\boldsymbol{C}^{A}\right)^{-1/2}\left(\boldsymbol{R}^{A}\right)^{-1}\left(\hat{\boldsymbol{C}}^{B}\right)^{-1}\left(\boldsymbol{R}^{A}\right)^{-t}\left(\boldsymbol{C}^{A}\right)^{-t/2}\nabla_{\boldsymbol{p}}\varphi\right].\end{aligned}$$

The difficulty in derive the above equation is clear; then, if necessary, we recommend to calculate this term by using numerical derivatives. For Sec. 5.2, we calculated it by using complex numerical derivatives as show bellow (HAVEROTH; STAHLSCHMIDT; MUÑOZ-ROJAS, 2015):

$$\frac{\partial\mathcal{I}_p^A}{\partial E_q^A} = \frac{\mathrm{Im}\left(\mathcal{I}_{n+1}^A\left((E_{n+1}^A) + j\hat{\delta}\right)_p\right)_q}{\hat{\delta}}, \tag{E.20}$$

where $p, q = 1, 2, 3$, $\hat{\delta}$ is a small perturbation ($\hat{\delta} \in [10^{-100}, 10^{-300}]$) and j the imaginary unit.

E.4 On the Obtaining of $\partial_{\boldsymbol{E}^B}\boldsymbol{S}^B$

Here, we indicate how to calculate the derivative in the first term of Eq. (4.22). By using Eq. (2.53), we can write

$$\partial_{\boldsymbol{E}^B_{n+1}}\boldsymbol{S}^B_{n+1} = \det(\boldsymbol{F}^A_n)\left(\boldsymbol{F}^A_n\right)^{-1}\partial_{\boldsymbol{E}^B_{n+1}}\hat{\boldsymbol{T}}^B_{n+1}\left(\boldsymbol{F}^A_n\right)^{-1}. \tag{E.21}$$

Remember that, as discussed in Sec. 4.1.2, we use $\boldsymbol{F}^A_n$ know. By Eq. (E.21), it is necessary to calculate $\partial_{\boldsymbol{E}^B_{n+1}}\hat{\boldsymbol{T}}^B_{n+1}$. In order to simplify the following computations, we suppress the last two terms in Eq. (3.25) and consider $\tilde{b} = 0$ (no viscous damping) to obtain the approximation

$$\begin{aligned}\hat{\boldsymbol{T}}^B \simeq\ &= \frac{1}{\det\left(\boldsymbol{F}^A\right)}\left\{G_h^B\left[\mu^B\left(\boldsymbol{I} - \left(\hat{\boldsymbol{C}}^B\right)^{-1}\right) + \lambda^B\ln\left(\det\left(\hat{\boldsymbol{C}}^B\right)\right)^{1/2}\left(\hat{\boldsymbol{C}}^B\right)^{-1}\right]\right. \\ &\quad -g_c\gamma\left[\left(\hat{\boldsymbol{C}}^B\right)^{-1}\left(\boldsymbol{F}^A\right)^{-t}\nabla_{\boldsymbol{p}}\varphi\right]\otimes\left[\left(\hat{\boldsymbol{C}}^B\right)^{-1}\left(\boldsymbol{F}^A\right)^{-t}\nabla_{\boldsymbol{p}}\varphi\right] \\ &\quad \left.+\frac{G_m^B}{\rho_0}\boldsymbol{\mathcal{A}} : {}_0\mathrm{D}_t{}^{\alpha}(\hat{\boldsymbol{E}}_t^B)\right\}.\end{aligned} \tag{E.22}$$

Particularly, Costa-Haveroth et al. (2022) shown a detailed discussion that validates the simplifications adopted in the last equation.

By considering Eq. (E.22), we can write

$$\begin{aligned}\partial_{\hat{\boldsymbol{E}}^B}\hat{\boldsymbol{T}}^B = \; = \; & \frac{1}{\det\left(\boldsymbol{F}^A\right)}\left\{G_h^B\partial_{\hat{\boldsymbol{E}}^B}\left[\mu^B\left(\boldsymbol{I}-\left(\hat{\boldsymbol{C}}^B\right)^{-1}\right)+\lambda^B\ln\left(\det\left(\hat{\boldsymbol{C}}^B\right)\right)^{1/2}\left(\hat{\boldsymbol{C}}^B\right)^{-1}\right]\right. \\ & -g_c\gamma\partial_{\hat{\boldsymbol{E}}^B}\left[\left(\left(\hat{\boldsymbol{C}}^B\right)^{-1}\left(\boldsymbol{F}^A\right)^{-t}\nabla_{\boldsymbol{p}}\varphi\right)\otimes\left(\left(\hat{\boldsymbol{C}}^B\right)^{-1}\left(\boldsymbol{F}^A\right)^{-t}\nabla_{\boldsymbol{p}}\varphi\right)\right] \\ & \left.+\frac{G_m^B}{\rho_0}\partial_{\hat{\boldsymbol{E}}^B}\left(\boldsymbol{\mathcal{A}}:{}_0\mathrm{D}_t{}^{\alpha}\left(\hat{\boldsymbol{E}}_t^B\right)\right)\right\}. \end{aligned} \tag{E.23}$$

The derivative in the first term of Eq. (E.23) can be obtained similarly to that show in Eq. (D.6):

$$\begin{aligned}&\partial_{\hat{\boldsymbol{E}}^B}\left[\mu^B\left(\boldsymbol{I}-\left(\hat{\boldsymbol{C}}^B\right)^{-1}\right)+\lambda^B\ln\left(\det\left(\hat{\boldsymbol{C}}^B\right)\right)^{1/2}\left(\hat{\boldsymbol{C}}^B\right)^{-1}\right] \\ &= 2\left(\mu^B-\lambda^B\ln(\det(\hat{\boldsymbol{C}}^B)^{1/2}\right)\boldsymbol{\mathcal{I}}+\lambda(\hat{\boldsymbol{C}}^B)^{-1}\otimes(\hat{\boldsymbol{C}}^B)^{-1}, \end{aligned} \tag{E.24}$$

where $\boldsymbol{\mathcal{I}}$ is the fourth order identity tensor.

The derivative in the second term of Eq. (E.23) is calculated by using Eq. (B.3). In terms of components, we have

$$\begin{aligned}[\partial_{\boldsymbol{C}^B}\mathcal{I}]_{mn} \; &= \; -g_c\frac{\gamma}{2}\left[\nabla_{\boldsymbol{p}}(\varphi_0)\right]_i\left[(F^A)^{-1}\right]_{ij}\left[(F^A)^{-t}\right]_{kl}\left[\nabla_{\boldsymbol{p}}(\varphi_0)\right]_l\left[(C^B)^{-1}\right]_{jm}\left[(C^B)^{-1}\right]_{nk} \\ &= \; -g_c\frac{\gamma}{2}\left[(C^B)^{-t}\right]_{mj}\left[(F^A)^{-t}\right]_{ji}\left[\nabla_{\boldsymbol{p}}(\varphi_0)\right]_i\left[(C^B)^{-1}\right]_{nk}\left[(F^A)^{-t}\right]_{kl}\left[\nabla_{\boldsymbol{p}}(\varphi_0)\right]_l. \end{aligned} \tag{E.25}$$

that implies in

$$\partial_{\boldsymbol{C}^B}\mathcal{I} = -\left((\boldsymbol{C}^B)^{-1}(\boldsymbol{F}^A)^{-t}\nabla_{\boldsymbol{p}}(\varphi_0)\right)\otimes\left((\boldsymbol{C}^B)^{-1}(\boldsymbol{F}^A)^{-t}\nabla_{\boldsymbol{p}}(\varphi_0)\right), \tag{E.26}$$

The last term in Eq. (E.23) is calculated as

$$\partial_{\hat{\boldsymbol{E}}^B}\left(\boldsymbol{\mathcal{A}}:{}_0\mathrm{D}_t{}^{\alpha}(\hat{\boldsymbol{E}}_t^B)\right) = \partial_{\hat{\boldsymbol{E}}^B}\left(\boldsymbol{\mathcal{A}}\right):{}_0\mathrm{D}_t{}^{\alpha}(\hat{\boldsymbol{E}}_t^B)+\boldsymbol{\mathcal{A}}:\partial_{\hat{\boldsymbol{E}}^B}\left(\mathrm{D}_t{}^{\alpha}(\hat{\boldsymbol{E}}_t^B)\right). \tag{E.27}$$

The derivative $\partial_{\hat{\boldsymbol{E}}^B}\left(\boldsymbol{\mathcal{A}}\right)$ is dependent on the choice for $\boldsymbol{\mathcal{A}}$ (see some suggestions in Sec. 5.1.1.2). On the other hand, the derivative $\partial_{\hat{\boldsymbol{E}}^B}\left(\mathrm{D}_t{}^{\alpha}(\hat{\boldsymbol{E}}_t^B)\right)$ is calculated in this work by adopting the numerical approximation given by the algorithm G1 show in Eq. (4.45). Then,

$$\begin{aligned}\partial_{\hat{\boldsymbol{E}}^B}\left[\mathrm{D}_t{}^{\alpha}(\hat{\boldsymbol{E}}_t^B)\right] \; &= \; \partial_{\hat{\boldsymbol{E}}^B}\left[(\Delta t)^{-\alpha}\sum_{m=0}^{N-1}B_{m+1}\hat{\boldsymbol{E}}^B(t-m\Delta t)\right] \\ &= \; \partial_{\hat{\boldsymbol{E}}^B}\left[(\Delta t)^{-\alpha}\left[B_1\hat{\boldsymbol{E}}^B(t)+B_2\hat{\boldsymbol{E}}^B(t-\Delta t)+\right.\right. \\ &\quad \left.\left.\cdots+B_N\hat{\boldsymbol{E}}^B(t-(N)\Delta t)\right]\right] \\ &= \; (\Delta t)^{-\alpha}B_1. \end{aligned} \tag{E.28}$$

Alternatively, the derivative $\partial_{\boldsymbol{E}^B}\hat{\boldsymbol{T}}^B$, can also be obtained by using numerical derivatives. In particular, Costa-Haveroth et al. (2022) comment on how to use complex numerical derivatives to calculate this tensor.

E.5 On the Obtaining of $\partial_{\boldsymbol{E}^A}\boldsymbol{C}$ and $\partial_{\boldsymbol{E}^A}\boldsymbol{S}^B$

Consider the derivative that follows, in terms of components:

$$\begin{aligned}\frac{\partial[E^B]_{ij}}{\partial[C]_{pq}} &= \frac{\partial}{\partial[C]_{pq}}\left[\frac{1}{2}\left(\left[\left(F^A\right)^{-t}\right]_{ik}C_{kl}\left[\left(F^A\right)^{-1}\right]_{lj}-I_{ij}\right)\right]\\ &= \frac{1}{2}\left[\left(F^A\right)^{-t}\right]_{ik}\underbrace{\frac{\partial C_{kl}}{\partial C_{pq}}}_{\delta_{kp}\delta_{lq}}\left[\left(F^A\right)^{-1}\right]_{lj}\\ &= \frac{1}{2}\left[\left(F^A\right)^{-t}\right]_{ip}\left[\left(F^A\right)^{-1}\right]_{qj}.\end{aligned}$$

This means that we can use the approximation

$$\left(\partial_{\partial\boldsymbol{C}}\hat{\boldsymbol{E}}^B\right)_{n+1} \simeq \left(\frac{1}{2}\left(\boldsymbol{F}_n^A\right)^{-t}\otimes\left(\boldsymbol{F}_n^A\right)^{-1}\right). \tag{E.29}$$

Now, we use Eq. (3.5) and (3.39) to write

$$\boldsymbol{C} = \left(\boldsymbol{F}^B\right)^t\boldsymbol{C}_A\boldsymbol{F}^B = \left(\boldsymbol{F}^B\right)^t(2\boldsymbol{E}^A-\boldsymbol{I})\boldsymbol{F}^B, \tag{E.30}$$

which implies in

$$\partial_{\boldsymbol{E}^A}\boldsymbol{C} = 2\left(\boldsymbol{F}^B\right)^t\otimes\boldsymbol{F}^B = 2(\boldsymbol{F}^A)^{-t}\boldsymbol{F}^t\otimes\boldsymbol{F}(\boldsymbol{F}^A)^{-1}. \tag{E.31}$$

Then, the derivative $\partial_{\boldsymbol{E}^A}\boldsymbol{S}^B$ can be obtained by the chain rule:

$$\partial_{\boldsymbol{E}^A}\boldsymbol{S}^B \;=\; \partial_{\hat{\boldsymbol{E}}^B}\boldsymbol{S}^B\partial_{\boldsymbol{C}}\hat{\boldsymbol{E}}^B\partial_{\boldsymbol{E}^A}\boldsymbol{C}. \tag{E.32}$$

The term $\partial_{\hat{\boldsymbol{E}}^B}\boldsymbol{S}^B$ is given in Sec. (E.4); $\partial_{\boldsymbol{C}}\hat{\boldsymbol{E}}^B$ is given in Eq. (4.24) and $\partial_{\boldsymbol{E}^A}\boldsymbol{C}$ is shown in Eq. (E.31).

E.6 Simplifications in the Linearization of the Motion Equation

Here we discuss the obtaining of Eq. (4.31). Consider the following manipulation:

$$\boldsymbol{S}^B:\left[\frac{1}{2}\left(\delta\dot{\boldsymbol{F}}^t\nabla_{\boldsymbol{p}}(\boldsymbol{w})+\nabla_{\boldsymbol{p}}(\boldsymbol{w})^t\delta\dot{\boldsymbol{F}}\right)\right] \;=\; \frac{1}{2}\boldsymbol{S}^B:\left(\delta\dot{\boldsymbol{F}}\nabla_{\boldsymbol{p}}(\boldsymbol{w})\right)+\frac{1}{2}\boldsymbol{S}^B:\left(\nabla_{\boldsymbol{p}}(\boldsymbol{w})^t\delta\dot{\boldsymbol{F}}\right)$$

By using Eq. (C.92) and $\boldsymbol{S}^B = \left(\boldsymbol{S}^B\right)^t$ in the above equation, we obtain

$$\begin{aligned}
\boldsymbol{S}^B : \left[\frac{1}{2}\left(\delta\dot{\boldsymbol{F}}^t\nabla_{\boldsymbol{p}}(\boldsymbol{w}) + \nabla_{\boldsymbol{p}}(\boldsymbol{w})^t\delta\dot{\boldsymbol{F}}\right)\right] &= \frac{1}{2}\mathrm{tr}\left(\left(\boldsymbol{S}^B\right)^t\delta\dot{\boldsymbol{F}}\nabla_{\boldsymbol{p}}(\boldsymbol{w})\right) + \frac{1}{2}\mathrm{tr}\left(\left(\boldsymbol{S}^B\right)^t\nabla_{\boldsymbol{p}}(\boldsymbol{w})^t\delta\dot{\boldsymbol{F}}\right)\\
&= \frac{1}{2}\mathrm{tr}\left(\delta\dot{\boldsymbol{F}}\nabla_{\boldsymbol{p}}(\boldsymbol{w})\boldsymbol{S}^B\right) + \frac{1}{2}\mathrm{tr}\left((\delta\dot{\boldsymbol{F}}^t\nabla_{\boldsymbol{p}}(\boldsymbol{w})\left(\boldsymbol{S}^B\right)^t\right)\\
&= \frac{1}{2}\mathrm{tr}\left(\delta\dot{\boldsymbol{F}}\nabla_{\boldsymbol{p}}(\boldsymbol{w})\boldsymbol{S}^B\right) + \frac{1}{2}\mathrm{tr}\left(\delta\dot{\boldsymbol{F}}^t\nabla_{\boldsymbol{p}}(\boldsymbol{w})\boldsymbol{S}^B\right)\\
&= \frac{1}{2}\left(\nabla_{\boldsymbol{p}}(\boldsymbol{w})^t\delta\dot{\boldsymbol{F}} : \boldsymbol{S}^B\right) + \frac{1}{2}\left(\nabla_{\boldsymbol{p}}(\boldsymbol{w})^t\delta\dot{\boldsymbol{F}} : \boldsymbol{S}^B\right)\\
&= \frac{1}{2}\left(\delta\dot{\boldsymbol{F}} : \nabla_{\boldsymbol{p}}(\boldsymbol{w})\boldsymbol{S}^B\right) + \frac{1}{2}\left(\delta\dot{\boldsymbol{F}} : \nabla_{\boldsymbol{p}}(\boldsymbol{w})\boldsymbol{S}^B\right)\\
&= \left(\delta\dot{\boldsymbol{F}} : \nabla_{\boldsymbol{p}}(\boldsymbol{w})\boldsymbol{S}\right).
\end{aligned}$$

Now, to obtain Eq. (4.30), we consider

$$\begin{aligned}
&\frac{1}{2}\left(\delta\dot{\boldsymbol{F}}^t\boldsymbol{F} + \boldsymbol{F}^t\delta\dot{\boldsymbol{F}}\right) : \boldsymbol{\mathcal{A}} : \left[\frac{1}{2}\left(\nabla_{\boldsymbol{p}}(\boldsymbol{w})^t\boldsymbol{F} + \boldsymbol{F}^t\nabla_{\boldsymbol{p}}(\boldsymbol{w})\right)\right]\\
= \;&\frac{1}{2}\left(\delta\dot{\boldsymbol{F}}^t\boldsymbol{F}\right) : \boldsymbol{\mathcal{A}} : \left[\frac{1}{2}\left(\nabla_{\boldsymbol{p}}(\boldsymbol{w})^t\boldsymbol{F}\right)\right] + \frac{1}{2}\left(\delta\dot{\boldsymbol{F}}^t\boldsymbol{F}\right) : \boldsymbol{\mathcal{A}} : \left[\frac{1}{2}\left(\boldsymbol{F}^t\nabla_{\boldsymbol{p}}(\boldsymbol{w})\right)\right] +\\
&\frac{1}{2}\left(\boldsymbol{F}^t\delta\dot{\boldsymbol{F}}\right) : \boldsymbol{\mathcal{A}} : \left[\frac{1}{2}\left(\nabla_{\boldsymbol{p}}(\boldsymbol{w})^t\boldsymbol{F}\right)\right] + \frac{1}{2}\left(\boldsymbol{F}^t\delta\dot{\boldsymbol{F}}\right) : \boldsymbol{\mathcal{A}} : \left[\frac{1}{2}\left(\boldsymbol{F}^t\nabla_{\boldsymbol{p}}(\boldsymbol{w})\right)\right]. \qquad \text{(E.33)}
\end{aligned}$$

As can be shown by using the symmetry of $\boldsymbol{\mathcal{A}}$, the terms in the above equation are identical. Consider the first term of Eq. E.33 (for the remaining terms the calculation is similar):

$$\begin{aligned}
\frac{1}{2}\left(\delta\dot{\boldsymbol{F}}^t\boldsymbol{F}\right)_{ij}A_{ijkl}\frac{1}{2}\left(\nabla_{\boldsymbol{p}}(\boldsymbol{w})^t\boldsymbol{F}\right)_{kl} &= \frac{1}{4}\nabla_{\boldsymbol{p}}(w)^t_{im}F_{mj}A_{ijkl}\delta\dot{F}^t_{kn}F_{nl}\\
&= \frac{1}{4}F^t_{jm}\nabla_{\boldsymbol{p}}(w)_{mi}A_{ijkl}F^t_{ln}\delta\dot{F}_{nk}\\
&= \frac{1}{4}\left(F^t\nabla_{\boldsymbol{p}}(w)\right)_{ji}A_{jilk}\left(F^t\delta\dot{F}\right)_{lk}\\
&= \frac{1}{4}\left(\boldsymbol{F}^t\delta\dot{\boldsymbol{F}}\right) : \boldsymbol{\mathcal{A}} : \left(\boldsymbol{F}^t\nabla_{\boldsymbol{p}}(\boldsymbol{w})\right).
\end{aligned}$$

Replacing the above equation in (E.33), we obtain (4.30).